GAS EJECTOR MODELING FOR DESIGN AND ANALYSIS

A Dissertation

by

CHAQING LIAO

Submitted to the Office of Graduate Studies of
Texas A&M University
in partial fulfillment of the requirements for the degree of

DOCTOR OF PHILOSOPHY

December 2008

Major Subject: Nuclear Engineering

GAS EJECTOR MODELING FOR DESIGN AND ANALYSIS

A Dissertation

by

CHAQING LIAO

Submitted to the Office of Graduate Studies of
Texas A&M University
in partial fulfillment of the requirements for the degree of

DOCTOR OF PHILOSOPHY

Approved by:

Chair of Committee,	Frederick R. Best
Committee Members,	Yassin A. Hassan
	Pavel V. Tsvetkov
	Debjyoti Banerjee
Head of Department,	Raymond Juzaitis

December 2008

Major Subject: Nuclear Engineering

ABSTRACT

Gas Ejector Modeling for Design and Analysis.

(December 2008)

Chaqing Liao, B.S., Zhejiang University;

M.E., Texas A&M University

Chair of Advisory Committee: Dr. Frederick R. Best

A generalized ejector model was successfully developed for gas ejector design and performance analysis. Previous 1-D analytical models can be derived from this new comprehensive model as particular cases. For the first time, this model shows the relationship between the cosntant-pressure and constant-area 1-D ejector models. The new model extends existing models and provides a high level of confidence in the understanding of ejector mechanics. “Off-design” operating conditions, such as the shock occurring in the primary stream, are included in the generalized ejector model. Additionally, this model has been applied to two-phase systems including the gas-liquid ejector designed for a Proton Exchange Membrane (PEM) fuel cell system.

The equations of the constant-pressure and constant-area models were verified. A parametric study was performed on these widely adopted 1-D analytical ejector models. FLUENT, commercially available Computational Fluid Dynamics (CFD) software, was used to model gas ejectors. To validate the CFD simulation, the numerical predictions

were compared to test data and good agreement was found between them. Based on this benchmark, FLUENT was applied to design ejectors with optimal geometry configurations.

DEDICATION

To my mother

ACKNOWLEDGEMENTS

I would like to express my appreciation to a number of individuals who helped produce this work. My appreciation is extended to Dr. Frederick Best who has spent significant time guiding me towards completion of this work. Sincere gratitude is extended to Dr. Yassin A. Hassan, Dr. Pavel V. Tsvetkov and Dr. Debjyoti Banerjee for their recommendations while reviewing this manuscript. I would also like to extend my appreciation to Dr. Ryoji Oinuma and Cable R. Kurwitz who provided me with significant inspiration during our numerous discussions on the analytical models. This work would not have been completed without the extensive time spent by the above mentioned and their help has been deeply appreciated.

NOMENCLATURE

A	Area
CFD	Computational fluid dynamics
CR	Compression ratio
c	Sound speed
c_p	Specific heat capacity at constant pressure
c_v	Specific heat capacity at constant volume
D	A temporary parameter defined by equation (5.19)
D	Diameter
E	A temporary parameter defined by equation (5.23)
ER	Entrainment ratio
η_n	Primary nozzle efficiency coefficient
η_d	Diffuser efficiency coefficient
γ	Specific heat ratio
h	Enthalpy
κ	Area ratio, $\kappa = A_{m2}/A_t$
L	Length
M	Mach number
m	Mass flow rate
μ	Pressure ratio, $\mu = P_1/P_{s0}$

ω	Entrainment ratio
P	Pressure
PEM	Proton exchange membrane
R	Gas constant
$\overline{R}$	Universal gas constant
ρ	Density
Δs	Entropy change
ψ	A temporary parameter defined by equation (3.59)
T	Temperature
τ	Pressure ratio, $\tau = P_{s0}/P_{m2}$
θ	Area ratio, $\theta = A_1/P_{m2}$
W	Molecular weight
V	Velocity
v	Specific volume
x	Liquid quality
ξ	A temporary parameter defined by equation (3.58)

Subscripts

0	Stagnation condition
1	Ejector section 1
2	Ejector section 2

3	Ejector section 3
4	Ejector section 4
*	Critical flow
a	Flow station a
b	Flow station b
e	Exit
g	Gas phase
i	Isentropic
l	Liquid phase
m	Ejector mixed flow
p	Ejector primary stream
s	Ejector secondary stream
t	Nozzle throat
tp	Gas-liquid two-phase mixture
x	Shock wave

TABLE OF CONTENTS

CHAPTER Page

Page

LIST OF FIGURES

Page

Page

Page

Page

Page

LIST OF TABLES

CHAPTER I

INTRODUCTION AND LITERATURE REVIEW

INTRODUCTION

Ejectors are devices used to induce a secondary fluid by momentum and energy transfer from a high velocity primary jet. Ejectors can be operated with incompressible fluids (liquids), and in this application are normally referred to as jet pumps or eductors. On the other hand when ejectors are operated with compressible fluids (gases and vapors) the terms ejector and injector are generally employed. A major difference between the two, besides the working fluid states, is the supersonic, choked flow nozzle of the gas ejector system. The supersonic approach allows a greater conversion of primary fluid energy to secondary fluid pressure head increase. However, this occurs with the penalty of considerable thermodynamic complexity in the mixing and diffusion sections. Fig. 1.1 and Fig. 1.2 are typical cross sectional views of liquid jet pumps and gas ejectors.

The working process in a liquid jet pump or in a gas ejector is the same. A high-pressure fluid with very low velocity at the primary inlet is accelerated to high velocity jet through a converging nozzle for the liquid jet pump or a converging-diverging supersonic nozzle for the gas ejector. The supply pressure at the inlet is partly converted

---

This dissertation follows the style of Journal of Fluids Engineering.

to be the jet momentum at the nozzle exit according to the Bernoulli equation. The high velocity, low static pressure primary jet induces a secondary flow from the suction port and accelerates it in the direction of the driving jet. The two streams then combine in the mixing section, and ideally the process is complete by the end of this section. A diffuser is usually installed at mixing chamber exit to lift the static pressure of mixed flow.

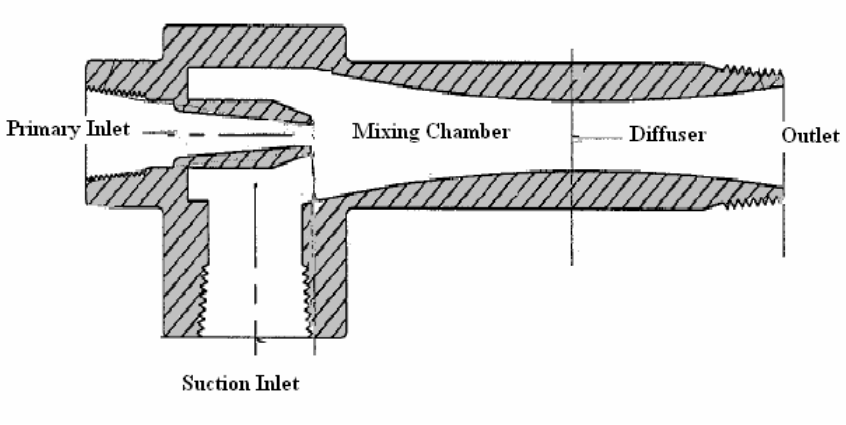

Fig. 1.1 Cross sectional view of a typical liquid jet pump

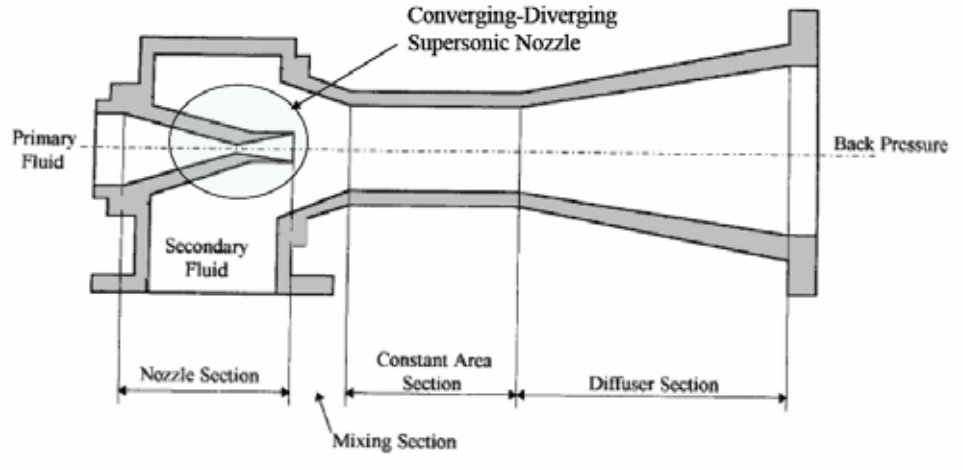

Fig. 1.2 Cross sectional view of a typical gas ejector

Ejectors have simple geometry and no moving parts. Their operation does not require electrical or mechanical shaft energy input. This greatly reduces equipment mass and increases reliability. Ejectors have found wide use in power plant, aerospace, propulsion and refrigeration application because of the above mentioned features. Liquid Jet pumps have very good resistance to cavitation compared to other types of pumps. Thus, jet pumping may be an attractive method for waste heat transport in new generations of spacecraft. The Inter-phase Transport Phenomenon (ITP) Laboratory of Texas A&M University [1] proposed a Rankine Cycle System, in which a liquid jet pump is used to increase pressure recovery for power generation systems of future spacecraft. However, the research and development of jet pump technology for incompressible fluids (liquid) is more mature than that for ejectors used for compressible fluids (gases). This dissertation focuses on gas ejector and discussion on liquid jet pump is limited.

Gas ejectors are also found in high-altitude aircraft, thrust augmentation of aircraft and hydrogen fuel cells, etc. Lee et al. [2] studied the ejector systems used for a hydrogen fuel cell. The Center of Space Power (CSP) at Texas A&M University is designing a gas-liquid separation system for a Proton Exchange Membrane (PEM) fuel cell. In order to pump the exhaust from a PEM fuel cell, a two-phase gas ejector is integrated into the system. Fig. 1.3 is the schematic of PEM fuel cell system test bed. A gas tank supplies high pressure gas to the ejector primary nozzle inlet and the PEM fuel cell exhaust line is connected to the ejector secondary inlet (suction) port. PEM cell exhaust is sucked into the ejector and mixed with the motive stream; the mixed flow then is directed into the

vortex separator. Gas and liquid are split by the separator; liquid is discharged and the gas is directed to the PEM inlet port.

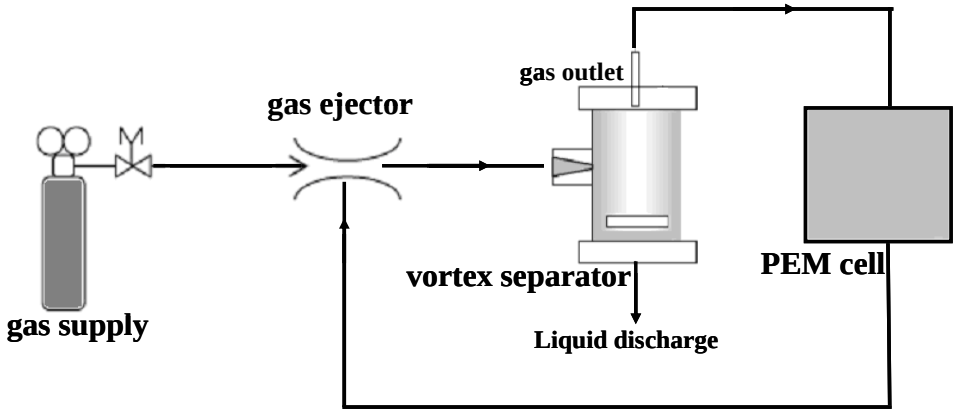

Fig. 1.3 Schematic of the PEM fuel cell system test bed

The goal of the dissertation is to perform a comprehensive theoretical study of ejector energy and momentum transfer, to develop a universal ejector model which embodies all existing ejector models and provide answers to the problems left unsolved by these existing models, and to investigate the feasibility as well as limitations of using gas ejector to work for gas-liquid two-phase flow.

The theoretical background of ejector working mechanism, the fundamental concepts and governing equations of aerodynamics are introduced as the first step. Equations of the constant-pressure ejector model and constant-area ejector model are then derived in great details. Parametric analysis is performed for these 1-D analytical models for gas ejector with single-phase flow. The general gas ejector design procedures and steps

using the 1-D analytical models are discussed. ESDUpac A9242, a computer program with comprehensive 1-D analytical models for gas ejector design, is introduced briefly.

In order to gain a better understanding of the mixing process in the ejector, the commercial Computational Fluid Dynamics (CFD) software FLUENT is used to model the gas ejector. It will be shown that there is good agreement between the CFD simulation results and experimental data. Based on this benchmark, FLUENT is employed to optimize the ejector geometric configuration.

Confidence in the ejector working mechanism is gained from the above-mentioned studies and simulations. A generalized, comprehensive ejector model is successfully developed based on the understanding of momentum and energy transfer between the primary and secondary streams. This novel model provides answers to the unsolved problems of existing models. Since the motivation of this research is to design a working ejector for the PEM fuel system, the new model was applied to study the limitations of design and operation of ejector working with a gas-liquid two-phase mixture.

GAS EJECTORS LITERATURE REVIEW

The ejector was introduced as an engineering device in the early 20th century. At the same time, researchers started to investigate its working mechanism. In a paper published in 1950, Keenan and Neumann [3] presented the first comprehensive

theoretical and experimental analysis of the ejector problem. The constant-pressure mixing model and the constant-area mixing model developed by Keenan and Neumann [3] became the basis of ejector design and performance analysis since then. Based on these 1-D analytical approaches, much research effort has been devoted to the improvement of ejector design methods and hundreds of papers relating to supersonic ejectors are published. In a review carried out by Bonnington and King [4], 413 ejector references about ejector dating prior to 1976 were cited; 1/3 of them are about gas ejectors. More recently, a comprehensive review of published research related to the design and application of supersonic ejectors is given by D.W. Sun and I.W. Eames (1995) [5].

In the derivation of constant-pressure mixing model, Keenan and Neumann [3] assumed that the fluids of the primary flow and secondary flow were the same gas. Keenan and Neumann [3] also neglected nozzle and diffuser efficiencies and frictional effects. This method is not very accurate, but it avoids the complicated expressions of thermodynamic properties for mixed flow as well as the use of experimentally determined constants. In general, experimental values of pressure-rise and flow entrainment are found to be approximately 85% of the calculated values.

DeFrate and Hoerl [6] modified the constant-pressure mixing model by taking the ideal gas law with molecular weight into their derivation, since gas constant is determined by the molecular weight and universal gas constant by the relationship of $R = \overline{R}/W$.

Different heat ratios of the primary and secondary fluids were also included in their method. Based on constant-pressure mixing and in terms of enthalpy, Emanuel [7] developed a simple analytical model for optimizing the steady-state performance of an ejector. Rice and Dandachi [8] derived equations for steam ejectors to predict the primary flow rate by including the friction and mixing losses which have usually been neglected. Huang et al. [9] assumed constant-pressure mixing to occur inside the constant-area section of the ejector with the entrained flow in a choking condition. Huang et al. [9] determined various loss factor coefficients in their approach by matching the test data with the analytical results.

Another 1-D analytical model, the constant-area mixing ejector, was also considered by Keenan and Neumann [3,10]. The mixing in a constant-area ejector operates in two distinct regimes, depending on whether the flow characteristics of the ejector are dependent or independent of the back pressure P_b. Fabri and Siestrunck [11] introduced the concept of "aerodynamic throat" and included the primary nozzle wall thickness in their constant-area mixing model. They referred to the P_b-dependent regime as the "mixed" regime (MR), and to the P_b-independent regime as the "supersonic" regime (SR) and/or the "saturated-supersonic" regime (SSR). For a better understanding of the mixing mechanism, Addy and Chow [12,13], Dutton and Carroll [14] showed these regimes on a three-dimensional solution surface as shown in Fig. 1.4. This solution surface is based on three variables: primary-to-secondary stagnation pressure ratio P_{p0}/P_{s0}, the static-to-secondary stagnation pressure-ratio P_b/P_{s0} and entrainment ratio

ω. A constant-area ejector is constrained to operate at some point on the solution surface. The entrainment ratio ω is predicted by the other two variables, P_{p0} / P_{s0} and P_b / P_{s0}.

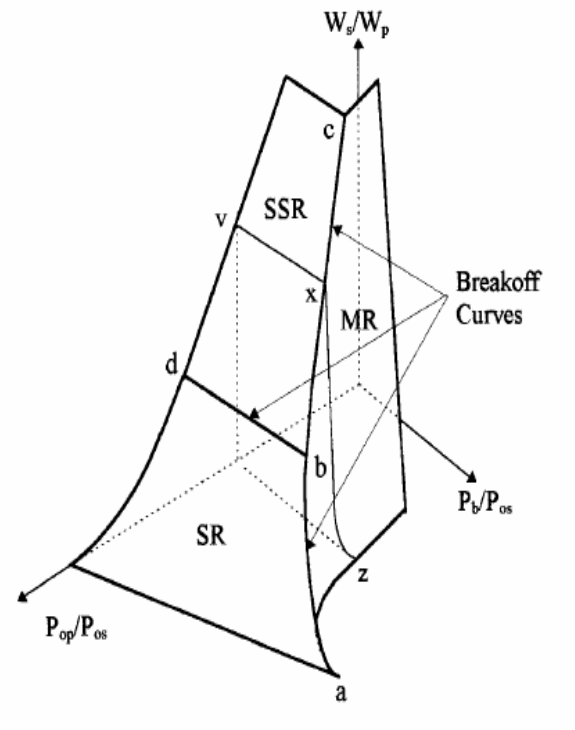

Fig. 1.4 Three-dimensional ejector solution surface, Addy & Dutton et al. [12, 13, 14]

The conditions required by 1-D models are not as restrictive as they may appear. As long as the flow can be simplified to 1-D or suitable mean values can be used, these models can be applied for non-uniform flow conditions. However, for turbulent flow through very short sections this is not the case. A 1-D analysis can be utilized for the purposes of engineering design because, despite its relative simplicity, it has been shown to give

consistent and reasonably accurate results within its limitations. Significant progress has been made for these widely used analytical models since 1950, but some problems are still unsolved. There is no way to determine the optimum shape of the mixing section for constant-pressure ejector. Also, nobody has yet established a definite link between the performance of constant-area and constant-pressure ejectors. It is highly desired to develop a new ejector model which would unify all ejector models and provide answers for the unsolved problems of existing models.

Many researchers have used various 2-D models in order to gain a better understanding of the flow process in ejectors, particularly within the mixing section. Goff and Coogan [15] were the first to consider the two-dimensional aspects of ejector performance. Mikhail [16] assumed various velocity profiles at each stage of the mixing process in a constant-area tube. The predictions of 2-D analytical models could be more accurate than those of 1-D models, but a number of disadvantages are associated with them. The 2-D models are inherently more complicated, and generally require more specialist knowledge to implement. Fruthermore, there are usually empirical coefficients or constants to be determined from experiment, and they are usually applicable only for certain particular ejectors.

Hedges and Hill [17] took a first step into Computational Fluid Dynamics (CFD) and developed a finite-difference scheme to model the flow process within a gas ejector. Gilbert and Hill [18] further refined this method and their theoretical results were

generally in good agreement with experimental results. Commercial CFD software programs now widely available enable researchers to look at the complicated supersonic flow and mixing problems in the gas phase. Neve [19] studied the flow in the diffuser section of an ejector. Riffat et al. [20] used CFD to analyze the performance of ejectors. A commercial code, FLUENT, was employed by Riffat et al. [20] to investigate the impact of the primary nozzle exit position on the performance of the ejector. In the CFD modeling, Riffat et al. [20] have adopted the standard $k-\varepsilon$ model and Renormalization Group (RNG) $k-\varepsilon$ model to solve the turbulence problems. Bartosiewicz et al. [21,22] also used FLUENT to simulate ejectors, but they concluded that the shear stress transport (SST) version of the $k-\omega$ turbulence model agrees best with the test data.

There is no study of the flow in a whole ejector channel, let alone using CFD to optimize the ejector design. Also, there are few comparisons between CFD predictions and data. In order to validate the CFD simulations, it is necessary to carry out more experimental-CFD and analytical-CFD comparisons. The feasibility of whether CFD methods are capable of dealing adequately with supersonic flow, particularly shock and expansion wave in ejectors, has not been previously investigated.

DISSERTATION ORGANIZATION

The theoretical background and some important concepts used in the derivation of analytical models for gas ejectors will be introduced in Chapter II. Chapter III will

introduce the existing analytical models for gas ejectors with single phase flow; the Engineering Science Data Unit (ESDU) program ESDUpac A9242 Version 2 also will be introduced and analyzed. Chapter IV consists of sing-phase gas ejector simulations using the CFD software FLUENT. This chapter also includes the introduction of simulation, benchmark, analysis of performance characteristics and flow field details of gas ejectors, and optimization of geometric configurations. Chapter V derives a novel generalized ejector model for the ejector design and performance analysis. Chapter VI studies the general features and limitations of design and operation of ejector working with gas-liquid two-phase flow. Chapter VII summarizes present work, address existing problems and suggest possible direction for future work.

CHAPTER II

THEORETICAL BACKGROUND AND NOZZLES

INTRODUCTION

The theoretical background used in the derivation of 1-D analytical models for gas ejectors is introduced in this chapter. All 1-D analysis of compressible gas streams in the ejector are made by application of conservation equations of continuity, momentum, and energy, as well as the ideal-gas law. For compressible flow, an important dimensionless parameter, Mach number, usually is utilized to represent the velocity. Isentropic expansion is an important assumption during the derivations, though some researchers also use loss factor coefficients obtained from experimental data to represent the friction or other loss. To achieve better performance, modern gas ejectors are normally operated in a supersonic condition at the exit of primary nozzle. Therefore, it is necessary to introduce the choking phenomena occurs at the throat of primary nozzle.

The basic idea of a gas ejector is to accelerate the motive flow to supersonic by a converging-diverging nozzle, primary flow exit at the suction chamber where secondary flow is induced by this high-velocity, depressurized flow. In most cases, there is also a diffuser installed at the exit of the mixing section to induce pressure recovery. The nozzles used to accelerate/decelerate or pressurize/depressurize the compressible flows are introduced in this chapter.

THEORETICAL BACKGROUND

Conservation and Ideal Gas Law

The conservation equations and idea gas law for steady 1-D compressible flow in an arbitrary variable-area control volume as sketched in Fig. 2.1 are given below. The definitions of termininologies can be found in the nomencluatre section.

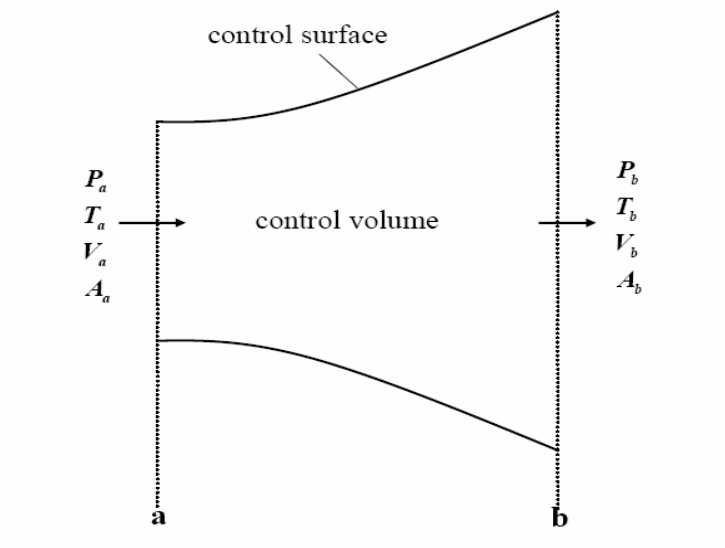

Fig. 2.1 Control volume for 1-D flow

Continuity equation

$$m = \rho_a V_a A_a = \rho_b V_b A_b \tag{2.1}$$

Momentum equation

$$P_a A_a + m_a V_a + \int_{A_a}^{A_b} P dA = P_b A_b + m_b V_b \tag{2.2}$$

Energy equation

$$h_a + \frac{V_a^2}{2} = h_b + \frac{V_b^2}{2} \tag{2.3}$$

Ideal gas law

$$\frac{P}{\rho} = RT \tag{2.4}$$

Where R is the gas constant with unit of $J/(kg.K)$. R is related to its molecular weight by following equation:

$$R = \frac{\overline{R}}{W} \tag{2.5}$$

In the above equation, $\overline{R}$ is the universal gas constant with unit of $J/(kmol.K)$ and W is the molecular weight with unit of $kg/(kmol)$.

Mach Number

Mach number, M , is a very important dimensionless parameter for compressible flow, specially, for supersonic flow. Mach number is defined as the ratio of the fluid velocity to the local sonic speed.

$$M = \frac{\text{local fluid velocity}}{\text{local sonic speed}} = \frac{V}{c} \tag{2.6}$$

The local sound speed c in a medium with temperature T is given by:

$$c = \sqrt{\gamma RT} \tag{2.7}$$

Isentropic Expansion of Ideal Gas

Equation (2.8) is the process equation for isentropic flow of an ideal gas:

$$\frac{P}{\rho^{\gamma}} = \text{constant} \tag{2.8}$$

The basic equations: continuity, momentum, energy, second law, equation of state, as well as the above-mentioned process equation, the local pressure, temperature and density can be related with their corresponding values at stagnation condition by isentropic flow functions expressed in Equations (2.9) through (2.11). The parameters with subscript 0 refer to the stagnation properties. Stagnation properties are constant throughout a steady, isentropic flow field.

Pressure: $$\frac{P_0}{P} = \left(1 + \frac{\gamma - 1}{2} M^2\right)^{\frac{\gamma}{\gamma - 1}} \quad (2.9)$$

Temperature: $$\frac{T_0}{T} = 1 + \frac{\gamma - 1}{2} M^2 \quad (2.10)$$

Density: $$\frac{\rho_0}{\rho} = \left(1 + \frac{\gamma - 1}{2} M^2\right)^{\frac{1}{\gamma - 1}} \quad (2.11)$$

Choking Phenomena

To explain the choking phenomena, a convergent-divergent nozzle with its static pressure distribution along the flow direction are shown in Fig. 2.2 [23]. Flow through the Converging-diverging nozzle of Fig. 2.2 is induced by an adjustable lower downstream pressure; upstream supply is constant and stagnation conditions with $V_0 \cong 0$. P_e and P_b represent the static pressure at the nozzle exit plane and the back pressure, respectively. Fig. 2.2 illustrates graphically the effect of variations in back pressure P_b on the pressure distribution through the nozzle.

The flow rate is low when back pressure P_b is slightly less than P_0; curve *i* shows the pressure distribution in the nozzle for this case. If the flow rate is low enough, the flow will be subsonic and essentially incompressible (if $M < 0.3$) at all points on this curve. Under this condition, the nozzle will behave as a venturi, with flow accelerating in the

converging portion until a point of maximum velocity and minimum pressure is reached at the throat, then decelerating in the diverging portion to the nozzle exit. When the back pressure is reduced further, the flow rate increases but, is still subsonic everywhere and the pressure distribution is shown as curve *ii* similar to curve *i* although the compressibility effects become important. As P_b continues to be reduced, the flow rate will continue to increase.

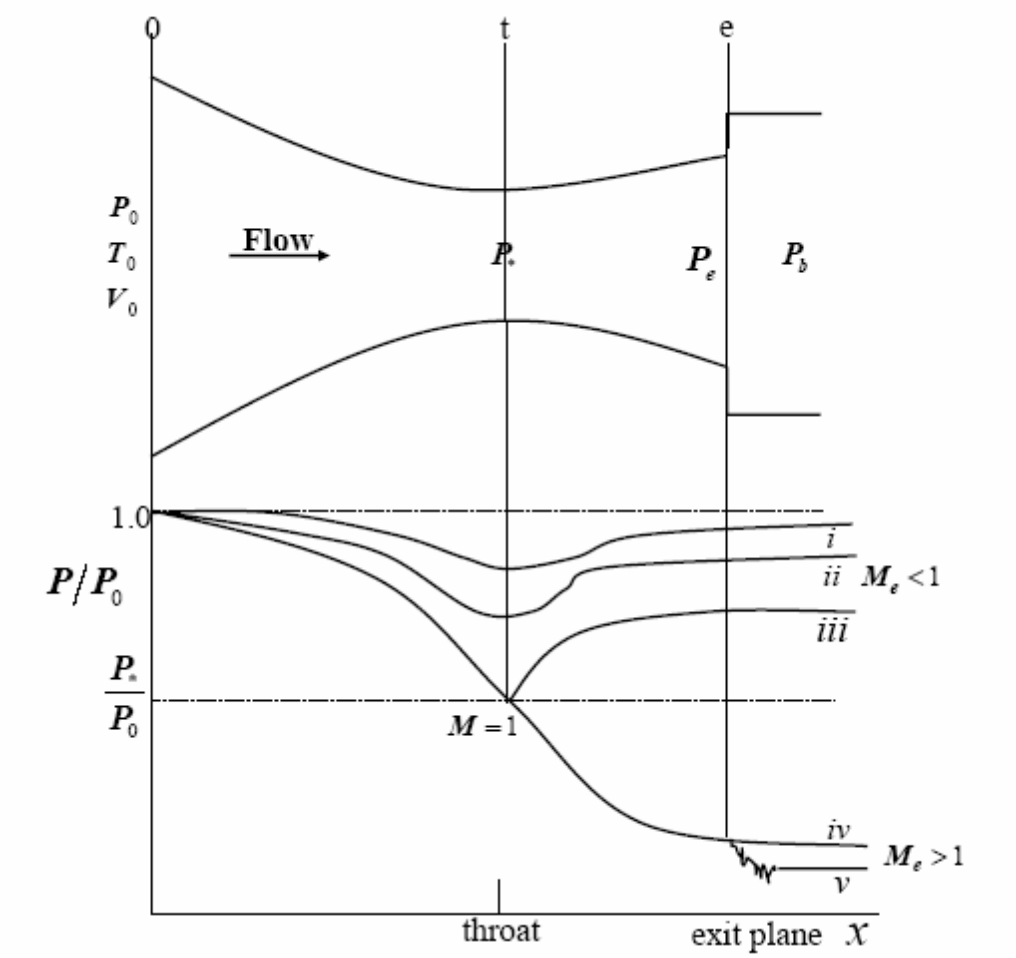

Fig. 2.2 Pressure pofile for isentropic flow in a converging-diverging nozzle [23]

If back pressure P_b is lowered far enough, ultimately the flow reaches $M = 1$ at nozzle throat—the section of minimum flow area, as shown on curve *iii* and the nozzle is choked. When curve *iii* is reached, critical conditions are present at the throat and the mass flow rate attains the maximum possible for the given nozzle and stagnation conditions. The corresponding pressure is the critical back pressure, P_*. The definition of critical condition is the state at which the Mach number is unity. Substituting $M = 1$ into Equations (2.9) through (2.11) and considering the definition of Mach number, we have following relationships.

$$\frac{P_*}{P_0} = \left(\frac{2}{\gamma+1}\right)^{\frac{\gamma}{\gamma-1}} \tag{2.12}$$

$$\frac{T_*}{T_0} = \frac{2}{\gamma+1} \tag{2.13}$$

$$\frac{\rho_*}{\rho_0} = \left(\frac{2}{\gamma+1}\right)^{\frac{1}{\gamma-1}} \tag{2.14}$$

$$V_* = c_* = \sqrt{\left(\frac{2\gamma}{\gamma+1}\right)RT_0} \tag{2.15}$$

For air, $\gamma = 1.4$, and $P_*/P_0 = 0.528$, $T_*/T_0 = 0.833$, $\rho_*/\rho_0 = 0.634$. The mass flow rate at critical condition is calculated by:

$$m = \rho_* V_* A_* \tag{2.16}$$

Where, $A_* = A_t$. Using the definition of critical condition, it can be shown that:

$$m = \frac{A_t P_0}{T_0}\sqrt{\frac{\gamma}{R}\left(\frac{2}{\gamma+1}\right)^{\frac{\gamma+1}{\gamma-1}}} \qquad (2.17)$$

Thus the maximum flow through a given nozzle depends only on the ratio $P_0/\sqrt{T_0}$. Fig. 2.3, mass flow rate vs. pressure for various throat diameters, was generated according to Equation (2.17) for air with stagnation temperature $T_0 = 300K$.

As shown in Fig. 2.2, when back pressure is reduced further, below P_*, such as conditions of *iv* and *v*, information about the throat downstream conditions cannot be transmitted upstream. Consequently, reductions in P_b below P_* has no effect on flow conditions in the converging nozzle portion; thus, neither the pressure distribution through the converging nozzle, throat exit pressure, nor mass flow rate is affected by lowering P_b below P_*.

The diverging section accelerates the flow to supersonic speed from $M = 1$ at the throat. Accelerating the flow in the diverging section results in a pressure decrease. This condition is illustrated by curve *iv* shown in Fig. 2.2. If the back pressure is set at P_{iv}, flow will be isentropic through the nozzle, and supersonic at the nozzle exit. Nozzles operating at $P_b = P_{iv}$ are said to operate at design conditions. Lowering the back pressure below condition *iv*, say to condition *v*, has no effect on flow in the nozzle. The flow is isentropic from the plenum chamber to the nozzle exit (same as condition *iv*) and then undergoes a three-dimensional irreversible expansion to the lower back pressure. A

nozzle operating under these conditions is said to be under-expanded, since additional expansion takes place outside the nozzle.

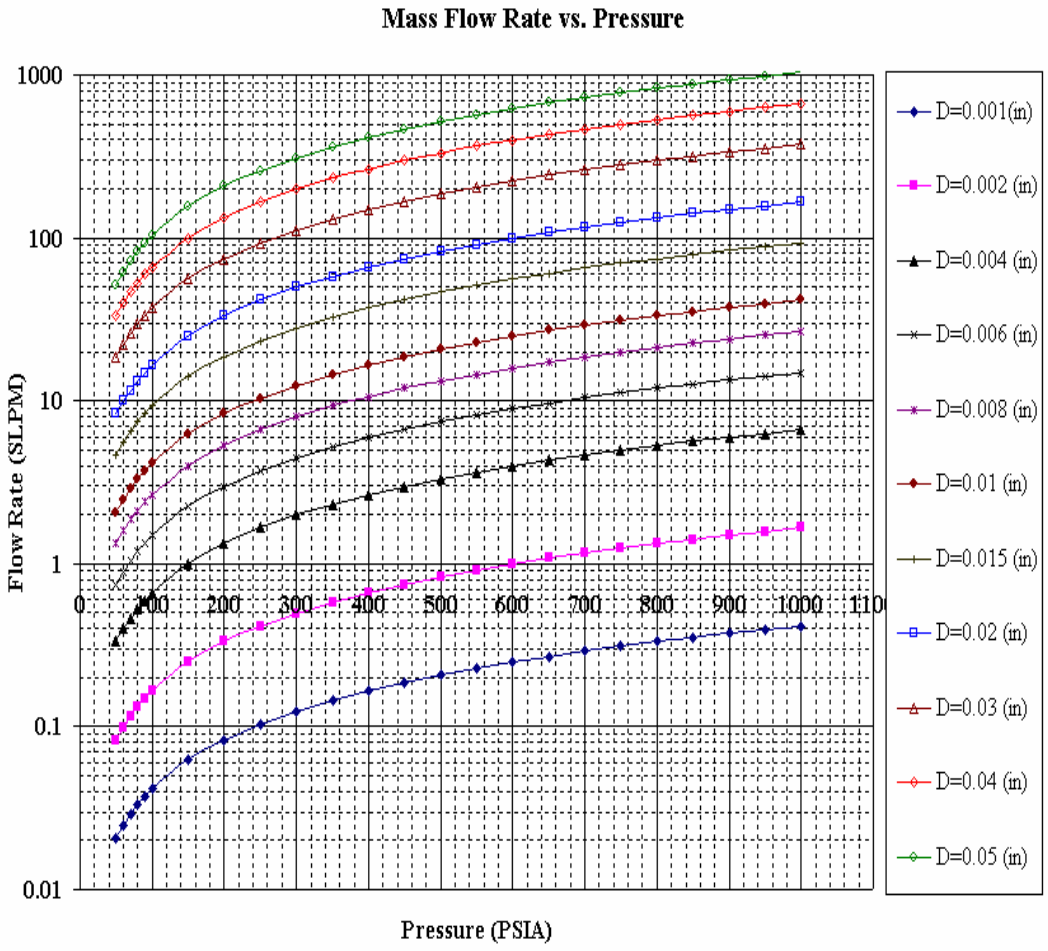

Fig. 2.3 Maximum mass flow rate vs. stagnation pressure for various throat diameters, with air at $T_0 = 300K$

Flow Acceleration and Deceleration

Equation (2.18) and Equation (2.19) are convenient differential forms of the momentum and continuity equations, respectively, for isentropic flow.

$$\frac{dP}{\rho} + d\left(\frac{V^2}{2}\right) = 0 \tag{2.18}$$

$$\rho VA = \text{constant} \tag{2.19}$$

Starting from the above two equations, a relationship between the flow area change and the velocity change can be derived as given by Equation (2.20).

$$\frac{dA}{A} = -\frac{dV}{V}\left(1 - M^2\right) \tag{2.20}$$

From the above equation, it is clear that for $M < 1$ an area change causes a velocity change of opposite sign and a pressure change of the same sign; for $M > 1$ an area change causes a velocity change of the same sign and a pressure change of opposite sign. Fig. 2.4 summarizes these relationships. For subsonic flows ($M < 1$), flow acceleration in a nozzle requires a passage of diminishing cross section; area must decrease to cause a velocity increase. A subsonic diffuser requires that the passage area increase to cause a velocity decrease. In supersonic flows ($M > 1$), the effects of area change are the opposite. A supersonic nozzle must be built with an area increase in the flow direction. A supersonic diffuser must be a converging channel. Where $M = 1$ and the above-

mentioned choking phenomena occurs, the channel area is at its minimum. At that point, it is called the throat.

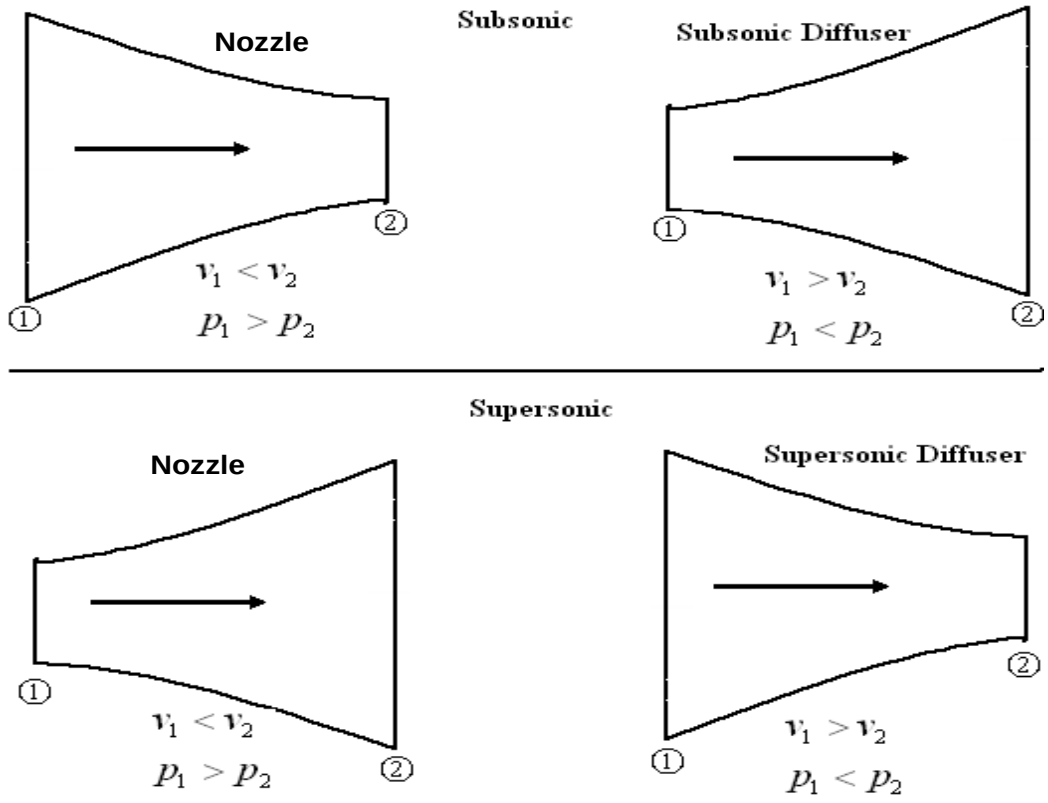

Fig. 2.4 Nozzle and diffuser shapes for subsonic flow and supersonic flow

To accelerate flow from rest to supersonic speed requires first a subsonic converging nozzle. Under proper conditions, the flow will be choked at the throat, where the area is a minimum. Further acceleration is possible if a supersonic divergent nozzle segment is added downstream of the throat. This is the reason for the primary nozzle of modern gas ejectors to be designed in the convergent-divergent shape, as shown in Fig. 2.2.

To decelerate flow from supersonic to subsonic speed requires first a supersonic converging diffuser. The flow will be at $M = 1$ at the throat, theoretically. In practice, supersonic flow cannot be decelerated to exactly $M = 1$ at a throat because sonic flow near a throat is unstable due to a rising, reverse, pressure gradient. Further isentropic deceleration could take place in a diverging subsonic diffuser section. Flow at the ejector mixing section exit is subsonic for this study, and a diverging subsonic diffuser is used.

PRIMARY NOZZLE OF EJECTOR

As discussed in previous paragraphs, a gas ejector is designed with a converging-diverging primary nozzle which is intended to produce supersonic flow at the nozzle exit plane. Primary flow leaves the nozzle exit as supersonic when the back pressure is at or below nozzle design pressure. The exit Mach number is fixed once the area ratio, A_e/A_*, is specified. Considering mass conservation and substituting Equations (2.7), (2.10) and (2.11) into Equation (2.17), the relationship between A_e/A_* and Mach number is given by Equation (2.21).

$$\frac{A_e}{A_*} = \frac{1}{M}\left(\frac{1+\frac{\gamma-1}{2}M^2}{1+\frac{\gamma-1}{2}}\right)^{\frac{\gamma+1}{2(\gamma-1)}} \tag{2.21}$$

Where, $A_* = A_t$ is the nozzle throat area. All other exit plane properties (for isentropic flow) are uniquely related to stagnation properties by the fixed plane Mach number

according to the isentropic expansion functions, Equation (2.9) through (2.11). The properties of isentropic flow at the diverging nozzle exit, i.e., T_e, P_e, ρ_e and A_e can therefore be calculated. Property ratios against Mach number at the nozzle exit plane are shown in Fig. 2.5.

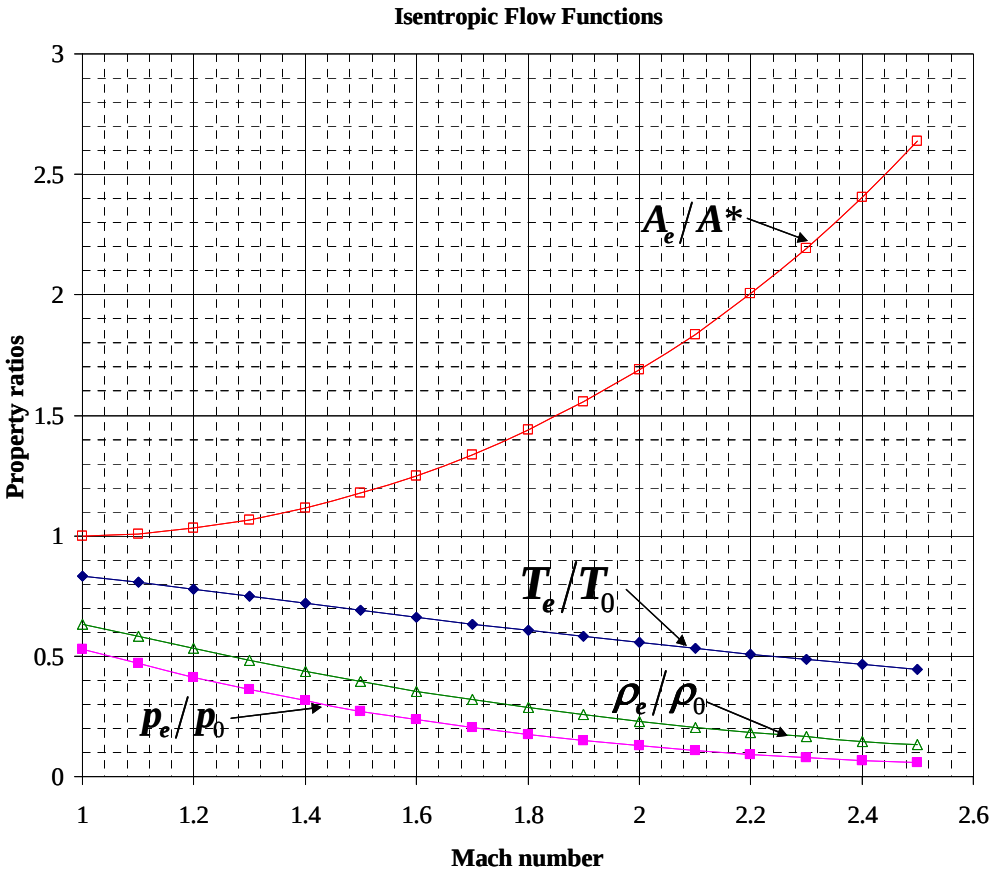

Fig. 2.5 Property ratios at the nozzle exit for given Mach numbers

In the design of a gas ejector, determining primary nozzle size is the first step. Based on the given operating range of stagnation conditions, i.e., T_0 and p_0 at the primary inlet and desired mass flow rate with known specific heat ratio γ, the throat diameter can be determined by Equation (2.17). For air flow, Fig. 2.3 can also be applied for this purpose. Equation (2.21) is utilized to calculate the diameter of supersonic nozzle exit for desired Mach number. Thus, the geometry of the primary nozzle is computed by Equation (2.17) and (2.21). Meanwhile, the flow properties at the nozzle exit plane can be calculated using Equation (2.9), (2.10) and (2.11).

SUMMARY

The basic concepts and governing equations of aerodynamics were introduced in this chapter. Since modern ejectors are usually designed and operated with supersonic primary flow, the mechanism of choking phenomena, supersonic flow and shock wave were described in detail. Fundamentals of isentropic nozzle and subsonic diffuser were provided so preliminary calculations could be made for the ejector design. These background knowledge enable the comprehensive theoretical study of ejector energy and momentum transfer.

CHAPTER III

GAS EJECTOR 1-D ANALYTICAL MODELS

INTRODUCTION

This chapter is focus on 1-D analytical models for the design and performance analysis of ejectors with single phase gas flow. Analysis in detail will be performed on each section of ejector: supersonic primary nozzle, mixing chamber, and diffuser. The flow model for the mixing chamber is the key issue for ejector design. The two widely adopted ejector mixing models are the constant-pressure mixing model and the constant-area mixing model [3, 6]. Equations of these analytical models, incorporating the different working gases with different molecular weight and different thermodynamic properties for the primary and secondary streams, are derived in great detail.

Parametric study was performed on both models so ejector behaviors and working mechanism could be understood. Computer codes for various flow models are developed to predict and analyze the general features of an ejector with single-phase gas flow. The merits and problems of 1-D analytical models will be summarized and discussed. Gas ejector design can be implemented by employing equations of constant-area mixing approach and their corresponding figures generated in the parametric study. A general gas ejector design guide was developed in the format of design procedure and steps.

ESDUpac A9242 Version 2, developed and released by the Engineering Science Data Unit (ESDU), is a computer program for use in the design and performance evaluation of ejectors with gases as working fluids. The 1-D analytical gas ejector flow models constant-pressure mixing and constant-area mixing models, the latest improvements, as well as many coefficients obtained by experimental data, are all integrated in ESDUpac A9242. As an example, this program will be introduced and used to design and evaluate a gas ejector performance.

SUPERSONIC PRIMARY NOZZLE

Fig. 3.1 shows a typical supersonic primary nozzle used in a gas ejector. The nozzle inlet section, throat section and exit section are represented by 0, t and 1, respectively. The supersonic primary nozzle has been mentioned in the previous chapter, and Equation (2.17) and Equation (2.21) were derived to calculate the maximum mass flow rate and the area ratio of nozzle exit to nozzle throat. However, those equations were derived based on the assumption of isentropic expansion in the primary nozzle. In reality, the downstream pressure of the ejector is normally not operated at the unique design conditions of the nozzle geometry. Irreversible over-expansion or under-expansion, i.e., shock waves, will occur outside the nozzle. Therefore a coefficient, η_n, relating to the isentropic efficiency of the compressible flow in the diverging expansion part of the nozzle is utilized.

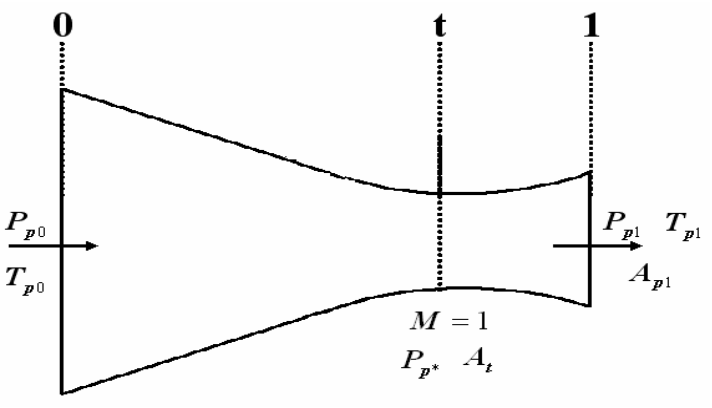

Fig. 3.1 Supersonic primary nozzle

For the converging part through the nozzle throat, the isentropic assumption is still adopted. The flow parameters: P_{p^*} , T_{p^*} , ρ_{p^*} and V_{p^*} at the nozzle throat can be calculated by using Equations (2.12), (2.13), (2.14) and (2.15). According to Equation (2.17), the mass flow rate of the primary stream is

$$m_p = \frac{A_t P_0}{\sqrt{T_0}} \sqrt{\frac{\gamma_p}{R_p} \left(\frac{2}{\gamma_p + 1} \right)^{\frac{\gamma_p + 1}{\gamma_p - 1}}} \tag{3.1}$$

The isentropic efficiency of diverging expansion part of the nozzle is defined as [24]:

$$\eta_n = \frac{h_{p0} - h_{p1}}{h_{p0} - h_{p1s}} \tag{3.2}$$

where h_{p0} is the stagnation enthalpy (total energy) of primary stream; h_{p1} is the exit enthalpy under real, operating conditions; h_{p1s} is the exit enthalpy under isentropic

conditions for the same exit pressure. The steady flow energy equation for the nozzle shown in Fig. 3.1 can be written as:

$$h_{p0} = h_{p1} + \frac{V_{p1}^2}{2} \tag{3.3}$$

With $h = c_p T$, Equation (3.4) can be obtained from Equation (3.2).

$$\frac{T_{p1s}}{T_{p0}} = 1 - \frac{1}{\eta_n}\left(1 - \frac{T_{p1}}{T_{p0}}\right) \tag{3.4}$$

According to the isentropic expansion function, the ratio of the stagnation to static temperature is

$$\frac{T_0}{T} = 1 + \frac{\gamma - 1}{2} M^2 \tag{3.5}$$

With the isentropic relations and Equations (3.4), (3.5) the primary nozzle pressure ratio can be derived as:

$$\frac{P_{p1}}{P_{p0}} = \left[1 - \frac{1}{\eta_n} + \frac{1}{\eta_n\left(1 + \frac{\gamma_p - 1}{2} M_{p1}^2\right)}\right]^{\frac{\gamma_p}{\gamma_p - 1}} = f_1\left(\gamma_p, M, \eta_n\right) \tag{3.6}$$

The mass flow rate through the nozzle is constant and can be expressed as:

$$m_p = \rho_p A V = PAM\left(\frac{\gamma_p}{R_p T}\right)^{\frac{1}{2}} \tag{3.7}$$

Considering mass conservation, i.e., $m_{p1} = m_{p^*}$, the primary nozzle area ratio of exit to throat becomes

$$\frac{A_{p1}}{A_t} = \frac{P_{p^*}}{P_{p1}} \frac{1}{M_{p1}} \left(\frac{T_{p1}}{T_{p^*}} \right)^{\frac{1}{2}} \tag{3.8}$$

By using Equation (3.5) and Equation (3.6), Equation (3.8) can be expressed as:

$$\frac{A_{p1}}{A_t} = \frac{1}{M_{p1}} \left(\frac{2}{\gamma + 1} \right)^{\frac{\gamma_p + 1}{2(\gamma_p - 1)}} \left[1 - \frac{1}{\eta_n} + \frac{1}{\eta_n \left(1 + \frac{\gamma_p - 1}{2} M_{p1}^2 \right)} \right]^{\frac{-(\gamma_p + 1)}{2(\gamma_p - 1)}} \tag{3.9}$$

CONSTANT- AREA MIXING MODEL

Fig. 3.2 shows the schematic of a gas ejector designed using the constant-area mixing model. The exit plane of the primary nozzle is located within the constant-area mixing section. The mixing process of primary stream and secondary stream starts at the inlet and completes at the exit of this mixing chamber. The aerodynamic throat as shown in Fig. 3.2, which could occur in the constant-area mixing chamber during ejector operation, is an important concept in Fabri's theory [11]. Such an aerodynamic throat would have significant impact on ejector performance. When the static pressure of the primary stream is higher than that of secondary stream in the section between 1 and 2, the primary stream expands against secondary stream. Thus, the primary steam behaves as

an aerodynamic nozzle for the secondary stream and causes an aerodynamic throat to occur within the mixing chamber. The secondary stream could be choked at the aerodynamic throat if the downstream pressure is low enough.

The first part of this section will derive the equations for a constant-area mixing model without an aerodynamic throat occurring in the mixing chamber. The second part of this section will derive equations including the aerodynamic throat phenomena.

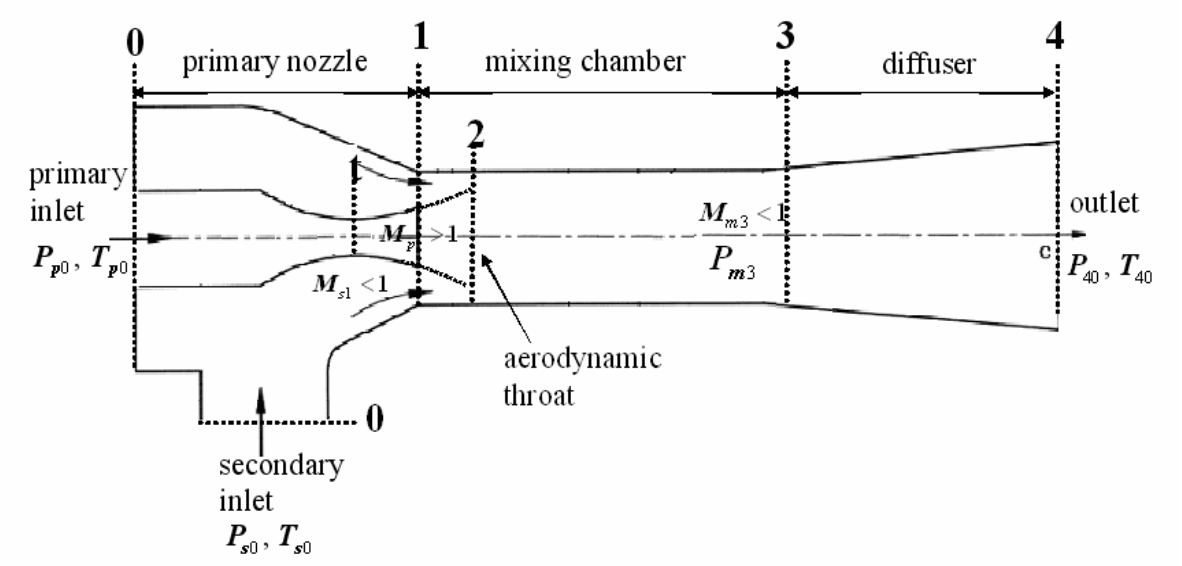

Fig. 3.2 Schematic of constant-area ejector model

Derivation of Constant-Area Mixing Model without Aerodynamic Throat

Fig. 3.3 is the control volume selected to analyze the flow in the mixing chamber of a constant-area ejector. Derivation of the constant-area model is based on the following assumptions:

1) Streams are in steady state;
2) The primary and secondary streams at section 1 are uniform and they are fully mixed at section 3;
3) Both streams can be considered as perfect gases;
4) The inner wall between sections 1 and 3 is adiabatic.

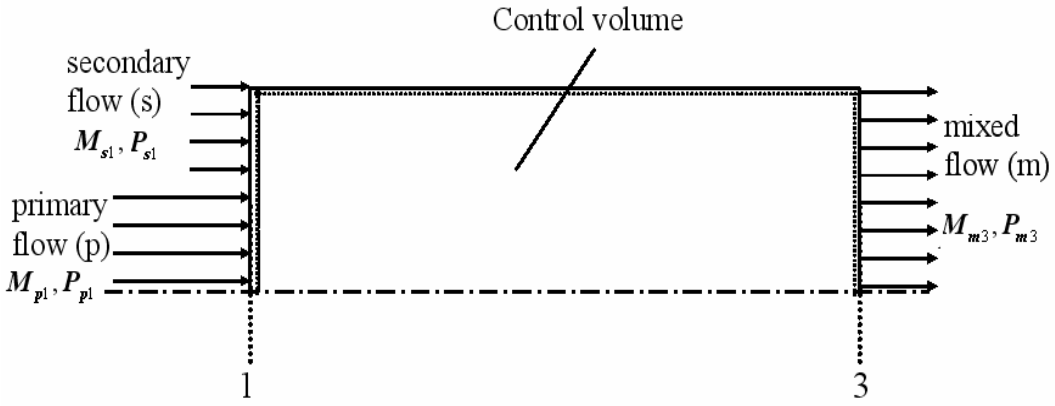

Fig. 3.3 Control volume for derivation of constant-area mixing model

The entrainment ratio (ER) ω, i.e., the mass flow ratio of secondary to primary, at the inlet of the mixing chamber is

$$\omega = \frac{m_{s1}}{m_{p1}} = \frac{P_{s1}}{P_{p1}} \frac{A_{s1}}{A_{p1}} \left(\frac{T_{p0}}{T_{s0}} \right)^{\frac{1}{2}} \left(\frac{R_p}{R_s} \right)^{\frac{1}{2}} \frac{f_2\left(\gamma_s, M_{s1}\right)}{f_2\left(\gamma_p, M_{p1}\right)} \tag{3.10}$$

Where, $f_2\left(\gamma, M\right)$ is the mass flow function,

$$f_2\left(\gamma, M\right) \equiv \frac{m}{PA}\left(RT_0\right)^{\frac{1}{2}} = M\left[\gamma\left(1+\frac{\gamma-1}{2}M^2\right)\right]^{\frac{1}{2}} \tag{3.11}$$

Solving for the static pressure ratio of the secondary stream to the primary stream at the mixing chamber inlet P_{s1}/P_{p1} from Equation (3.10), the following expression can be obtained:

$$\frac{P_{s1}}{P_{p1}} = \left(\frac{T_{s0}}{T_{p0}} \right)^{\frac{1}{2}} \left(\frac{R_s}{R_p} \right)^{\frac{1}{2}} \frac{A_{p1}}{A_{s1}} \frac{f_2\left(\gamma_p, M_{p1}\right)}{f_2\left(\gamma_s, M_{s1}\right)} \omega \tag{3.12}$$

Considering the continuity equation for the control volume in Fig. 3.3,

$$m_{p1} + m_{s1} = m_{m3} \tag{3.13}$$

According to Equation (3.11), mass flow rate can be expressed as:

$$m = \frac{PA}{\left(RT_0\right)^{\frac{1}{2}}} f_2\left(\gamma, M\right) \tag{3.14}$$

Substituting the mass flow rate expression of Equation (3.14) into mass conservation Equation (3.13), the following expression can be derived:

$$\frac{P_{m3}}{P_{p1}} = \left(\frac{T_{m0}}{T_{p0}}\right)^{\frac{1}{2}} \left(\frac{R_m}{R_p}\right)^{\frac{1}{2}} \frac{A_{p1}}{A_{m3}} \frac{f_2\left(\gamma_p, M_{p1}\right)}{f_2\left(\gamma_m, M_{m3}\right)} (1+\omega) \tag{3.15}$$

In the above equation, the gas constant R_m and specific heat ratio γ_m of the mixed flow are defined as:

$$R_m = \frac{R_p + \omega R_s}{1+\omega} \tag{3.16}$$

$$\gamma_m = \frac{\frac{\gamma_p}{\gamma_p - 1} + \frac{\gamma_s}{\gamma_s - 1}\frac{R_s}{R_p}\omega}{\frac{1}{\gamma_p - 1} + \frac{1}{\gamma_s - 1}\frac{R_s}{R_p}\omega} \tag{3.17}$$

Energy conservation over the control volume shown in Fig. 3.3, with the above assumptions, can be expressed as:

$$m_p h_{p0} + m_s h_{s0} = m_m h_{m0} \tag{3.18}$$

Using continuity Equation (3.13) and substituting $h_0 = c_p T_0$ into energy Equation (3.18), the stagnation temperature ratio of mixed flow to the primary flow is obtained:

$$\frac{T_{m0}}{T_{p0}} = \frac{\frac{\gamma_p}{\gamma_p - 1} + \frac{\gamma_s}{\gamma_s - 1}\frac{R_s}{R_p}\frac{T_{s0}}{T_{p0}}\omega}{\frac{\gamma_p}{\gamma_p - 1} + \frac{\gamma_s}{\gamma_s - 1}\frac{R_s}{R_p}\omega} \tag{3.19}$$

The stagnation pressure ratio of the secondary stream to the primary steam is

$$\frac{P_{s0}}{P_{p0}} = \frac{P_{s1}}{P_{p1}} \frac{f_1\left(\gamma_p, M_{p1}, \eta_n\right)}{f_3\left(\gamma_s, M_{s1}\right)} \tag{3.20}$$

Where,

$$f_3\left(\gamma_s, M\right) \equiv \frac{P_{s1}}{P_{s0}} = \left(1 + \frac{\gamma_s - 1}{2} M_{s1}^2\right)^{\frac{-\gamma_s}{\gamma_s - 1}} \tag{3.21}$$

The momentum conservation equation for the control volume is

$$P_{p1}A_{p1} + P_{s1}A_{s1} + \rho_{p1}A_{p1}V_{p1}^2 + \rho_{s1}A_{s1}V_{s1}^2 = P_{m3}A_{m3} + \rho_{m3}A_{m3}V_{m3}^2 \tag{3.22}$$

According to gas state equation, local gas density can be expressed as:

$$\rho = P/\left(RT\right) \tag{3.23}$$

The local velocity can be expressed as a function of Mach number:

$$V^2 = M^2 \gamma RT \tag{3.24}$$

Substituting local density Equation (3.23) and local velocity Equation (3.24) into Equation (3.22), the momentum conservation can be rewritten as:

$$\frac{P_{s1}}{P_{p1}} \frac{A_{s1}}{A_{p1}} \left(1 + \gamma_s M_{s1}^2\right) + \left(1 + \gamma_p M_{p1}^2\right) = \frac{P_{m3}}{P_{p1}} \frac{A_{m3}}{A_{p1}} \left(1 + \gamma_m M_{m3}^2\right) \tag{3.25}$$

The Mach number at the mixing chamber exit can be solved by substituting Equation (3.12) and Equation (3.15) into Equation (3.25).

$$M_{m3}=\sqrt{\frac{-\left(\alpha^2-2\right)\pm\sqrt{\left(\alpha^2-2\right)^2+2\left(\frac{\gamma_m-1}{\gamma_m}\right)\left(\alpha^2-\frac{2\gamma_m}{\gamma_m-1}\right)}}{\left(\gamma_m-1\right)\left(\alpha^2-\frac{2\gamma_m}{\gamma_m-1}\right)}} \tag{3.26}$$

Where,

$$\alpha=\frac{\left(\frac{T_{s0}}{T_{p0}}\right)^{\frac{1}{2}}\left(\frac{R_s}{R_p}\right)^{\frac{1}{2}} f_4\left(\gamma_s,M_{s1}\right)w+f_4\left(\gamma_p,M_{p1}\right)}{\left(\frac{T_{m0}}{T_{p0}}\right)^{\frac{1}{2}}\left(\frac{R_m}{R_p}\right)^{\frac{1}{2}}\left(1+w\right)} \tag{3.27}$$

and

$$f_4\left(\gamma,M\right)=\frac{1+\gamma M^2}{M}\left[\gamma\left(1+\frac{\gamma-1}{2}M^2\right)\right]^{-\frac{1}{2}} \tag{3.28}$$

So far, the flow field parameters at the mixing chamber exit are all obtained by solving the conservation equations of mass, momentum and energy over the control volume as shown in Fig. 3.3. The velocity which is represented by Mach number can be calculated by using Equation (3.26); the static pressure and the stagnation temperature can be calculated by using Equation (3.15) and (3.19), respectively. To calculate these parameters, it may be more convenient to make the entrainment ratio, ω, be a function of the area ratio.

Considering that $A_{s1} = A_{m3} + A_{p1}$ and using Equation (3.9), the area ratio of secondary stream to primary stream at the mixing chamber inlet can be expressed as:

$$\frac{A_{s1}}{A_{p1}} = \frac{A_{m3}}{A_t} \frac{1}{f_5\left(\eta_n, \gamma_p, M_{p1}\right)} - 1 \tag{3.29}$$

Where $f_5\left(\eta_n, \gamma_p, M_{p1}\right)$ is defined as:

$$f_5\left(\eta_n, \gamma_p, M_{p1}\right) = \frac{1}{M_{p1}} \left(\frac{2}{\gamma + 1} \right)^{\frac{\gamma_p + 1}{2\left(\gamma_p - 1\right)}} \left[1 - \frac{1}{\eta_n} + \frac{1}{\eta_n \left(1 + \frac{\gamma_p - 1}{2} M_{p1}^2 \right)} \right]^{\frac{-\left(\gamma_p + 1\right)}{2\left(\gamma_p - 1\right)}} \tag{3.30}$$

Rearranging Equation (3.20) to give,

$$\frac{P_{s1}}{P_{p1}} = \frac{P_{s0}}{P_{p0}} \frac{f_3\left(\gamma_s, M_{s1}\right)}{f_1\left(\gamma_p, M_{p1}, \eta_n\right)} \tag{3.31}$$

The relationship of ER with area ratio can be derived by substituting Equation (3.29) and Equation (3.31) into Equation (3.10), according to the definitions of $f_1\left(\gamma_p, M_{p1}, \eta_n\right)$, $f_2\left(\gamma, M\right)$ and $f_3\left(\gamma, M\right)$.

$$\omega = \frac{P_{s0}}{P_{p0}} \left(\frac{T_{p0}}{T_{s0}} \right)^{\frac{1}{2}} \left(\frac{R_p}{R_s} \right)^{\frac{1}{2}} \left(\frac{\gamma_s}{\gamma_p} \right)^{\frac{1}{2}} \frac{M_{s1}}{M_{p1}} \left(\frac{A_{m3}}{A_t} \frac{1}{f_5\left(\eta_n, \gamma_p, M_{p1}\right)} - 1 \right) \cdot \frac{\left(1 + \frac{\gamma_s - 1}{2} M_{s1}^2 \right)^{\frac{-\left(\gamma_s + 1\right)}{2\left(\gamma_s - 1\right)}}}{\left(1 + \frac{\gamma_p - 1}{2} M_{p1}^2 \right)^{\frac{-\left(\gamma_p + 1\right)}{2\left(\gamma_p - 1\right)}}} \left[\left(\frac{\eta_n - 1}{\eta_n} \right) \frac{\gamma_p - 1}{2} M_{p1}^2 + 1 \right]^{\frac{-\gamma_p}{\gamma_p - 1}} \tag{3.32}$$

Derivation of Constant-Area Mixing Model with Aerodynamic Throat

Fig. 3.4 shows a control volume of the initial interaction region in the constant-area mixing chamber. This control volume was used for derivation of equations for constant-area mixing model operating in the supersonic regime (SR). In order to analyze the flow in this region, the following additional assumptions are made:

5) Streams do not mix and are isentropic between sections 1 and 2.

6) The secondary stream is choked at section 2, i.e., $M_{s2} = 1$.

7) The primary static pressure at the inlet is greater than that of the secondary, i.e., $P_{p1} > P_{s1}$.

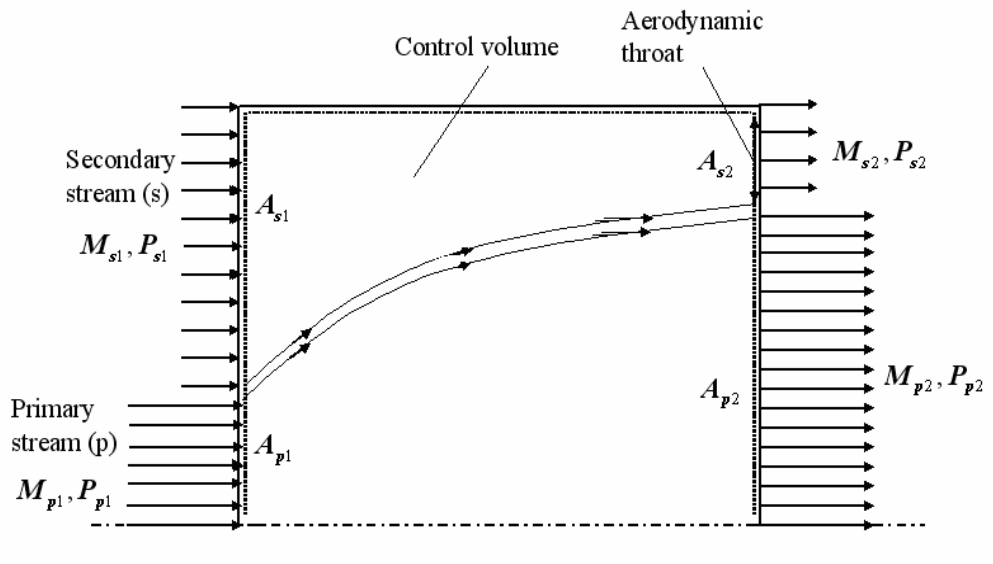

Fig. 3.4 Control volume for analysis of initial interaction region

The area ratio of primary stream at section 1 to nozzle throat can be derived starting from the following equation:

$$\frac{A_{p2}}{A_t} = \frac{A_{p2}}{A_{p1}} \frac{A_{p1}}{A_t} \tag{3.33}$$

Considering that $A_{p2} = A_{m3} - A_{s2}$ and $A_{s1} = A_{m3} - A_{p1}$ and substituting Equation (3.9) into Equation (3.33), Equation (3.34) is obtained:

$$\frac{A_{p2}}{A_t} = \frac{1 - \frac{1 - \left(A_{p1}/A_{m3} \right)}{A_{s1}/A_{s2}}}{A_{p1}/A_{m3}} \frac{1}{M_{p1}} \left(\frac{2}{\gamma + 1} \right)^{\frac{\gamma_p + 1}{2(\gamma_p - 1)}} \left[1 - \frac{\frac{\gamma_p - 1}{2} M_{p1}^2}{\eta_n \left(1 + \frac{\gamma_p - 1}{2} M_{p1}^2 \right)} \right]^{\frac{-(\gamma_p + 1)}{2(\gamma_p - 1)}} \tag{3.34}$$

The above area ratio can also be derived, similar to Equation (3.8), in the following form:

$$\frac{A_{p2}}{A_t} = \frac{P_{p^*}}{P_{p2}} \frac{1}{M_{p2}} \left(\frac{1 + \frac{\gamma_p - 1}{2}}{1 + \frac{\gamma_p - 1}{2} M_{p2}^2} \right)^{\frac{1}{2}} \tag{3.35}$$

The P_{p^*}/P_{p2} in Equation (3.35) can be expressed as:

$$\frac{P_{p^*}}{P_{p2}} = \frac{P_{p^*}}{P_{p0}} \frac{P_{p0}}{P_{p1}} \frac{P_{p1}}{P_{p2}} = \frac{P_{p^*}}{P_{p0}} \Bigg/ \left(\frac{P_{p2}}{P_{p1}} \frac{P_{p1}}{P_{p0}} \right) \tag{3.36}$$

From Equation (3.5) and the isentropic relations, the following equation can be written

$$\frac{P_{p2}}{P_{p1}} = \left(\frac{1+\frac{\gamma_p - 1}{2} M_{p1}^2}{1+\frac{\gamma_p - 1}{2} M_{p2}^2} \right)^{\frac{\gamma_p}{\gamma_p - 1}} \tag{3.37}$$

P_{p^*} / P_{p0} in Equation (3.36) can be derived similarly to Equation (3.6). Substituting the P_{p^*} / P_{p0} , Equation (3.6) and Equation (3.37) into Equation (3.35), the following expression is obtained:

$$\frac{A_{p2}}{A_t} = \frac{1}{M_{p2}} \left(\frac{2}{\gamma_p + 1} \right)^{\frac{\gamma_p + 1}{2(\gamma_p - 1)}} \left(1+\frac{\gamma_p - 1}{2} M_{p2}^2 \right)^{\frac{\gamma_p + 1}{2(\gamma_p - 1)}} \left[1+\frac{\eta_n - 1}{2\eta_n} (\gamma_p - 1) M_{p1}^2 \right]^{\frac{-\gamma_p}{\gamma_p - 1}} \tag{3.38}$$

Thus, M_{p2} can be found by using Equation (3.34) and Equation (3.38).

The momentum equation for the control volume shown in Fig. 3.4 is

$$\begin{aligned} &P_{p1}A_{p1} + P_{s1}A_{s1} + \rho_{p1}A_{p1}V_{p1}^2 + \rho_{s1}A_{s1}V_{s1}^2 \\ &= P_{p2}A_{p2} + P_{s2}A_{s2} + \rho_{p2}A_{p2}V_{p2}^2 + \rho_{s2}A_{s2}V_{s2}^2 \end{aligned} \tag{3.39}$$

Considering that $M_{s2} = 1$ and $A_{s1} = A_{m3} - A_{p1}$ from Fig. 3.4 and also solving for P_{s1} / P_{p1} from Equation (3.39), the inlet static pressure ratio can be obtained as:

$$\frac{P_{s1}}{P_{p1}} = \frac{\left(\frac{P_{p2}/P_{p0}}{P_{p1}/P_{p0}} \right) \left(\frac{A_{p2}/A_{p^*}}{A_{p1}/A_{p^*}} \right) \left(1+\gamma_p M_{p2}^2 \right) - \left(1+\gamma_p M_{p1}^2 \right)}{\frac{1-\left(A_{p1}/A_{m3} \right)}{A_{p1}/A_{m3}} \left[\left(1+\gamma_s M_{s1}^2 \right) - \frac{P_{s2}/P_{s0}}{P_{s1}/P_{s0}} \frac{1+\gamma_s}{A_{s1}/A_{s2^*}} \right]} \tag{3.40}$$

CONSTANT- PRESSURE MIXING MODEL

The basic principles of constant-pressure mixing approach were introduced by Keenan and Neumann [3]. It was assumed that the mixing of the primary and the secondary streams occurs in a chamber with a uniform, constant pressure. As shown in Fig. 3.5, the mixing chamber is between section 1 and section 2 within which the pressure is assumed to be uniform. If the velocity of the fully mixed flow is supersonic ($M_{m2} > 1$), a normal shock wave is assumed to occur in the constant-area chamber between section 2 and section 3. The static pressure of the mixed flow leaving section 3 at uniform subsonic velocity is increased in the diffuser.

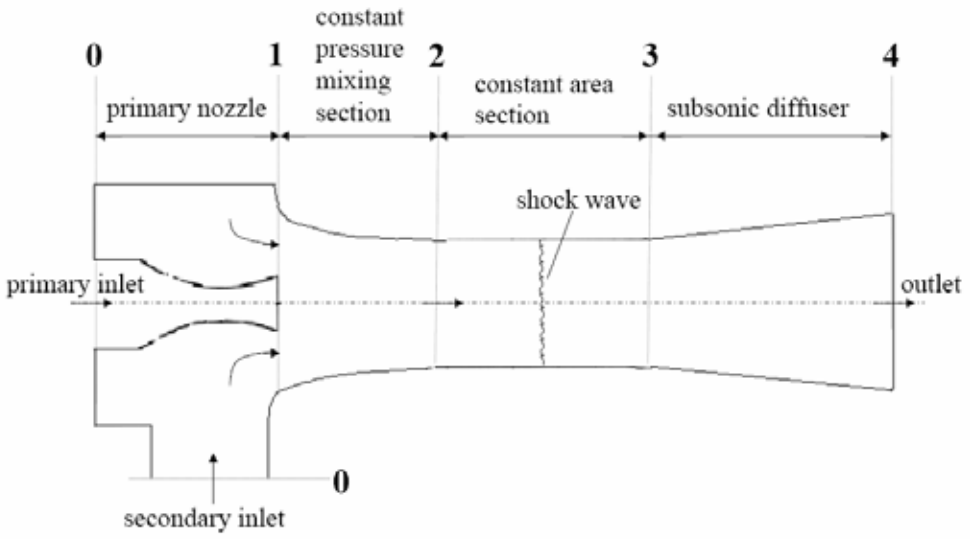

Fig. 3.5 Constant-pressure ejector flow model

In the derivation of the constant-pressure mixing ejector model, the following assumptions are generally made:

(1) The primary and secondary streams at the inlet of the ejector and the mixed flow at the exit of the ejector are at stagnation conditions.

(2) Velocities are uniform at all sections.

(3) Mixing of streams occurs at constant pressure between sections 1 and 2.

(4) If the mixed flow is supersonic at section 2, a shock wave will occur between sections 2 and 3 and the flow is subsonic at section 3.

The equations for supersonic primary nozzle and subsonic diffuser in the constant-pressure mixing ejector flow model are the same as those equations in the constant-area ejector model. This section will therefore focus on the equation derivations for the mixing process of the primary stream and secondary stream. The conservation equations of continuity, energy and momentum as well as the perfect gas relations under the above assumptions are applied to analyze the flow field in the control volume shown in Fig. 3.6.

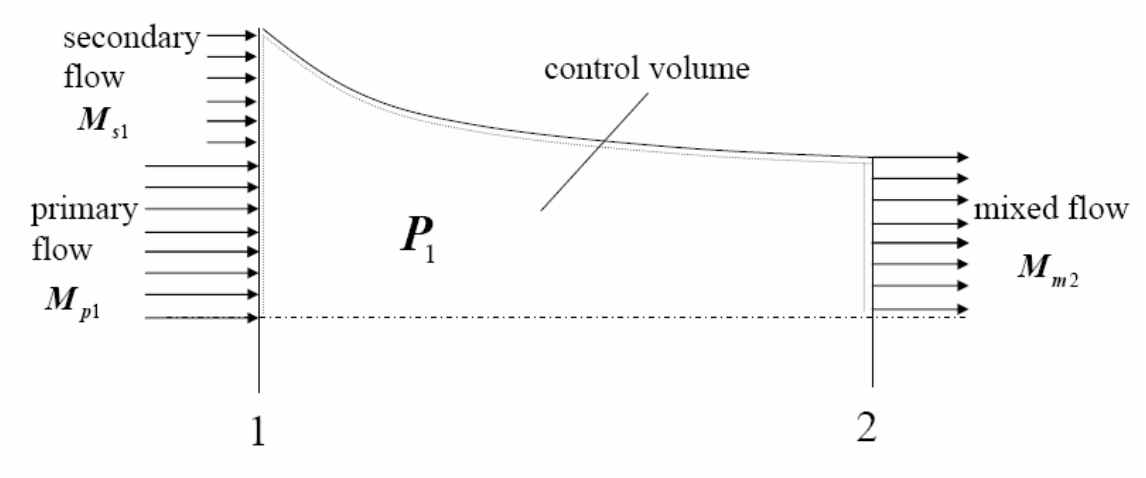

Fig. 3.6 Control volume of constant-pressure mixing chamber

According to the constant-pressure assumption,

$$P_{p1} = P_{s1} = P_{m2} = P_1 \tag{3.41}$$

Therefore, the mass flow ratio of secondary to primary at the inlet of the mixing chamber Equation (3.10) can be simplified to:

$$\omega = \frac{A_{s1}}{A_{p1}} \left(\frac{T_{p0}}{T_{s0}} \right)^{\frac{1}{2}} \left(\frac{R_p}{R_s} \right)^{\frac{1}{2}} \frac{f_2\left(\gamma_s, M_{s1}\right)}{f_2\left(\gamma_p, M_{p1}\right)} \tag{3.42}$$

Where, $f_2\left(\gamma, M\right)$ is the mass flow function defined by Equation (3.11); M_{p1} and M_{s1} are given by the following equations:

$$M_{p1} = \sqrt{\frac{2}{\gamma_p - 1} \frac{\eta_n \left[1 - \left(\frac{P_1}{P_{p0}} \right)^{\frac{\gamma_p - 1}{\gamma_p}} \right]}{1 - \eta_n \left[1 - \left(\frac{P_1}{P_{p0}} \right)^{\frac{\gamma_p - 1}{\gamma_p}} \right]}} \tag{3.43}$$

$$M_{s1} = \sqrt{\frac{2}{\gamma_s - 1} \left[\left(\frac{P_1}{P_{s0}} \right)^{-\frac{\gamma_s - 1}{\gamma_s}} - 1 \right]} \tag{3.44}$$

The area ratio of the secondary stream to the primary stream can be obtained by rearranging Equation (3.42).

$$\frac{A_{s1}}{A_{p1}} = \left(\frac{T_{s0}}{T_{p0}} \right)^{\frac{1}{2}} \left(\frac{R_s}{R_p} \right)^{\frac{1}{2}} \frac{f_2\left(\gamma_p, M_{p1}\right)}{f_2\left(\gamma_s, M_{s1}\right)} \omega \tag{3.45}$$

The continuity equation for the selected control volume in Fig. 3.6,

$$m_{p1} + m_{s1} = m_{m2} \tag{3.46}$$

The area ratio of mixing chamber exit to the primary nozzle exit can be derived by substituting the mass flow function $f_2\left(\gamma, M\right)$ into Equation (3.46).

$$\frac{A_{m2}}{A_{p1}} = \left(\frac{T_{m0}}{T_{p0}} \right)^{\frac{1}{2}} \left(\frac{R_m}{R_p} \right)^{\frac{1}{2}} \frac{f_2\left(\gamma_p, M_{p1}\right)}{f_2\left(\gamma_m, M_{m2}\right)} \left(1 + \omega\right) \tag{3.47}$$

Where, R_m, γ_m and T_{m0} can be calculated by using Equation (3.16), Equation (3.17) and Equation (3.19), respectively. To design a constant-pressure gas ejector, it is desired to relate the entrainment ratio to the area ratio of the mixing chamber throat to the primary nozzle throat. This relationship can be derived by substituting Equation (3.9) and Equation (3.2) into Equation (3.48).

$$\frac{A_{m2}}{A_t} = \frac{A_{m2}}{A_{p1}} \frac{A_{p1}}{A_t} \tag{3.48}$$

$$\frac{A_{m2}}{A_t} = (1+\omega)\left(\frac{T_{m0}}{T_{p0}}\right)^{\frac{1}{2}} \left(\frac{R_m}{R_p}\right)^{\frac{1}{2}} \frac{(\gamma_p)^{\frac{1}{2}}}{f_2(\gamma_m, M_{m2})} \left(\frac{2}{\gamma_p+1}\right)^{\frac{\gamma_p+1}{2(\gamma_p-1)}} \cdot \left[1 - \frac{(\gamma_p-1)M_{p1}^2}{2\eta_n + \eta_n(\gamma_p-1)M_{p1}^2}\right]^{\frac{-\gamma_p}{\gamma_p-1}} \tag{3.49}$$

Since the static pressure in the mixing chamber is uniform and constant, the momentum conservation equation over the control volume in Fig. 3.6 can be simplified to be

$$m_{p1}V_{p1} + m_{s1}V_{s1} = m_{m2}V_{m2} \tag{3.50}$$

Considering the continuity equation as well as the definition of ω, Equation (3.48) can be further simplified to be

$$V_{p1} + \omega V_{s1} = (1+\omega)V_{m2} \tag{3.51}$$

The uniform velocity of the flow at the mixing chamber exit is

$$V_{m2} = \frac{V_{p1} + \omega V_{s1}}{1+\omega} \tag{3.52}$$

Using Mach numbers to substitute for the velocities in Equation (3.50),

$$M_{m2} = \frac{M_{p1} + \omega M_{s1}\left(\frac{\gamma_s}{\gamma_p}\right)^{\frac{1}{2}}\left(\frac{R_s}{R_p}\right)^{\frac{1}{2}}\left(\frac{T_{s1}}{T_{p1}}\right)^{\frac{1}{2}}}{(1+\omega)\left(\frac{\gamma_m}{\gamma_p}\right)^{\frac{1}{2}}\left(\frac{R_m}{R_p}\right)^{\frac{1}{2}}\left(\frac{T_{m2}}{T_{p1}}\right)^{\frac{1}{2}}} \tag{3.53}$$

The T_{s1}/T_{p1} and T_{m2}/T_{p1} in above equation can be obtained by using the isentropic relationship between temperature and pressure:

$$\frac{T_{s1}}{T_{p1}} = \frac{T_{s0}}{T_{p0}}\left(\frac{P_{p0}}{P_1}\right)^{\frac{\gamma_p - 1}{\gamma_p}}\left(\frac{P_{s0}}{P_1}\right)^{-\frac{\gamma_s - 1}{\gamma_s}} \tag{3.54}$$

$$\frac{T_{m2}}{T_{p1}} = \frac{T_{m0}}{T_{p0}}\left(\frac{P_{p0}}{P_1}\right)^{\frac{\gamma_p - 1}{\gamma_p}}\left(\frac{P_{m0}}{P_1}\right)^{-\frac{\gamma_m - 1}{\gamma_m}} \tag{3.55}$$

The T_{m0}/T_{p0} in Equation (3.53) can be calculated by using Equation (3.19). The P_{m0}/P_1 can be obtained by using the isentropic function:

$$\frac{P_{m0}}{P_1} = \left(1 + \frac{\gamma_m - 1}{2} M_{m2}^2\right)^{\frac{\gamma_m}{\gamma_m - 1}} \tag{3.56}$$

Substituting Equation (3.53) and Equation (3.54) into Equation (3.51), the Mach number at the mixing chamber exit is obtained:

$$M_{m2} = \frac{\xi}{\psi}\sqrt{1-\frac{\gamma_m - 1}{2}\left(\frac{\xi}{\psi}\right)^2} \tag{3.57}$$

Where,

$$\xi = M_{p1} + \omega M_{s1}\left(\frac{\gamma_s}{\gamma_p}\right)^{\frac{1}{2}}\left(\frac{R_s}{R_p}\right)^{\frac{1}{2}}\left(\frac{T_{s1}}{T_{p1}}\right)^{\frac{1}{2}} \tag{3.58}$$

$$\psi = (1+\omega)\left(\frac{\gamma_m}{\gamma_p}\right)^{\frac{1}{2}}\left(\frac{R_m}{R_p}\right)^{\frac{1}{2}}\left(\frac{T_{m0}}{T_{p0}}\right)^{\frac{1}{2}}\left(\frac{P_{p0}}{P_1}\right)^{\frac{\gamma_p - 1}{2\gamma_p}} \tag{3.59}$$

If the velocity is supersonic after constant-pressure mixing, i.e., $M_{m2} > 1.0$, a normal shock wave will occur between section 2 and section 3. Assuming the mixed flow after the shock undergoes an isentropic process, it has a uniform pressure P_{m3} in the constant-area section. The follow parameters after the shock wave can be calculated by the following gas dynamic relationships.

$$\frac{P_{m3}}{P_{m2}} = \frac{2\gamma_m}{\gamma_m + 1}M_{m2}^2 - \frac{\gamma_m - 1}{\gamma_m + 1} \tag{3.60}$$

$$\frac{T_{m3}}{T_{m2}} = \left(\frac{\gamma_m - 1}{\gamma_m + 1}\right)^2\left(\frac{2\gamma_m}{\gamma_m - 1}M_{m2}^2 - 1\right)\left[\frac{2}{(\gamma_m - 1)M_{m2}^2} + 1\right] \tag{3.61}$$

$$M_{m3}^2 = \frac{M_{m2}^2 + \frac{2}{\gamma_m - 1}}{\frac{2\gamma_m}{\gamma_m - 1}M_{m2}^2 - 1} \tag{3.62}$$

SUBSONIC DIFFUSER

By using the definition of diffuser efficiency, which is similar to that of the nozzle efficiency defined in Equation (3.2), the diffuser pressure ratio can be obtained:

$$\frac{P_{40}}{P_{m3}} = \left[1 + \eta_d \frac{\gamma_m - 1}{2} M_{m3}^2\right]^{\frac{\gamma_m}{\gamma_m - 1}} \tag{3.63}$$

In addition, the over-all compression ratio through the gas ejector can be found from the following expression:

$$\frac{P_{40}}{P_{s0}} = \frac{P_{40}}{P_{m3}} \frac{P_{m3}}{P_{p1}} \frac{P_{p1}}{P_{p0}} \frac{P_{p0}}{P_{s0}} \tag{3.64}$$

PARAMETRIC ANALYSIS

Supersonic Primary Nozzle

As presented in Chapter II, the geometry of a supersonic primary nozzle could be designed based the desired mass flow rate and desired Mach number at the nozzle exit by using Equation (2.17) and (2.21), respectively. A set of unique flow parameters, i.e., the ratio of static pressure, static temperature and density to the stagnation values of the flow at the nozzle exit would be determined by Equation (2.9), (2.10) and (2.11). These flow parameters are unique for a particular nozzle design. The supersonic nozzle is

operated at its design condition when the back pressure P_1 or P_{p1} of the ejector, is equal to the exact value determined by its geometry. In this case, there is a continuous pressure distribution through the nozzle. In reality, the nozzle is normally operated with the downstream back pressure P_1 in a certain range instead of at a particular designed value. When the nozzle is operated in off design conditions, a shock may occur and the pressure distribution would no longer be continuous.

A nozzle is called under-expanded if the nozzle exit area is too small so that designed P_1 is above the operating back pressure. On the other hand, a nozzle is called over-expanded if the nozzle exit area is too large so that a shock will occur and other phenomena such as separation. In any case of off design operation, the flow experiences irreversible expansion process in the nozzle and there is energy loss in this process. That's why the isentropic efficiency coefficient η_n is defined and utilized in the previous derivations. The isentropic efficiency coefficient η_n should be determined from experimental data. For different nozzles, η_n is different and it would even be different under various operation conditions.

Plots of the area ratio of nozzle exit to nozzle throat against the desired exit Mach number for various η_n using Equation (3.9) are shown in Fig. 3.7. As a comparison, the area ratio curve obtained by Equation (2.21) with isentropic assumption ($\eta_n = 1$) is also plotted in Fig. 3.7. It is observed from Fig. 3.7 that a larger nozzle area ratio is required

to achieve the same desired exit Mach number if η_n decrease, i.e., the energy loss in the nozzle increases. Fig. 3.8 shows the relationship of pressure ratio of nozzle exit to throat against exit Mach number for various η_n. For the smaller η_n, the same Mach number will result in much smaller pressure ratios.

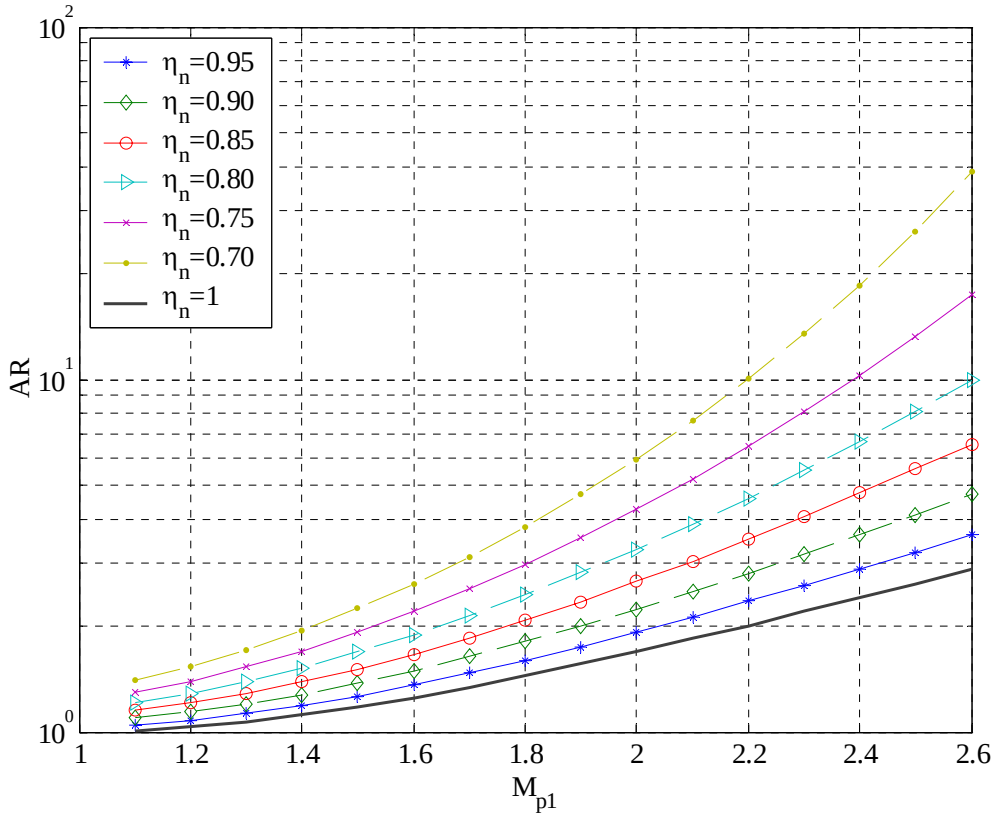

Fig. 3.7 Area ratio of nozzle exit to its throat vs. M_{p1} for various η_n

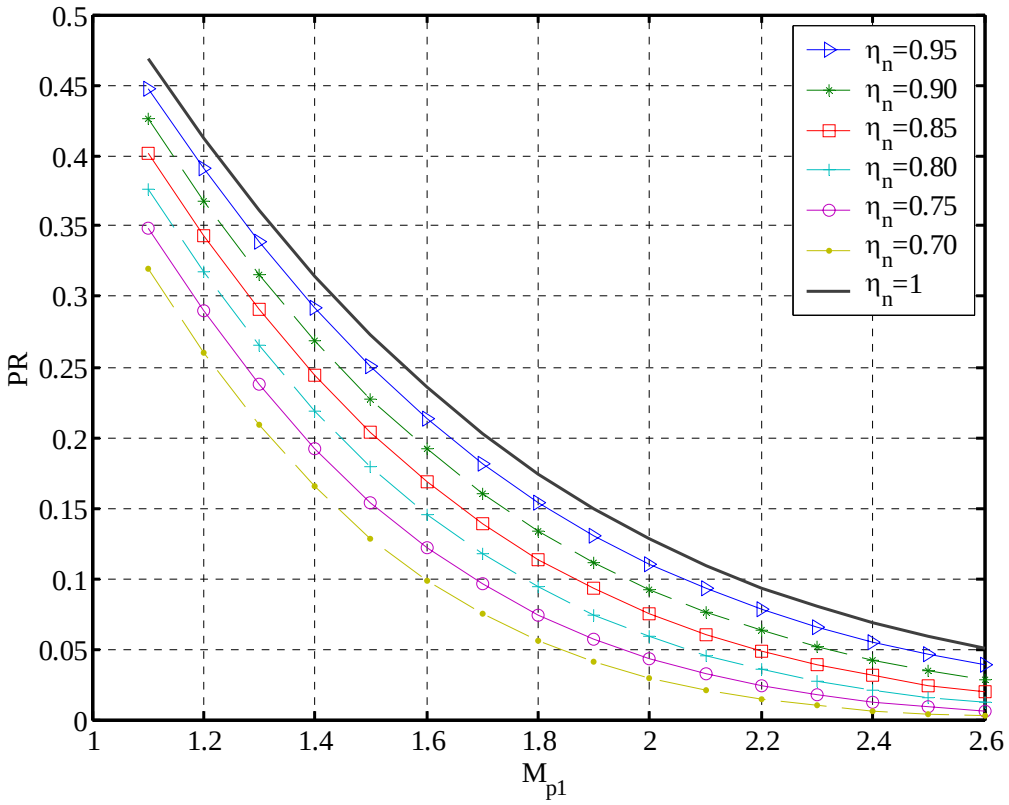

Fig. 3.8 Pressure ratio of nozzle exit to its throat vs. M_{p1} for various η_n

Theoretically, the nozzle exit Mach number M_{p1} can be obtained by solving Equation (3.9) if the isentropic efficiency coefficient η_n and the area ratio A_{p1}/A_t are given. Two solutions are expected for Equation (3.9); one is subsonic, $M_{p1}<1$ and the other is supersonic, $M_{p1}>1$. As discussed, the primary stream is designed to be supersonic at the nozzle exit and the solution of $M_{p1}>1$ is the correct answer for this case.

Once M_{p1} is determined, the pressure ratio, P_{p1}/P_{p0} can be calculated from Equation (3.6). However, it is not possible to solve M_{p1} analytically from Equation (3.9). There are two approaches used to avoid this trouble. One approach is to solve Equation (3.9) by using a numeric approach. The alternative method is use arbitrary but reasonable values of P_{p1}/P_{p0} , then solve for M_{p1} from Equation (3.6) which can be solved analytically. The area ratio A_{p1}/A_t can be calculated by using Equation (3.9) once M_{p1} is determined.

A least square data fit was used to solve Equation (3.9) numerically. The first step is to generate a set of arbitrary M_{p1} values, which would cover the typical operating range of M_{p1}. $1 < M_{p1} < 2.6$ could represent the M_{p1} range of most ejectors according to Fig. 3.8. A set of A_{p1}/A_t values can be calculated from (3.9) corresponding to the M_{p1} values. An explicit function $M_{p1} = f\left(A_{p1}/A_t\right)$, such as in the form of polynomials, can be established by using a least square data fit on these two sets of data. Mach number M_{p1} then can be calculated easily by using this data fit function for any given A_{p1}/A_t . As an example, Fig. 3.9 shows the data fit curve obtained by the above-described method. This curve is generated by an 8^{th} order polynomial.

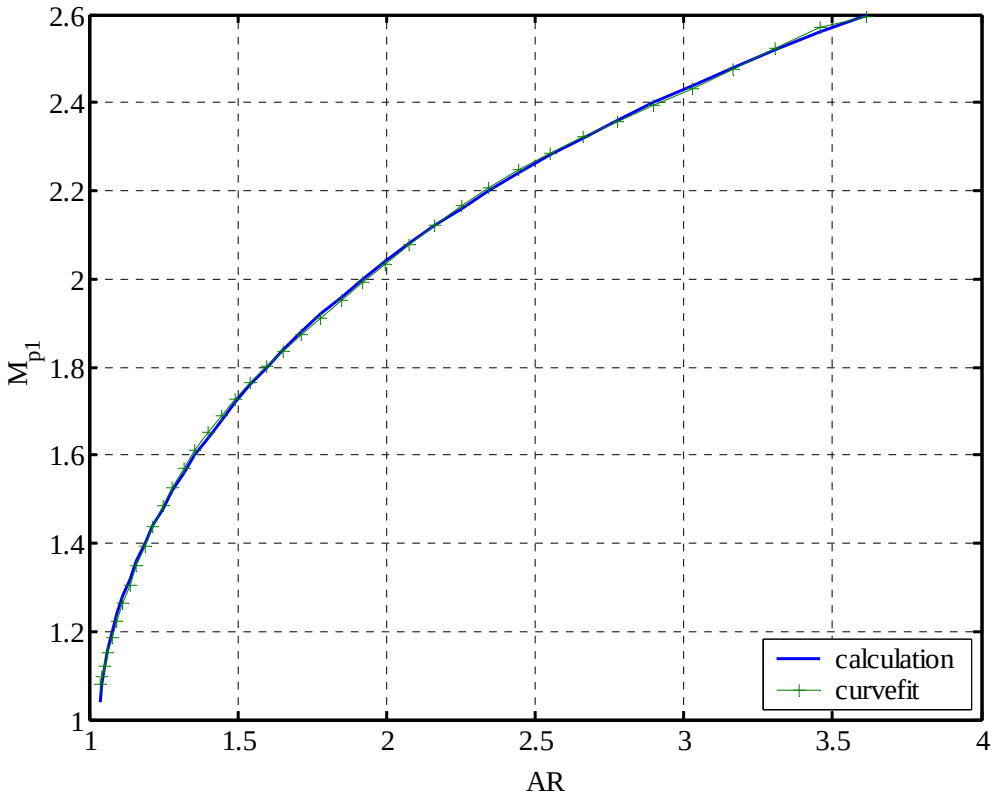

Fig. 3.9 M_{p1} calculated by using least square data fit

Constant-Area Mixing Model

The plot of entrainment ratio (ER) against area ratio (AR) of mixing chamber to nozzle throat is an important gas ejector performance curve. To plot ER by using Equation (3.32), M_{p1} and M_{s1} should be calculated first. $P_{s1} = P_{p1} = P_1$ is a reasonable assumption made to calculate M_{s1}. M_{p1}, thus, P_{p1} and M_{s1} can be calculated by employing the previous numerical method for any given A_{p1}/A_t. Fig. 3.10 is developed in this way for

primary nozzles with various area ratios of nozzle exit to nozzle throat A_{p1}/A_t . For the purpose of design convenience, a performance curve of ER against the diameter ratio (for cylindrical ejectors) is also plotted as Fig. 3.11.

The investigated range for the nozzle area ratio parameter A_{p1}/A_t is very narrow in these calculations—from 1.77 to 2.17. According to Fig. 3.9, this A_{p1}/A_t range corresponds to a range of 1.8 to 2.1 for M_{p1}, a typical ejector operational range. If the area ratio A_{p1}/A_t is too small, the corresponding static pressure P_{p1} could be higher than P_{s0} and no suction would happen. On the other hand, too big A_{p1}/A_t would result an unreasonable high M_{p1} which results a very low P_{p1}. That's why the range of $A_{p1}/A_t = [1.77,\ 2.17]$ was selected for the study.

As expected, increased nozzle expansion area ratio A_{p1}/A_t should enhance ejector entrainment ratio since the bigger expansion results in a higher Mach number and lower static pressure at the nozzle exit. If the primary nozzle is always operated on its design point (corresponds to the value of A_{p1}/A_t), large A_{p1}/A_t may result an unreasonable low P_{p1} such that $P_{p1} \ll P_{s0}$, even a supersonic secondary flow. In reality, this phenomena never happen and P_{p1} will not be much lower than P_{s0}. The reason for this discrepancy is that the isentropic efficiency coefficient η_n was given as a fixed value in

our calculations, while over-expansion shock, corresponding to different η_n values, will happen in real operation.

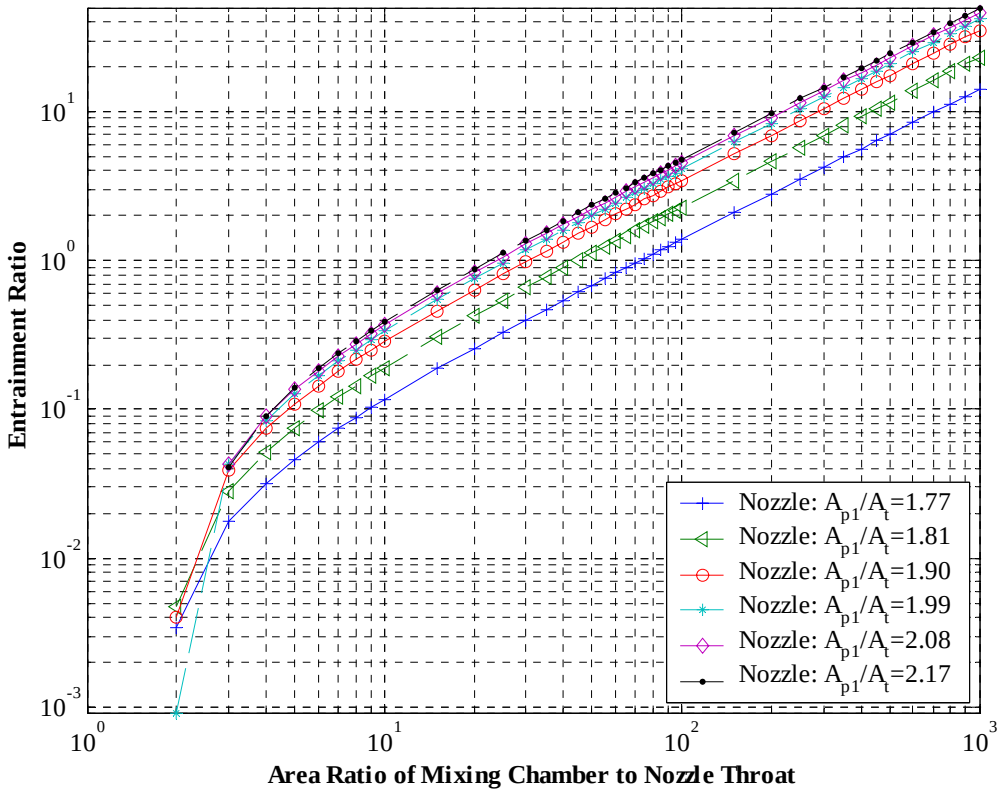

Fig. 3.10 Constant-area ejector ER vs. area ratio for various primary nozzles

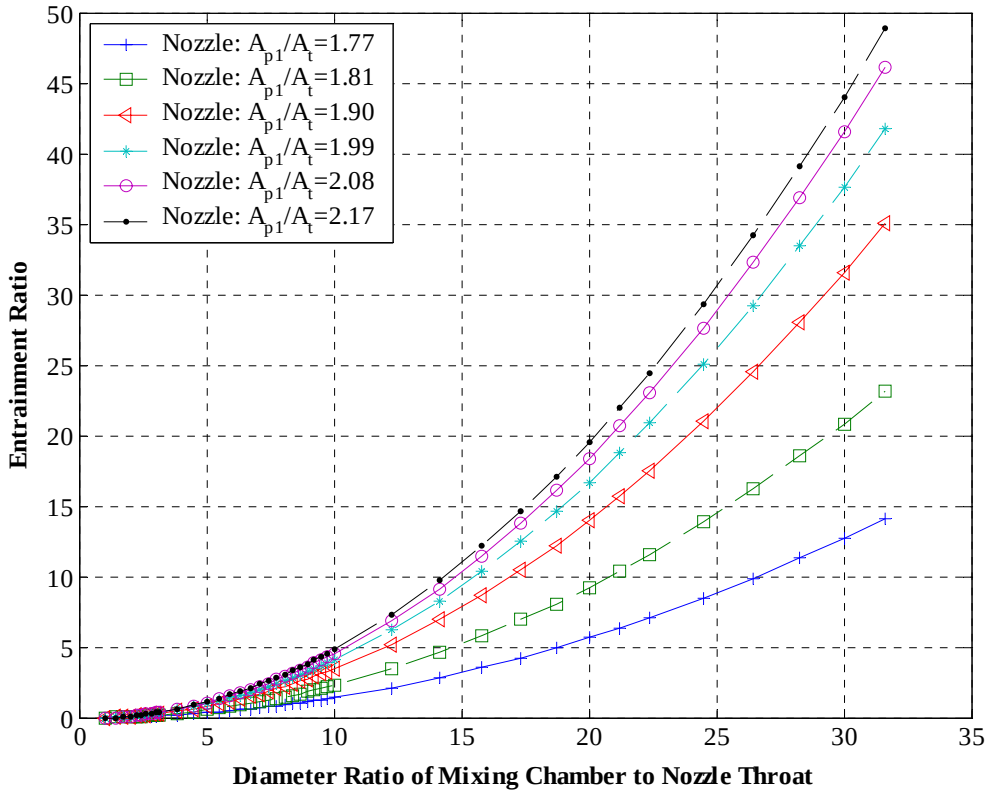

Fig. 3.11 Constant-area ejector ER vs. diameter ratio for various primary nozzles

An alternative approach for obtaining the ejector performance curve would be to use arbitrary but reasonable values of $P_{p1} = P_{s1} = P_1$. To operate the ejector, the P_1 value must be in a practical range such that $0 < P_1/P_{s0} < 1$. Fig. 3.12 shows the ER curves obtained by this method for various P_1. Fig. 3.11 and Fig. 3.12 are very similar to each other, since they are predictions for the same nozzle but using different solution assproaches.

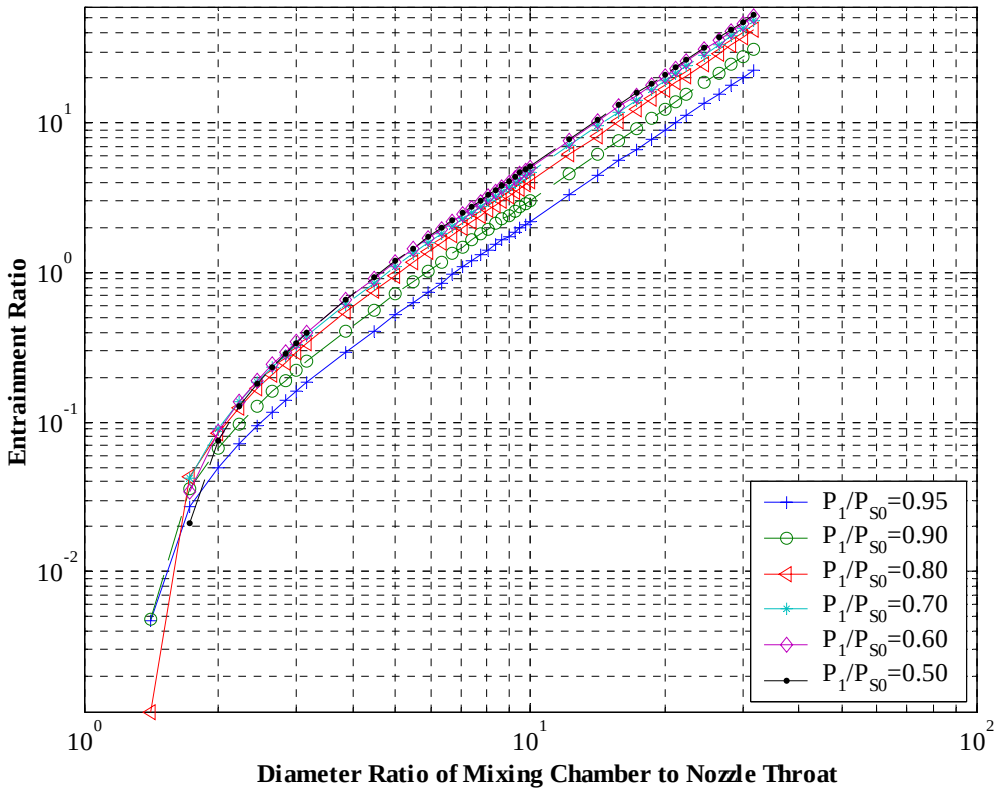

Fig. 3.12 Constant-area ejector ER curve for various P_1 values

Ejector performance is affected by the temperatures of the primary stream and the secondary stream. Fig. 3.13 shows the impact of temperature ratio of secondary to primary streams on jector performance curve of ER against area ratio. Fig. 3.14 is a similar curve, but ER is plotted against the diameter ratio instead of area ratio for the purpose of design convenience. The investigation range of temperature ratio T_{s0}/T_{p0} was arbitrarily selected in the range of $T_{s0}/T_{p0} = [0.90,\ 1.30]$. T_{p0} was set as a fixed

value, $T_{p0} = 300K$. Therefore, the secondary flow inlet temperature was in the range of $T_{s0} = [270K,\ 390\text{K}]$, which includes the most practical operating conditions.

It is observed from Fig. 3.13 and Fig. 3.14 that ER is higher for the cooler secondary flow. The impact of T_{s0}/T_{p0} is more obvious in the big area/diameter ratio range. In the small area/diameter ratio range, the temperature ratios do not have significant influence on the ejector performance curve.

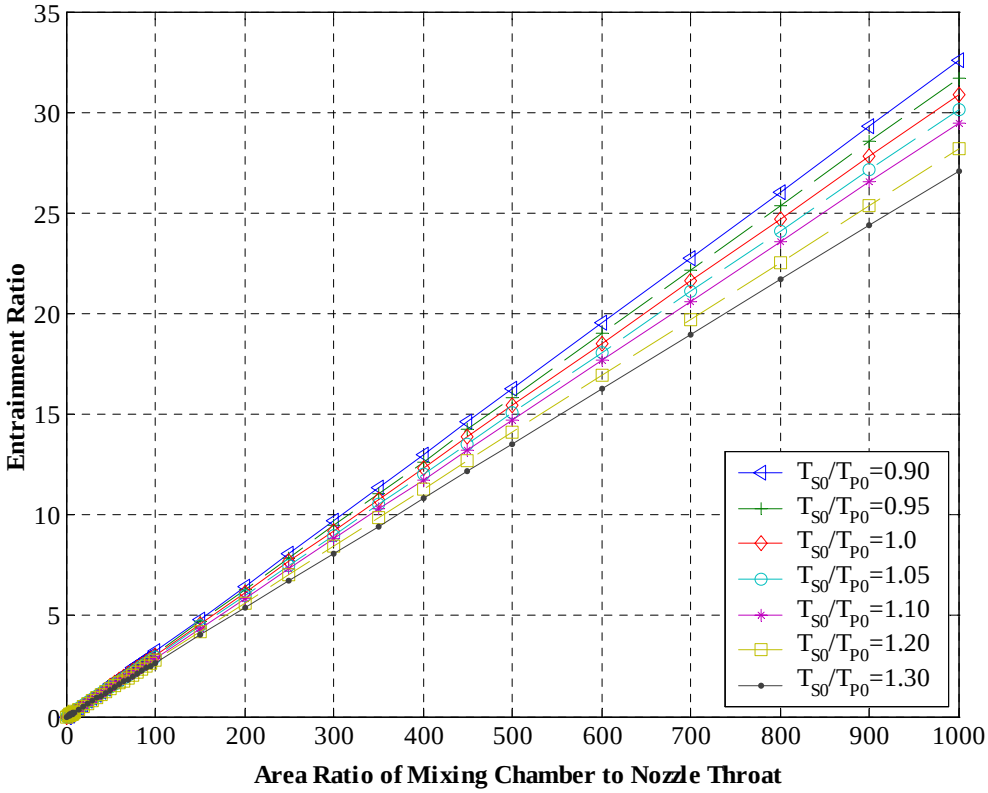

Fig. 3.13 Constant-area ejector ER vs. AR for various T_{s0}/T_{p0}

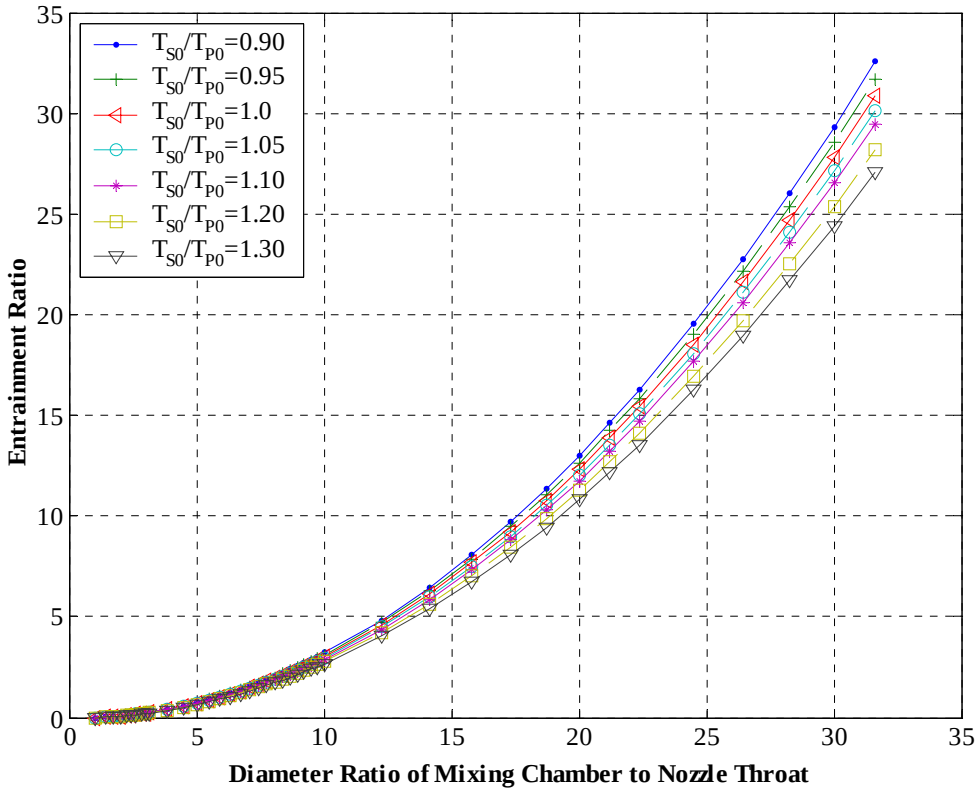

Fig. 3.14 Constant-area ejector ER vs. DR for various T_{s0}/T_{p0}

The specific heat ratio γ is a very important parameter in the gas ejector analytical model. Fig. 3.15 shows the influence of specific heat ratio on the ejector ER curve. In the plot of the performance curve, arbitrary values of γ_s are set as the specific heat ratio for the secondary stream. Air, with $\gamma_p = 1.4$, is set for the primary stream. It is observed from Fig. 3.15 that specific heat ratio does have some impact on the ejector performance curve. However, the influence of γ_s/γ_p on the ER is not significant.

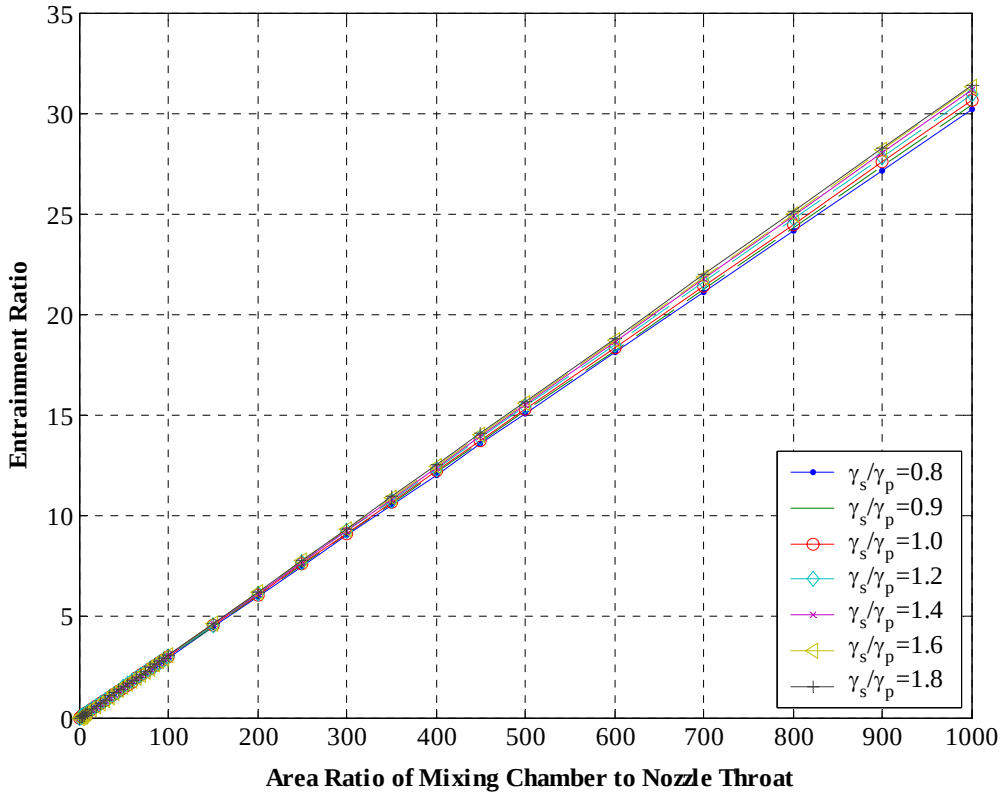

Fig. 3.15 Impact of specific heat ratio on the constant-area ejector performance

In practical ejector design, the details of the geometry are calculated. In previous discussions, a lot of effort has been put on the design of the primary nozzle and the mixing chamber. The previous discussion gives adequate information to determine the geometric parameters of those two parts in the design of a constant-area gas ejector for a desired entrainment ratio.

More detail may be desired in the design of section 1 (suction station) in Fig. 3.2. A desired parameter of this station is the area ratio of secondary flow channel to primary

flow channel, A_{s1}/A_{p1} . Actually, A_{s1}/A_{p1} can be calculated by using Equation (3.29) for desired entrainment ratio. Fig. 3.16 shows the relationship of A_{s1}/A_{p1} with the entrainment ratio of a constant-area gas ejector.

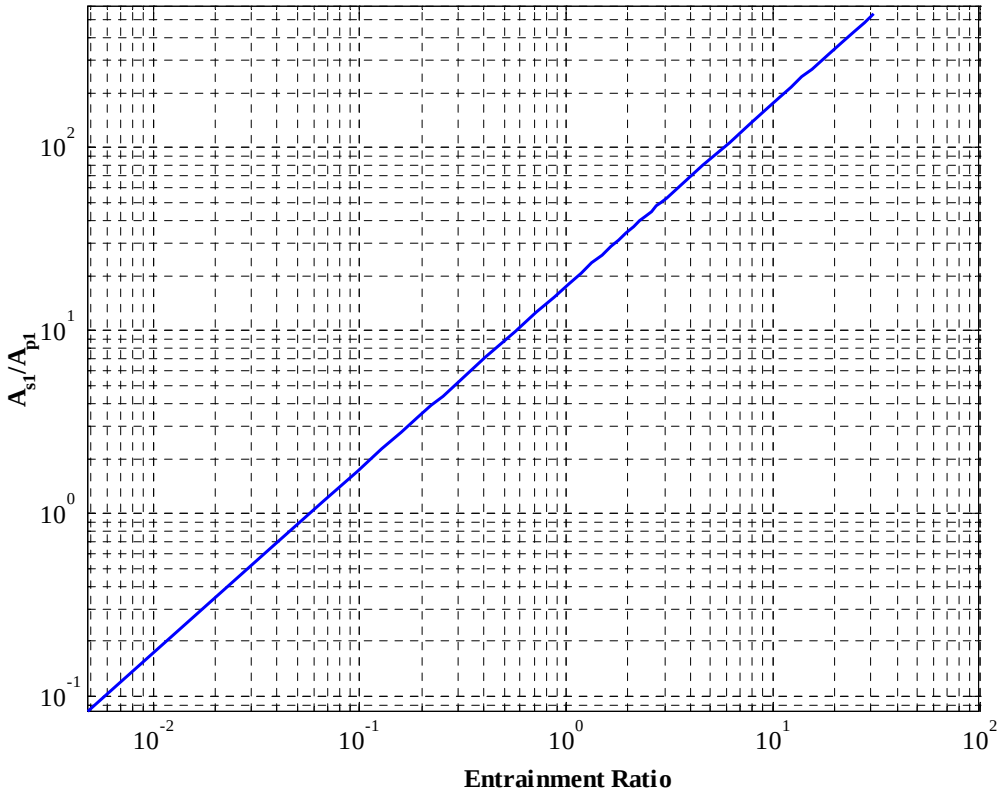

Fig. 3.16 Relationship of A_{s1}/A_{p1} with constant-area ejector ER

The mixing chamber exit Mach number M_{m3} is calculated by using Equation (3.26) for the desired entrainment ratio. Two real solutions are possible for Equation (3.26), though sometimes there is only one real solution. Should two real solutions happen, one is

supersonic value $M_{m3} > 1$ and the other one is subsonic value $M_{m3} < 1$. The subsonic solution is the one for our design and the supersonic solution is abandoned. Fig. 3.17 shows the relationship of M_{m3} with constant-area ejector entrainment ratio.

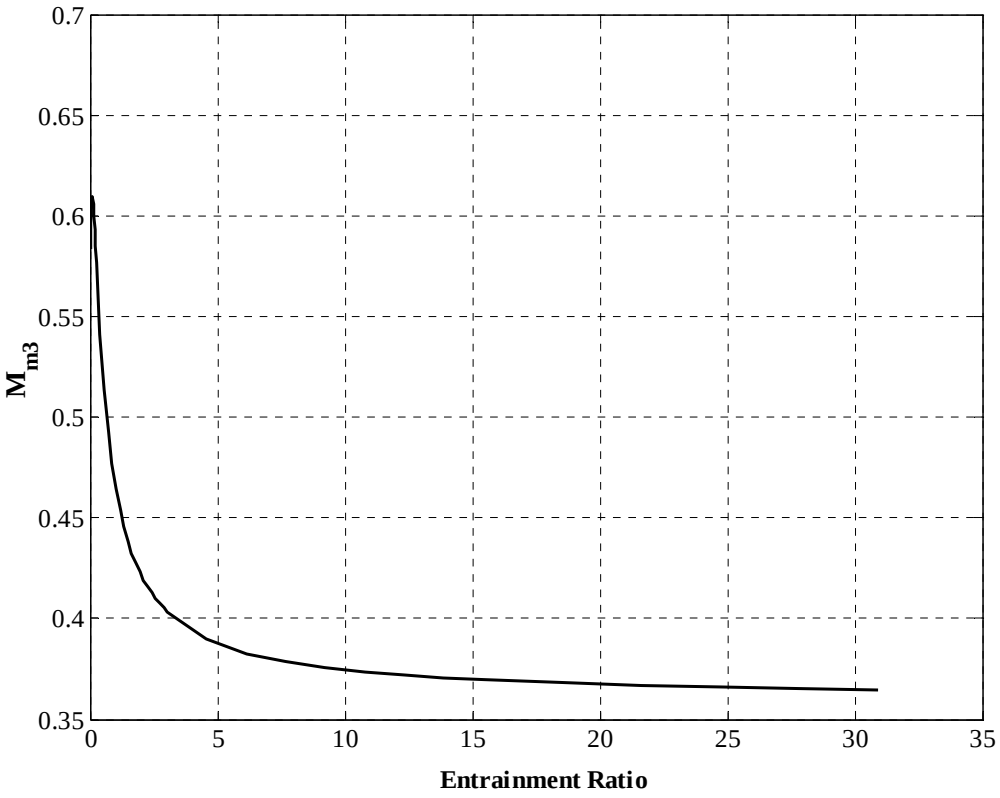

Fig. 3.17 Relationship of mixed flow Mach number with constant-area ejector ER

The compression ratio (CR) is an important parameter in practical gas ejector design. It is desired to design an ejector which introduces more secondary flow and gain higher pressure recovery for the secondary flow. Fig. 3.18 is the plot of CR against ER on a

semi-log scale for a constant-area gas ejector. CR can be as higher as 4.0 if ER is extremely low, and it decreases sharply with the increase of ER. CR is below 1.2 when ER is more than 1.0. This phenomenon can be explained by momentum conservation. Larger ER means the same amount of momentum transferred from primary stream is shared by more mass of secondary stream; thus, lower pressure increase will be gained by each unit mass of secondary flow. On the other hand, smaller ER means the same amount of momentum transferred from primary stream is shared by less mass of secondary stream, and higher pressure increase will be gained. Fig. 3.19 shows this performance curve for a constant-area ejector in the region where ER is higher than 1.0 – the range of practical ejectors are usually operated.

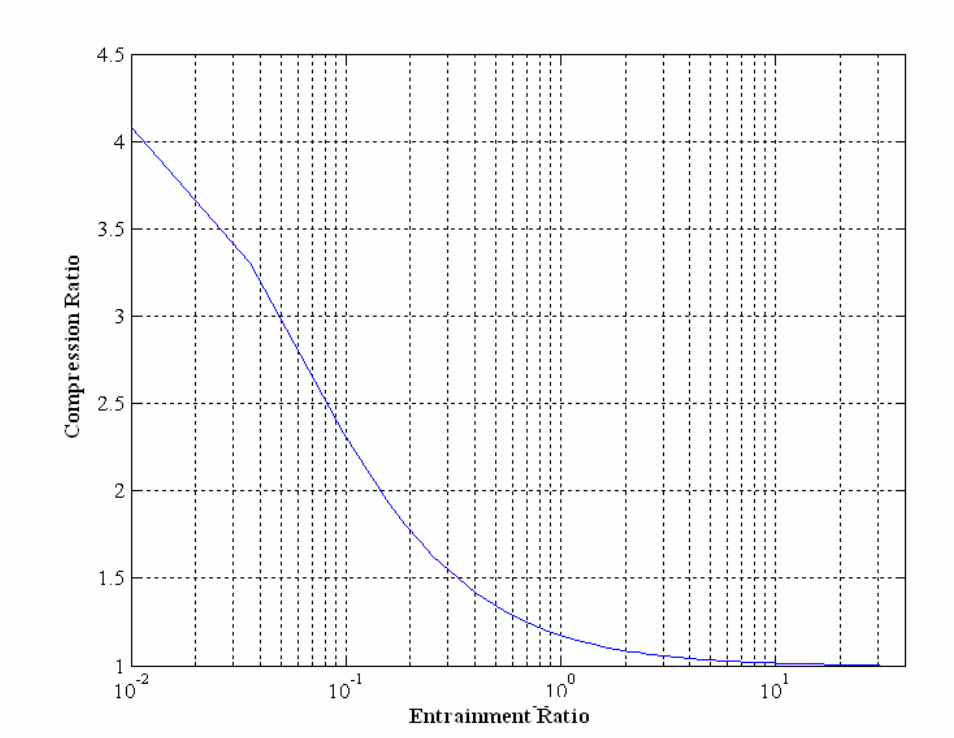

Fig. 3.18 Plot of CR vs. ER in semi-log scale for constant-area ejector

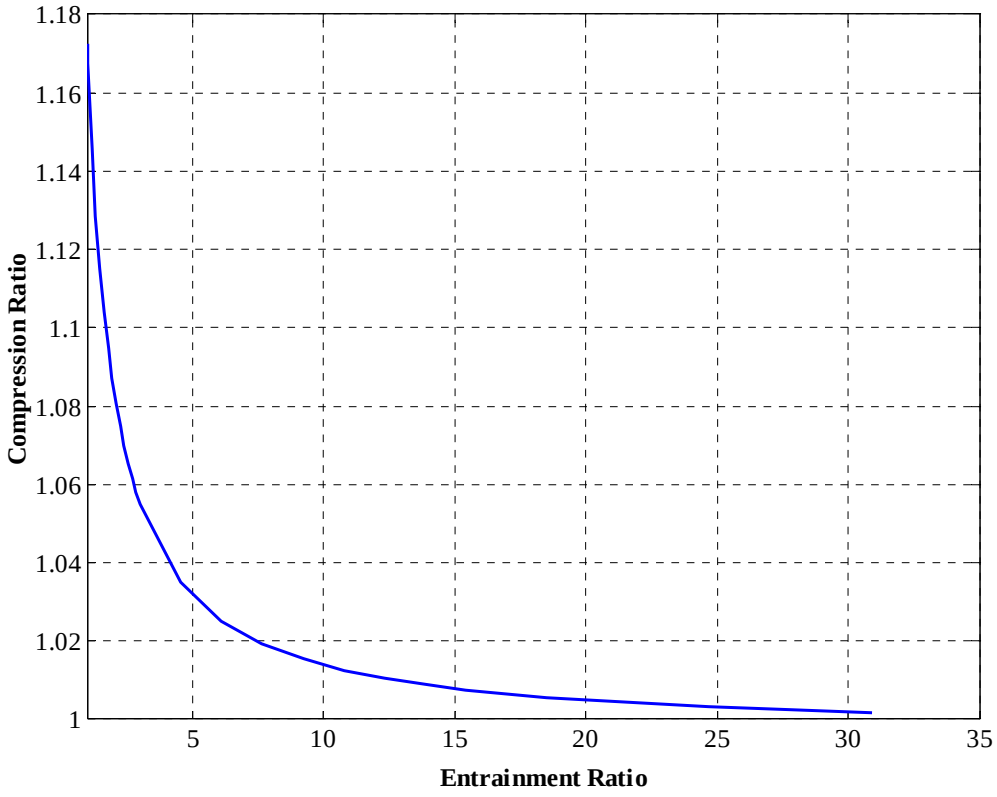

Fig. 3.19 Plot of CR vs. ER in higher ER region for constant-area ejector

Constant-Pressure Mixing Model

The calculations for the constant-pressure mixing ejector model can be performed similarly to the calculations for the constant-area mixing model. Since the design and performance analysis for constant-area ejector have been executed in great detail in the previous section, the analysis of constant-pressure ejector will not be in the same detail.

As for the constant-area model, the analysis for constant-pressure model is focused on ejector performance curves.

It is possible that the mixed flow can be supersonic at the mixing chamber exit, i.e., $M_{m2} > 1$, and a normal shock will occur between section 2 and section 3. This will happen in an ejector with a small area ratio of mixing chamber exit to the nozzle throat and extremely low entrainment ratio. In this case, shock wave Equations (3.60), (3.61) and (3.62) could be utilized to correct the flow field parameters. In reality, most practical ejectors are not designed in such configurations and it is not necessary to consider the situations of $M_{m2} > 1$. In this section, calculations will be performed only for the subsonic mixed flow cases, i.e., $M_{m2} < 1$ and $M_{m3} = M_{m2}$.

The flow parameters at the nozzle exit M_{p1}, P_{p1} can be calculated for a given nozzle area ratio of A_{p1}/A_t by using least square fit numerical approach. As discussed in the previous section, it may be better to use arbitrary values of P_1 to solve M_{p1} and M_{s1} with the assumption of $P_{P1} = P_{s1} = P_1$. Fig. 3.20 shows the relationship among entrainment ratio and the area ratio of mixing chamber exit to nozzle throat for various P_1 values.

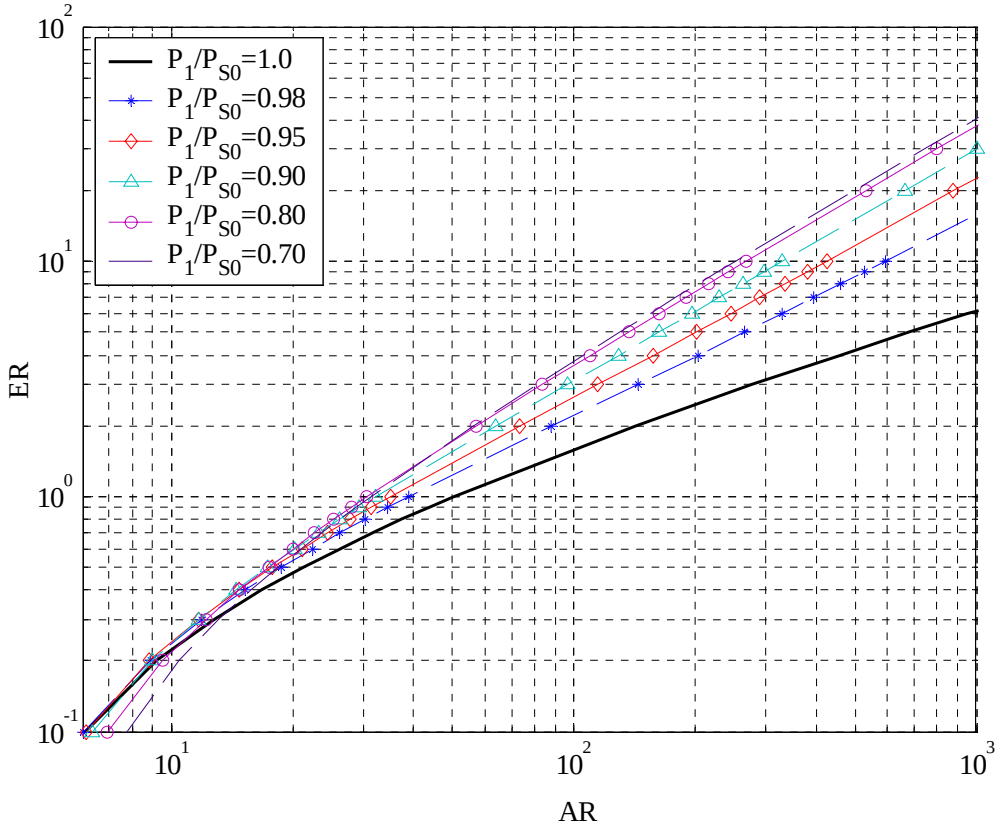

Fig. 3.20 Relationship of ER with AR for constant-pressure ejector with various P_1

As a comparison, the ER calculations for constant-area ejector and for constant-pressure ejector are plotted together on Fig. 3.21. Solid lines represent the ER curves of constant-pressure ejector and the dash lines represent the ER curves of constant-area ejector. In high ER region (ER>1.0), there is no significant difference between the plots obtained by these two mixing models. In low ER region, the difference between these two approaches could be obvious. Generally, the constant-pressure ejector has higher ER when $P_1/P_{s0} > 0.90$, while the constant-area ejector has a higher ER if $P_1/P_{s0} < 0.90$.

This observation is different from conclusions in the literature. In the literature, it is widely believed that a constant-pressure ejector has a better performance [3], though some researchers do not agree.

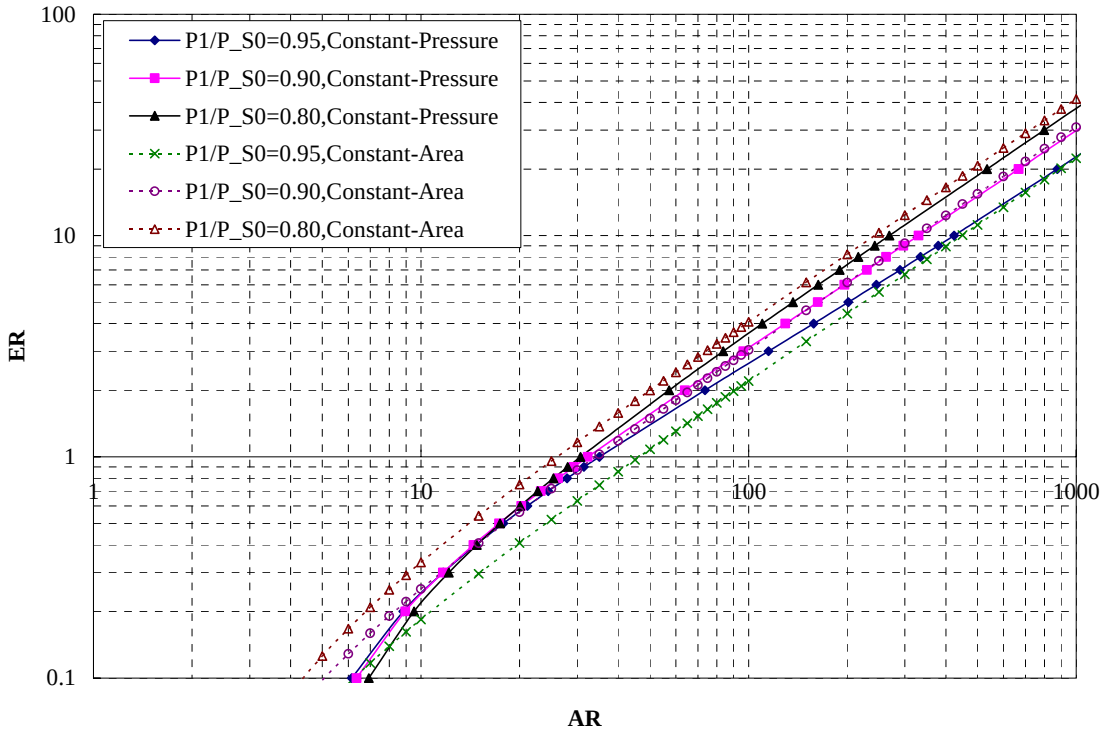

Fig. 3.21 ER curves for constant-area ejector and constant-pressure ejector

The mixing chamber exit Mach number M_{m2} is calculated by using Equation (3.57), thus the velocity and other flow parameters of this location can be determined. Unlike the constant-area model which may have two solutions of M_{m3}, only one solution can be obtained from Equation (3.57). Intuitively, M_{m2} is certainly related with ER and the AR

of mixing chamber to nozzle throat. To explore this relationship, M_{m2} is plotted against the AR in Fig. 3.22. The M_{m2} value drops rapidly with the increase of AR. The possible supersonic mixed flow, i.e. $M_{m2} > 1$, happens in a limited region with small AR. Practically, it is not desired to design an ejector with a small AR, since small AR corresponds to small ER.

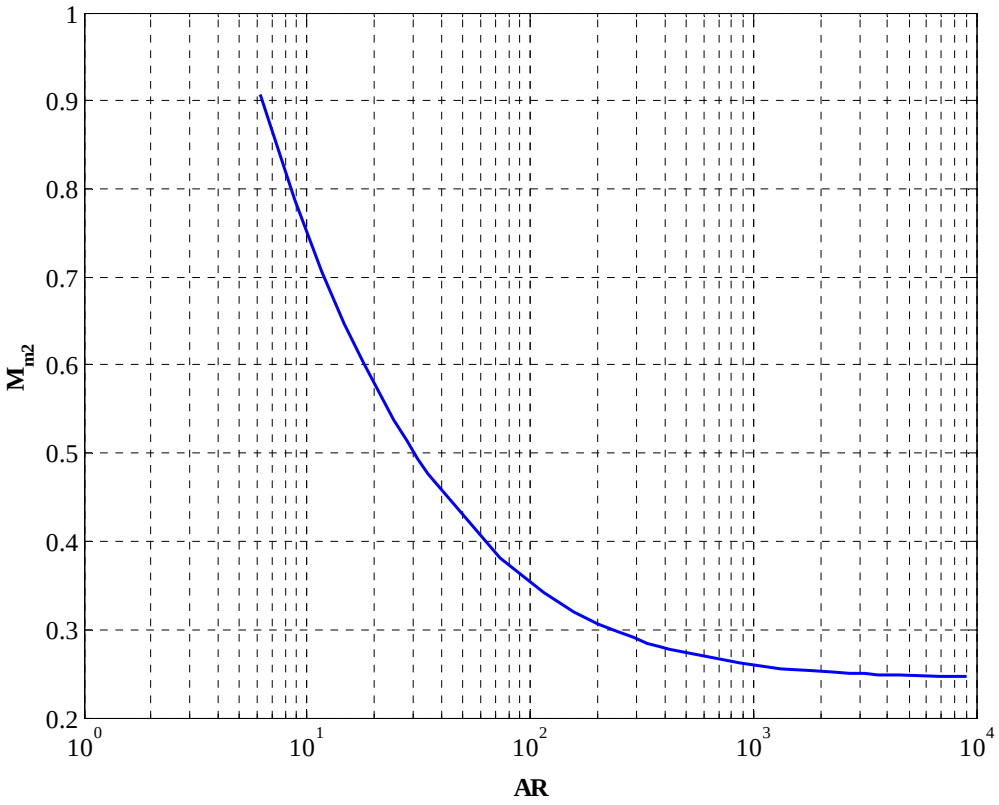

Fig. 3.22 Plot of M_{m2} against A_{m2}/A_t for constant-pressure ejector

As stated before, the CR and ER are the two most important design parameters. Higher ER as well as higher CR is desired. Fig. 3.23 shows the relationship between CR and ER for a constant-pressure ejector. The value of CR can be as high as 1.6 at the point of ER=0.1. However, it deceases rapidly with increase of ER, and CR is less than 1.2 when ER is higher than 1.0. The design goal of "higher CR as well as higher ER" is difficult to implement, but it is possible to design an ejector with a reasonable balance between ER and CR. The relationship between CR and M_{m2} is potted in Fig. 3.24. The CR increases with increasing M_{m2}, since bigger M_{m2} means smaller AR and smaller ER.

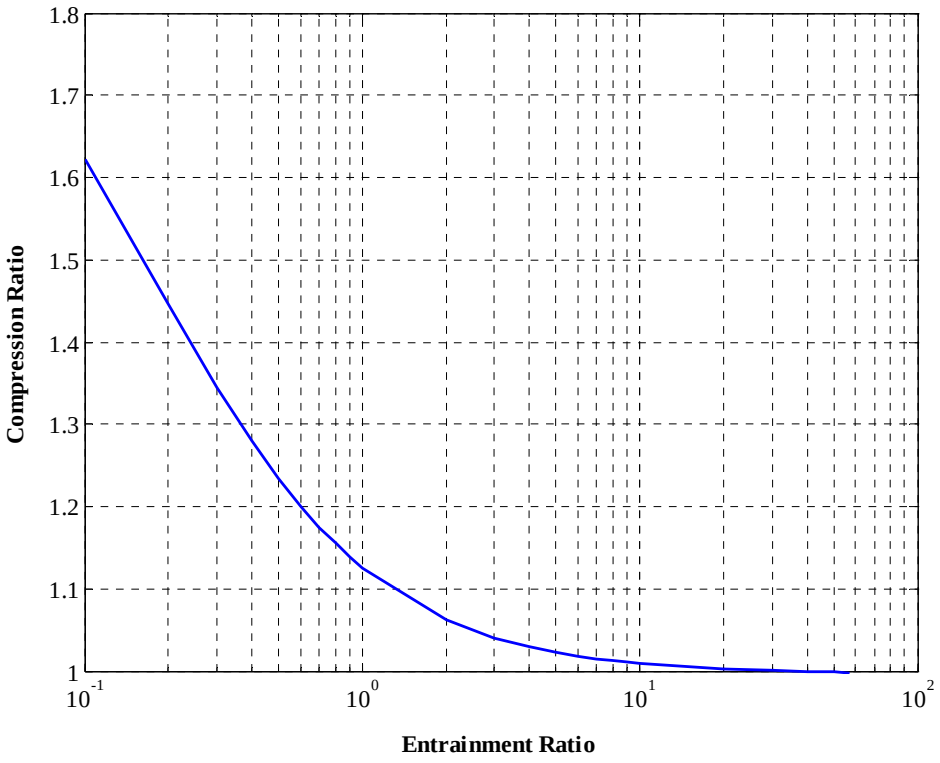

Fig. 3.23 Relationship between CR and ER for constant-pressure ejector

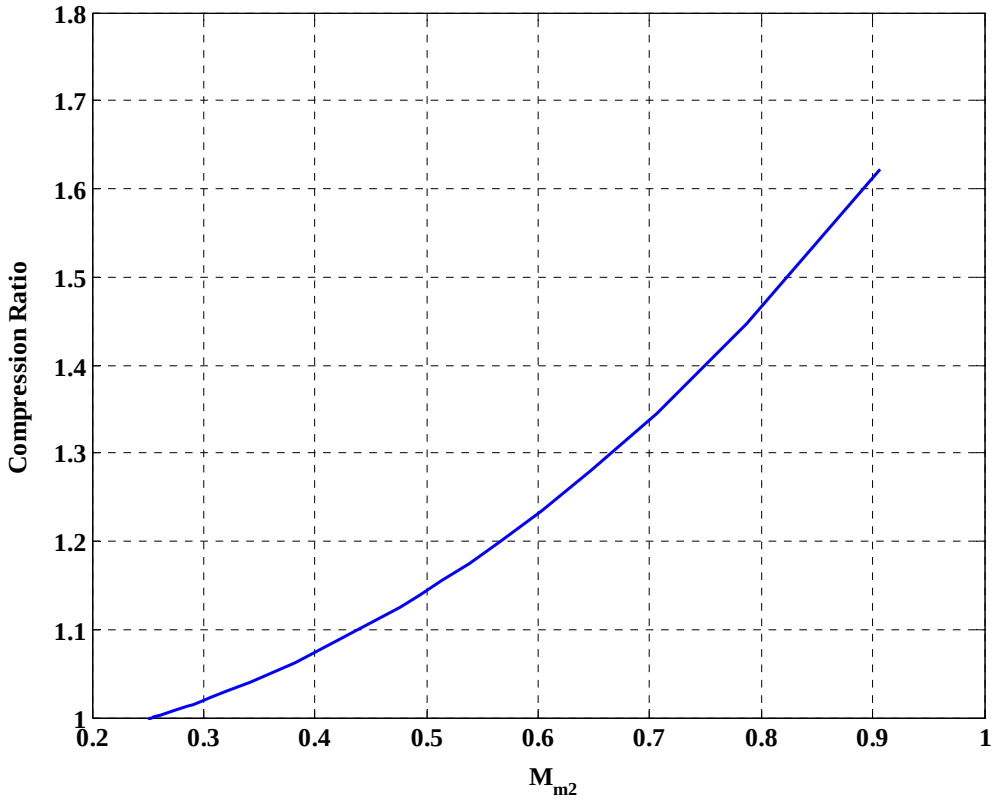

Fig. 3.24 Plot of CR against M_{m2} for constant-pressure ejector

EJECTOR DESIGN USING 1-D MODELS

Gas ejectors are usually integrated into systems for specific operational conditions and limitations, which are specified in terms of temperature, pressure and flow rate. The designed ejectors should meet these constraints and other design specifications. Following is the procedure of a gas ejector design:

1) Determine the ejector operation conditions or boundary conditions;

2) Determine desired ER and CR;
3) Determine primary nozzle geometry according to operational conditions;
4) Determine mixing model, constant-area approach or constant-pressure approach;
5) Determine the mixing chamber geometry according to the relationship of ER vs. AR;
6) Determine diffuser dimension for desired CR.

The above design procedure can be implemented according to the equations and figures derived for the constant-area approach or constant-pressure approach accordingly.

A computer program, ESDUpac A9242 Version 2, developed and released by the Engineering Science Data Unit (ESDU) can be used to do the calculations for the ejector design. All 1-D analytical models as well as their latest improvements are included in the package of ESDUpac A9242. Sets of coefficients collected from many experiments are utilized to correct the calculations due to various loss factors. It is a convenient and practical tool for gas ejector design and performance analysis.

ESDUpac A9242 provides the following design and performance prediction procedures.

A) Quick Design Procedure. Given a selection of entry and required exit pressures, temperatures, mass flow rates and dimensions the program will calculate primary nozzle and exit dimensions, using empirical data for air-air ejectors. The scope of Quick Design Method is restricted to ejectors with constant-area mixing and air as both working fluids.
B) Detailed Design Procedure. Give a selection of entry and required exit pressures,

temperatures, mass flow rates, dimensions and loss factors as well as user defined constraints on the flow conditions, the program will calculate the primary nozzle and exit dimensions and flow conditions throughout the ejector.

C) Performance Prediction Calculation. Given the ejector dimensions, loss factors and a range of flow conditions at entry, the program will calculate the outlet conditions and the flow conditions through the ejector.

Fig. 3.25 is the typical gas ejector configuration utilized by ESDUpac A9242 for the calculations of design and performance prediction. The procedure and steps of deign a gas ejector which meets the system operational flow conditions and constraints are shown in Fig. 3.26.

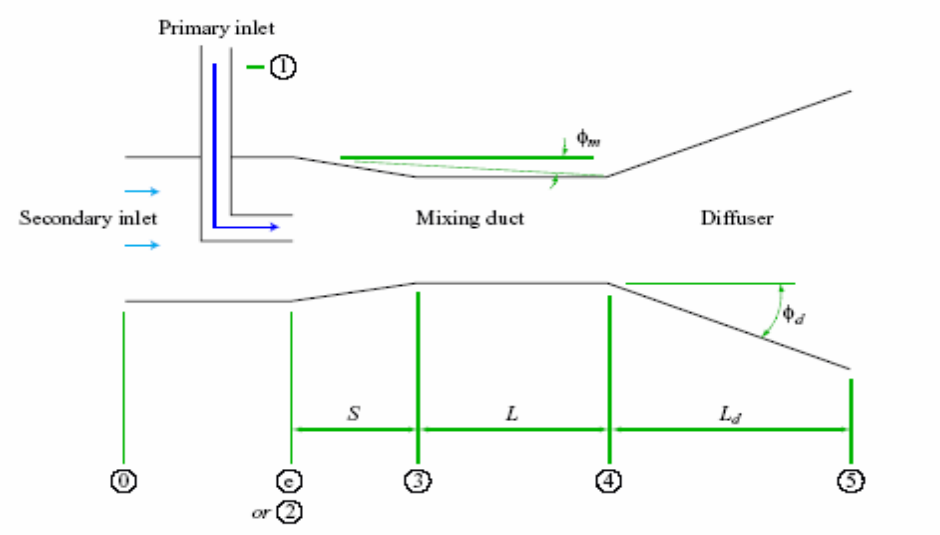

Fig. 3.25 Typical ejector configuration used by ESDUpac A9242

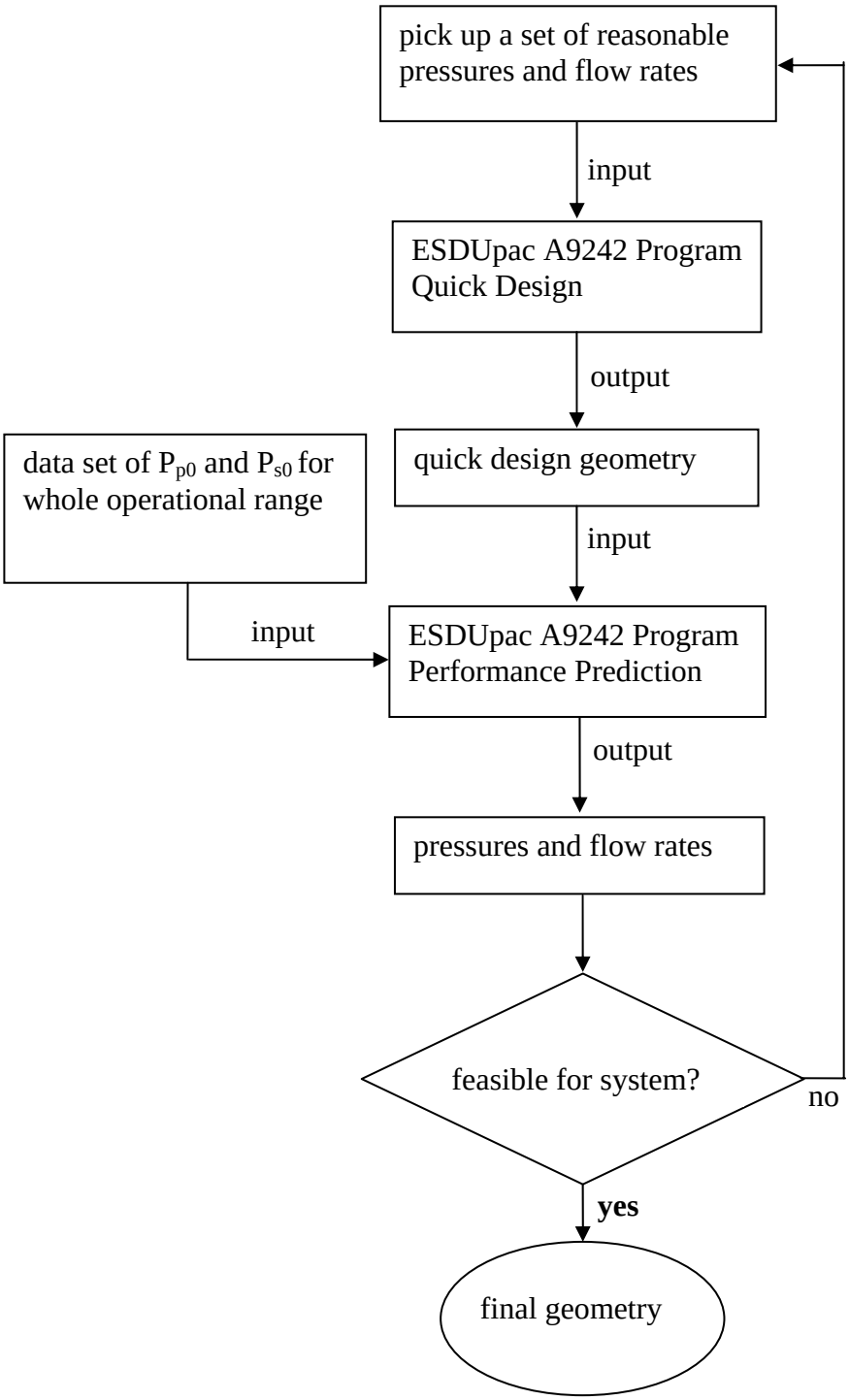

Fig. 3.26 Ejector design procedure for using ESDUpac A9242

SUMMARY AND DISCUSSION

Two general 1-D models for gas ejector design, the constant-pressure mixing model and constant-area mixing model, have been derived based on the conservation equations of continuity, momentum and energy. A parametric study was performed on both models. Gas ejector design can be implemented by employing equations of constant-area mixing and their corresponding figures generated in the parametric study. The general gas ejector design procedure and steps were discussed. ESDUpac A9242, a computer program with comprehensive 1-D analytical models for gas ejector design, has been introduced briefly. A flow chart of gas ejector design using ESDUpac A9242 has been developed.

It is widely believed that the constant-pressure mixing approach results in ejectors with superior performance. However, this belief is not supported by the present work. These calculations show that a constant-pressure mixing ejector could have better performance than that of constant-pressure mixing ejector for certain operating conditions, while it could be the reverse for other operating conditions. Actually, Keenan and Neumann also expressed the opinion that the theoretical results obtained by using the constant area ejector flow model agreed with experimental results and that it was difficult to obtain an agreement between the theoretical and experimental results for the constant pressure ejector flow model.

The ideal design method should provide information on flow-channel shape to give the best performance. In reality, it is impossible to determine the optimal shape and the dimensions of a constant-pressure mixing chamber. Even if it could be determined for one operating condition, different ejector geometries would be required for every different operating condition. It is still not practical to design a gas ejector with the constant-pressure mixing approach. Although a number of modifications have been proposed, there appears to be a need for further improvement.

As discussed preciously, ejector design procedures determine performance at the primary nozzle “on-design” point—a unique operating point. However, the practical ejector may be required to operate over a range of primary pressures or secondary Mach numbers. Actually, operating conditions critically affect the optimum performance of an ejector. Slight changes in operating conditions result in the ejector operating away from its designed optimum performance. Therefore, in this study, arbitrary but reasonable P_1 and $P_{p1} = P_{s1} = P_1$ were adopted for the calculations for the constant-pressure model and the constant-area model, respectively.

To design and predict the performance of a gas ejector integrated in a system with a range of operation conditions, more definitive design and prediction methods are needed. Theoretically, 2-D analytical methods could be utilized for this purpose; however, the technique is ruled out as an effective method because of the number of empirical coefficients required.

Commercial Computational Fluid Dynamics (CFD) software are now widely available. These CFD programs allow researchers to model complicated supersonic flows and mixing problems in complicated geometries. Local details of flow fields can be also obtained by CFD software, thus, it enable researchers to gain better understanding of the mixing process in a ejector. In next chapter, a CFD program will be used to model and design gas ejectors.

CHAPTER IV

SINGLE PHASE GAS EJECTOR CFD SIMULATIONS

INTRODUCTION

Previously introduced 1-D analytical approaches do not provide the details of the flow field, such as the local velocity, pressure, temperature profiles of the streams in the ejector. Knowledge of these details is very important to understand the complex compressible phenomena happening in the nozzles and the mixing process occuring in the mixing chamber. This understanding is crucial to model and predict the performance of ejectors with better accuracy and to design ejectors with optimal performance curves. Those flow parameters could be obtained by 2-D analytical models. However, 2-D analytical models are complicated and haven't been well established yet. The alternative is numerical simulation using CFD codes. The computer program FLUENT, a commercial CFD software, is utilized for this simulation purpose.

A brief introduction of the FLUENT code and the details of ejector simulation procedure is the first part of this chapter. The second part is a benchmark of the simulation. Data of ejectors are compared with the simulation results, reasonable agreement is found. The next part of this study is to find the best geometrical configuration which achieves the optimal ejector performance curves in terms of entrainment ratio (ER) or compression ratio (CR). Details of the flow field in a gas-ejector with single-phase flow obtained

from the CFD simulations are included in the fourth part. As an example of using the CFD tool to design a particular gas ejector, the fifth part of this chapter talks about ejector design for a scalable PEM fuel system.

FLUENT AND SIMULATION ASPECTS

FLUENT is a commercial CFD software released by Fluent Inc. [25]. It is designed to simulate dynamics of flow processes. In simulations, the system or device is constructed as a computational model—geometry and grid system using a preprocessor. The computational model is then imported to the appropriate solver. The computation can be executed after the boundary conditions, initial conditions, and the fluid flow physics are applied to this virtual prototype. The solver can output the various predictions of the fluid dynamics, including the fluid flow behavior, heat transfer and mass transfer etc.

Preprocessing is the first step in building and analyzing a flow model. It includes building the model, applying a mesh, and entering the data. Three preprocessing tools, GAMBIT, G/Turbo and TGrid are provided by FLUENNT Inc. Third-party preprocessing tools, such as ANSYS, PATRAN, GridGen, can also be used. The meshes generated by GAMBIT can be structured or unstructured. After preprocessing, the CFD solver of FLUENT does the calculations and produces the results. This solver is capable of complicated geometry simulation, and has complete mesh flexibility. It is capable of solving flows of all speed regimes from the low subsonic flow to transonic, supersonic,

and hypersonic flows. The flow can be steady-state or transient; it can be inviscid, laminar, or turbulent.

GAMBIT 2.2 was used as the preprocessor for all simulations in this study. The ejector geometry was constructed to be 2-D axis-symmetric as shown in Fig. 4.1. The computational domain was discretized to be a grid system with structured or unstructured meshes. The geometry and grid system were then imported to the solver FLUENT 6.3. As shown in Fig. 4.1, the boundaries of the geometry were defined as pressure-inlet, pressure-outlet, axis (symmetric) and wall. The wall was set to be a stationary, non-slip wall. The fluid in the domain was set to be air or nitrogen with the density being that of ideal gas, and other properties being constant. In solving the flow field, standard gravity was considered as the operating condition.

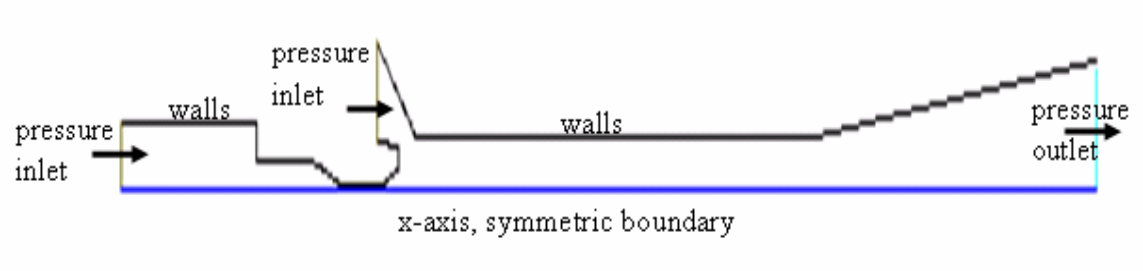

Fig. 4.1 2-D axis-symmetric ejector design

A density-based solver was used instead of pressure-based solver for all calculation cases. As mentioned before, “2-D axis-symmetric” was adopted as the spatial approach.

The fluid flow was set as steady state. Though Reynolds number could be low in certain areas, the flow is generally turbulent in the computational domain. Spalart-Allmaras turbulence model, with “Strain/Vorticity” as eddy generation method, was employed for all calculations. Heat transfer was enabled.

BENCHMARK

The Inter-Phase Transport Phenomena (ITP) Laboratory at Texas A&M University (TAMU) has designed ejectors which meet the operating condition of PEM fuel system. FLUENT was applied to design the ejector and predict its performance. A system with ejector was developed to validate the CFD predictions. Fig. 4.2 shows a schematic of ejector test system used for the benchmark test.

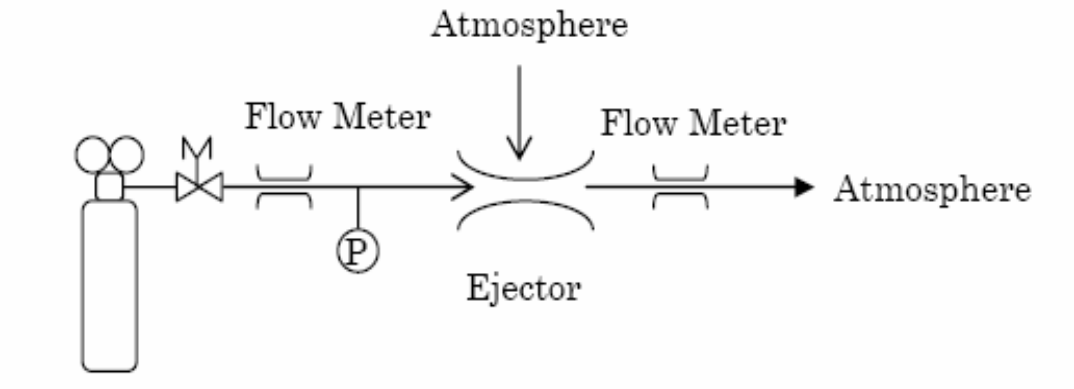

Fig. 4.2 Schematic of ejector performance test system

Initially, ejector performance is evaluated for open loop system, i.e. the suction port and the outlet port are open to atmosphere. Fig. 4.3 shows the schematic of ITP homemade ejector. A Thread to Barb Orifice with 0.0145" orifice diameter was used as a primary nozzle and 1/4" tube with the inner diameter of 0.152" was used as mixing section. On the outlet side of the port connector, a hole was bored through the connector body and ultra-torr fitting was attached so that 1/4" stainless tube can be moved through the connector body.

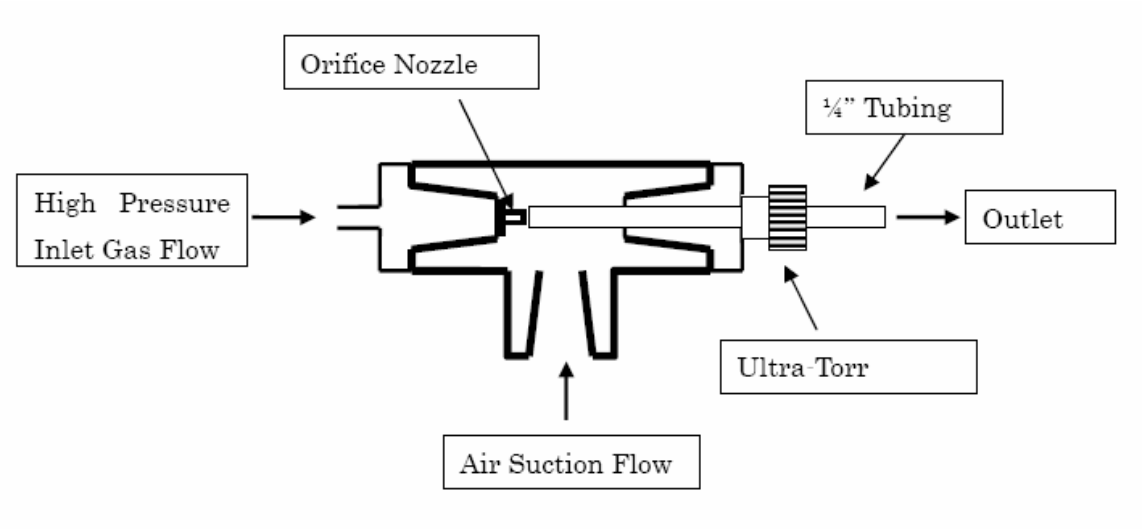

Fig. 4.3 ITP ejector structure

To evaluate ejector performance, the ratio of outlet flow rate to primary flow rate was plotted against the primary flow rate as shown in Fig. 4.4. At the low end of primary flow rate, the ER is also low. ER increases rapidly with the increase of primary flow rate, and it reaches the maximum value of 5.5 at the primary flow rate of 3 SLPM. ER turns

down at primary flow rate of 4 SLPM, and it decrease with further increases of primary flow rate.

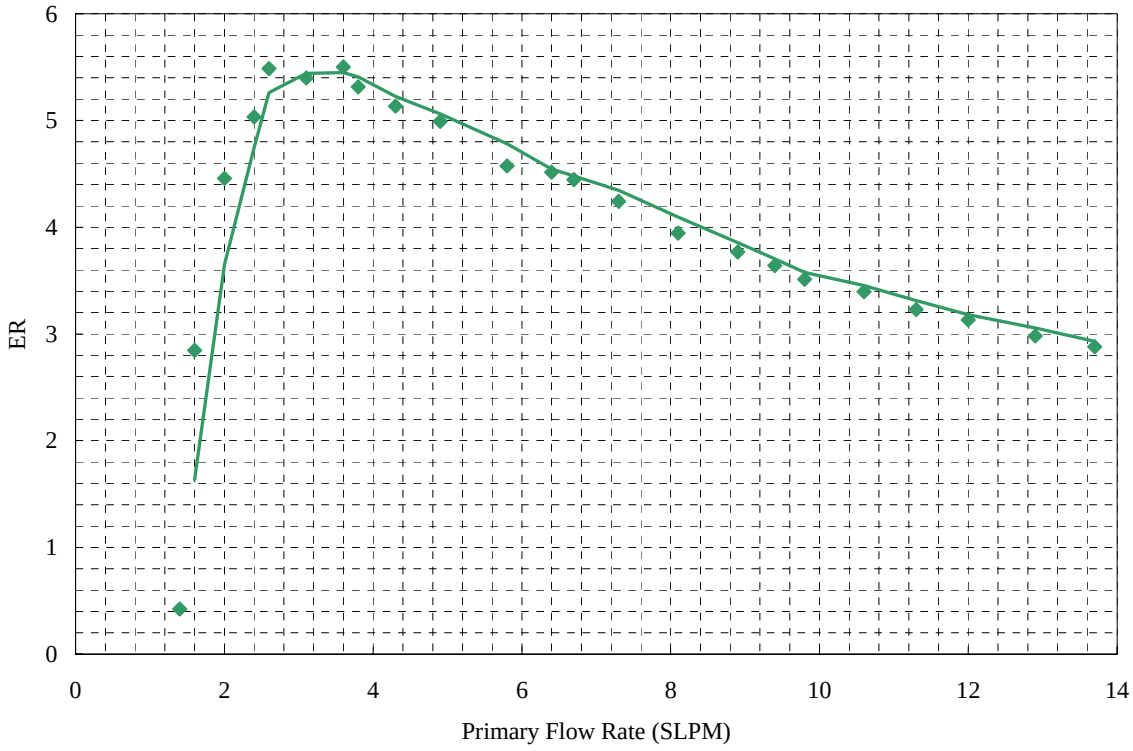

Fig. 4.4 ITP ejector performance curve

This ejector was simulated by using FLUENT with the geometry shown in Fig. 4.5. Numerical simulation results and test data of primary flow rate vs. driving pressure are plotted in Fig. 4.6. Fig. 4.6 shows that the relationship between primary flow rate and driving pressure is linear. Very good agreement was found between CFD results and test data.

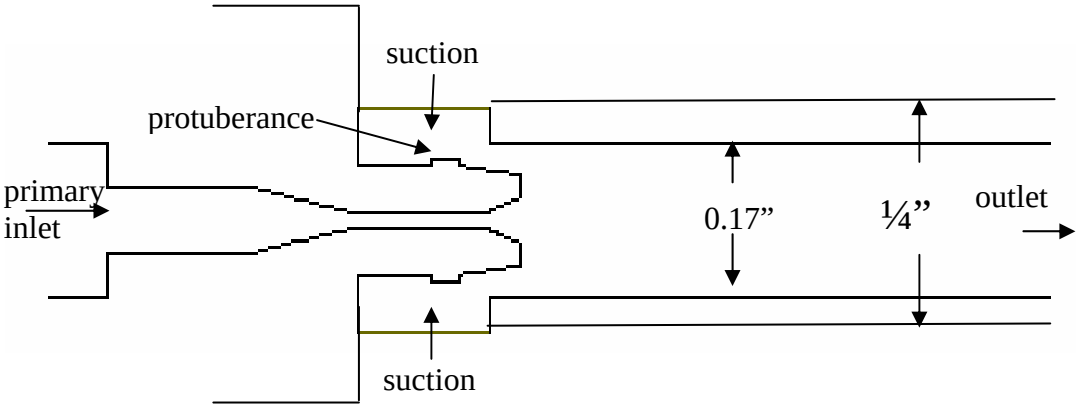

Fig. 4.5 Ejector geometry configuration simulated by FLUENT

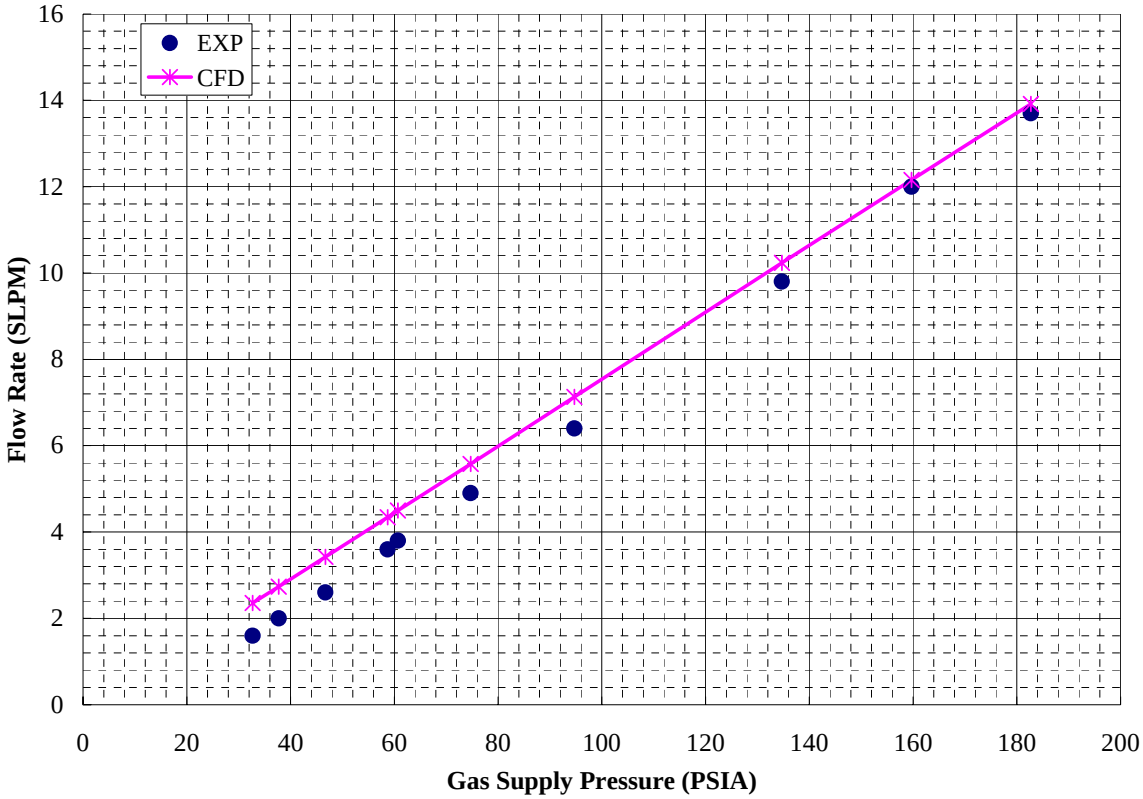

Fig. 4.6 Primary flow rate vs. gas supply pressure

Fig. 4.7 shows ejector flow ratio against driving pressure. The error bar of data is $\pm 10\%$. The optimal performance region in terms of ER is in the driving pressure range of 40-80 psia. The simulation results show a good agreement with data. These compare very well in the ejector optimal performance region. Bigger discrepancies are found in the higher driving pressure region. A possible reason is that the friction effect of tubing in the experimental tests is no longer negligible for the higher flow rate. The CFD simulation only considered the configuration of ejector itself, and the simulated length of mixing tube is 1 inch. However, the actual length of orifice downstream tube is about 20 inches with flow meter, which causes a pressure drop. For higher flow rates, the pressure drop across this tube and flow meter will be relatively significant.

Based on the comparisons of CFD simulation results with data from the Texas A&M University ITP group, it is proper to conclude that there is very good agreement between the CFD predictions and test data, validating CFD simulations. Commercial CFD software FLUENT can be used to simulate the supersonic gas ejector, and it is capable of predicting the performance of an ejector to a satisfactory degree.

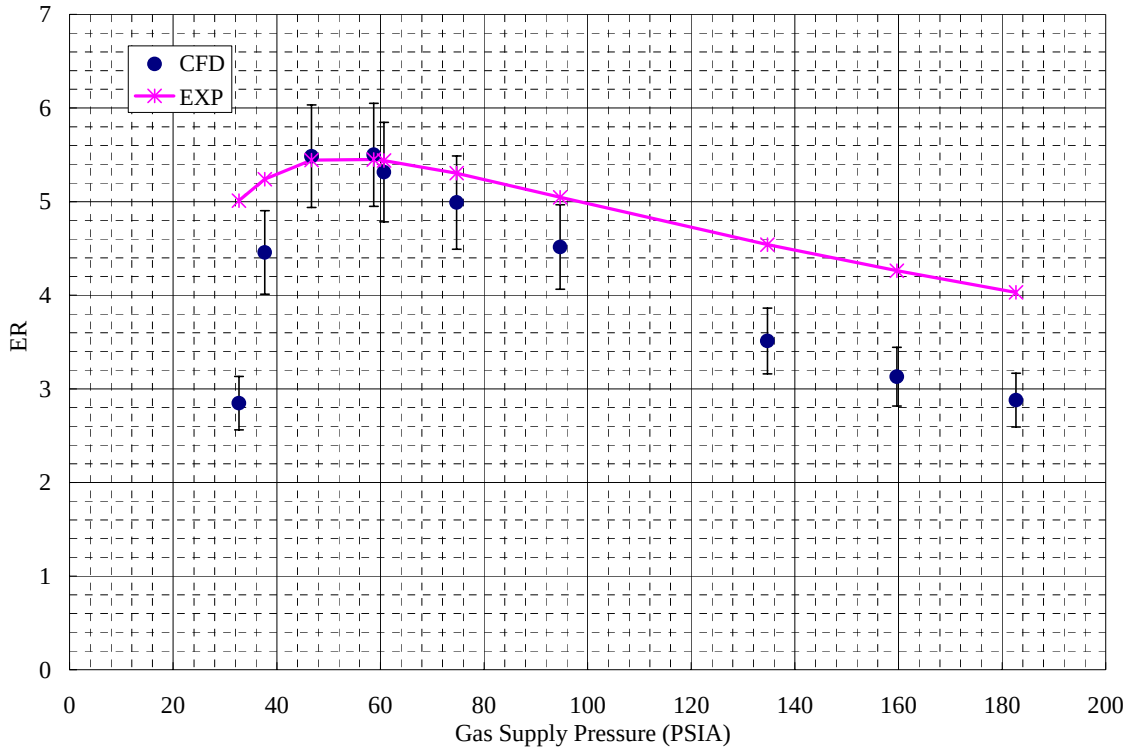

Fig. 4.7 ER vs. driving pressure

EJECTOR OPTIMIZATION

The ejector geometry optimization goal is to find the optimal geometry configuration which can achieve the highest entrainment ratio (ER) as well as reasonable pressure recovery. The optimal configuration is obtained by investigating the influence of geometry parameters on the ejector performance. The investigation includes adjustment of the following geometry parameters: the diameter ratio of mixer to throat (D_m/D_t), the

position of nozzle exit to the entrance of constant-area mixer, the mixing tube length, the subsonic diffuser angle etc.

The ejector configurations shown in Fig. 4.5 and Fig. 4.8 were used as the basic geometric set up. Geometry modifications and parameter adjustments were done based on Fig. 4.5 or Fig. 4.8 to obtain the optimal configuration.

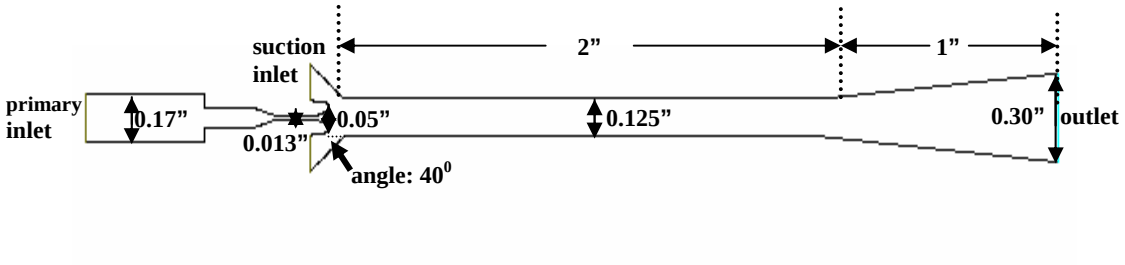

Fig. 4.8, Ejector geometry used for optimization

To investigate the impact of a certain geometry parameter on ejector performance, that parameter was adjusted while other parts of the ejector geometry were fixed. The same boundary conditions and operating conditions were then set up for all these configurations. The performance curve was obtained by plotting the resulting ERs of all simulation cases against the values of that geometry parameter.

To set boundary conditions in absolute pressure, the operating environment pressure is set to be zero. The operating environment temperature was set to be 300 K. Also, gravity was included in the operating conditions. For the purpose of comparison, the same

boundary conditions were set for all simulation cases which were based on adjusting the geometry configuration shown in Fig. 4.8. The primary inlet was 164.7 psia and 300K; the suction inlet was 59.3 psia and 300K; the outlet was 59.7 psia and 300K. The investigation of the influence of primary nozzle exit position on performance was based on modifying the geometry configuration shown in Fig. 4.5. Boundary conditions for this investigation were 59 psia, 14.7 psia and 14.7 psia for primary pressure inlet, suction pressure inlet and pressure outlet respectively. 300 K is the temperature set for all boundaries.

Primary Nozzle Exit Position

For a given nozzle geometry, L_s in Fig. 4.9 describes the geometry between the suction plenum and the mixing tube, i.e., $L_s = L_n + L_{gap}$. Where, L_n is the nozzle length and L_{gap} is the distance between the nozzle exit and constant-mixing tube entrance. The position of the nozzle exit to the entrance of the constant-area mixer can be represented by L_s. $L_s < L_n$ means that the nozzle is inserted to the constant-area tube; $L_s > L_n$ means there is certain distance between the nozzle exit and the entrance of constant-area mixing tube.

The simulation results are shown in Fig. 4.9. The entrainment ratio, ER, is plotted against the value of L_s. It is observed that ER is much higher for $L_s > L_n$ than that of for $L_s < L_n$, i.e., the ejector has better performance when its nozzle was taken out of

mixing tube than the nozzle was inserted in the mixing tube. This phenomenon is consistent with our expectation. The cross sectional area of secondary flow path is smaller when the nozzle was inserted in the mixing tube than when the nozzle exit located at outside of the mixing tube. A dimensionless parameter L_{gap}/D_m, the ratio of L_{gap} to mixer diameter D_m, is more convenient to use in gas ejector design when $L_s > L_n$. It is observed from Fig. 4.9 that the gas ejector has the best performance when L_{gap}/D_m is in the range of $0.25 \sim 1.5$. When L_{gap}/D_m increases further, the ER starts to decrease rapidly.

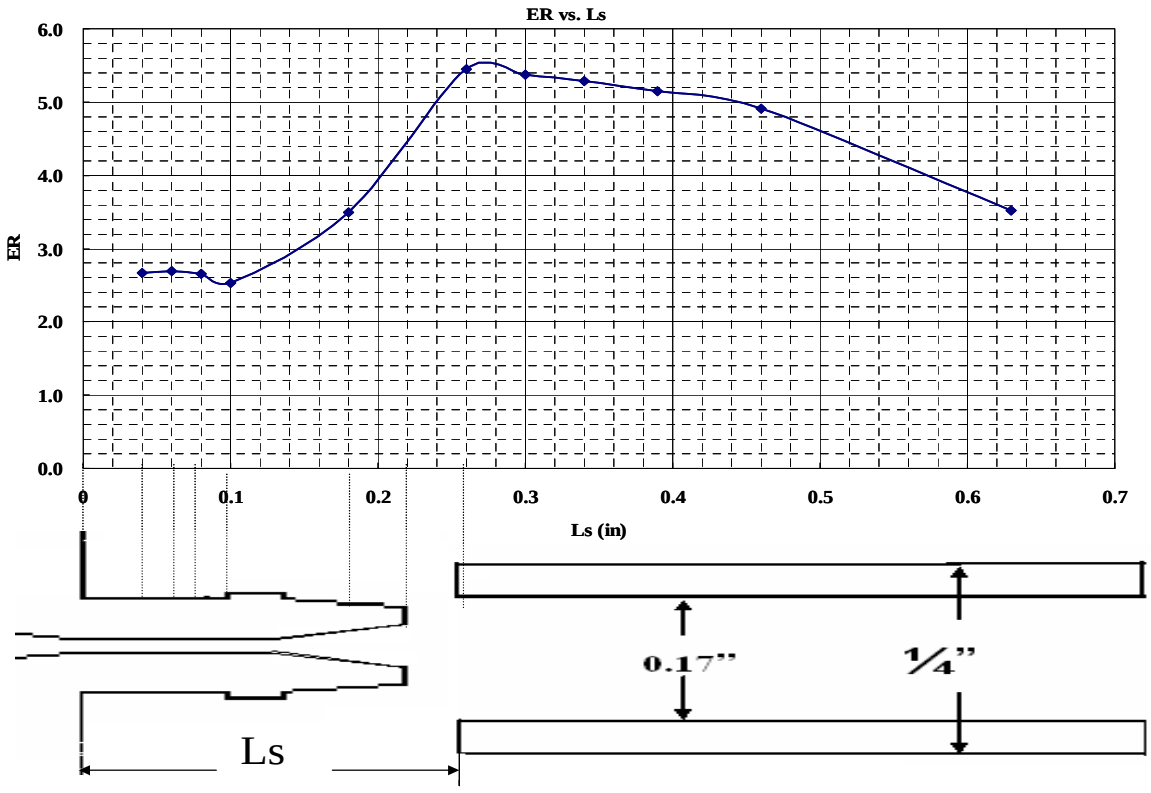

Fig. 4.9 Ejector performance against L_s

Diameter Ratio of Mixer to Throat

Investigation of the influence of diameter ratio D_m/D_t on ejector performance was based on the gas ejector configuration shown in Fig. 4.8. The nozzle throat diameter D_t was fixed at 0.013" and the mixer diameter D_m was then adjustable. Fig. 4.10 shows that ER increases with the increase of D_m/D_t and reaches its maximum value at $D_m/D_t = 11$. The ER then decreases rapidly with the further increase of D_m/D_t. The ejector has the best performance when D_m/D_t is in the range of 8 to 14. When D_m/D_t is larger than 17, the ejector can not induce any secondary flow.

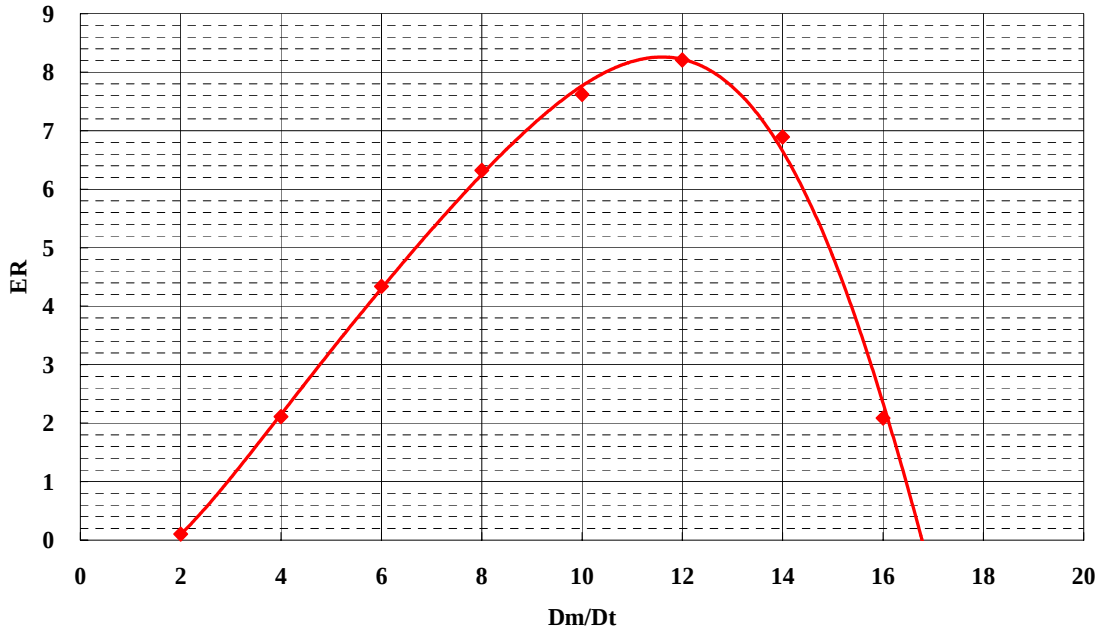

Fig. 4.10 Influence of diameter ratio D_m/D_t on ejector performance

Mixer Length

Investigation of the influence of mixing tube length L_m on ejector performance was again based on the gas ejector configuration shown in Fig. 4.10. The ratio of mixing tube length to mixing tube diameter, L_m/D_m, was used as a dimensionless parameter. The ejector performance curve was obtained by plotting ER against the L_m/D_m value as shown in Fig. 4.11. The ER decreases slightly with the increase of L_m/D_m. In reality, L_m/D_m is usually designed to be in the range of 8 to 12.

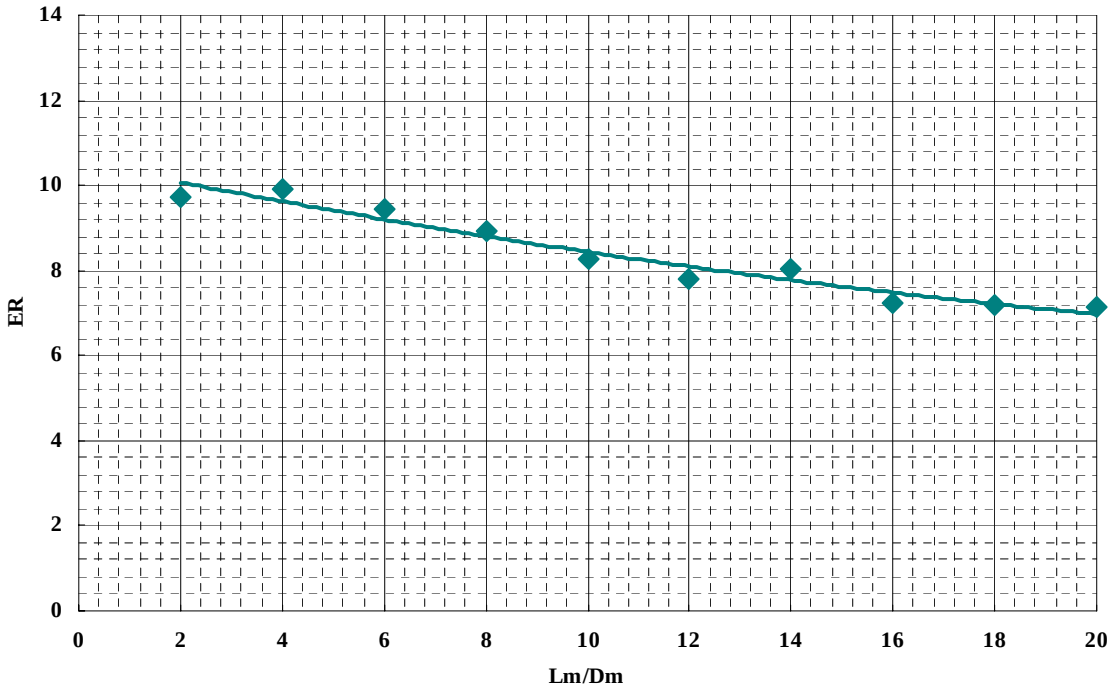

Fig. 4.11 Influence of mixing tube length on ejector performance

Diffuser Angle

A subsonic diffuser is adopted to enhance pressure recovery. Diffuser exit cross-sectional area should determine ejector pressure recovery. The diffuser exit flow area is determined by its expansion angle and its length. It is more practical to adjust expansion angle rather than to adjust length. The simulation results are shown in Fig. 4.12. The ER increases slightly with the increase of diffuser expansion angle and it reaches a maximum value at diffuser angle of 5 degree, then, the ER decreases slightly with the increase of diffuser expansion angle. The optimal diffuser expansion angle is in the range of 2 to 6 degrees.

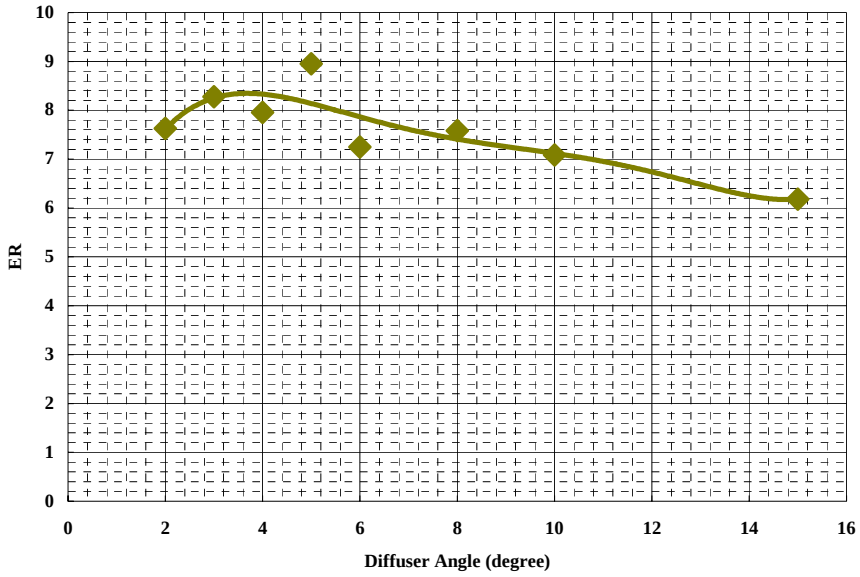

Fig. 4.12 Influence of diffuser expansion angle on ejector performance

The ejector configuration optimization was performed in order to achieve the highest ER as well as reasonable pressure recovery. The investigations have been implemented on 4 geometry parameters: the diameter ratio of mixer to throat (D_m/D_t), the position of nozzle exit to the entrance of constant-area mixer, the mixing tube length, and the subsonic diffuser angle. The study shows that the diameter ratio of mixer to throat and the position of nozzle exit to the entrance of constant-area mixer have the most significant impact on the gas ejector ER curve. The influence of mixing tube length and the subsonic diffuser angle is relatively less important. To achieve optimal performance, the gas ejector may designed in such a way that the D_m/D_t is in the range of 8~12, the L_{gap}/D_m is in the range of $0.25 \sim 1.5$, the L_m/D_m is in the range of 8 to 12, and the diffuser expansion angle is in the range of 2 to 6 degrees.

FLOW FIELD DETAILS OF GAS EJECTOR

The detailed information of the flow field in a gas ejector is very helpful in understanding its performance characteristics. Obtaining the local details of the flow field is one of the purposes of using CFD to simulate gas ejector. Static pressure and velocity are the most important flow field parameters. Gas density, temperature and local Mach number are also desired information for compressible gas flow, especially for supersonic flow. The local profiles of these parameters are provided by post-processing of CFD simulations in forms of contours, vector plots or X-Y plots.

A gas ejector with following boundary conditions: (1) $P_0 = 164.7$ psia, $T_0 = 300$ K for primary pressure inlet, (2) $P_0 = 59.3$ psia, $T_0 = 300$ K for secondary pressure inlet, and (3) $P_0 = 59.7$ psia, $T_0 = 300$ K for pressure outlet is simulated using FLUENT. The local information on gas ejector obtained from the simulation results are shown in the following figures. Fig. 4.13, Fig. 4.14 and Fig. 4.15 are contours of static pressure, axial velocity and static temperature respectively. Since the primary nozzle is very small compared to other parts of the ejector and it is this location that the flow experiences the most significant change, the contours of this part are enlarged.

A shock wave due to the overexpansion of supersonic flow is observed clearly at the exit of the nozzle throat as shown in the contours of static pressure, axial velocity and static temperature. This demonstrates that FLUENT has the ability to capture supersonic shock wave phenomenon, which used to be a difficult task for CFD simulations.

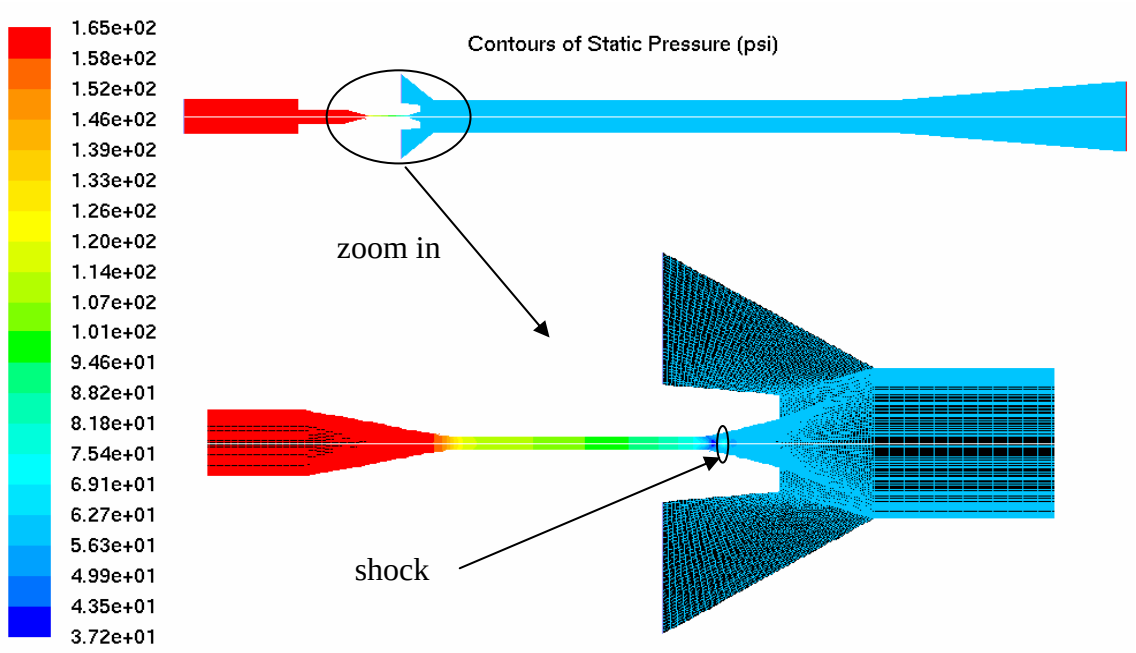

Fig. 4.13 Contours of static pressure in gas ejector

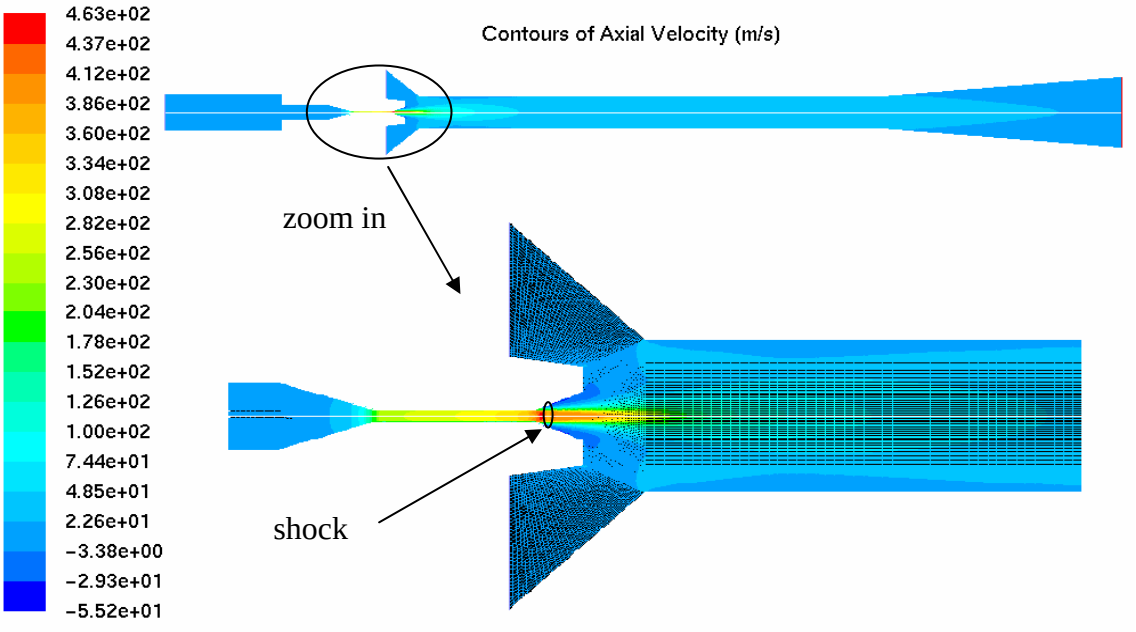

Fig. 4.14 Contours of axial velocity in gas ejector

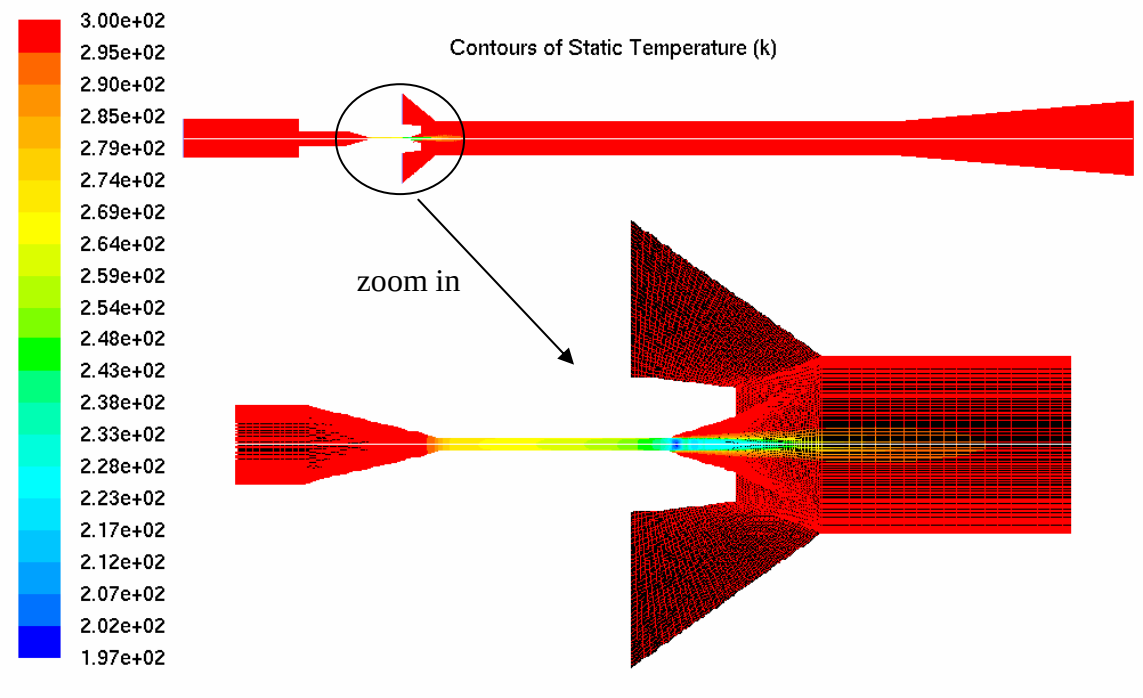

Fig. 4.15 Contours of static temperature in gas ejector

Fig. 4.16, Fig. 4.17 and Fig. 4.18 are plots of local gas density, Mach number and static temperature along the centerline of the gas ejector respectively. Due to the static pressure change, the gas density experiences a big change. The gas density is around 12.8 kg/m^3 at the primary inlet where static pressure is highest; the density is as low as 4.4 kg/m^3 at the nozzle throat exit where static pressure is lowest; the density suddenly jumps back to about 6 kg/m^3 after a shock wave which increase static pressure; then, the density decreases along the centerline since the flow cross sectional area increases. The Mach number plot indicates that the primary flow is almost stagnation at the primary inlet; the stream is accelerated to supersonic by the convergent-divergent nozzle and the

Mach number is as high as 1.7 at the exit of nozzle throat (a little bit down stream of the throat); then, an overexpansion shock wave occurrs at this location and the down stream flow becomes subsonic. The plot of static temperature shows the expected opposite trend of Mach number.

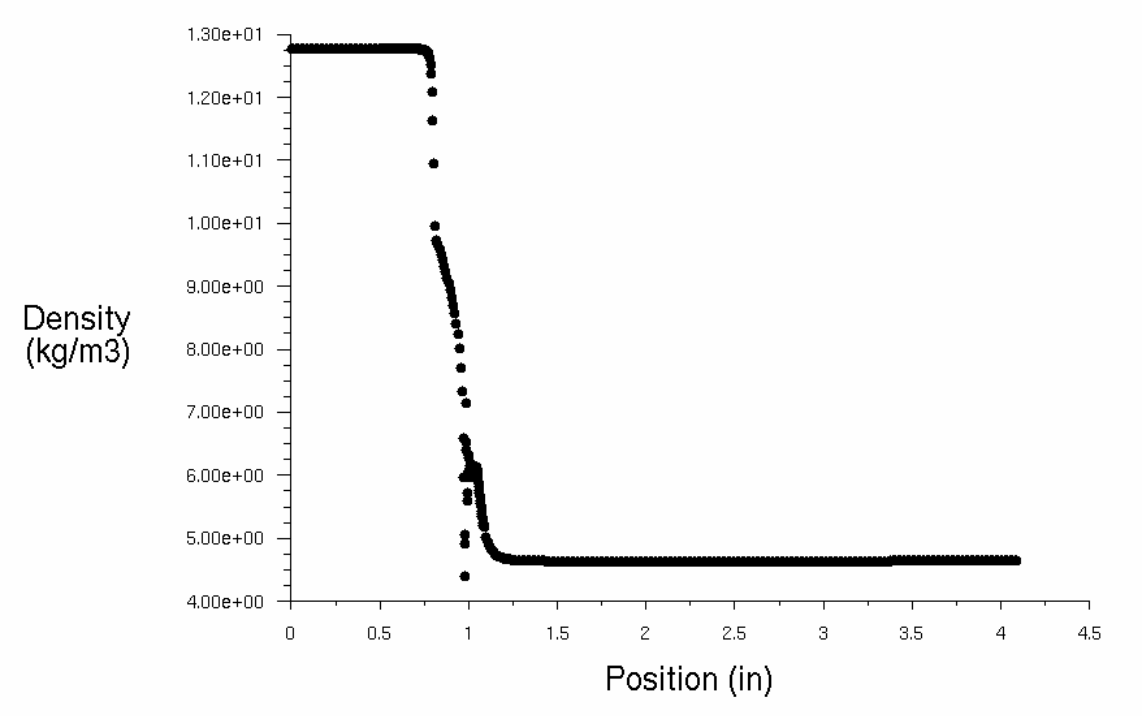

Fig. 4.16 Plot of gas density along the centerline of gas ejector

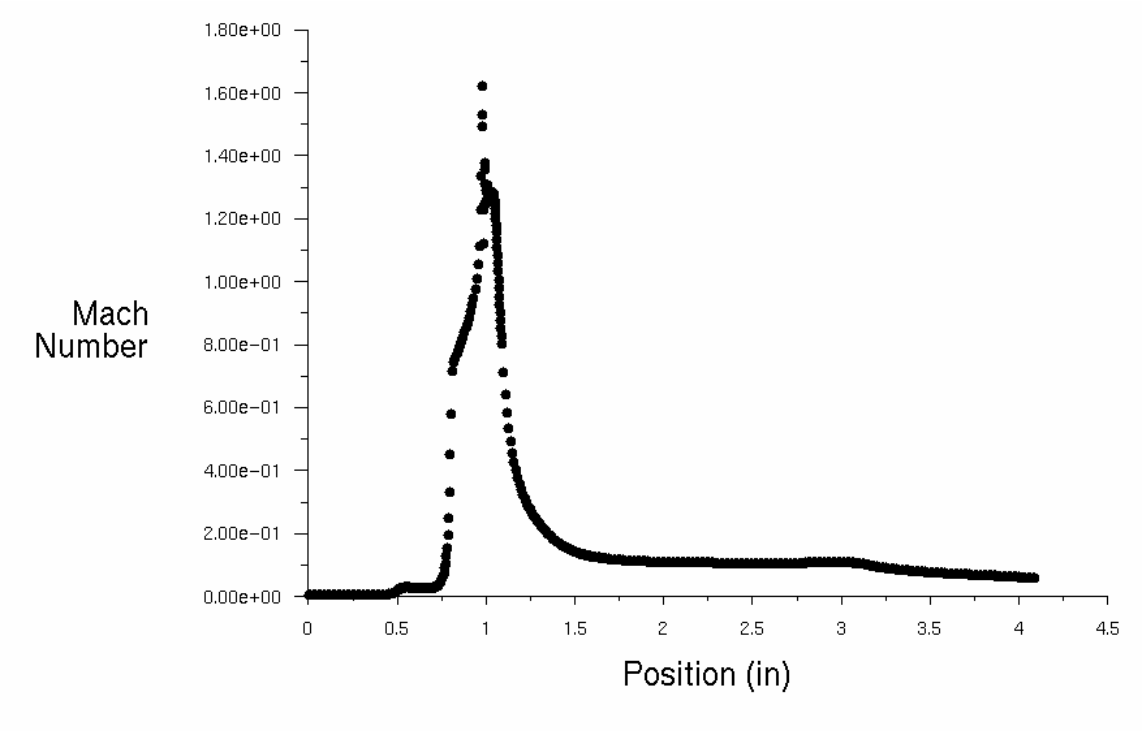

Fig. 4.17 Plot of Mach number along the centerline of gas ejector

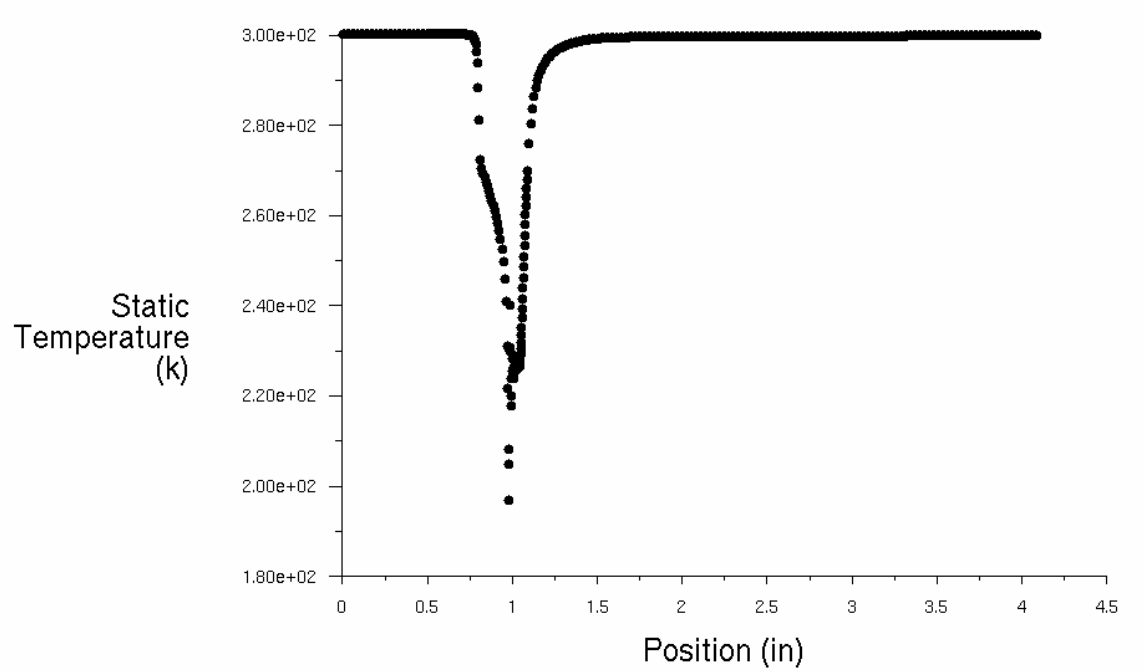

Fig. 4.18 Plot of static temperature along the centerline of gas ejector

EJECTOR DESIGN FOR SCALABLE PEM FUEL SYSTEM

Efforts have been made to design a gas ejector which meets the operating conditions of a PEM fuel cell system with gas-driven vortex separator. Fig. 4.19 shows the schematic of the PEM fuel system. Both vortex separator driving flow and gas ejector motive flow are supplied by a high pressure gas bottle. The separator gas outlet is connected to the suction port of the gas ejector. The mixed flow is then supplied to PEM fuel cell. The two-phase flow coming from the PEM fuel cell, including gas and liquid, is introduced into the vortex separator through a low pressure drop nozzle.

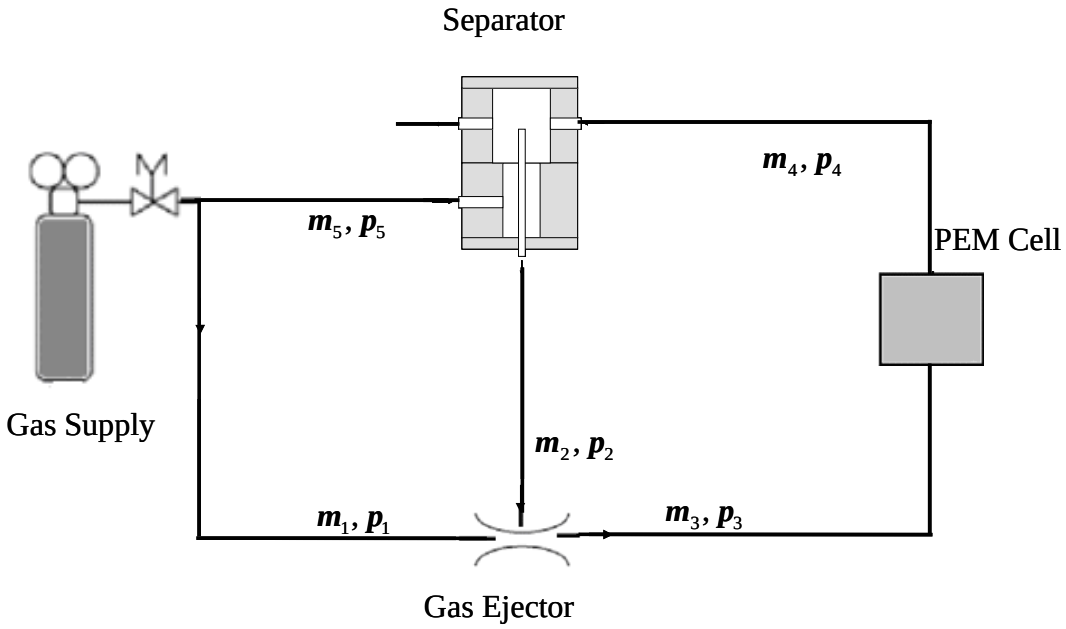

Fig. 4.19 Schematic of PEM fuel system

The constraints on gas ejector are: (1) the PEM fuel cell consuming flow rate 1.5 SLPM to 10 SLPM, (2) the lowest limit of vortex driving flow rate at 4 SLPM or less, (3) pressure recovery from ejector suction to outlet, which is equal to pressure difference (DP) from gas ejector outlet port to suction port through the PEM fuel cell. As shown in Fig. 4.20, ejector performance is very sensitive to the DP which includes the pressure drop due to tubing friction, PEM cell itself and instrumentation, etc. DP is assumed to be 0.4 psi for this design purpose. To meet with these constraints, it desirable to design an ejector that can induce at least 4 SLPM secondary flow with motive flow rate as low as possible, ideally, 1-2 SLPM, as well as 0.4 psi pressure recovery.

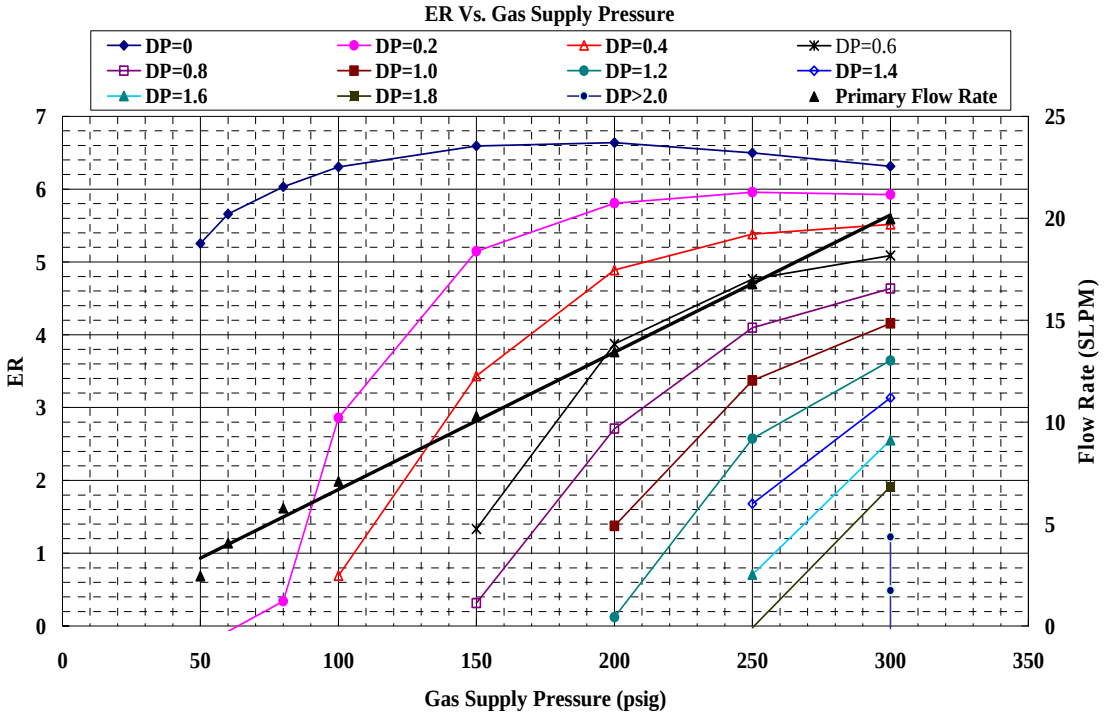

Fig. 4.20 ER sensitivity

The first step of the design is to determine the primary nozzle. To achieve the best performance, it is desired to operate ejector motive flow at supersonic speed at nozzle exit as stated previously. A convergent-divergent nozzle is adopted in order to accelerate the motive flow to supersonic. Since the motive flow is choked at nozzle throat, its flow rate is linear against supply pressure if supply gas temperature is constant. Fig. 4.21 is a plot of primary flow rate against supply pressure for various nozzle diameters.

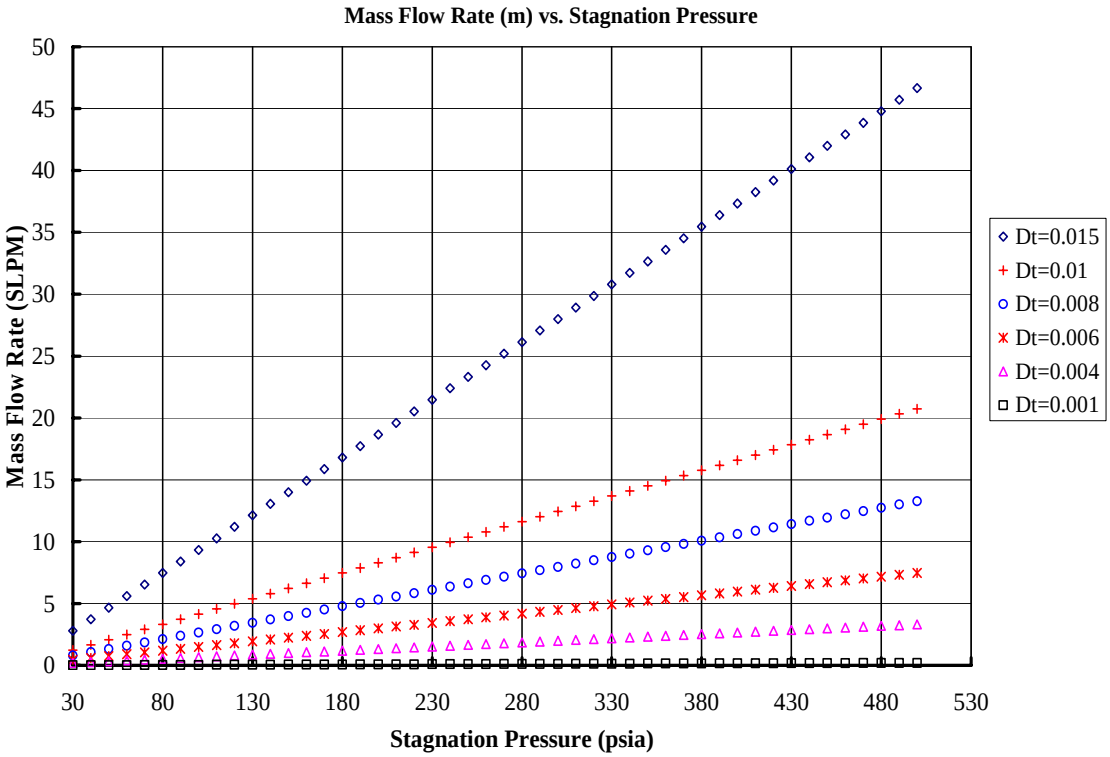

Fig. 4.21 Primary flow rate vs. gas supply pressure

An ejector with nozzle diameter $D_t = 0.013"$ and mixer diameter $D_m = 0.125"$ has been studied previously. The low limit of motive flow rate is about 7 SLPM to operate this ejector to gain 0.4 psi pressure recovery. To decrease the low limit of motive flow rate, a smaller nozzle diameter is desired. Fig. 4.22 shows the interpolation of ejector performance for the purpose of this scoping study. ER curve for $D_t = 0.013"$ is obtained by CFD simulations using FLUENT, and ER curves for other nozzles are interpolated from the $D_t = 0.013"$ curve according to the linear relationship between the motive flow rate and supply gas pressure. It is observed from Fig. 4.22 that the nozzle diameter should be $0.006"$ or smaller for the ejector to be operable within the system constraints.

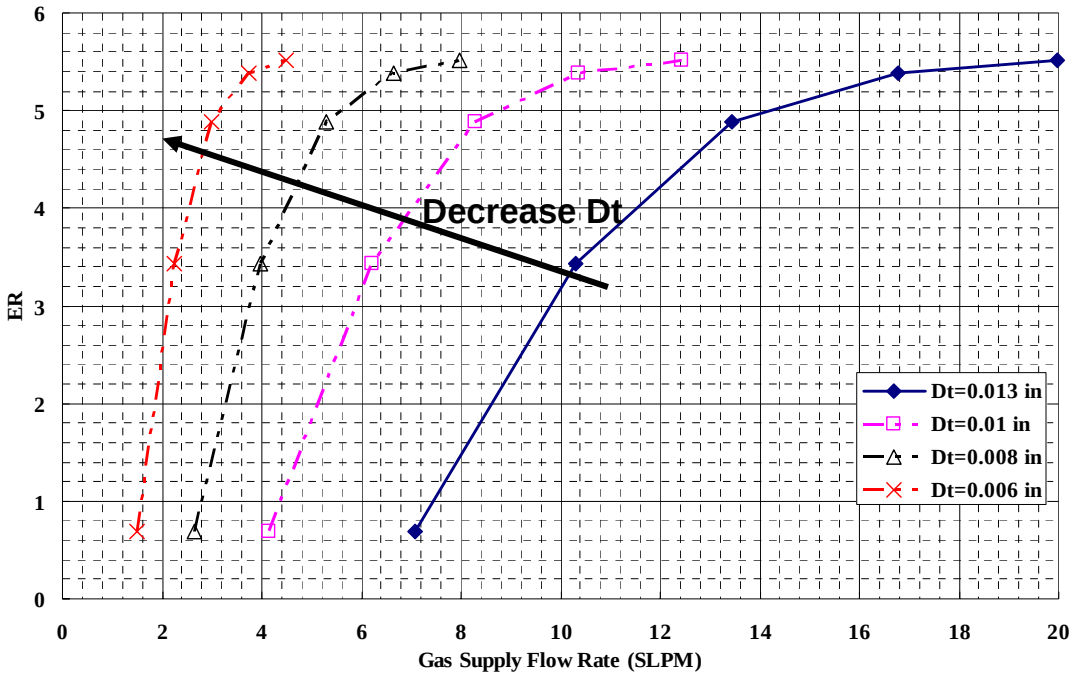

Fig. 4.22 Interpolation of ejector performance curve

According to the above analysis, ejectors with nozzle diameters of $D_t = 0.008"$, $0.007"$, $0.006"$, $0.005"$ and $0.004"$, with corresponding optimal mixer diameters ($D_m / D_t = 12$), were investigated. The investigation found that the ejector with $D_t = 0.005"$ is operable for a PEM fuel system. The geometry details of the designed ejector are shown in Fig. 4.23 and Table 4.1. The performance curve of this ejector is shown in Fig. 4.24.

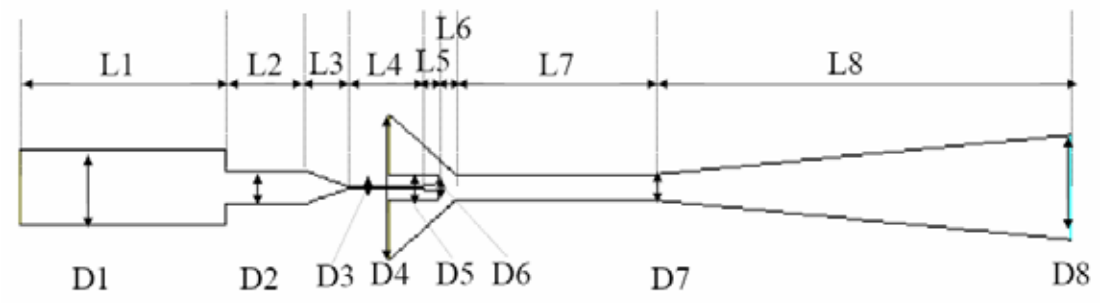

Fig. 4.23 Geometry details of designed gas ejector

Table 4.1 Geometry parameters of gas ejector with D_t=0.005”

L1 (in)	L2 (in)	L 3(in)	L4 (in)	L5 (in)	L6 (in)	L7 (in)	L8 (in)
0.5	0.2	0.1	0.17	0.05	0.04	0.5	1
D1 (in)	D2 (in)	D3 (in)	D4 (in)	D5 (in)	D6 (in)	D7 (in)	D8 (in)
0.17	0.07	0.005	0.328	0.06	0.019	0.06	0.235

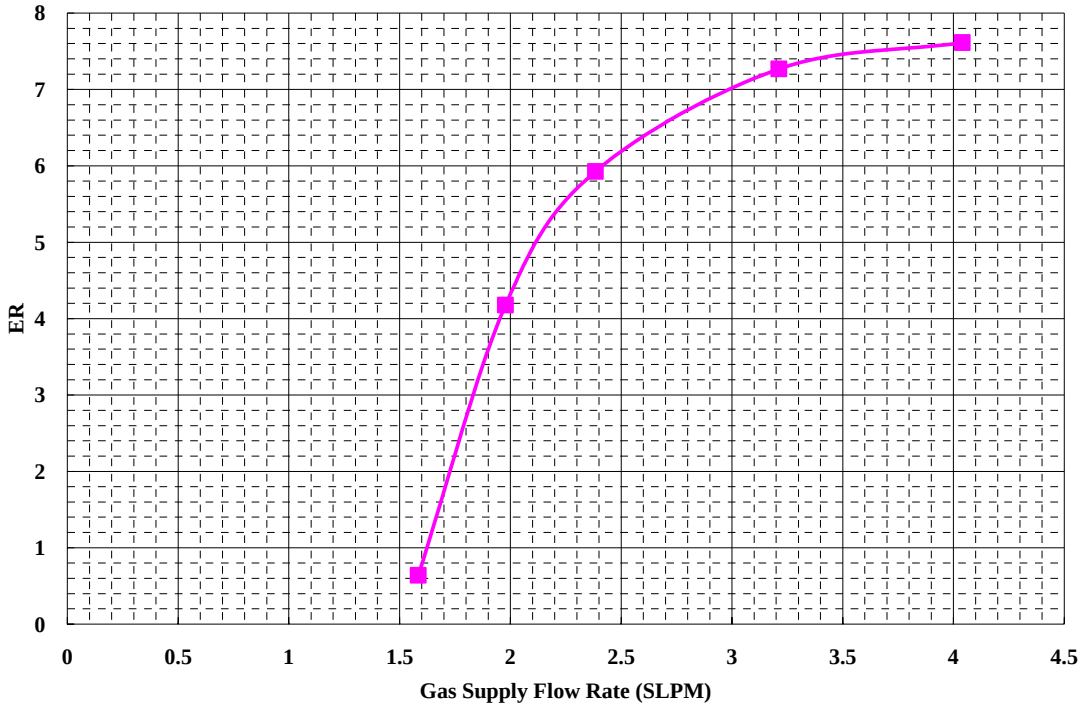

Fig. 4.24 Performance curve of designed gas ejector

Table 4.2 are the PEM fuel system operating parameters with this gas ejector design. The listed parameters, m_1, ..., m_5, and P_1, P_2, P_3 refer to those parameters in Fig. 4.19. $\dot{m}_{PEM}$ is the PEM fuel cell consuming mass flow rate.

One of the advantages of this design is that the gas ejector motive flow rate can be set to a constant value, i.e. the ejector flow would not require any active flow controls. PEM fuel cell consuming rate can be adjusted by adapting the separator driving flow rate only, which would be able to be controlled passively by a pressure regulator with external

sensing line connecting to outlet of the PEM fuel cell. This feature can greatly reduce the number of system control devices and increase the stability of system operation.

Table 4.2 PEM fuel system operating parameters

m_1 (SLPM)	2.2	2.2	2.2	2.2	2.2
m_2 (SLPM)	11.4	11.4	11.4	11.4	11.4
m_3 (SLPM)	13.6	13.6	13.6	13.6	13.6
m_4 (SLPM)	7.44	6.44	5.44	4.44	3.44
m_5 (SLPM)	4	5	6	7	8
$m_{\_PEM}$ (SLPM)	6.2	7.2	8.2	9.2	10.2
p_1 (psia)	289.2	289.2	289.2	289.2	289.2
p_2 (psia)	59.3	59.3	59.3	59.3	59.3
p_3 (psia)	59.7	59.7	59.7	59.7	59.7

CONCLUSIONS

Commercial CFD software, FLUENT, was used to simulate a gas ejector with single-phase gas flow. The simulation procedure as well as FLUENT itself was introduced in this chapter. The simulation results have very good agreement with experimental data. FLUENT was then used to optimize the ejector geometric configuration. The optimization study shows that the diameter ratio of mixing tube to throat and the primary

nozzle exit position have the most significant impact on ejector performance. The geometry parameters optimal ranges are obtained by this optimization study. The results of CFD simulations give very detailed profiles of flow field in a gas ejector, which are very helpful to understand the mixing process of the primary and secondary streams. The simulations also demonstrated that FLUENT has the ability to capture the supersonic shock waves occurring in the ejector. Also, a specific gas ejector for scalable PEM fuel system was designed as an example of using FLUENT as a design tool.

CHAPTER V

A NOVEL GENERALIZED EJECTOR MODEL

INTRODUCTION

A new 1-D generalized ejector model was developed for gas ejector design and analysis. In an important literature review, Sun and Eames [5] wrote “These advances have not been matched by the progress in constant-pressure mixing methods; ... and the question of the optimum shape of mixing section has still not been answered.” The generalized model provides an answer for this question. In the same paper, Sun and Eames also wrote “However, nobody has yet established a definite link between the performance of constant-area and constant-pressure ejectors”. This problem can also be solved by the present generalized ejector model. A definite link is established between the performance of these ejectors by using the new model.

Unlike the widely used constant-pressure model and constant-area model, this new model does not require the assumption of either constant-area mixing chamber or constant, uniform pressure in the mixing chamber. The geometry of the mixing chamber can be any configuration, and both the constant-pressure model and the constant-area model can be derived from this model as particular cases.

For most of the existing models, there are three ways to determine the static pressures at the mixing chamber entrance (P_{p1} and P_{s1} or P_1): (1) the unique design value for a given nozzle, (2) the design value corrected by coefficients obtained from experimental data for some particular ejectors, (3) arbitrarly given. In the presnet novel model, P_1 is represented by the product of two parameters, μ and τ , which relate the boundary conditions to ejector performance. The parameter τ is a parameter given as a down stream boundary condition.

The first part of this chapter is the derivation of the new model. The general features of gas ejectors are analyzed and discussed in the second part by applying this model. The third part of this chapter discusses optimal ejector performance. Definite links between the new model and the constant-pressure model, between the new model and constant-area model, as well as between the constant-pressure model and the constant-area model are established in the fourth part. The performance of constant-area ejectors and constant-pressure ejectors could be compared based on these links. The new model is employed to discuss gas ejector operation and design limitations in the fifth part. The last part is a summary section.

GENERALIZED EJECTOR MODEL

The generalized ejector model is developed for gas ejectors having the schematic as shown in Fig. 5.1. Similar to the constant-pressure ejector, these ejectors could be

divided into four sections, i.e., supersonic primary nozzle, mixing chamber, constant-area section and subsonic diffuser. In practical applications, the subsonic diffuser may or may not be installed. Different from the constant-pressure mixing ejector, the area ratio of mixing chamber entrance to mixing chamber exit can be any given value as long as it is not less than unity. If this area ratio is equal to unity, it becomes the constant-area mixing ejector.

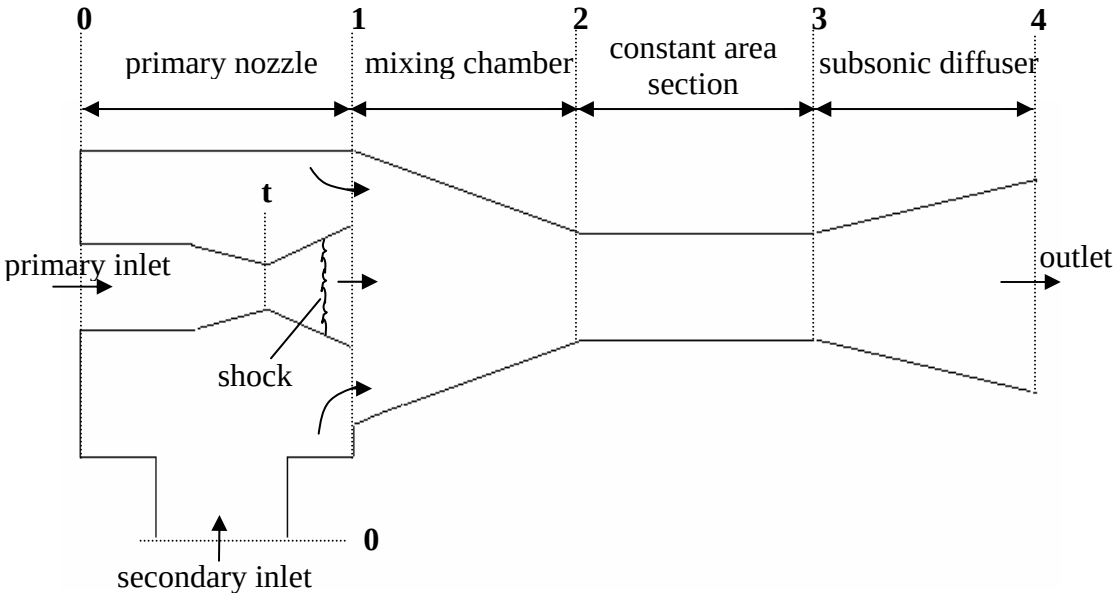

Fig. 5.1 Schematic of generalized ejector model

As discussed in previous chapters, the geometry of the primary nozzle determines a unique nozzle exit static pressure, but practical ejectors are usually not operated at this design point. It is very difficult to determine the exact value of nozzle exit static pressure. Some researchers use the design value to calculate the optimal ejector performance, and

others use coefficients obtained from experimental data for some particular ejectors to correct the design values, while some researchers use arbitrary values to calculate a range of the ejector performance.

In practical operation, a shock will happen due to under-expansion or over-expansion. The under-expansion shock usually happens at the nozzle exit. The over-expansion shock may occur in the nozzle supersonic part or at the nozzle exit. If the shock occurs in the nozzle due to overexpansion, separation may also happen in the nozzle. There is no way to determine the exact location of the overexpansion shock. In this model, it is assumed that $P_{p1} = P_{s1} = P_1$. P_1 will be calculated by entropy analysis or determined by the given down stream operational conditions. A parameter μ is used to relate P_1 with secondary supply pressure P_{s0}. μ is defined by Equation (5.1).

$$\mu = \frac{P_1}{P_{s0}} \tag{5.1}$$

Therefore,

$$P_{p1} = P_{s1} = P_1 = \mu P_{s0} \tag{5.2}$$

The following assumptions are made for the generalized ejector model.

1) The inner wall of the ejector is adiabatic.
2) Friction loss is negligible.
3) The flow streams are uniform 1-D and in steady state.
4) Gases are in stagnation at the primary inlet and suction port.

5) The secondary flow is not supersonic.
6) The primary stream and secondary stream have the same static pressure at the entrance of the mixing chamber, i.e., $P_{p1} = P_{s1} = P_1$
7) The mixed flow is subsonic.
8) Both primary stream and secondary stream can be considered as perfect gases with constant specific heat ratio γ.

Mixing Chamber Entrance Flow Properties

It is reasonable to assume that the secondary stream expands from suction port to the mixing chamber entrance isentropically. According to Equation (2.9), the secondary stream pressure ratio, P_1/P_{s0}, is related to the Mach number M_{s1} by Equation (5.3).

$$\frac{P_1}{P_{s0}} = \mu = \left(1 + \frac{\gamma_s - 1}{2} M_{s1}^2\right)^{\frac{-\gamma_s}{\gamma_s - 1}} \tag{5.3}$$

Rearranging the above equation,

$$M_{s1}^2 = \frac{2}{\gamma_s - 1}\left(\mu^{\frac{\gamma_s}{\gamma_s - 1}} - 1\right) \tag{5.4}$$

Substituting M_{s1} expressed by Equation (5.4) into Equation (2.10), the secondary stream temperature ratio, T_{s1}/T_{s0}, is expressed in Equation (5.5).

$$\frac{T_{s1}}{T_{s0}} = \left(1 + \frac{\gamma_s - 1}{2} M_{s1}^2\right)^{-1} = \mu^{\frac{\gamma_s - 1}{\gamma_s}} \tag{5.5}$$

If the primary nozzle is operated at its design condition, the primary flow experiences isentropic expansion from the nozzle throat to the nozzle exit. The isentropic Mach number M_{p1i} can be obtained by solving Equation (5.6) and the static pressure P_{p1i} is given by Equation (5.7).

$$\frac{A_{p1}}{A_t} = \frac{1}{M_{p1i}} \sqrt{\left(\frac{1 + \frac{\gamma_p - 1}{2} M_{p1i}^2}{\frac{\gamma_p + 1}{2}}\right)^{\frac{\gamma_p + 1}{\gamma_p - 1}}} \tag{5.6}$$

$$\frac{P_{p1i}}{P_{p0}} = \left(1 + \frac{\gamma_p - 1}{2} M_{p1i}^2\right)^{-\frac{\gamma_p}{\gamma_p - 1}} \tag{5.7}$$

If the nozzle is operated under off-design conditions, the shock will occur in the nozzle or at the nozzle exit. The subscript x represents the flow properties after the shock. The primary stream static pressure and Mach number at the nozzle exit are $P_{p1} = P_1 = \mu P_{s0}$ and M_{p1}, respectively. For off-design operations, $P_{p1} \neq P_{p1i}$ and $M_{p1} \neq M_{p1i}$. After the shock, the total pressure will change $P_{p0i} \neq P_{p0x}$, but the stagnation temperature will not change $T_{p0i} = T_{p0x} = T_{p0}$ since it is an adiabatic process. M_{p1} can be related to P_{p1} by the mass conservation equation. The primary mass flow rate is given by Equation (2.17).

$$m_p = \frac{P_{p0} A_t}{\sqrt{T_0}} \sqrt{\frac{\gamma_p}{R_p} \left(\frac{2}{\gamma_p + 1} \right)^{\frac{\gamma_p + 1}{\gamma_p - 1}}} \tag{2.17}$$

According to Equation (3.11), the definition of mass flow function $f_2(\gamma, M)$, mass flow rate can also be expressed by Equation (3.14).

$$f_2(\gamma, M) \equiv M \left[\gamma \left(1 + \frac{\gamma - 1}{2} M^2 \right) \right]^{\frac{1}{2}} \tag{3.11}$$

$$m = \frac{PA}{(RT_0)^{\frac{1}{2}}} f_2(\gamma, M) \tag{3.14}$$

Therefore,

$$\frac{P_{p1} A_{p1}}{(R_p T_{p0})^{\frac{1}{2}}} f_2(\gamma_p, M_{p1}^2) = \frac{P_{p0} A_t}{(R_p T_{p0})^{\frac{1}{2}}} \left(\gamma_p \left(\frac{2}{\gamma_p + 1} \right)^{\frac{\gamma_p + 1}{\gamma_p - 1}} \right)^{\frac{1}{2}} \tag{5.8}$$

Substitute $P_{p1} = \mu P_{s0}$ into the above equation and rearrange into the following form:

$$f_2(\gamma_p, M_{p1}^2) = \frac{P_{p0} A_t}{\mu P_{s0} A_{p1}} \left(\gamma_p \left(\frac{2}{\gamma_p + 1} \right)^{\frac{\gamma_p + 1}{\gamma_p - 1}} \right)^{\frac{1}{2}} \tag{5.9}$$

According to Equation (3.11), the definition of mass flow function $f_2(\gamma, M)$,

$$M_{p1}\left(\left(1+\frac{\gamma_p-1}{2}M_{p1}^2\right)\right)^{\frac{1}{2}}=\frac{P_{p0}A_t}{\mu P_{s0}A_{p1}}\left(\left(\frac{2}{\gamma_p+1}\right)^{\frac{\gamma_p+1}{\gamma_p-1}}\right)^{\frac{1}{2}} \tag{5.10}$$

Rearranging the above equation,

$$\left(\gamma_p-1\right)\mu^2M_{p1}^4+2\mu^2M_{p1}^2-2\left(\frac{P_{p0}A_t}{P_{s0}A_{p1}}\right)^2\left(\frac{2}{\gamma_p+1}\right)^{\frac{\gamma_p+1}{\gamma_p-1}}=0 \tag{5.11}$$

$$M_{p1}^2=\frac{-\mu+\sqrt{\mu^2+2\left(\gamma_p-1\right)\left(\frac{P_{p0}A_t}{P_{s0}A_{p1}}\right)^2\left(\frac{2}{\gamma_p+1}\right)^{\frac{\gamma_p+1}{\gamma_p-1}}}}{\left(\gamma_p-1\right)\mu} \tag{5.12}$$

The primary stream total pressure after the shock wave can be expressed by the following equation.

$$P_{p0x}=P_{p1}\left(1+\frac{\gamma_p-1}{2}M_{p1}^2\right)^{\frac{\gamma_p}{\gamma_p-1}}=\mu P_{s0}\left(1+\frac{\gamma_p-1}{2}M_{p1}^2\right)^{\frac{\gamma_p}{\gamma_p-1}} \tag{5.13}$$

The ratio of total pressure before shock to total pressure after the shock is

$$\frac{P_{p0i}}{P_{p0x}}=\frac{P_{p0}}{\mu P_{s0}\left(1+\frac{\gamma_p-1}{2}M_{p1}^2\right)^{\frac{\gamma_p}{\gamma_p-1}}} \tag{5.14}$$

Momentum Conservation Equation

The momentum conservation equation over a control volume shown in Fig. 5.2 is solved to find M_{m2}^2, the Mach number at the mixing chamber exit. Equation (5.15) is the 1-D, x-direction momentum equation expressed in Mach numbers.

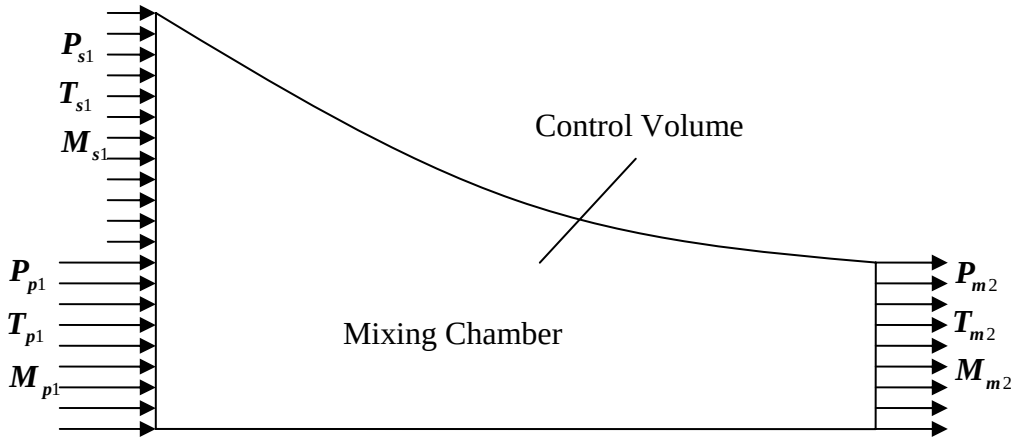

Fig. 5.2 Control volume of mixing chamber for generalized ejector model

$$P_{p1}A_{p1}\left(1+\gamma_p M_{p1}^2\right)+P_{s1}A_{s1}\left(1+\gamma_s M_{s1}^2\right)=P_{m2}A_{m2}\left(1+\gamma_m M_{m2}^2\right) \tag{5.15}$$

Rearranging Equation (5.15),

$$\frac{\mu P_{s0}A_{p1}}{P_{m2}A_{m2}}\left(1+\gamma_p M_{p1}^2\right)+\frac{\mu P_{s0}A_{s1}}{P_{m2}A_{m2}}\left(1+\gamma_s M_{s1}^2\right)=\left(1+\gamma_m M_{m2}^2\right) \tag{5.16}$$

Define a pressure ratio parameter τ ,

$$\tau \equiv \frac{P_{s0}}{P_{m2}} \tag{5.17}$$

Rearranging Equation (5.16), the M_{m2}^2 can be expressed in Equation (5.18).

$$M_{m2}^2 = \frac{D\mu\tau - 1}{\gamma_m} \tag{5.18}$$

Where,

$$D = \frac{A_{p1}}{A_{m2}}\left(1+\gamma_p M_{p1}^2\right) + \frac{A_{s1}}{A_{m2}}\left(1+\gamma_s M_{s1}^2\right) \tag{5.19}$$

There are two unknown variables, μ and τ , in the expression of M_{m2}^2. It is desired to express one of these variables as a function depending on the other variable. To find such a function, the mass conservation equation is used. The mass flow rate at the mixing chamber exit is related to the mass flow rate of the secondary stream by Equation (5.20).

$$\frac{m_m}{m_s} = \frac{1+\omega}{\omega} = \frac{P_{m2}A_{m2}}{P_{s1}A_{s1}} \frac{\left(R_s T_{s0}\right)^{\frac{1}{2}}}{\left(R_m T_{m0}\right)^{\frac{1}{2}}} \frac{f_2\left(\gamma_m, M_{m2}\right)}{f_2\left(\gamma_s, M_{s1}\right)} \tag{5.20}$$

According to the definitions of μ and τ , Equation (5.21) can be readily obtained.

$$\frac{1+\omega}{\omega}=\frac{1}{\mu\tau}\frac{A_{m2}}{A_{s1}}\frac{\left(R_sT_{s0}\right)^{\frac{1}{2}}}{\left(R_mT_{m0}\right)^{\frac{1}{2}}}\frac{f_2\left(\gamma_m,M_{m2}\right)}{f_2\left(\gamma_s,M_{s1}\right)} \tag{5.21}$$

Substituting the expression of $f_2\left(\gamma_m,M_{m2}\right)$ into Equation (5.21) and rearranging,

$$\frac{1+\omega}{\omega}\mu\tau=EM_{m2}\left[\gamma_m\left(1+\frac{\gamma_m-1}{2}M_{m2}^2\right)\right]^{\frac{1}{2}} \tag{5.22}$$

Where,

$$E=\frac{A_{m2}}{A_{s1}}\frac{\left(R_sT_{s0}\right)^{\frac{1}{2}}}{\left(R_mT_{m0}\right)^{\frac{1}{2}}}\frac{1}{f_2\left(\gamma_s,M_{s1}\right)} \tag{5.23}$$

Substituting the M_{m2} expressed by Equation (5.18) into Equation (5.22), the following equation is obtained.

$$\left(\frac{1+\omega}{\omega}\frac{\mu\tau}{E}\right)^2=\left(D\mu\tau-1\right)\left[1+\frac{\gamma_m-1}{2\gamma_m}\left(D\mu\tau-1\right)\right] \tag{5.24}$$

Rearrange the above equation in the following form,

$$\left[2\gamma_m\left(\frac{1+\omega}{\omega}\frac{\mu}{E}\right)^2-\left(\gamma_m-1\right)D^2\mu^2\right]\tau^2-2D\mu\tau+\left(\gamma_m+1\right)=0 \tag{5.25}$$

In Equation (5.25), variable τ has two solutions. Correspondingly, the M_{m2}^2 also has two solutions. Further calculations show that one of them corresponding to the

supersonic mixed flow and the other one is a stable, subsonic solution. In this study, the supersonic solution is discarded.

$$\tau = \frac{D - \sqrt{D^2 - \left[2\gamma_m \left(\frac{1+\omega}{\omega}\frac{1}{E}\right)^2 - (\gamma_m - 1)D^2\right](\gamma_m + 1)}}{2\gamma_m \left(\frac{1+\omega}{\omega}\frac{1}{E}\right)^2 \mu - (\gamma_m - 1)D^2\mu} \tag{5.26}$$

Substituting the expression for τ into Equation (5.18), the Mach number at the mixing chamber exit, M_{m2}^2, is given by following equation.

$$M_{m2}^2 = \frac{D}{\gamma_m}\frac{D - \sqrt{D^2 - \left[2\gamma_m \left(\frac{1+\omega}{\omega}\frac{1}{E}\right)^2 - (\gamma_m - 1)D^2\right](\gamma_m + 1)}}{2\gamma_m \left(\frac{1+\omega}{\omega}\frac{1}{E}\right)^2 - (\gamma_m - 1)D^2} - \frac{1}{\gamma_m} \tag{5.27}$$

With the knowledge of τ and M_{m2}, the parameters P_1/P_{m2} and T_{m2}/T_{p1} can be calculated by using their relationship with these two parameters.

$$\frac{P_1}{P_{m2}} = \frac{P_1}{P_{s0}}\frac{P_{s0}}{P_{m2}} = \mu\tau \tag{5.28}$$

$$\frac{P_1}{P_{m2}} = \frac{D - \sqrt{D^2 - \left[2\gamma_m \left(\frac{1+\omega}{\omega}\frac{1}{E}\right)^2 - (\gamma_m - 1)D^2\right](\gamma_m + 1)}}{2\gamma_m \left(\frac{1+\omega}{\omega}\frac{1}{E}\right)^2 - (\gamma_m - 1)D^2} \tag{5.29}$$

$$\frac{T_{m2}}{T_{p1}} = \frac{T_{m0}}{T_{p0}} \frac{T_{p0}}{T_{p1}} \Bigg/ \left(1 + \frac{\gamma_m - 1}{2} M_{m2}^2 \right) \tag{5.30}$$

Entrainment Ratio And Area Ratio

In previous derivations, entrainment ratio ω is treated as a known value. Actually, ω is determined by the flow properties at the entrance of the mixing chamber if the mixing chamber geometry configuration is given. For the 1-D analytical model, the mixing chamber geometry configuration can be represented by two area ratio parameters, κ and θ, which are defined by following equations.

$$\kappa \equiv \frac{A_{m2}}{A_t} \tag{5.31}$$

$$\theta \equiv \frac{A_1}{A_{m2}} \tag{5.32}$$

All dimensions of the mixing chamber are determined by the given parameters of primary nozzle geometry together with κ and θ.

$$\frac{A_{m2}}{A_{p1}} = \kappa \frac{A_t}{A_{p1}} \tag{5.33}$$

According to the definition of θ given by Equation (5.32),

$$\theta = \frac{A_{p1} + A_{s1}}{A_{m2}} = \frac{1 + A_{s1}/A_{p1}}{A_{m2}/A_{p1}} \tag{5.34}$$

Therefore,

$$\frac{A_{s1}}{A_{p1}} = \frac{A_t}{A_{p1}}\kappa\theta - 1 \tag{5.35}$$

According to its definition, ω is given by the following equation.

$$\omega = \frac{m_s}{m_p} = \frac{\dfrac{P_{s1}A_{s1}}{\left(R_sT_{s0}\right)^{\frac{1}{2}}} f_2\left(\gamma_s, M_{s1}\right)}{\dfrac{P_{p1}A_{p1}}{\left(R_pT_{p0}\right)^{\frac{1}{2}}} f_2\left(\gamma_p, M_{p1}\right)} \tag{5.36}$$

Since $P_{p1} = P_{s1}$, Equation (5.36) can be simplified and rearranged to Equation (5.37).

$$\omega = \frac{A_{s1}}{A_{p1}}\left(\frac{R_pT_{p0}}{R_sT_{s0}}\right)^{\frac{1}{2}} \frac{f_2\left(\gamma_s, M_{s1}\right)}{f_2\left(\gamma_p, M_{p1}\right)} \tag{5.37}$$

Substituting the expression of A_{s1}/A_{p1} into Equation (5.37), ω is related to κ and θ as well as the Mach numbers of each stream.

$$\omega = \left(\frac{A_t}{A_{p1}}\kappa\theta - 1\right)\left(\frac{R_pT_{p0}}{R_sT_{s0}}\right)^{\frac{1}{2}} \frac{f_2\left(\gamma_s, M_{s1}\right)}{f_2\left(\gamma_p, M_{p1}\right)} \tag{5.38}$$

Entropy Change

The total entropy change includes (1) the entropy change due to the primary stream shock, and (2) the entropy change due to the mixing of the two streams.

$$\Delta s = \Delta s_x + \Delta s_m \tag{5.39}$$

Where, Δs_x is the entropy change due to the primary stream shock; Δs_m is entropy change due to the two streams mixing.

$$\Delta s = \frac{m_p \left(\Delta s\big|_p^{p1i \to p1} + \Delta s\big|_p^{p1 \to m2} \right) + m_p \, \Delta s\big|_s^{s1 \to m2}}{m_m} \tag{5.40}$$

Considering mass conservation and the definition of ER, $\omega = m_s / m_p$, Equation (5.40) can be rewritten as:

$$\Delta s = \frac{1}{1+\omega} \Delta s\big|_p^{p1i \to p1} + \frac{1}{1+\omega} \Delta s\big|_p^{p1 \to m2} + \frac{\omega}{1+\omega} \Delta s\big|_s^{s1 \to m2} \tag{5.41}$$

Th definition of entropy is

$$ds = \frac{dq}{T} = \frac{du + Pdv}{T} \tag{5.42}$$

Substituting the ideal gas law to Equation (5.42), the following equation can be derived.

$$ds = c_v d\left[\ln\left(Pv^{\gamma} \right) \right] \tag{5.43}$$

The entropy change of a stream experiencing a certain process from state *a* to state *b* can be obtained by integrating Equation (5.43).

$$\Delta s\Big|_{a\to b} = R\ln\left[\frac{P_a}{P_b}\left(\frac{T_b}{T_a}\right)^{\frac{\gamma}{\gamma-1}}\right] \tag{5.44}$$

According to Equation (5.44),

$$\Delta s\Big|_{p}^{p1i\to p1} = R_p \ln\left[\frac{P_{p1i}}{P_{p1}}\left(\frac{T_{p1}}{T_{p1i}}\right)^{\frac{\gamma_p}{\gamma_p-1}}\right] \tag{5.45}$$

$$\Delta s\Big|_{p}^{p1i\to p1} = R_p \ln\left[\frac{P_{p0i}}{P_{p0x}}\left(\frac{T_{p0i}}{T_{p1i}}\right)^{-\frac{\gamma_p}{\gamma_p-1}}\left(\frac{T_{p0x}}{T_{p1}}\right)^{\frac{\gamma_p}{\gamma_p-1}}\left(\frac{T_{p1}}{T_{p1i}}\right)^{\frac{\gamma_p}{\gamma_p-1}}\right] \tag{5.46}$$

Equation (5.46) can be simplified to Equation (5.47)

since it is an adiabatic process and stagnation temperature will not change, i.e., $T_{p0i} = T_{p0x} = T_{p0}$.

$$\Delta s\Big|_{p}^{p1i\to p1} = R_p \ln\left(\frac{P_{p0i}}{P_{p0x}}\right) \tag{5.47}$$

P_{p0i}/P_{p0x} is given by Equation (5.14). Substituting Equation (5.14) into Equation (5.47) an explicit expression of $\Delta s\Big|_{p}^{p1i\to p1}$ with respect to the variable μ is derived.

$$\Delta s\Big|_{p}^{p1i\to p1} = R_p\left\{\ln\left(\frac{P_{p0}}{P_{s0}}\right)+\ln\left(\frac{1}{\mu}\right)-\frac{\gamma_p}{\gamma_p-1}\ln\left(1+\frac{\gamma_p-1}{2}M_{p1}^2\right)\right\} \tag{5.48}$$

Similarly,

$$\Delta s\Big|_{p}^{p1\to m2} = R_p\ln\left[\frac{P_{p1}}{P_{m2}}\left(\frac{T_{m2}}{T_{p1}}\right)^{\frac{\gamma_p}{\gamma_p-1}}\right] \tag{5.49}$$

$$\Delta s\Big|_{s}^{s1\to m2} = R_s\ln\left[\frac{P_{s1}}{P_{m2}}\left(\frac{T_{m2}}{T_{s1}}\right)^{\frac{\gamma_s}{\gamma_s-1}}\right] \tag{5.50}$$

Considering $P_{p1} = P_{s1} = P_1$ and substituting Equations (5.49), (5.50) into Equations (5.39) (5.41), Δs_m is given by the following equation.

$$\Delta s_m = \frac{1}{1+\omega}\left\{\begin{array}{l}\left(R_p+\omega R_s\right)\ln\left(\frac{P_1}{P_{m2}}\right)+\omega R_s\frac{\gamma_s}{\gamma_s-1}\ln\left(\frac{T_{p1}}{T_{s1}}\right)\\ +\left(R_p\frac{\gamma_p}{\gamma_p-1}+\omega R_s\frac{\gamma_s}{\gamma_s-1}\right)\ln\left(\frac{T_{m2}}{T_{p1}}\right)\end{array}\right\} \tag{5.51}$$

To calculate Δs_m using Equation (5.51), it is necessary to find the expressions for P_1/P_{m2} , T_{p1}/T_{s1} and T_{m2}/T_{p1} . T_{p1}/T_{s1} may be expanded as Equation (5.52), while P_1/P_{m2} and T_{m2}/T_{p1} are given by Equations (5.29) and (5.30).

$$\frac{T_{p1}}{T_{s1}} = \frac{T_{p1}}{T_{p0}} \frac{T_{p0}}{T_{s0}} \frac{T_{s0}}{T_{s1}} \tag{5.52}$$

Where,

$$\frac{T_{p1}}{T_{p0}} = \left(1 + \frac{\gamma_p - 1}{2} M_{p1}^2\right)^{-1} \tag{5.53}$$

$$\frac{T_{s0}}{T_{s1}} = \left(1 + \frac{\gamma_s - 1}{2} M_{s1}^2\right) \tag{5.54}$$

Find μ by Entropy Minimization

Should there exist a minimum value of total entropy change, a μ value corresponding to the ejector optimal performance could be found. A curve of total entropy change with respect to the μ values is plotted in Fig. 5.3. In the physically meaningful range of $0 < \mu < 1$, the total entropy change curve does have a minimum point. This optimal value of μ is found at the point of $d(\Delta s)/d\mu = 0$.

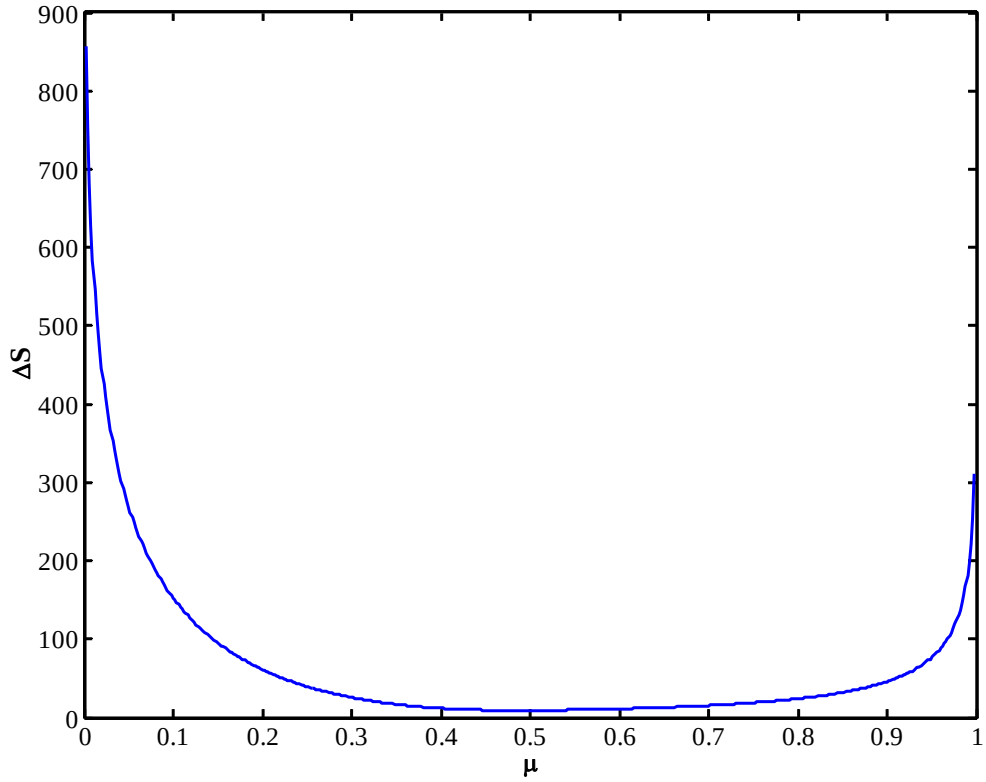

Fig. 5.3 Plot of total entropy change with respect to μ

Differentiating the total entropy change function Δs respect to μ is the first step to find the optimal μ value.

$$\frac{d(\Delta s)}{d\mu} = \frac{d(\Delta s_x)}{d\mu} + \frac{d(\Delta s_m)}{d\mu} \tag{5.55}$$

$$\frac{d(\Delta s_x)}{d\mu} = \frac{1}{1+\omega}\left[\frac{d}{d\mu}\left(\Delta s\big|_p^{p1i\to p1}\right) - \Delta s_x \frac{d\omega}{d\mu}\right] \tag{5.56}$$

Assuming the parameter P_1/P_{m2} be a constant respect to μ, since it only weakly depends on μ.

$$\frac{d(\Delta s_m)}{d\mu}=\frac{1}{1+\omega}\left\{\frac{\omega R_s\gamma_s}{\gamma_s-1}\frac{d}{d\mu}\left[\ln\left(\frac{T_{p1}}{T_{s1}}\right)\right]+\left(\frac{R_p\gamma_p}{\gamma_p-1}+\frac{\omega R_s\gamma_s}{\gamma_s-1}\right)\frac{d}{d\mu}\left[\ln\left(\frac{T_{m2}}{T_{p1}}\right)\right]\right\} + \frac{1}{1+\omega}\left\{R_s\ln\left(\frac{P_1}{P_{m2}}\right)+R_s\frac{\gamma_s}{\gamma_s-1}\ln\left(\frac{T_{m2}}{T_{s1}}\right)-\Delta s_m\right\}\frac{d\omega}{d\mu} \tag{5.57}$$

Each derivative component in Equation (5.56) and Equation (5.57) is given in following.

1) $\dfrac{d}{d\mu}\left(\Delta s\big|_p^{p1i\to p1}\right)$

$$\frac{d}{d\mu}\left(\Delta s\big|_p^{p1i\to p1}\right)=-R_p\left\{\frac{1}{\mu}+\frac{\gamma_p}{2+(\gamma_p-1)M_{p1}^2}\frac{d}{d\mu}\left(M_{p1}^2\right)\right\} \tag{5.58}$$

Where,

$$\frac{d}{d\mu}\left(M_{p1}^2\right)=\frac{-2\left(\dfrac{P_{p0}A_{pt}}{P_{s0}A_{p1}}\right)^2\left(\dfrac{2}{\gamma_p+1}\right)^{\frac{\gamma_p+1}{\gamma_p-1}}\mu^{-3}}{\sqrt{1+2(\gamma_p-1)\left(\dfrac{P_{p0}A_{pt}}{P_{s0}A_{p1}}\right)^2\left(\dfrac{2}{\gamma_p+1}\right)^{\frac{\gamma_p+1}{\gamma_p-1}}\dfrac{1}{\mu^2}}} \tag{5.59}$$

2) $\dfrac{d\omega}{d\mu}$

$$\frac{d\omega}{d\mu}=\omega\left\{\frac{\frac{d}{d\mu}f_2\left(\gamma_s,M_{s1}\right)}{f_2\left(\gamma_s,M_{s1}\right)}-\frac{\frac{d}{d\mu}f_2\left(\gamma_p,M_{p1}\right)}{f_2\left(\gamma_p,M_{p1}\right)}\right\} \tag{5.60}$$

It can be shown that,

$$\frac{d}{d\mu}f_2\left(\gamma,M\right)=\frac{1}{2}\left[\frac{1}{M^2}+\frac{\gamma-1}{2+\left(\gamma-1\right)M^2}\right]f_2\left(\gamma,M\right)\frac{d}{d\mu}\left(M^2\right) \tag{5.61}$$

Therefore,

$$\frac{d\omega}{d\mu}=\frac{\omega}{2}\left\{\begin{array}{l}\left[\frac{\gamma_s-1}{2+\left(\gamma_s-1\right)M_{s1}^2}+\frac{1}{M_{s1}^2}\right]\frac{d}{d\mu}\left(M_{s1}^2\right)\\-\left[\frac{\gamma_p-1}{2+\left(\gamma_p-1\right)M_{p1}^2}+\frac{1}{M_{p1}^2}\right]\frac{d}{d\mu}\left(M_{p1}^2\right)\end{array}\right\} \tag{5.62}$$

Where,

$$\frac{d}{d\mu}\left(M_{s1}^2\right)=-\frac{2}{\gamma_s}\mu^{\frac{-2\gamma_s+1}{\gamma_s}} \tag{5.63}$$

3) $\frac{d}{d\mu}\left[\ln\left(\frac{T_{p1}}{T_{s1}}\right)\right]$

$$\frac{d}{d\mu}\left[\ln\left(\frac{T_{p1}}{T_{s1}}\right)\right]=\frac{d}{d\mu}\left[\ln\left(\frac{T_{p1}}{T_{p0}}\frac{T_{p0}}{T_{s0}}\frac{T_{s0}}{T_{s1}}\right)\right]=\frac{d}{d\mu}\ln\left(\frac{T_{p1}}{T_{p0}}\right)+\frac{d}{d\mu}\ln\left(\frac{T_{s0}}{T_{s1}}\right) \tag{5.64}$$

The two parts of Equation (5.64) are presented by Equations (5.65) and (5.66).

$$\frac{d}{d\mu}\ln\left(\frac{T_{p1}}{T_{p0}}\right)=\left(1+\frac{\gamma_p-1}{2}M_{p1}^2\right)\frac{\gamma_p-1}{2}\frac{d}{d\mu}\left(M_{p1}^2\right) \tag{5.65}$$

$$\frac{d}{d\mu}\ln\left(\frac{T_{s0}}{T_{s1}}\right)=\left(1+\frac{\gamma_s-1}{2}M_{s1}^2\right)^{-1}\frac{\gamma_s-1}{2}\frac{d}{d\mu}\left(M_{s1}^2\right) \tag{5.66}$$

Therefore, the term of $\frac{d}{d\mu}\left[\ln\left(\frac{T_{p1}}{T_{s1}}\right)\right]$ can be expressed as Equation (5.67).

$$\begin{aligned}\frac{d}{d\mu}\left[\ln\left(\frac{T_{p1}}{T_{s1}}\right)\right]=&\left(1+\frac{\gamma_p-1}{2}M_{p1}^2\right)\frac{\gamma_p-1}{2}\frac{d}{d\mu}\left(M_{p1}^2\right)\\&+\left(1+\frac{\gamma_s-1}{2}M_{s1}^2\right)^{-1}\frac{\gamma_s-1}{2}\frac{d}{d\mu}\left(M_{s1}^2\right)\end{aligned} \tag{5.67}$$

4) $\frac{d}{d\mu}\left[\ln\left(\frac{T_{m2}}{T_{p1}}\right)\right]$

$$\frac{d}{d\mu}\left[\ln\left(\frac{T_{m2}}{T_{p1}}\right)\right]=-\frac{d}{d\mu}\ln\left(\frac{T_{p1}}{T_{p0}}\right)+\left(1+\frac{\gamma_m-1}{2}M_{m2}^2\right)\frac{\gamma_m-1}{2}\frac{d}{d\mu}\left(M_{m2}^2\right) \tag{5.68}$$

Where,

$$\frac{d}{d\mu}\left(M_{m2}^2\right)=\frac{1}{\gamma_m}\left(\frac{P_1}{P_{m2}}\right)\left[\frac{A_{p1}}{A_{m2}}\gamma_p\frac{d}{d\mu}\left(M_{p1}^2\right)+\frac{A_{s1}}{A_{m2}}\gamma_s\frac{d}{d\mu}\left(M_{s1}^2\right)\right] \tag{5.69}$$

The μ value corresponding to the minimum total entropy change is one of the solutions of Equation (5.70). It is very difficult if not impossible to solve Equation (5.70)

analytically due to the complexity of the equation itself. Numerical approaches may be used to find the solutions of Equation (5.70).

$$\frac{d(\Delta s)}{d\mu} = 0 \tag{5.70}$$

GENERAL FEATURES OF GENERALIZED EJECTOR MODEL

Entropy change is a function of variable μ if the ejector geometry and the boundary conditions are given. The specified geometric parameters are A_t and A_{p1}/A_t for the primary nozzle and κ and θ for the mixing chamber. The given boundary conditions are the stagnation pressure and temperature at the inlets, i.e., P_{p0}, T_{p0}, P_{s0} and T_{s0}. Of course, the thermodynamic properties of working fluids for the primary stream and the secondary stream should be specified as well. An ejector with geometry and operating conditions listed in Table 5.1 is used for the general investigation of this new model. Air is supplied as the working fluid for both the primary flow and the secondary flow.

Table 5.1 Geometry and operating parameters used for the new model investigation

A_t (m^2)	A_{p1}/A_t	κ	θ	P_{p0} (psia)	T_{p0} (K)	P_{s0} (psia)	T_{s0} (K)
1.07e-7	7.61	80	1.2	364.7	300	34.7	300

To investigate the features of entropy change function of $\Delta s = f(\mu)$, the total entropy change Δs and its two components Δs_x and Δs_m are plotted against μ in Fig. 5.4. As discussed before, μ should be in the range of $0 < \mu < 1$ for it to have physical meaning. It is observed that the entropy change curves increase or drop dramatically in the regions of very low μ ($\mu < 0.15$) and very high μ ($\mu > 0.95$). Obviously, a gas ejector can not be operated in these two regions. Actually, Δs_x is less than zero in the $\mu < 0.15$ region. It violates the second law of thermodynamics, which means that the shock will not occur in this region at all. The entropy change curves are relatively flat in the region of $0.30 < \mu < 0.95$, which can be the stable operation range. Since the total entropy change is arbitrary decomposed of Δs_x and Δs_m, some portion of entropy change due to the two stream mixing or primary stream separation may be lined out from Δs_m and included into the Δs_x. Therefore, even if $\Delta \boldsymbol{s_m} < 0$ the two streams mixing is physically possible as long as the total entropy change Δs and its component of Δs_x are positive.

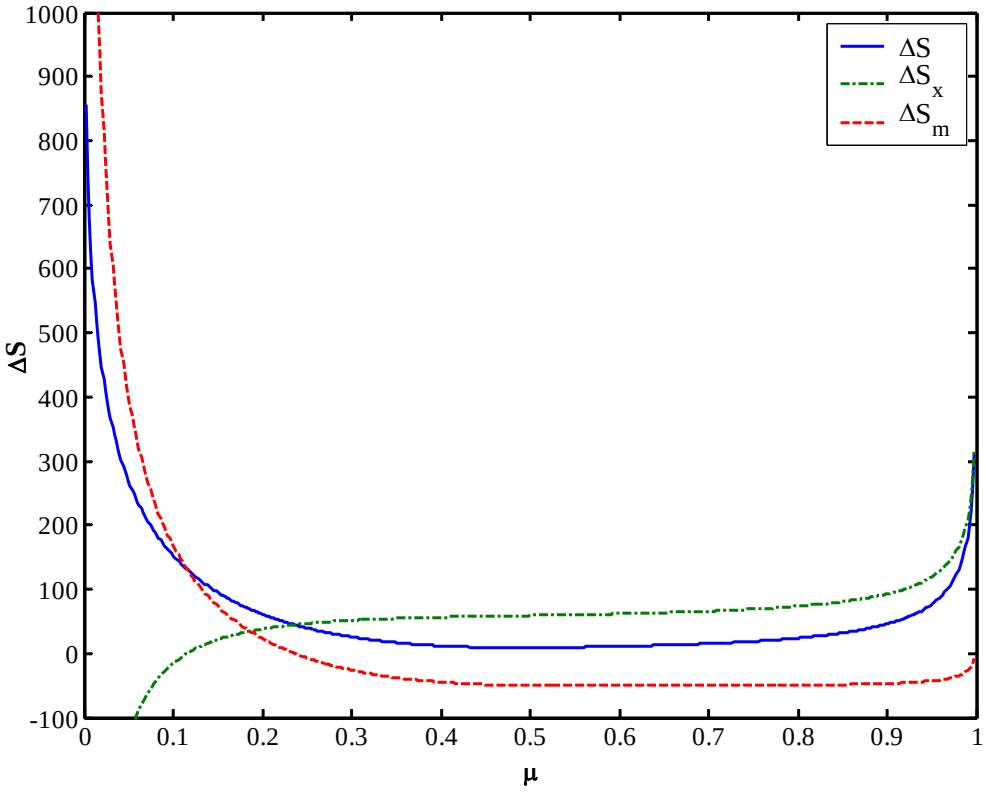

Fig. 5.4 Plots of the total entropy change and its two components

Fig. 5.5 is the plot of entrainment ratio against the parameter μ. ER increases rapidly with the increase of μ and will reach its maximum value at the point of $d\omega/d\mu = 0$; after that point, ER decreases. The location of the highest ER should be different from the point of minimum total entropy change, since they are determined by different equations, i.e., Equation (5.62) and Equation (5.55) respectively. However, the total entropy change curve in Fig. 5.4 and the entrainment ratio curve in Fig. 5.5 show that these two points are very close. In other words, the ejector has the best performance in

term of ER when it is operated in a region around the location of minimum total entropy change.

The value of entropy change indicates the irreversibility of a process. Mixing is a process in which the primary stream transfers part of its momentum to the secondary stream. Therefore, the irreversibility of this adiabatic mixing process represents the conversion degree of momentum to enthalpy which is irreversible. Higher entropy change means higher irreversibility—more momentum is converted to be enthalpy; in other word, lower entropy change means less momentum is converted to be enthalpy. In a region around the point of minimum entropy change, the conversion of momentum to enthalpy is the least and the secondary stream gains the maximum momentum from the primary stream. Higher secondary mass flow rate results if more momentum is provided for suction with a given, fixed flow area A_{s1}. This explains the optimal ER is achieved when the total entropy change is the minimum value.

The Mach number at the mixing chamber exit is plotted in Fig. 5.6. Similar to the entrainment ratio, M_{m2} increases with the decrease of Δs and reaches the maximum point when Δs is the least. The reason is similar to the explanation of relationship between ER and Δs, since the M_{m2} is the crucial indicator of mixed flow momentum. Lower Δs means less momentum is converted to be enthalpy and higher momentum provided for mixed flow; thus bigger M_{m2} results.

There are two solutions of τ corresponding to each μ value. One corresponds to the supersonic mixed flow, and the other corresponds to the subsonic mixed flow. The supersonic solution is discarded. Fig. 5.7 is the plot of subsonic solution of τ vs. μ. It is interesting to notice that in the regions of very low μ and very high μ, there is a one to one relationship between μ and τ. Between the above-mentioned two regions, there could be two or even three μ correspond to each τ. Of course, it is not feasible to operate the gas ejector in the very low μ region since $\Delta s_x < 0$ as previously discussed. Even so, it is still possible for one τ to have two solutions of μ.

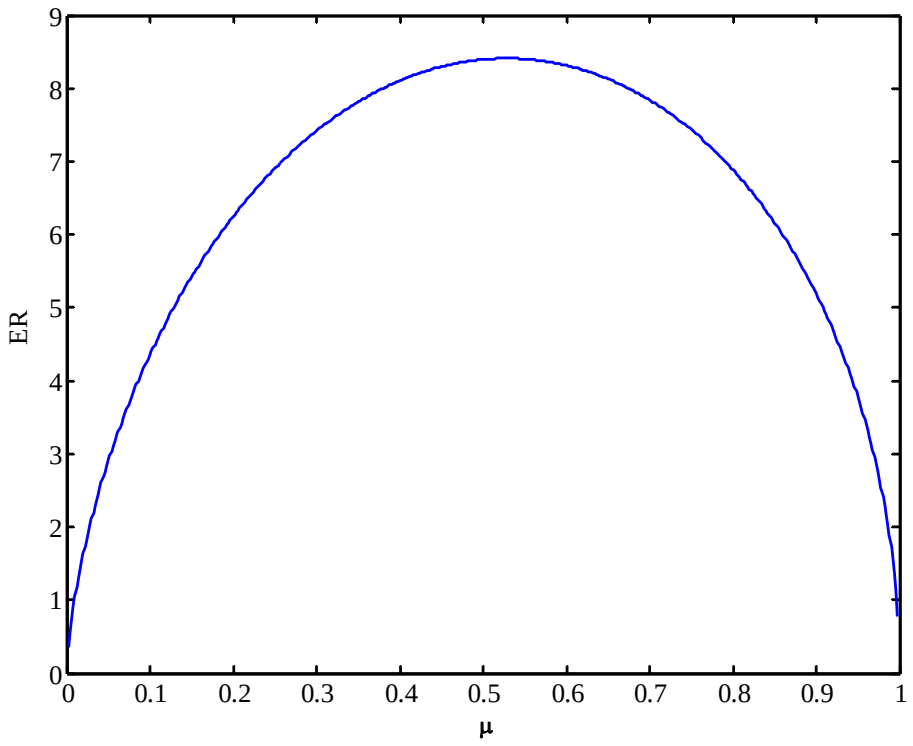

Fig. 5.5 Plot of entrainment ratio against variable μ

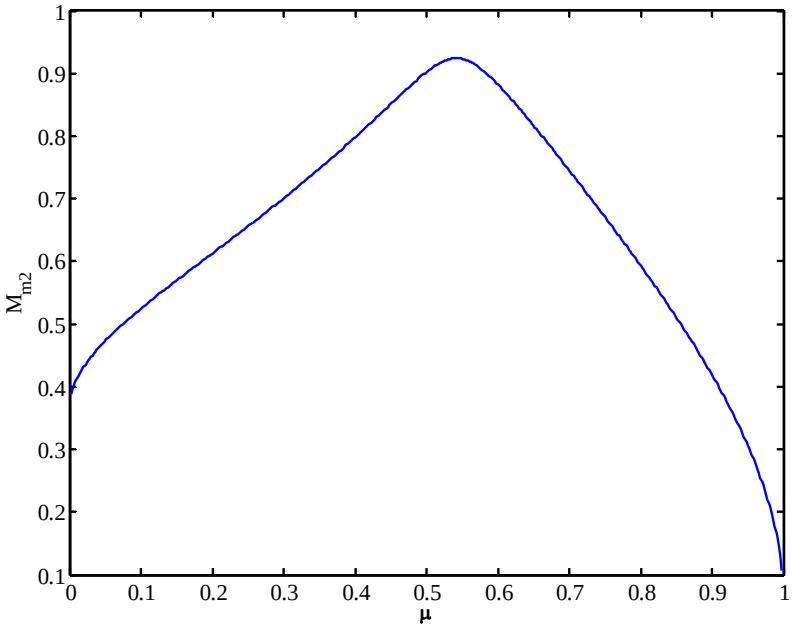

Fig. 5.6 Plot of the mixing chamber exit Mach number against μ

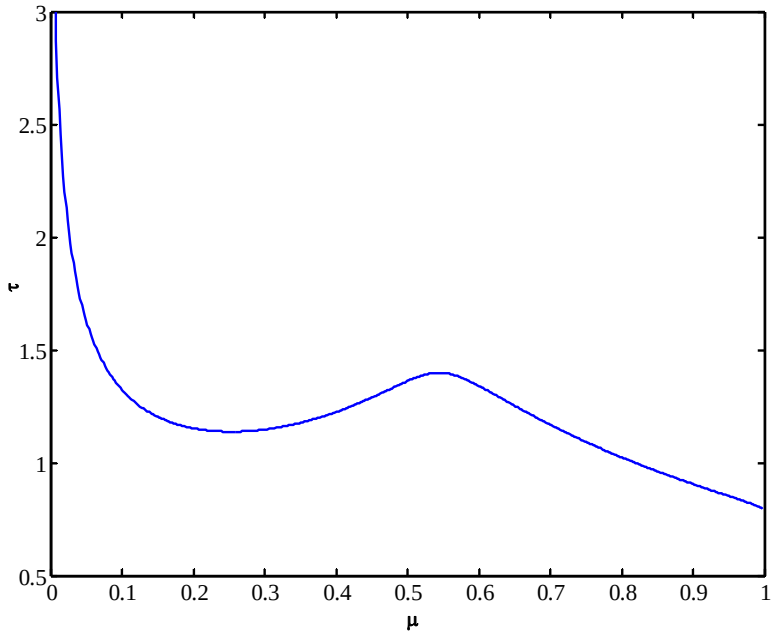

Fig. 5.7 Plot of τ against μ

OPTIMAL EJECTOR PERFORMANCE

The optimal μ for the highest ER is solved from $d\omega/d\mu = 0$, where $d\omega/d\mu$ is given by Equation (5.62). It is very difficult to solve this equation analytically due to the complexity of Equation (5.62). Numerically, it is very easy to obtain the solution for $d\omega/d\mu = 0$ since $d\omega/d\mu$ is explicitly expressed in variable μ by Equation (5.62). The numerical solution can also be calculated directly from the expression of $\omega = f(\mu)$ itself. If the operating domain of $\mu \in (0,1)$ is uniformly discretized to be $\{\mu_1, \mu_2, ..., \mu_N\}$ with the cell size of $\Delta\mu$, $d\omega/d\mu$ can also be expressed in discrete form given by Equation (5.71) according to the definition of derivative.

$$\left.\frac{d\omega}{d\mu}\right|_{\mu_k + \frac{\Delta\mu}{2}} = \frac{\omega(\mu_{k+1}) - \omega(\mu_k)}{\Delta\mu} \tag{5.71}$$

The numerical solution of $d\omega/d\mu = 0$ is $\mu_{opt} = \mu_I + \frac{\Delta\mu}{2}$, if

$$\left.\frac{d\omega}{d\mu}\right|_{\mu_{opt}} = \min\left(\left|\left.\frac{d\omega}{d\mu}\right|_{\mu_k + \frac{\Delta\mu}{2}}\right|\right) \tag{5.72}$$

Similarly, the solutions of $d(\Delta s)/d\mu = 0$, $d(M_{m2})/d\mu = 0$ and $d\tau/d\mu = 0$, etc. can be found by this numerical approach.

To investigate the relationship between ER and the stream Mach numbers at the mixing chamber entrance, normalized ER, M_{p1} and M_{s1} are plotted together in Fig. 5.8. There is an intersection between the M_{s1} curve and normalized ER. The intersection locates the point of maximum ER and $M_{s1}=1$. This means that the ejector best performance happens when secondary stream is choked at the mixing chamber entrance. The calculations also support this observation. The solution of $d\omega/d\mu=0$ can be found by using the above-introduced numerical approach, the calculation result is $\mu_{opt}=0.529$. Substituting the secondary flow (air) properties and $M_{s1}=1$ into Equation (5.3), the calculation shows that choking happens at $\mu_{choking}=0.528$. Considering the error due to the numerical calculation, μ_{opt} does equal to $\mu_{choking}$. Intuitively, this is physically true. The higher ER means the higher secondary mass flow rate is induced. As well known, the maximum mass flow rate is reached when the flow is choked.

The relationship between optimal ER and the area ratio of mixing chamber exit to the primary nozzle throat (AR or κ) is linear as shown in Fig. 5.9. The optimal ER is obtained at $M_{s1}=1$ as discussed previously. It is observed from the figure that the

parameter θ has significant impact on the ejector performance. Actually, the secondary mass flow rate is linearly proportion to θ which represents the flow channel area A_{s1} when the flow is choked at this point.

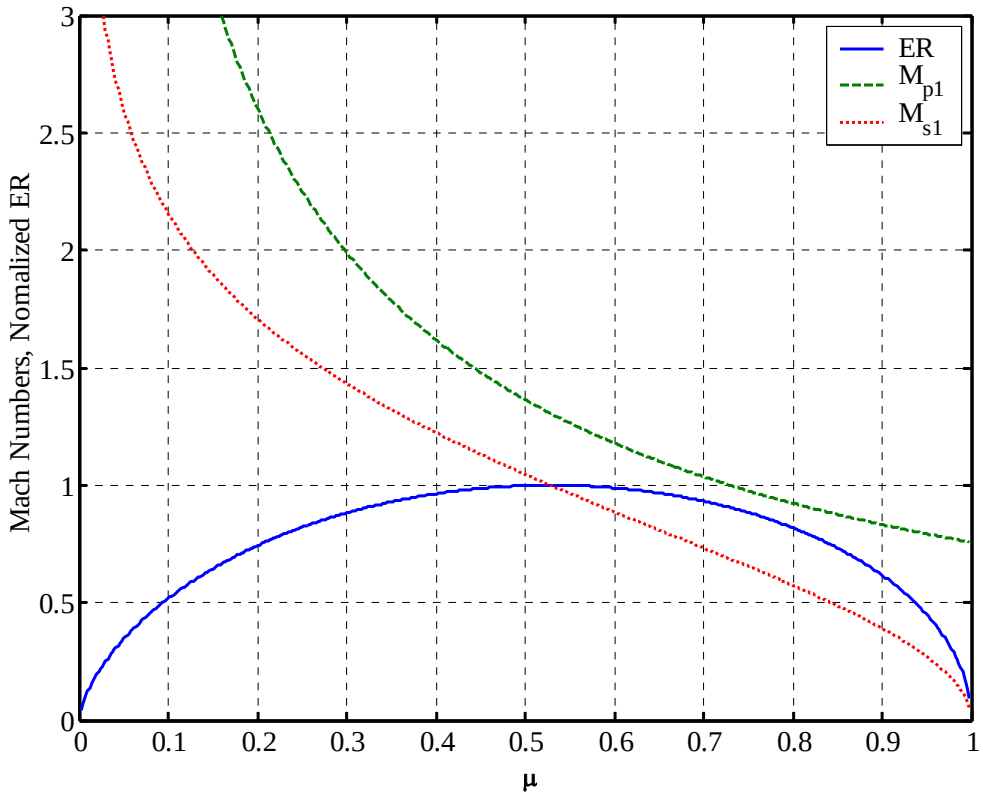

Fig. 5.8 Plots of M_{p1}, M_{s1} and normalized ER

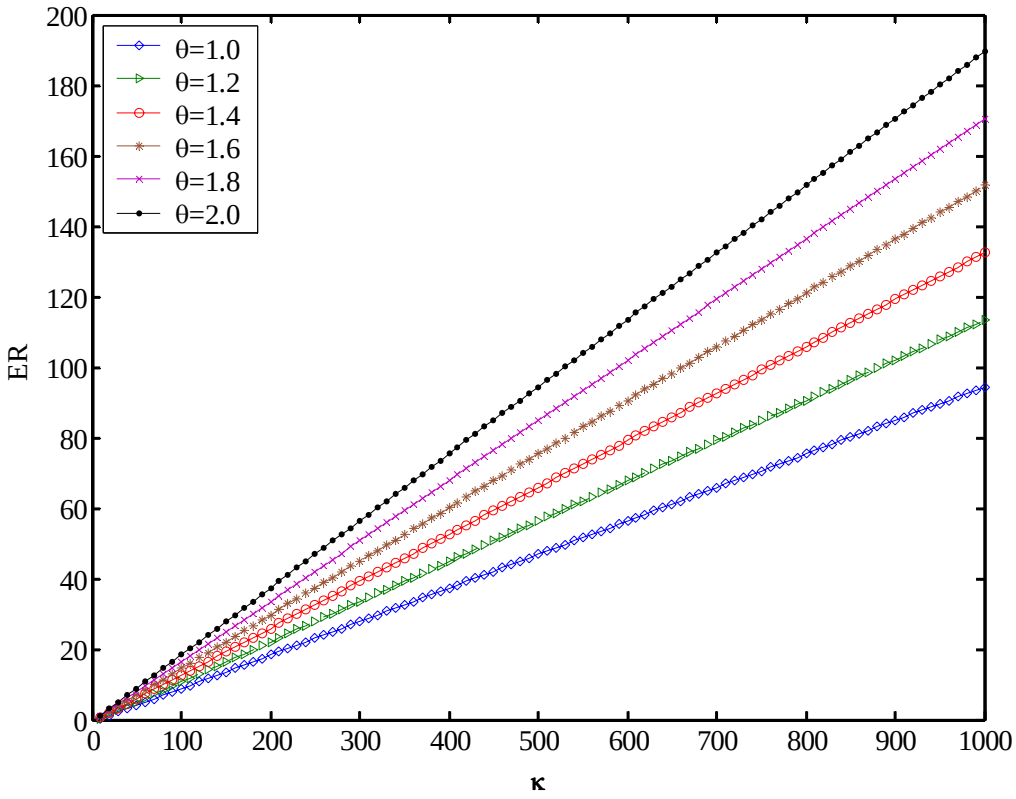

Fig. 5.9 Plots of optimal ER against κ for various θ

Fig. 5.10 shows the relationship between optimal compression ratio (CR) and κ. CR decreases rapidly with the increase of κ in low κ ($\kappa < 100$) region. In high κ region, CR may still decrease but very slowly, almost a constant. The reason is that lower κ corresponds to smaller ER, which means that the portion of momentum transferred from the primary stream is shared by less secondary flow. The large κ results in big ER. When κ is high enough, the limited portion of momentum provided by the primary stream is shared by a high secondary flow rate so that the momentum gained by per unit mass is negligible compared to their own momentum.

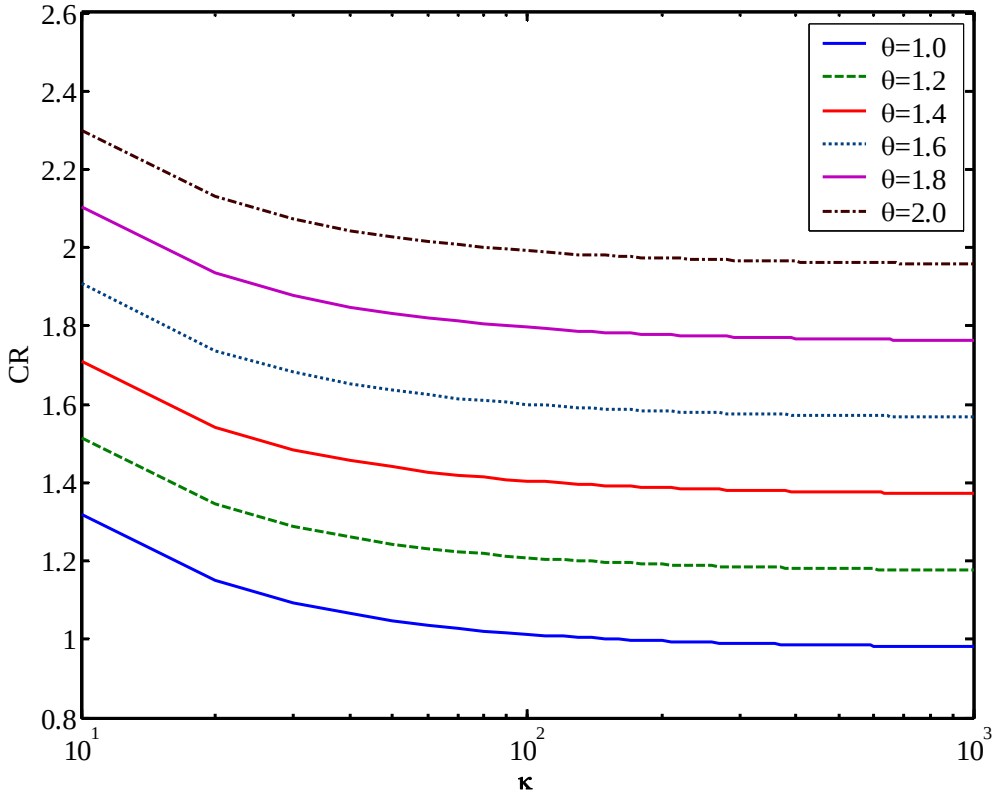

Fig. 5.10 Plots of optimal CR against κ for various θ

LINKS AMONG VARIOUS EJECTOR MODELS

The constant-pressure mixing model assumes that the static pressure in the mixing chamber is uniform and constant, i.e., $P_{p1} = P_{s1} = P_{m2} = P_1$. In the generalized ejector model, $P_{p1} = P_{s1} = P_1$ and P_1/P_{m2} is related to μ and τ by Equation (5.28). This model becomes the constant-pressure mixing model if the ejector is operated under such conditions that $P_1/P_{m2} = \mu\tau = 1$, i.e., $\tau = 1/\mu$. Should the constant-pressure mixing

operation exist, it will be located at the intersection point or the overlap parts between the curve of τ determined by Equation (5.26) and the curve of $\tau = 1/\mu$.

To find the parameters of μ and τ for the constant-pressure mixing operation, the τ curves for various θ, at $\kappa = 200$, are plotted together with $\tau = 1/\mu$ in Fig. 5.11. The influence of parameter θ on τ is obvious—τ decreases with the increase of θ for a given μ. All τ curves are below the $\tau = 1/\mu$ curve. For $\theta = 1.0$, part of the τ curve in the high μ region ($\mu > 0.6$) is very close to the curve of $\tau = 1/\mu$, though they do not actually overlap and there is no any intersection. For $\theta > 1.0$, the τ curves are further apart from the $\tau = 1/\mu$ curve. Therefore, true constant-pressure mixing operation is impossible. The assumptions made for the constant-pressure mixing model are valid for an ejector with geometric parameter θ small enough (close to 1.0). The constant-pressure model can predict the ejector performance accurately under such condition. If θ is large and far from $\theta = 1.0$, the assumptions made for the constant-pressure mixing model are invalid.

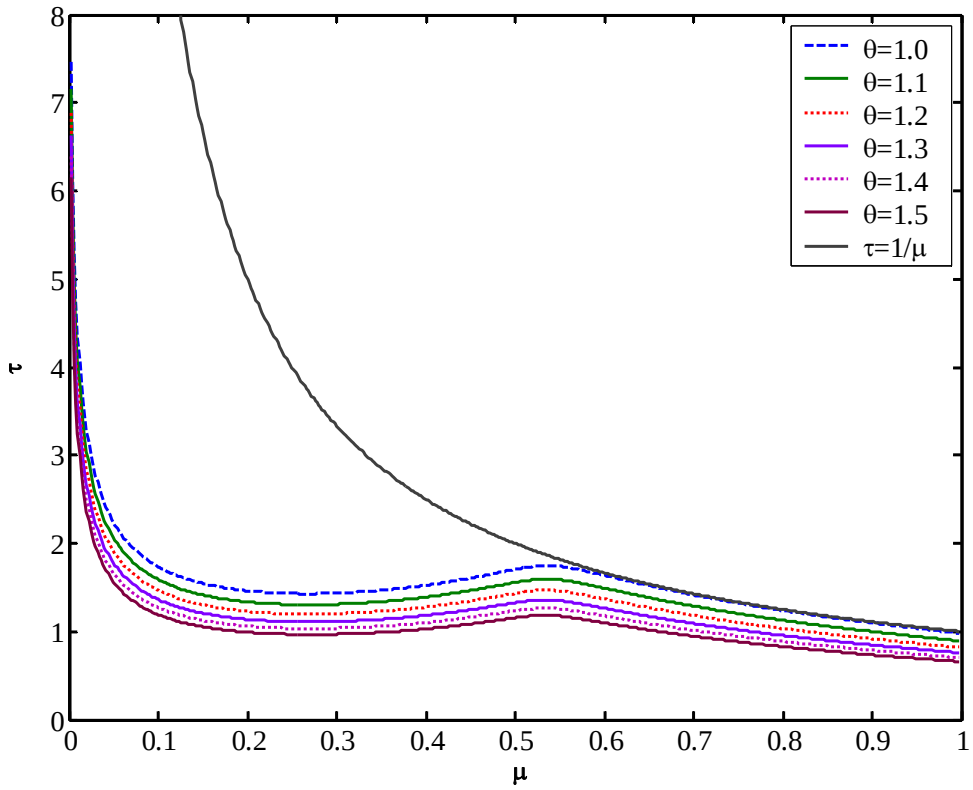

Fig. 5.11 Plots of τ against μ for various θ

To investigate the influence of another geometric parameter κ, the τ curves for various κ at $\theta = 1.0$ are plotted together with $\tau = 1/\mu$ as shown in Fig. 5.12. For $\kappa > 60$, the part of τ curves in the high μ region ($\mu > 0.6$) are very close to that part of the $\tau = 1/\mu$ curve and all curves are indistinguishable from each other. The τ curves for $\kappa < 60$ are distinguishable from the $\tau = 1/\mu$ curve.

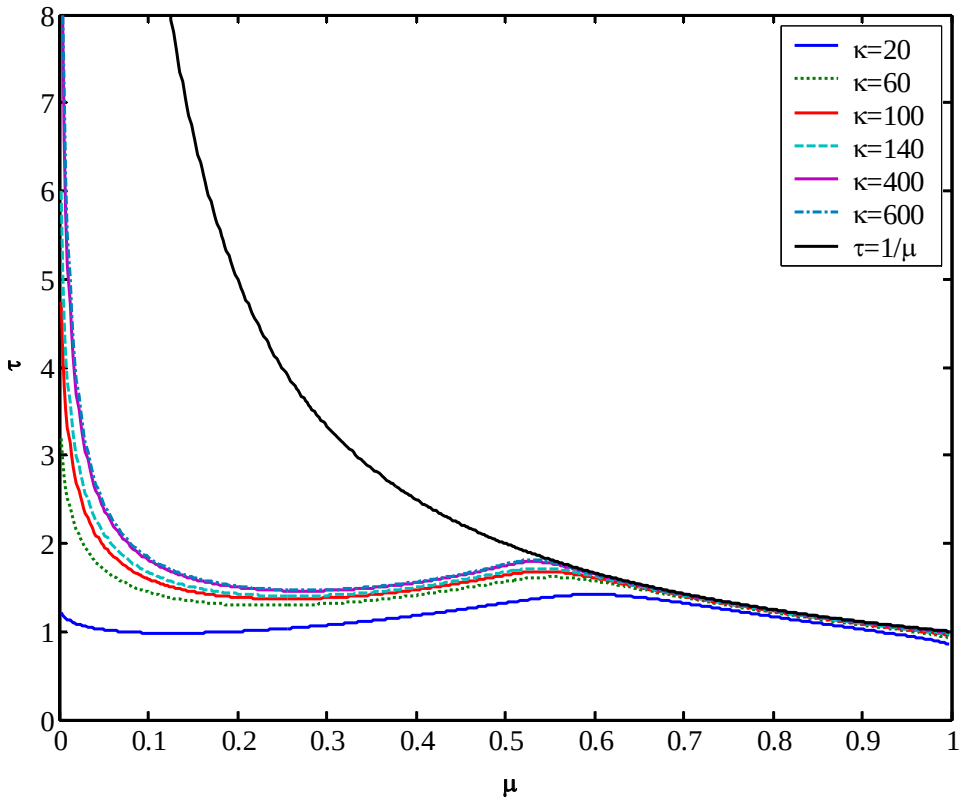

Fig. 5.12 Plots of τ against μ for various κ

The constant-area mixing ejector is a particular case, i.e. $\theta = 1$, for this new ejector model. All equations of the new model are valid for this particular case, though some of them could be simplified. The constant-area mixing ejector also has all generic features predicted for other ejectors. As a particular case, the constant-area mixing ejector has its own special characters. From the standpoint of geometry configuration, unity is the lowest possible value for parameter θ. It is observed from Fig. 5.9 and Fig. 5.10, this particular ejector has the lowest optimal performance in terms of both entrainment ratio and compression ratio. Actually, the constant-area mixing ejector gives the lowest

performance not only at the optimal point but also in the whole range of μ. This can be proved clearly by Fig. 5.13, the plots of ER against μ for various θ. Fig. 5.13 is plotted at $\kappa = 100$.

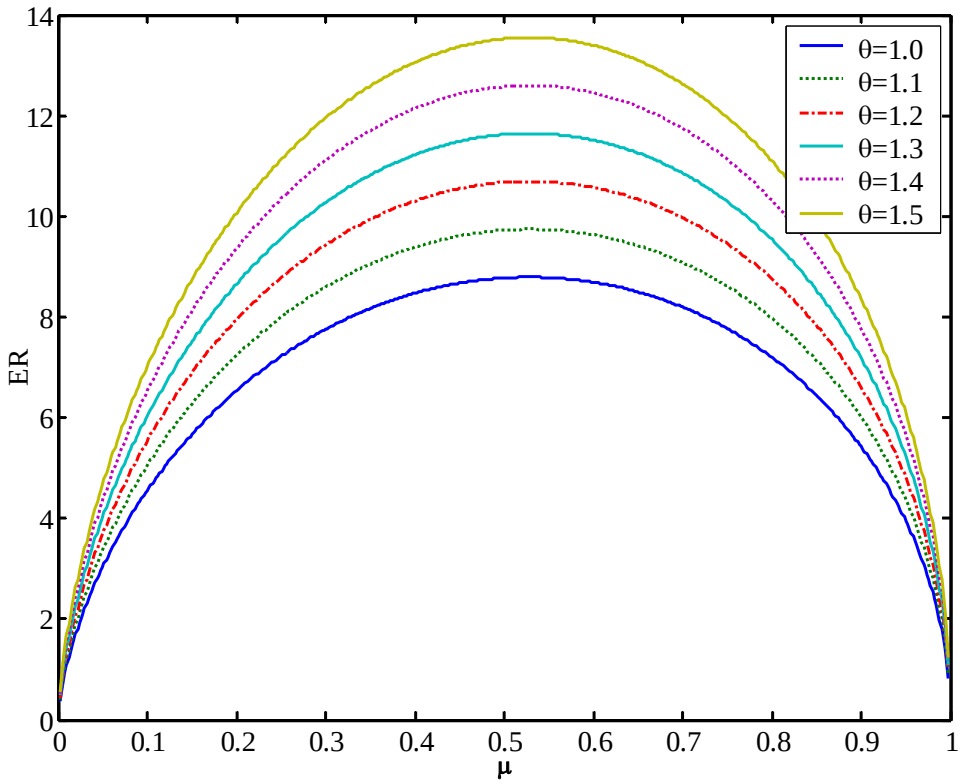

Fig. 5.13 Plots of ER against μ for various θ

The observations and discussions of Fig. 5.11 and Fig. 5.12 show that the assumptions made for constant-pressure mixing ejector are most close to the truth when $\theta = 1$. The constant-pressure model makes its most accurate predictions when the ejector has a constant-area mixing chamber. There is almost no difference between the predictions of

the constant-pressure ejector model and constant-area ejector model when the area ratio is bigger than 60 ($\kappa > 60$). For a constant-area mixing ejector with small area ratio ($\kappa < 20$), the predictions made by those two models may be significantly different.

LIMITATIONS ON EJECTOR DESIGN AND OPERATION

This new comprehensive model can be applied to design ejectors with specified requirements and operating conditions. The performance of any ejector with a given geometric configuration can be predicted theoretically by using this model. However, it is impossible to design an ejector which meets any arbitrary given requirements and operating conditions. It is infeasible for an ejector with any arbitrarily given geometry to function properly. Instead, every particular ejector has its own operational range; some ejector designs are practical and feasible for operation, but others are not. The performance features are analyzed and the operation ranges are calculated for arbitrary ejectors by adopting this new model in following sections. These analysis and calculations give definite limitations for ejector design and operation.

Design Limitations

Ejectors are usually designed to be components of certain systems. Each ejector has its

own particular boundary conditions, operating conditions and constraints determined by the system. Defining those conditions and constraints clearly is the first step of designing an ejector. Once the operating parameters and constraints are specified, the requirements on ejector performance could be determined. With the ejector performance range given, the second step of designing is to investigate the feasible geometry configurations according to their limitations of ER or CR.

As an example, Fig. 5.14 is the optimal ER surface (upper limits) for ejectors with various mixing chamber configurations. Fig. 5.14 is generated for the case of working fluids, operating conditions and other geometric parameters listed in Table 5.1. Similar limitation surfaces could be plotted for ejectors under other operating conditions by using this new model. Fig. 5.14 shows that the upper limit of ER increases with the increase of parameters θ and κ. The upper limit of ER is lowest at $\theta = 1$ (the constant-area mixing ejector) for a given, fixed κ.

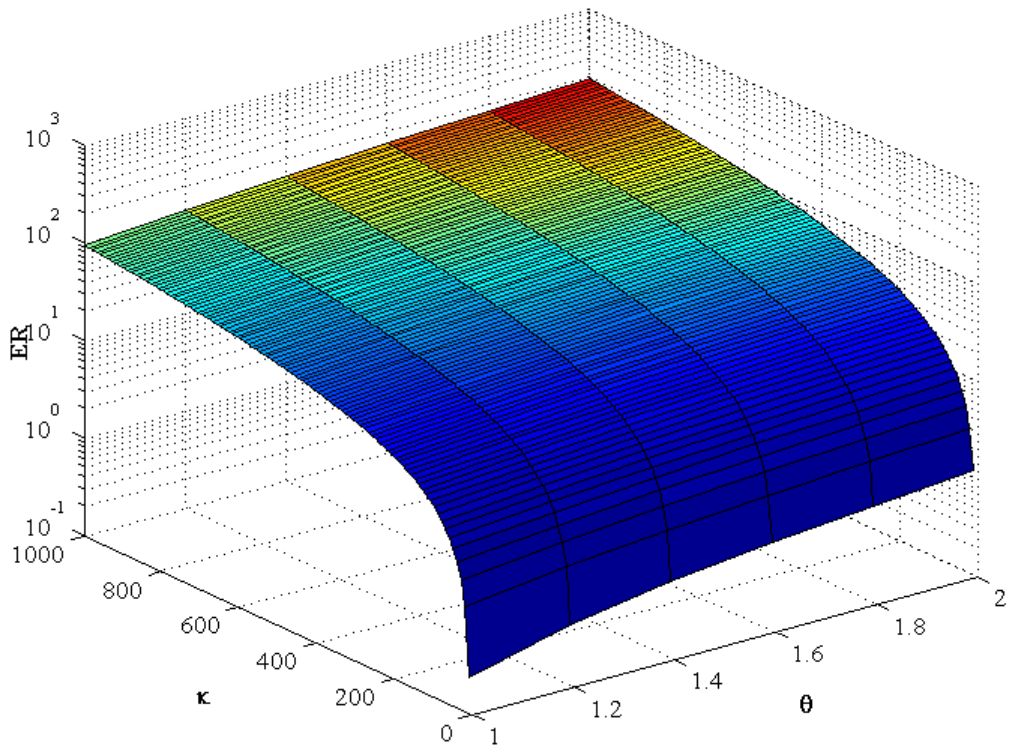

Fig. 5.14 Upper limits of ER for ejectors

According to Fig. 5.14, the ejector should be designed with large θ and κ if high ER is desired. It is intuitively understandable that θ and κ can not be infinity. What are the limits for θ and κ? The calculations of total entropy change during the mixing process will answer this question.

As discussed previously, the mixing process is physically possible only when the total entropy change is positive. In other words, ejectors fail to work if total entropy change is negative, i.e., $\Delta s<0$. Fig. 5.15 is the surface plot of Δs for various ejectors under the

working conditions specified in Table 5.1. Obviously, a large part of this surface is below the plane of $\Delta s = 0$, which means many ejectors can not achieve the optimal ER values given by the surface shown in Fig. 5.14.

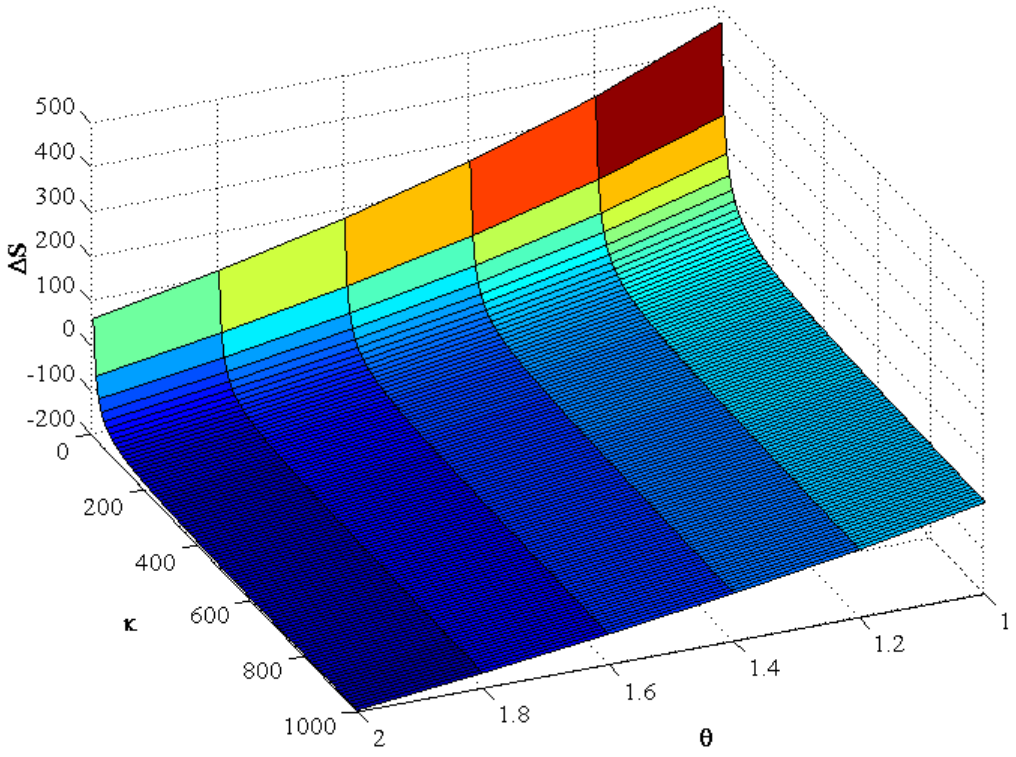

Fig. 5.15 Δs surface for ejectors working at the optimal point

To give a more definitive picture of operable range of mixing chamber configurations, the Δs surface shown in Fig. 5.15 is intercepted by $\Delta s = 0$ plane. Fig. 5.16 is the top-downward view of this intercepted Δs surface. The shadowed area is the $\Delta s > 0$ area,

and the blank area is the $\Delta s < 0$ area. It is obvious that very limited geometric configurations could achieve the optimal ER. Generally, an ejector could work at the optimal point only if it is designed with small κ or small θ. At $\theta = 1.0$ (constant-area mixing ejector), the κ can be as high as 1000 or even beyond 1000. When θ is within 1.1, the value of κ can be up to 200. At $\theta = 1.2$, κ can not be bigger than 100. From the stand point of another parameter κ, the ejectors can achieve optimal ER even at $\theta = 2.0$ if κ is less than 10. However, the feasible θ value decreases very rapidly.

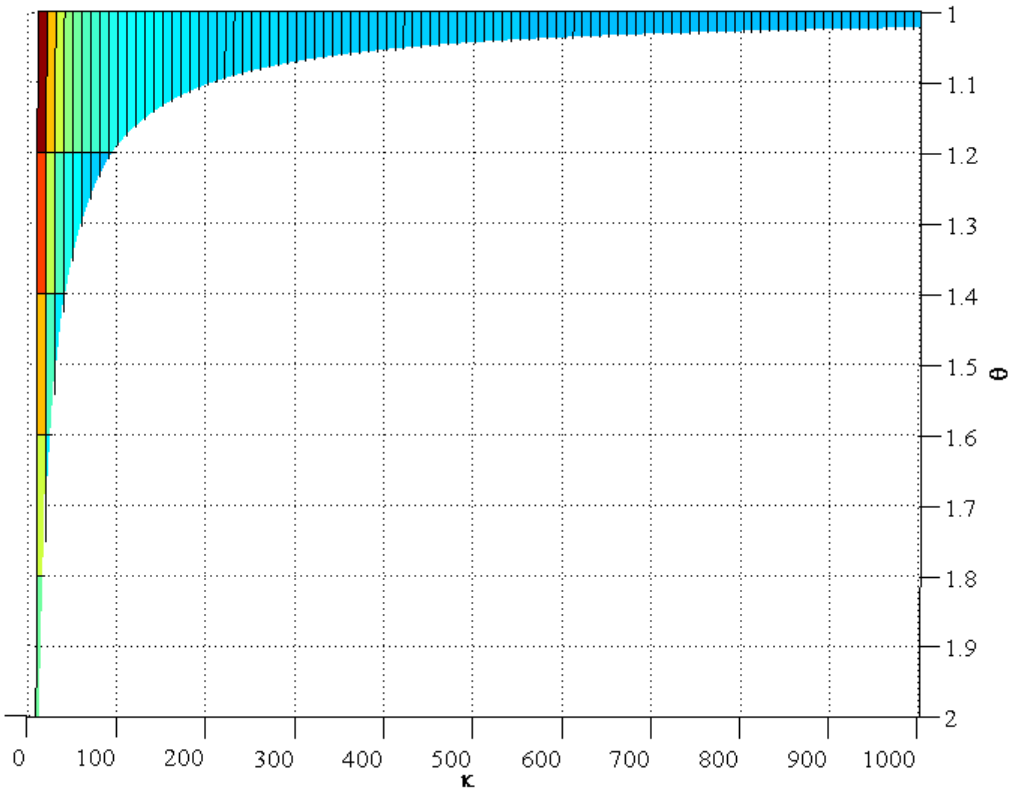

Fig. 5.16 Top-downward view of Δs surface intercepted by $\Delta s = 0$ plane

Fig. 5.14 through Fig. 5.16 and the corresponding discussions are made for upper limits of ejector performance. Usually, ejector designers pay more attention to the operable range instead of the particular optimal point though it may be desired. To meet this interest, it is necessary to investigate the operation feasibility of the whole operation range for each ejector. In the new model, μ is the parameter which describes the range of ejector operation. Theoretically, μ can be any value between 0 and 1. This study does not consider the supersonic flow for secondary stream, and the lower boundary of μ is $\mu = P_{s*}/P_{s0}$. Therefore, the operation range means $P_{s*}/P_{s0} \le \mu < 1.0$. In order to develop a guide for ejector design, the relationships among the parameters μ, κ, θ and Δs are investigated.

Constant-area mixing ejectors, i.e., ejectors with $\theta = 1.0$, are particular interesting to designers since they are the most widely used ejectors. Fig. 5.17 is the Δs surface plot of the whole operation range of μ for constant-area mixing ejectors with κ up to 1000. The Δs is positive in the whole operation range of μ as well as the investigated κ range. From this standpoint, the constant-area mixing ejector has the widest possible geometry choice in whole operation range of μ, though its performance is the worst.

Fig. 5.18 is the surface plot of Δs against parameters of μ and θ, for the ejectors with AR=100 and operating parameters listed in Table 5.1. Fig. 5.19 is the top-downward view of Fig. 5.18 intercepted by the $\Delta s = 0$ plane. It is clearly observed that the operable

range of μ shrinks rapidly with the increase of parameter θ. The whole range of $P_{s*}/P_{s0} \le \mu < 1.0$ is feasible for operation if θ is less than 1.2. At $\theta = 1.3$, the operable range shrinks to be $0.9 \le \mu < 1.0$, and the ejectors can not be operated at all when θ is bigger than 1.8.

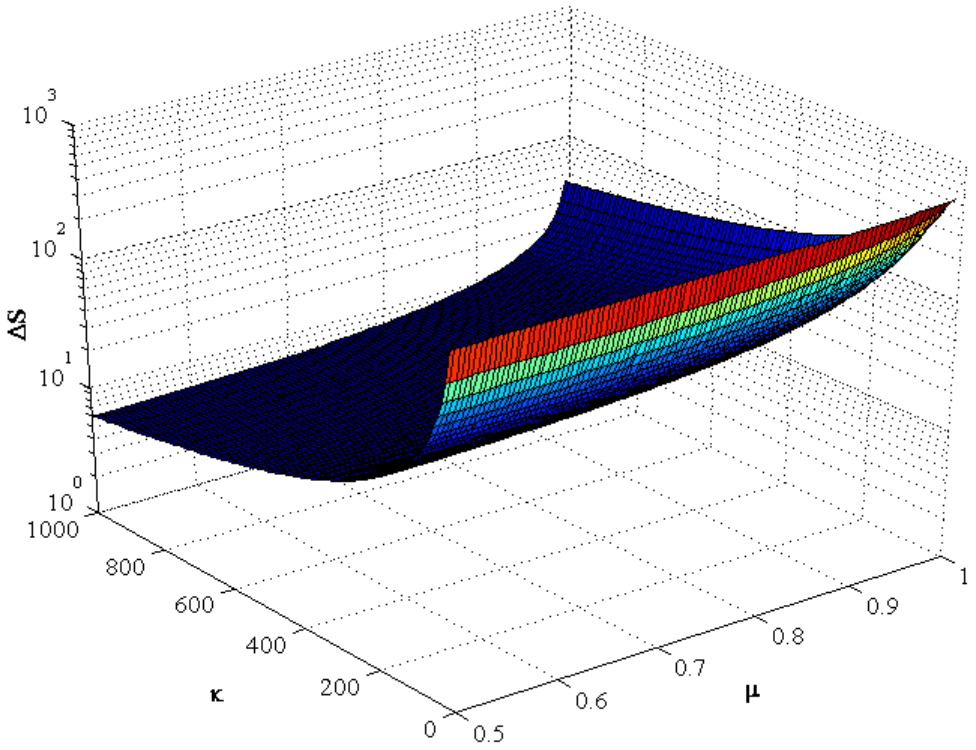

Fig. 5.17 Δs surface for constant-area mixing ejector

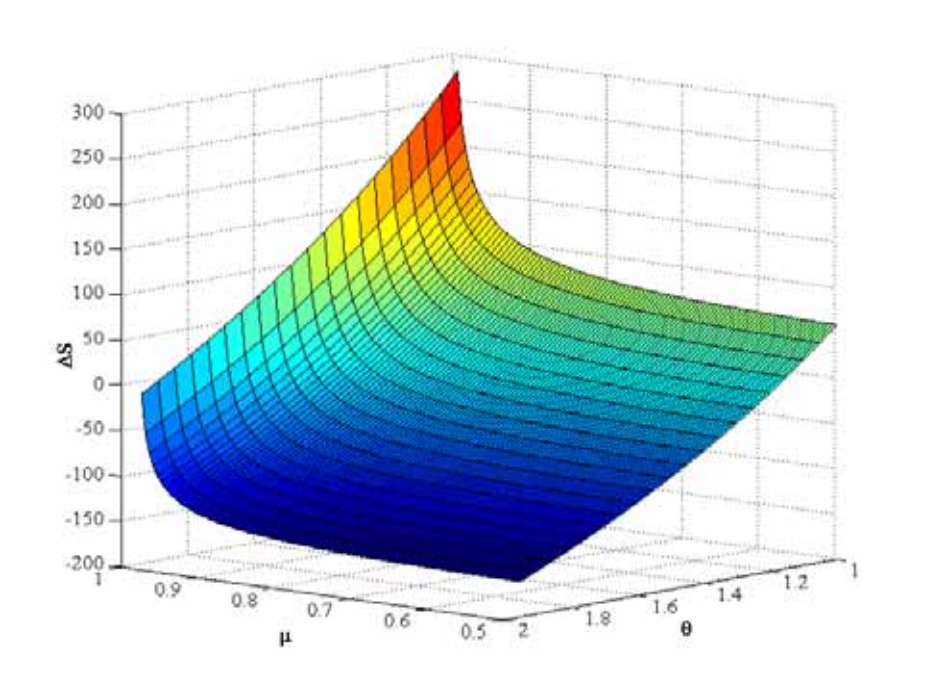

Fig. 5.18 Δs surface of ejectors with various θ

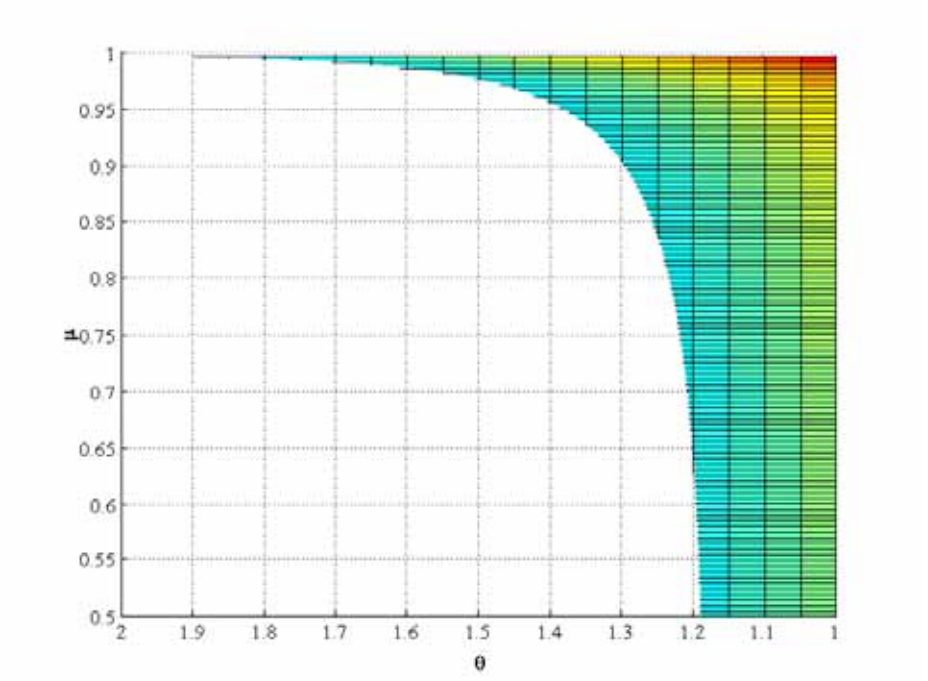

Fig. 5.19 Δs surface of ejectors with various θ, intercepted by $\Delta s = 0$ plane

Operation Limitations

In the new model, the two important operational parameters μ and τ are related to each other by Equation (5.26). If one of them is given, the other can be calculated. It is more practical and convenient to specify the ejector outlet static pressure as a boundary condition, thus, τ is usually given. Due to its complexity, it is very difficult if not impossible to obtain μ by solving Equation (5.26) analytically. In this study, a numerical technique is applied to circumvent this trouble. The least square curve fitting approach, similar to the method introduced in Chapter III, is employed to solve μ from Equation (5.26).

To investigate the relationships between ejector performance and boundary conditions— pressures of primary inlet, secondary inlet and outlet, a performance surface is plotted against pressure rations of P_{p0}/P_{s0} and P_b/P_{s0}. Where P_b is the back pressure, or the outlet static pressure, for an ejector without diffuser. Fig. 5.20 is such a surface plot for a constant-area mixing ejector with $\kappa = 100$. Fig. 5.20 is similar and comparable to the "three-dimensional ejector solution surface" as shown in Fig. 1.4, constructed by Addy and Dutton et al. [12, 13, 14] for a constant-area ejector. The entrainment ratio of the ejector could be predicted once the boundary conditions— all boundary pressures are given. It is observed from the performance surface that the outlet pressure P_b is constrained in a certain range. Actually, the operable range of P_b/P_{s0} is very limited.

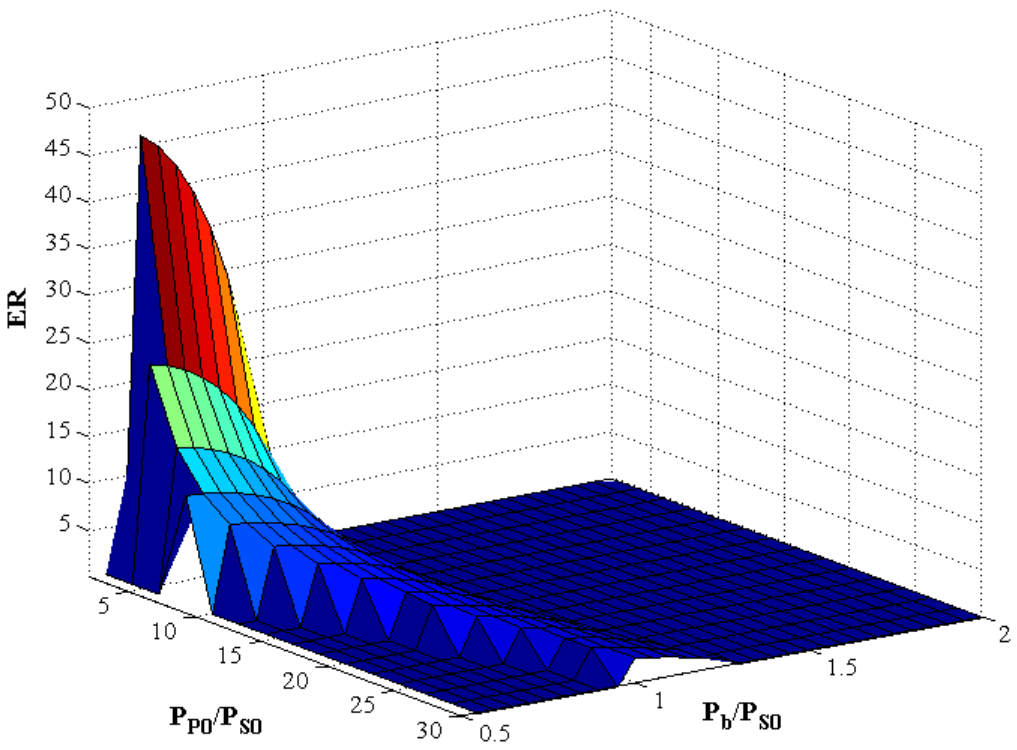

Fig. 5.20 Performance surface plotted against ejector boundary pressures

Obviously, the range of operable P_b/P_{s0} is related to the ratio of inlet supply pressures, i.e., P_{p0}/P_{s0}. To investigate the relationship between the range of operable P_b/P_{s0} and the ratio of inlet supply pressures, both maximum P_b/P_{s0} and minimum P_b/P_{s0} are plotted against P_b/P_{s0} in the same figure, Fig. 5.21. For a given P_{p0}/P_{s0}, the ejector would work properly if P_b/P_{s0} is a value between maximum P_b/P_{s0} and minimum P_b/P_{s0}. In Fig. 5.21, the zone between the maximum P_b/P_{s0} curve and minimum P_b/P_{s0} curve is ejector operable area.

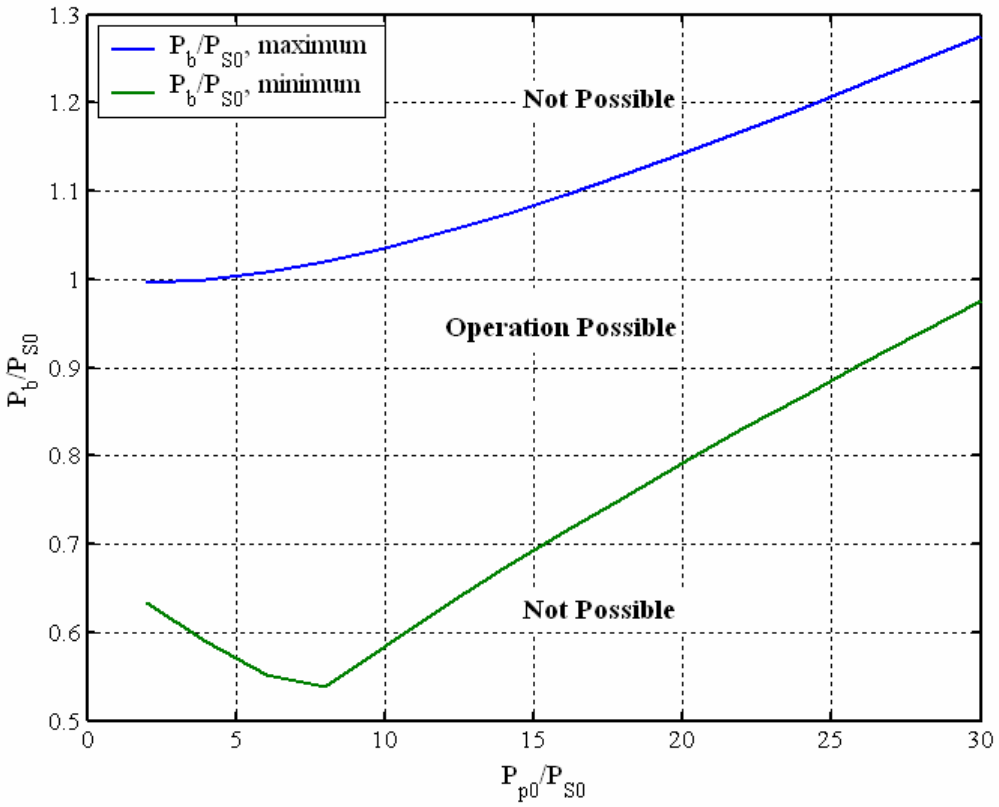

Fig. 5.21 Operable range of pressure ratio of outlet flow to secondary supply

CONCLUSIONS

A novel generalized comprehensive gas ejector analytical model is developed. A definite link is established between the widely used constant-pressure model and constant-area model, which are two particular cases of the new model. Analysis shows that it is physically impossible to build an ejector with an exact constant-pressure mixing chamber. However, the predictions of the constant-pressure ejector model could be very

accurate if the geometry of the ejector is close to the constant-area mixing ejector. If the mixing chamber is far different from constant-area mixing, a big error could result from the predictions of the constant-pressure model. The constant-area mixing ejector has the lowest performance, but it has the widest operating range. Also, the constant-area ejector has the biggest range of AR, the area ratios of mixing exit to primary nozzle throat.

CHAPTER VI

EJECTOR WORKING WITH TWO-PHASE FLOW

INTRODUCTION

The motivation for this research is to design an ejector for a Proton Exchange Membrane (PEM) fuel system. In this system, an ejector is used to transfer and compress the PEM fuel cell exhaust which contains gas and very small portion of liquid water. Theoretically, the portion of liquid water in PEM exhaust can be any value depends on operating conditions. To improve the transport of both reactants and exhaust, high reactant flow rates are desired. The reactant delivery flow rate associated with delivering exactly the reactant needed by the electrochemical reaction taking place is called the stoichiometric flow rate [26]. The use of these higher-than-stoichiometric flow rates not only improves transport, but it also helps to ensure that no portion of the fuel cell is ever starved for reactants. Usually, more than 2.0 stoichiometric flow rate of hydrogen/oxygen is required to circulate in a recirculation scheme [26].

The proportion of liquid water is so low that the exhaust behaves like a gas. The thermodynamic properties of this gas-like mixture will be discussed in this chapter. The generalized ejector model developed in last chapter is applied to design of the ejector working for such kind of two-phase mixture.

Theoretical development of the gas-liquid mixture model is the first part of this chapter. The second part performs parametric analysis and discussions on the thermodynamic properties of this two-phase mixture. In the third part, the generalized ejector model is used to design an ejector working with this mixture; the ejector performance will be studied parametrically. The summary and conclusions are made in the last part.

GAS-LIQUID MIXTURE MODEL

The gas-liquid two-phase mixture is assumed to behave like a gas since the proportion of the liquid is so low [27]. In addition, thermal equilibrium was assumed to exist between the gas and the liquid. The homogeneous two-phase model is applied to determine the thermodynamic properties of the mixture.

Gas, liquid and gas-liquid two-phase mixtures are denoted by the subscripts of “g”, “l” and “tp” respectively. The proportion of liquid is described by the liquid quality x, which is defined as the mass flow ratio of liquid to gas. In this study, the liquid quality is very small, $x \le 1$. Otherwise, a liquid jet pump instead of a gas ejector should be adopted, since the dimensions of the gas ejector do not allow it to transport high flow rate liquid.

$$x = \frac{m_l}{m_g} \tag{6.1}$$

The density of the mixture is related to the gas density by:

$$\rho_{tp} = (1+x)\,\rho_g \tag{6.2}$$

The state equations for the gas and the gas-like mixture are

$$\frac{P_g}{\rho_g} = R_g T_g \tag{6.3}$$

$$\frac{P_{tp}}{\rho_{tp}} = R_{tp} T_{tp} \tag{6.4}$$

Since the gas and liquid are in thermal equilibrium, $P_g = P_{tp} = P$ and $T_g = T_{tp} = T$. Combining Equations (6.2), (6.3) and (6.4), the gas constant is obtained for the mixture.

$$R_{tp} = \frac{R_g}{1+x} \tag{6.5}$$

Let $c_{p,l}$ represent the specific heat of the liquid phase. The liquid phase entropy change accompanying the gas-liquid mixing process is given by Equation (6.6).

$$ds_l = \frac{dQ}{T} = c_{p,l} m_l \frac{dT}{T} \tag{6.6}$$

While, the gas phase entropy change is given by following equation, if the gas has the specific heats of $c_{p,g}$ and $c_{v,g}$.

$$ds_g = \frac{dQ}{T} = c_{p,g} m_g \frac{dT}{T} - R_g m_g \frac{dP}{P} \tag{6.7}$$

The total entropy should remain constant if the gas and liquid are in thermal equilibrium. Therefore, the total entropy change is zero.

$$ds_l + ds_g = 0 \tag{6.8}$$

Substituting Equations (6.6) and (6.7) into Equation (6.8),

$$c_{p,l} m_l \frac{dT}{T} + c_{p,g} m_g \frac{dT}{T} - R_g m_g \frac{dP}{P} = 0 \tag{6.9}$$

Equation (6.10) is derived by rearranging the above equation,

$$\frac{dT}{T} = \frac{R_g}{x c_{p,l} + c_{p,g}} \frac{dP}{P} \tag{6.10}$$

Integrating Equation (6.10),

$$\ln T = \frac{R_g}{x c_{p,l} + c_{p,g}} \ln P + C \tag{6.11}$$

Where, C is an arbitrary constant. Therefore,

$$TP^{-\frac{R_g}{x c_{p,l} + c_{p,g}}} = \text{constant} \tag{6.12}$$

According to the isentropic expansion law, the state properties P and T of the gas-like mixture have following relationship,

$$TP^{\frac{\gamma_{tp}-1}{\gamma_{tp}}} = \text{constant} \tag{6.13}$$

Comparing Equation (6.12) and (6.13), γ_{tp} is related to the gas and liquid properties by Equation (6.14).

$$\gamma_{tp} = \frac{c_{p,g} + xc_{p,l}}{c_{v,g} + xc_{p,l}} \tag{6.14}$$

Therefore, the mixture behaves as if it possessed a specific gas constant given by Equation (6.5) and a value of the specific heat ratio γ_{tp} given by Equation (6.14).

PARAMETRIC ANALYSIS OF MIXTURE PROPERTIES

To study the thermodynamic properties of the gas-like flow, the derived R_{tp} and γ_{tp} are analyzed parametrically. In the parametric analysis, air is used as the gas phase and the water is used as the liquid phase. The investigation rang of x is from 0 to 1.0. Fig. 6.1 is the plot of R_{tp} against liquid quality x. As a comparison, the gas constant of the air is plotted on the same figure. At the point of $x = 0$, the R_{tp} has the highest value, $R_{tp} = R_g$; then, the parameter R_{tp} decreases with the increase of liquid quality x.

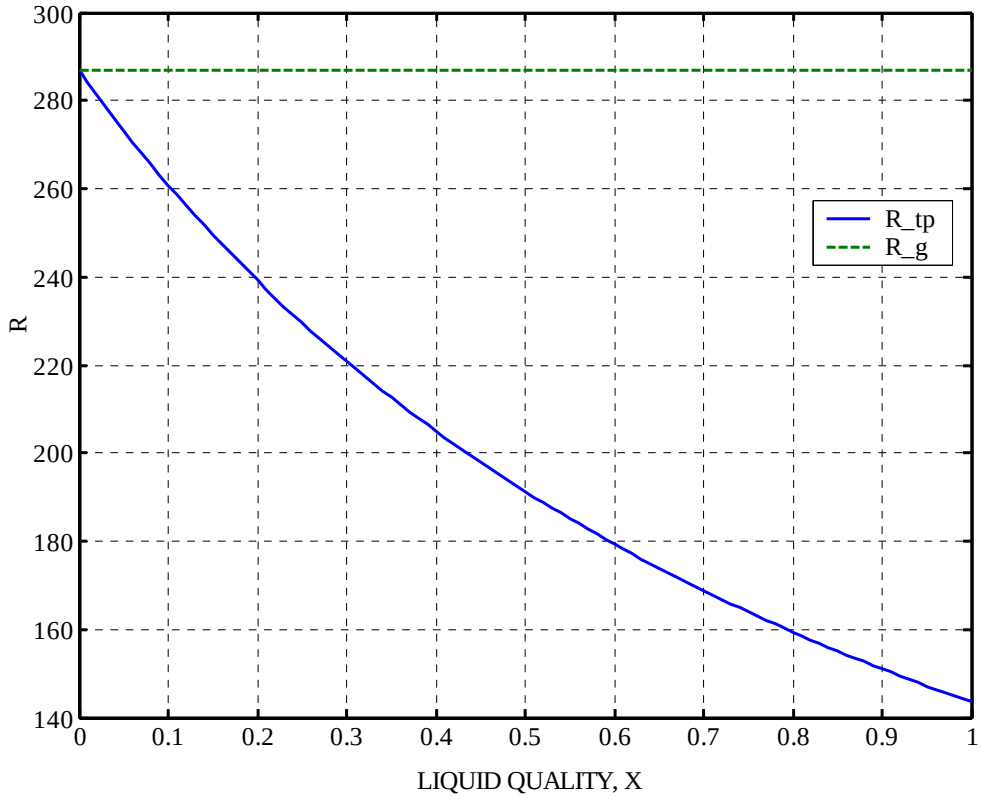

Fig. 6.1 Plot of mixture gas constant against the liquid quality x

The specific heat ratio of mixture is plotted against the liquid quality x is plotted in Fig. 6.2. Similar to the R_{tp}, γ_{tp} has the highest value at the point of $x = 0$ and then decreases with the increase of x. Unlike the R_{tp} curve, the γ_{tp} does not decrease as fast as R_{tp}. At $x = 1.0$, R_{tp} is only half of the R_g, but the γ_{tp} is about 75% of γ_g.

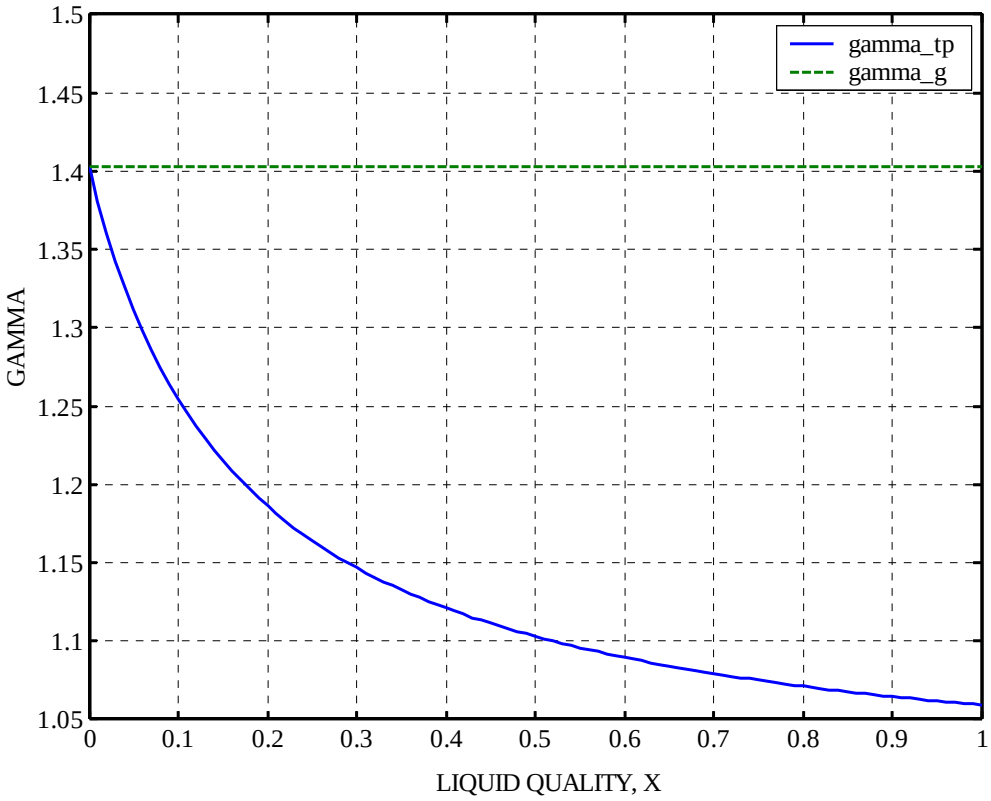

Fig. 6.2 Plot of mixture specific heat ratio against the liquid quality x

EJECTOR WORKING WITH TWO-PHASE MIXTURE

The gas-like mixture has its own equivalent specific heat ratio and molecular weight, which are different from the original single-phase gas. Both the ejector operational range and its performance are affected by the thermodynamic properties of working fluids, γ and R (reflecting the molecular weight). It is desired to investigate the impact of the liquid quality x on the ejector operability and ejector performance.

In this study, the generalized ejector model is used to design an ejector working with this gas-like two-phase flow. The impact of the liquid quality x on the ejector entrainment ratio is investigated for two cases: (1) the two-phase mixture supplied as the primary stream and the single-phase gas supplied as the secondary stream, (2) the two-phase mixture supplied as the secondary stream and the single-phase gas supplied as the primary stream. The operational range of gas ejector is also investigated for each case by the analysis of the total entropy change.

Mixture Supplied as Primary Stream

First case of investigation is that the two-phase mixture is supplied at the primary inlet and the single-phase gas is supplied at the suction port. The ejector operation range in terms of the boundary pressure ratio, P_b/P_{s0}, is calculated and plotted for liquid quality from $x=0.0$ to $x=1.0$. Since the liquid portion is assumed to be very low, this study didn't include the case of $x>1.0$ though it could be much higher.

Fig. 6.3 shows the operational range of P_b/P_{s0} in 3-D plot. The bottom surface is the plot of minimum operable P_b/P_{s0} against the P_{p0}/P_{s0} and x, while the top surface is that plot of maximum operable P_b/P_{s0}. These two surface define the lower and upper limits of P_b/P_{s0}, and the space between them are the operation range. It is observed that

the operable P_b/P_{s0} range is bigger for smaller P_{p0}/P_{s0} and it shrinks with the increase of the liquid quality x.

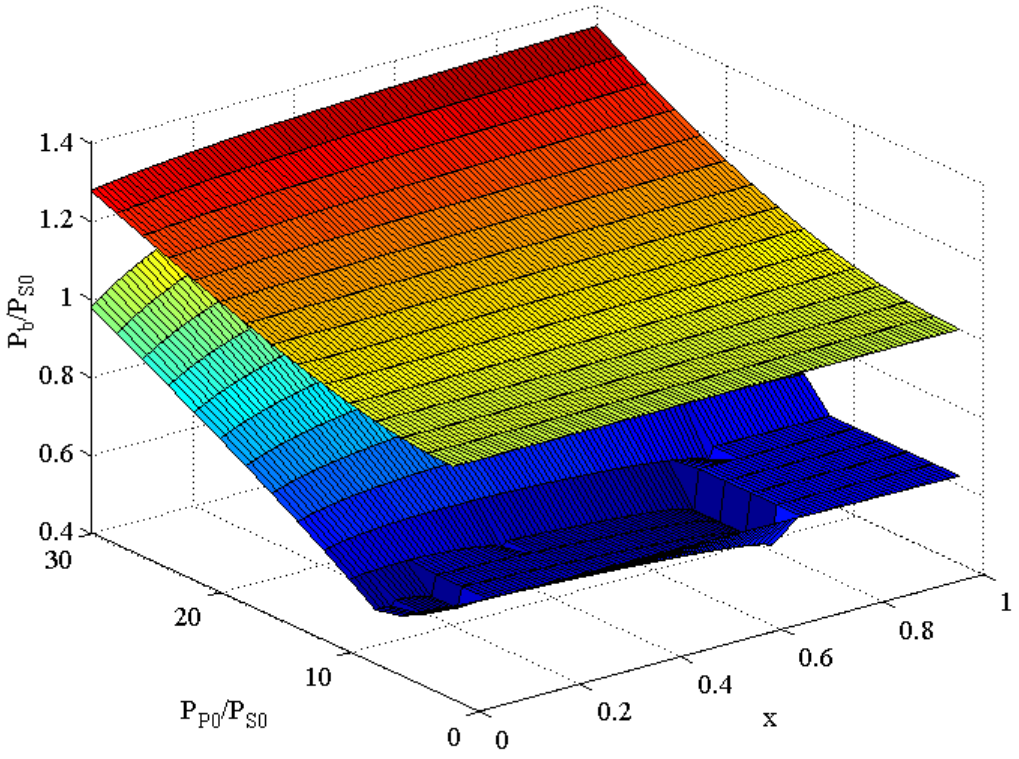

Fig. 6.3 3-D plot of operational P_b/P_{s0} against P_{p0}/P_{s0} and x, two-phase mixture supplied as the primary stream

The above 3-D plot gives a general picture of the operational P_b/P_{s0} range. To provide closer and more parametrical observation, a 2-D plot of this range is made. The curves of maximum P_b/P_{s0} and minimum P_b/P_{s0} are plotted against P_{p0}/P_{s0} for various x together in Fig. 6.4. For a given x, the operation range narrows with the increase of the

P_{p0}/P_{s0}. The upper limit P_b/P_{s0} curves do not differ much from each other for various x. Actually, those curves overlap together when P_{p0}/P_{s0} is less than 20, and they deviate from each other when P_{p0}/P_{s0} is bigger than 20. In contrast, the lower limit P_b/P_{s0} curves clearly differ from each other in the whole range of P_{p0}/P_{s0}.

The zone between curves of upper limit and lower limit is the rang of operable P_b/P_{s0}. As observed from Fig. 6.4, the operation range shrinks with the increase of P_{p0}/P_{s0} for all x , and the operable P_b/P_{s0} range of big x shrinks fast than that of the small x. When P_{p0}/P_{s0} is less than 15, the ranges are almost the same for all x. At $P_{p0}/P_{s0}=30$, the operable P_b/P_{s0} range is about 0.3 for $x=0$, but it is less than 0.05 for $x=1.0$.

To investigate the influence of mixture properties on ejector performance, the optimal ER is plotted against liquid quality x together with geometry parameters of κ and θ, respectively. These surfaces are generated for the ejectors with boundary conditions of $P_{p0}=364.7$ psia and $P_{s0}=34.7$ psia. Fig. 6.5 is the surface plot of optimal ER against κ combined with x, for a constant-area mixing ejector ($\theta=1$). It is obvious that the upper limit of ER decreases with the increase of x for a given κ. This trend is also reflected in Fig. 6.6, the surface plot of optimal ER against θ combined with x, for ejector with κ=100. The optimal ER decreases with the increase of x for a given θ.

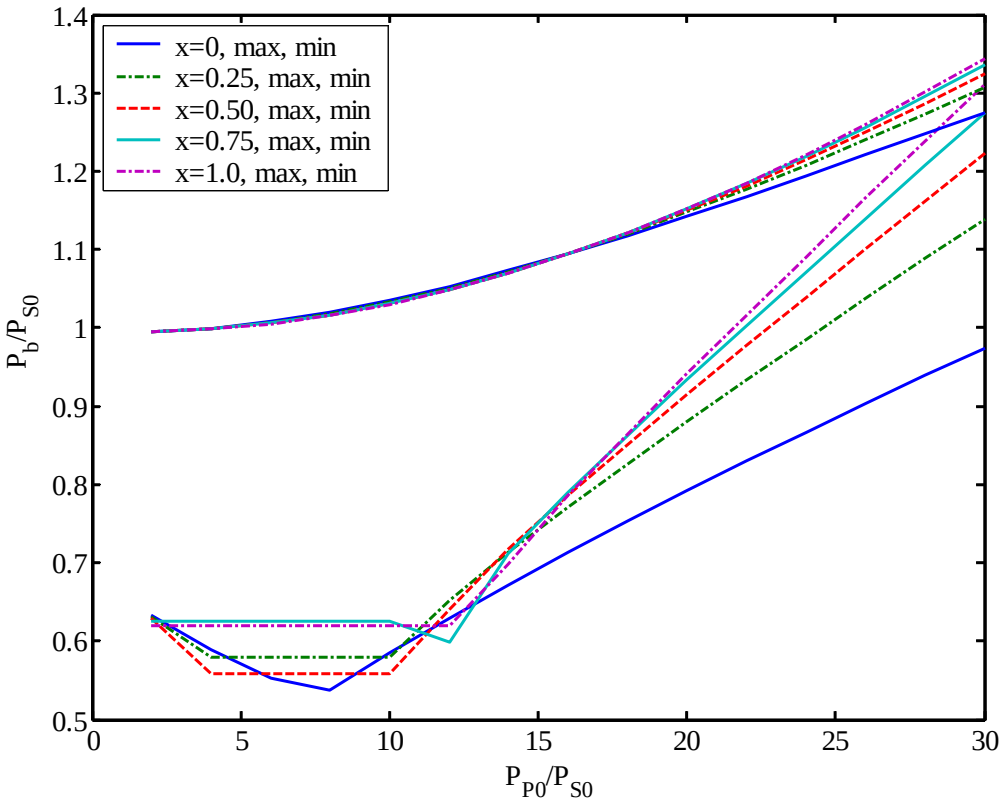

Fig. 6.4 2-D plot of operational P_b/P_{s0} against P_{p0}/P_{s0} for various x, two-phase mixture supplied as the primary stream

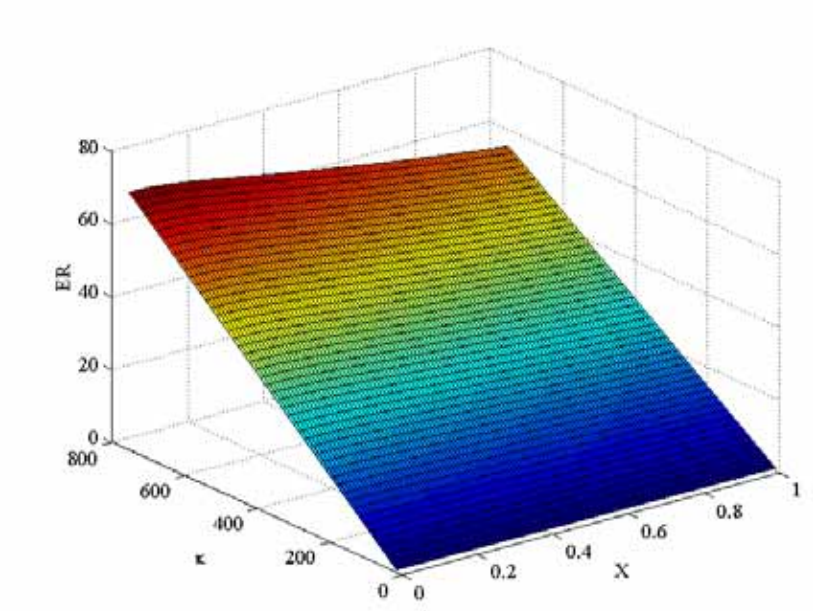

Fig. 6.5 Optimal ER surface against κ and x, two-phase mixture supplied as the primary stream

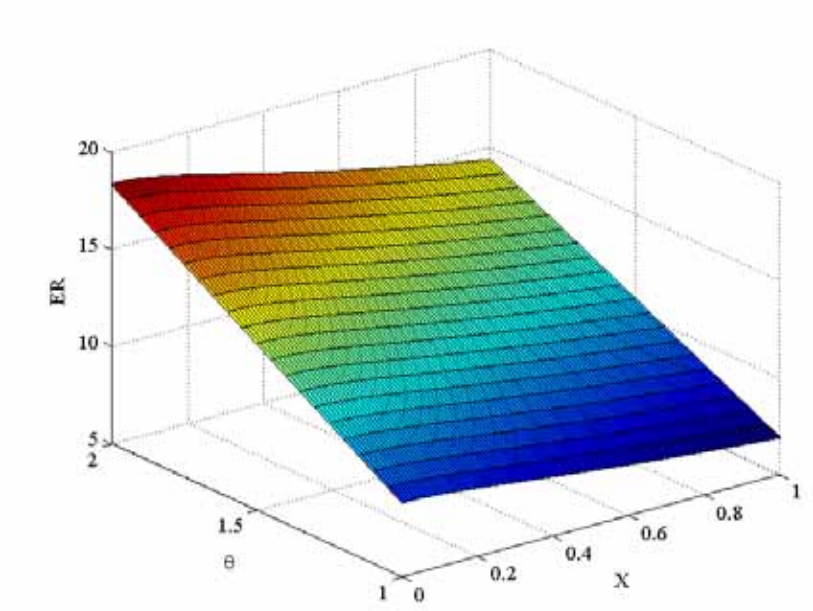

Fig. 6.6 Optimal ER surface against θ and x, two-phase mixture supplied as the primary stream

Mixture Supplied as Secondary Stream

Similar to the study for the case of two-phase mixture supplied as the primary stream, Fig. 6.7 through Fig. 6.10 are plotted to analyze the operation range and performance of the ejector with mixture supplied as secondary stream. Fig. 6.8 shows that the curves of P_b/P_{s0} upper limit overlap with each other for all x and the lower limit curves of P_b/P_{s0} do differ from each other for various x. The operation range also shrinks slowly with the increase of P_{p0}/P_{s0} for a given x. The shrinking rates are almost the same for various x values. When P_{p0}/P_{s0} is bigger than 20, these curves are almost parallel lines.

Fig. 6.9 and Fig. 6.10 are surface plots of optimal ER against κ combined with x and θ combined with x, respectively. Contrast to the case of mixture supplied as primary stream, the optimal ER increases with the increase of liquid quality x for given κ or given θ. This may imply that the ejector performance could be enhanced by adding small portion of liquid droplets to the secondary gas stream. Of course, the feasibility of this operation needs investigation. The test data from experiments could be very helpful to analyze this feature. In this study, the total entropy change method is employed to investigate this feasibility theoretically.

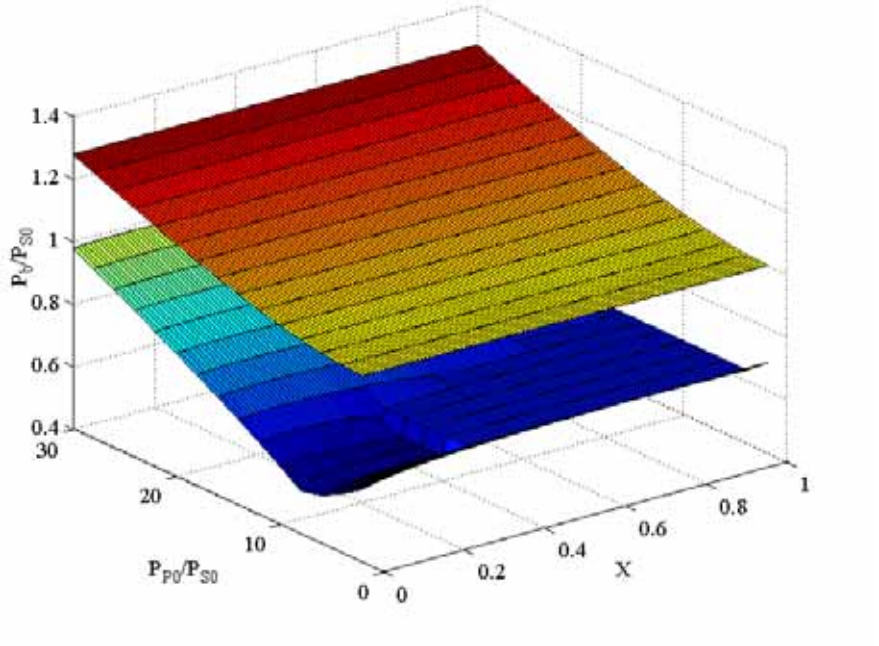

Fig. 6.7 3-D plot of P_b/P_{s0} vs. P_{p0}/P_{s0} and x, mixture supplied at suction port

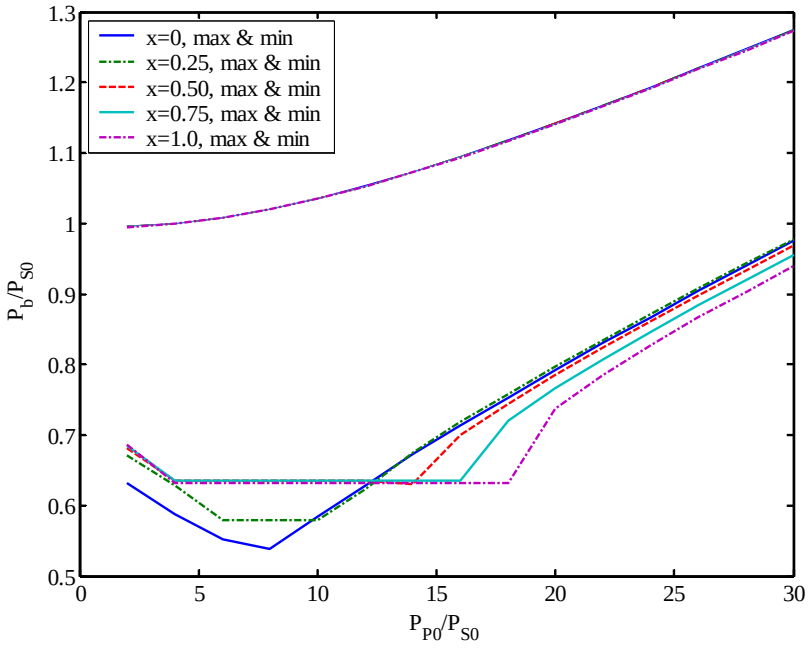

Fig. 6.8 2-D plot of P_b/P_{s0} vs. P_{p0}/P_{s0} for various x, mixture supplied at suction port

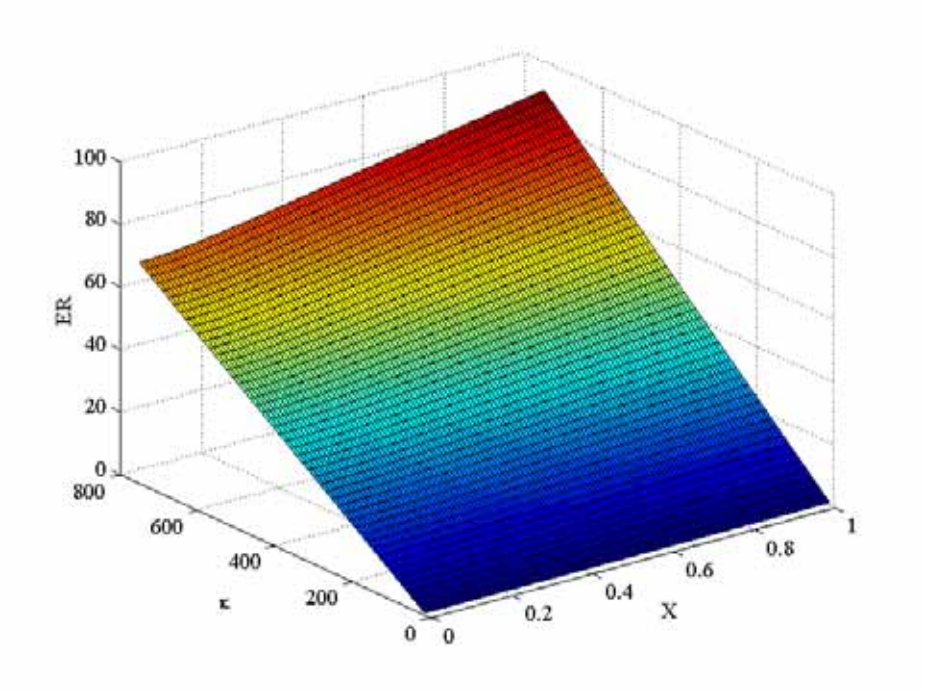

Fig. 6.9 Optimal ER surface vs. κ and x, mixture supplied at suction port

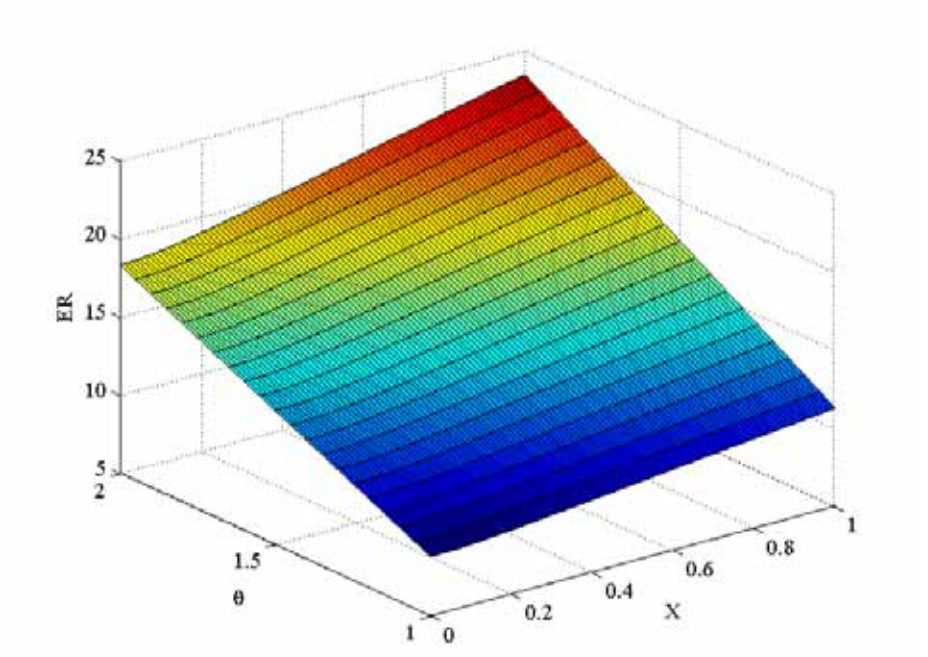

Fig. 6.10 Optimal ER surface vs. θ and x, mixture supplied at suction port

Operation Range Obtained by Entropy Analysis

In the previous sections, the optimal ER surface were generated for arbitrary ranges of κ, θ and x. Can ejectors be operated in those arbitrary ranges? This question will be answered by the analysis of the total entropy change.

The total entropy change is plotted against parameters of κ, θ and x, for both the case of mixture supplied as primary stream and the case of mixture supplied as the secondary stream. The ejector operation is feasible only when Δs is real and positive. The calculations shows that complex Δs could result in certain unreasonable ranges of κ, θ and x. The practical operation ranges are obtained by ruling out the areas of complex Δs and negative Δs. In order to plot Δs, the complex Δs are removed by converting them to be negative real numbers, which will be categorized to be "un-operable range". The Δs surface then is intercepted by the $\Delta s = 0$ plane and only the positive Δs part is left.

Fig. 6.11 and Fig. 6.12 are Δs surfaces for the case of two-phase mixture supplied as primary stream. Fig. 6.11 is Δs plotted against κ and x for constant-area mixing ejector. The impact of liquid quality x on the operational κ range is significant. When x is less than 0.3, the ejector could work properly in the whole given κ range. At the point of $x = 0.4$, κ can not be designed to more than 100. Fig. 6.12 is Δs plotted against θ and x. This figure shows that the operable θ range is very limited.

Fig. 6.13 and Fig. 6.14 are Δs surfaces for the case of mixture supplied at the suction port. These plots are very similar to those for the case of two-phase mixture supplied as primary stream. The operable ranges of κ and θ are even narrower than those shown in previous case.

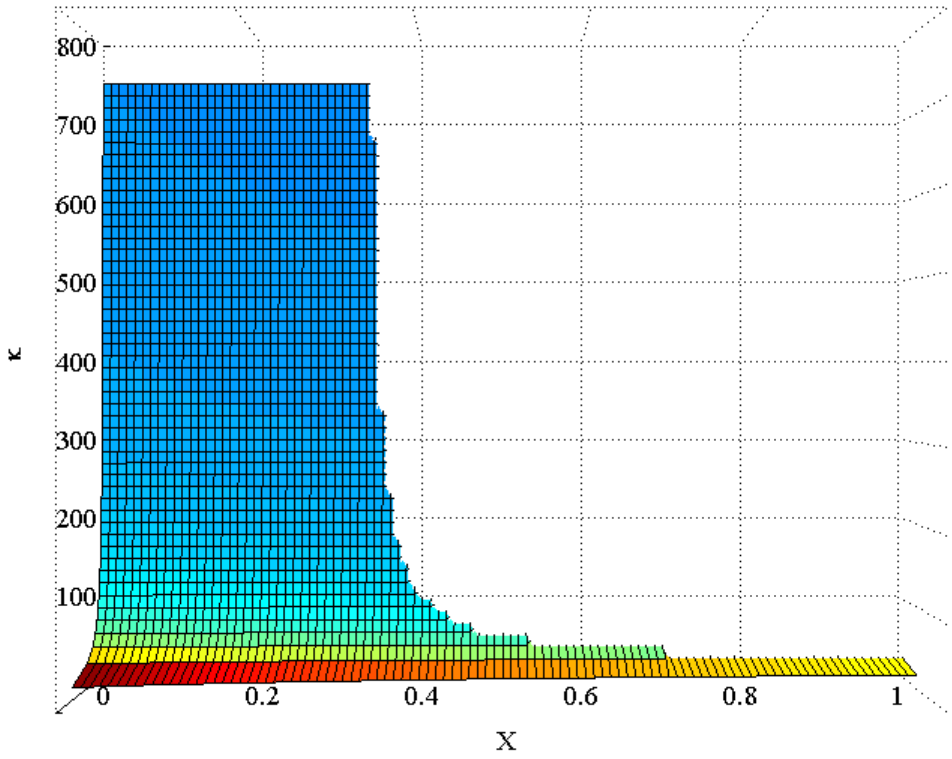

Fig. 6.11 Top-down view of Δs surface intercepted by $\Delta s = 0$ plane, mixture supplied as primary stream, $\theta = 1$

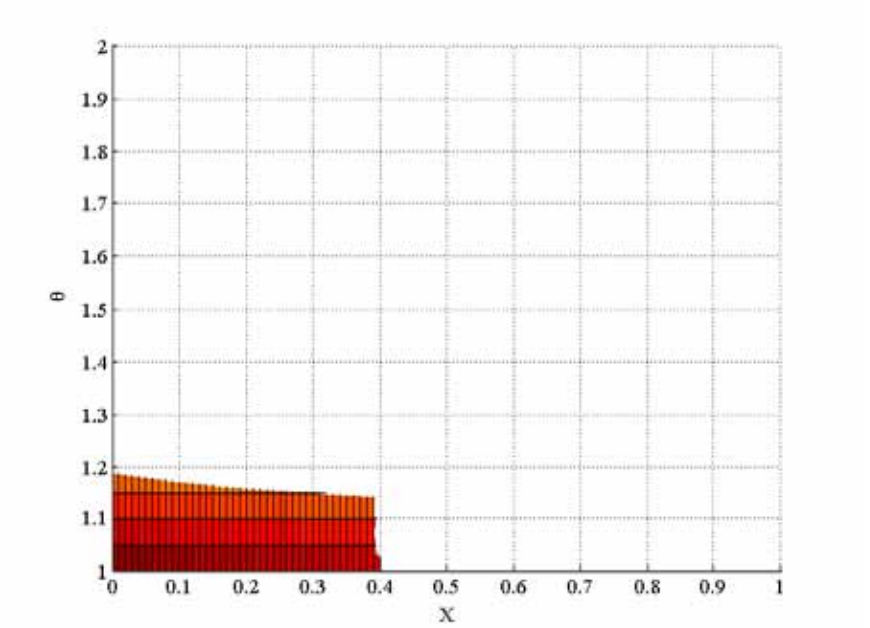

Fig. 6.12 Top-down view of Δs surface intercepted by $\Delta s = 0$ plane, mixture supplied as primary stream, $\kappa = 100$

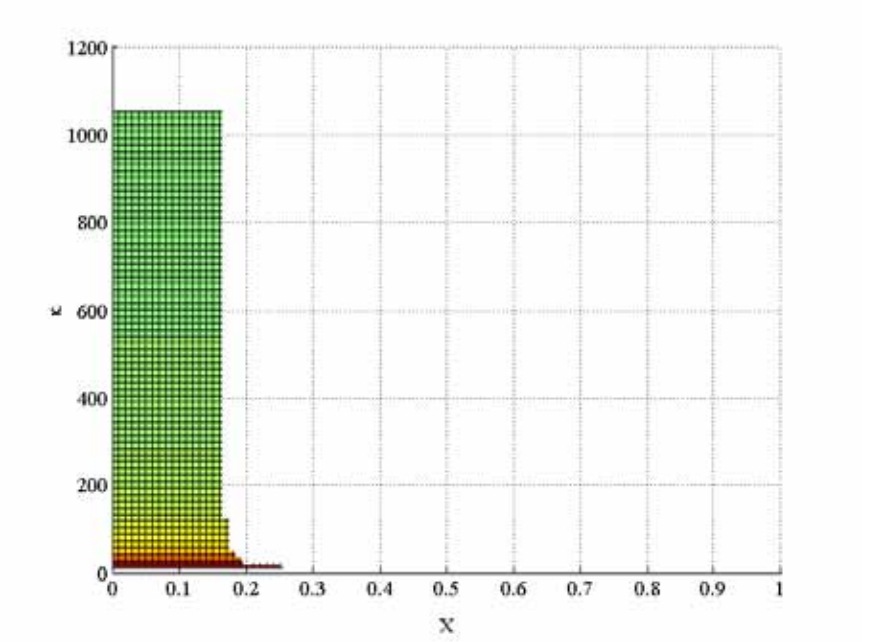

Fig. 6.13 Top-down view of Δs surface intercepted by $\Delta s = 0$ plane, mixture supplied at suction port, $\theta = 1$

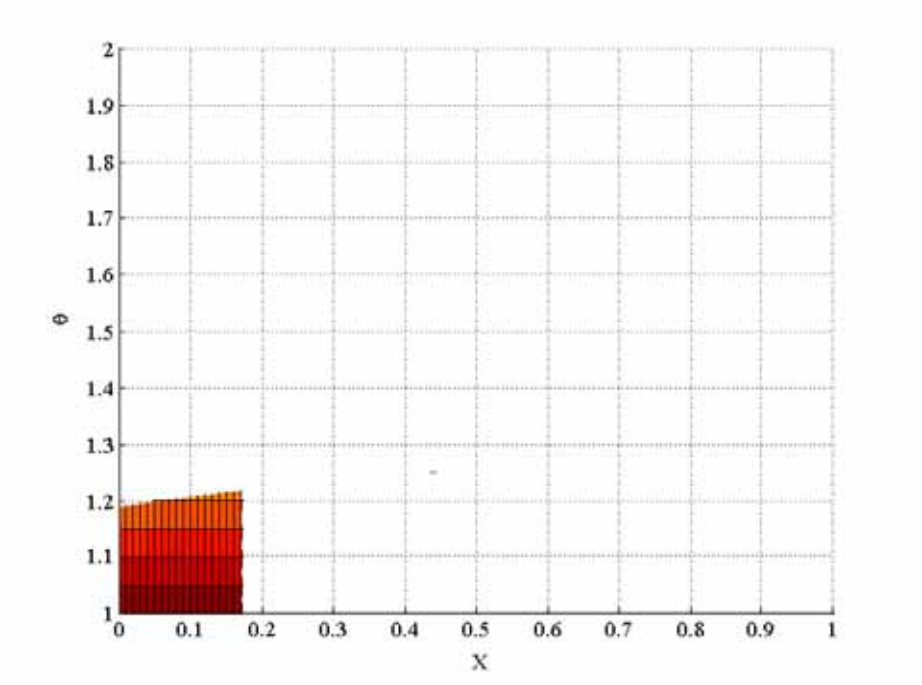

Fig. 6.14 Top-down view of Δs surface intercepted by $\Delta s = 0$ plane, mixture supplied at suction port, $\kappa = 100$

CONCLUSIONS

The thermodynamic properties of gas-like two-phase mixture flow are studied since the motivation of the dissertation research is to design a gas ejector which could work for gas-liquid flow. The ejector performance and operation range are investigated for two cases of operating conditions. One case is that mixture is supplied as the primary stream and the other case is that mixture is supplied as the secondary stream. The operational feasibility and operational ranges are analyzed and obtained by using the total entropy change method.

CHAPTER VII

SUMMARY AND CONCLUSIONS

SUMMARY

The ejector was introduced in the early 20th century. In a paper published in 1950, Keenan and Neumann [3] presented the first comprehensive theoretical and experimental analysis of an ejector. Since then, the constant-pressure mixing model and the constant-area mixing model developed, both by Keenan and Neumann [3], have become the basis of ejector design and performance analysis. Based on these methods, much research has been devoted to the improvement of ejector design methods including hundreds of papers related to supersonic ejectors. Significant progress has been made for these widely used ejector analytical models, but some problems remain outside their scope. The objective of this research was to develop a comprehensive ejector model which would embody all existing 1-D analytical ejector models and provide answers to the problems left unsolved by these existing models.

In the comprehensive theoretical study of ejector energy and momentum transfer, the basic concepts and governing equations of aerodynamics were introduced. The mechanism of choking phenomena, supersonic flow and shock wave have been described before the derivations of ejector models (since ejectors are usually designed and operated with supersonic primary flow). Fundamentals of an isentropic nozzle and

subsonic diffuser were provided before preliminary calculations were made for the ejector design.

Effort has been devoted to the detailed derivations and verifications of constant-pressure ejector model and constant-area ejector model. A parametric study was then performed on these models. The figures generated by the parametric analysis could be utilized to determine the geometry configurations for ejector design or to predict the ejector performance. An ejector design procedure and steps were developed for the use of the constant-area mixing model. It is still not practical to design a gas ejector with a constant-pressure mixing chamber since the geometry of a constant-pressure ejector can not be determined. Both the constant-area model and constant-pressure model were integrated into ESDUpac A9242, which is a computer program with comprehensive 1-D analytical models for gas ejector design and performance analysis. A flow chart of gas ejector design using ESDUpac A9242 has been developed.

The geometry of the supersonic primary nozzle determines a unique “on-design” point, but the practical ejector may be required to operate over a certain range. Thus, ejectors are usually operated under “off-design” conditions. Operating conditions critically affect the performance of an ejector. Some researchers have used coefficients and constants obtained from experimental data for particular ejectors to correct their performance predictions. However, these constants are only valid for the tested ejectors.

The CFD simulations provide the local details of the flow field which would be very helpful in understanding the complex mixing process. FLUENT, a commercial CFD software, was used to simulate gas ejector with single-phase gas flow. Very good agreement was found between the numerical calculations and the test results. The simulations also demonstrated FLUENT's ability to capture the supersonic shock waves which occurred in the primary nozzle. Upon validation, FLUENT was used to optimize the ejector geometric configuration. The optimization study shows that two parameters which most significantly impact ejector performance: the ratio of the mixing tube diameter to the nozzle throat diameter, the primary nozzle exit position. As an example of using FLUENT as a design tool, a specific gas ejector for a scalable PEM fuel system was designed.

CONCLUSIONS

A generalized ejector model was successfully developed for the gas ejector design and analysis. This new model has the following features.

1) It is a comprehensive model without assumptions made to simplify the momentum conservation equation for the mixing chamber. The geometry of the mixing chamber can be any given configuration; the mixing chamber entrance pressure can be different from mixing chamber exit pressure.
2) It is a generalized model. Both the constant-pressure model and the constant-area model can be derived from this model as particular cases.

3) For the first time, this novel model shows the relationship between the constant-pressure and constant-area 1-D ejector models.
4) The "off-design" operations are included in this new model. As discussed before, shock waves usually occur in the primary nozzle or at the nozzle exit. This phenomena is considered in the new model and the nozzle geometry determined unique "design value" of P_{p1} and M_{p1} are not adopted.
5) The static pressure at the mixing chamber entrance P_1 ($P_{p1} = P_{s1} = P_1$) is represented by the product of two parameters, μ and τ, which relate the boundary conditions to ejector performance.
6) The limitations of gas ejector design and operation can be obtained by the analysis of total entropy change. The total entropy change is split into two parts, the entropy change due to the shock of primary stream and the entropy change due to the mixing of the two streams.

Both the constant-pressure model and the constant-area model can be derived as particular cases of the new model. The generalized ejector model is simplified to be the constant-pressure model, when $P_1/P_{m2} = \mu\tau = 1$, i.e., $\tau = 1/\mu$. The constant-area ejector model is derived from the new model at $\theta = 1$.

The generalized ejector model provides answers for the unresolved problems of existing models. Currently, there is no way to determine the geometry of an ejector constant-pressure mixing chamber. The generalized model demonstrates that an ejector with an

exact constant-pressure mixing chamber is physically impossible to build. Also, It is generally believed in literature that the constant-pressure mixing ejector has better performance than the constant-area mixing ejector. The definitive or parametric explanation of this phenomenon is currently not available in the existing literature. The parametric analysis, used in this new model proves that the constant-area mixing ejector has the lowest performance. However, the new model also shows that the constant-area mixing ejector has the widest operating range as well as the biggest range of κ, the area ratios of mixing exit to primary nozzle throat.

For the first time, the generalized ejector model shows the relationship between the constant-pressure and constant-area models. The uniform, constant mixing pressure can not exactly established, but it can be very close to the real operation condition in a constant-area ejector. The predictions of constant-pressure ejector model could be very accurate if the geometry of the ejector is close to the constant-area mixing ejector. If the mixing chamber is far different from the constant-area mixing, large error could result from the predictions of the constant-pressure model.

The gas ejector and liquid jet pump have different design features. Using a gas ejector to transfer two-phase flow with a very high portion of liquid is impractical, however it is feasible if the liquid portion is very low and the mixture behaves like a gas. This dissertation studied the thermodynamic properties of gas-like two-phase mixture flow. The generalized ejector model is used to design an ejector working with this kind of two-

phase mixtures. The two-phase mixture can be supplied as the primary or secondary stream. The ejector performance and operation range are investigated for both operating cases. The operation feasibility and ranges are analyzed by the total entropy change method.

RECOMMENDATIONS

As discussed previously, there are two solutions of τ for each given μ; one corresponds to the supersonic mixed flow, and the other corresponds to the subsonic mixed flow. The supersonic solution is not considered since this study is limited to the design of a gas ejector for a PEM fuel cell system. The static pressure at the ejector downstream is either higher or slightly lower than the pressure at the suction port. Thus, the ejector mixed flow will be subsonic for this system. For most of the ejectors designed to compress secondary flow in a closed system, the mixed flow would be subsonic. In some applications, the ejector mixed flow could be supersonic. For example: the ejectors used for thrust in aerospace, the ejector used in the refrigeration system and discharging to a condenser. This is an area worthy of exploration using the generalized ejector model.

The generalized ejector model neglects wall friction and assumes the ejector inner wall to be adiabatic. This model would be more accurate if the friction, form loss and wall heat transfer were included. Two kinds of shock waves are possible within the nozzle or at the nozzle exit—the over-expansion shock or under-expansion shock. Should the

over-expansion shock occur, separation would usually happen. This is another area of study that can improve the predictions of analytical ejector models.

The generalized ejector model is a 1-D model, which only considers the areas of the flow channel. For the purpose of ejector design, it is necessary to know more about the details of the ejector geometry, such as the optimal length of the mixing chamber. Therefore, the development of a 2-D analytical model could be very helpful for gas ejector design.

This dissertation analyzed the performance of a gas ejector by use of the analytical models. It is desired to have further tests to compare the data with the analytical predictions. A better understanding of the behavior of a gas-like mixture in an ejector could be gained from numerical simulatioins. However, the feasibility of using CFD simulations to model gas ejectors working with gas-liquid two-phase flow is yet to be demonstrated.

REFERENCES

[1] Supak, K., 2007, “Reduced Gravity Rankine Cycle System Simulation and Design with Passive Vortex Phase Separation,” Texas A&M University Thesis.

[2] Lee, J. H., Sameen, A., Sanal Kumar, V. R., Kim, H. D., Choi, B. G. and Kim, K. H., 2005, “Studies on Ejector Systems for Hydrogen Fuel Cell,” Proceedings of 41st AIAA/ASME/SAE/ASEE Joint Propulsion Conference & Exhibit, Tucson, Arizona.

[3] Keenan, J.H. and Neumann, E.P., 1950, “An Investigation of Ejector Design by Analysis and Experiment,” J. Applied Mechanics, Trans ASME, **72**, pp. 299-309.

[4] Bonnington, S. T. and King, A. L., 1976, *Jet Pumps and Ejectors, A State of the Art Review and Bibliography*, 2nd Edition, BHRA Fluid Engineering, Cranfield, Bedford, UK.

[5] Sun, D.W. and Eames, I. W., 1995, “Recent Developments in the Design Theories and Applications of Ejectors—A Review,” Journal of the Institute of Energy, **68**, pp. 65-79.

[6] DeFrate, L. A. and Hoerl, A. E., 1959, “Optimum Design of Ejectors Using Digital Computers,” Computer Techniques, Chemical Engineering Progress Symposium Series, **55**(21), pp. 43-51.

[7] Emanuel, G., 1976, “Optimum Performance for a Single-Stage Gaseous Ejector,” AIAA J., **14**(9), pp. 1292-1296.

[8] Rice, P. and Dandachi, J., 1991, “An Equation for the Prediction of Steam Flowrate Required in the Design of Ejectors,” Trans I Chem E, **69A**, pp. 332-334.

[9] Huang, B.J., Chang, J.N., Wang, C.P. and Petrenko, V.A., 1999, “A 1-D Analysis of Ejector Performance,” International Journal of Refrigeration, **22**, pp. 354-364.

[10] Keenan, J.H. and Neumann, E.P., 1942, “A Simple Air Ejector,” Journal of Applied Mechanics, **9**(2), pp. A75-A81.

[11] Fabri, J. and Siestrunck R., 1958, “Supersonic Air Ejectors,” Advances in Appied Mechanics, Vol. **V**, pp. 1-34.

[12] Addy, A. L. and Chow, W. L., 1964, “On the Starting Characteristics of Supersonic Ejector Systems,” Journal of Basic Engineering, Trans ASME, **86**(4), pp. 861-868.

[13] Chow, W. L. and Addy, A. L., 1964, “Interaction between Primary and Secondary Streams of Supersonic Ejector Systems and Their Performance Characteristics,” AIAA Journal, **2**(4), pp. 686-695.

[14] Dutton, J. C. and Carroll B. F., 1986, “Optimal Supersonic Ejector Designs,” Journal of Fluids Engineering, **108**, pp. 415-420.

[15] Goff, J. A. and Coogan, C. H., 1942, “Some Two Dimensional Aspects of the Ejector Problem,” Journal of Applied Mechanics, Trans ASME, **9**(4), pp. A151-A154.

[16] Mikhail, S., 1960, “Mixing of Coaxial Streams inside a Closed Conduit,” Journal of Mechanical Engineering Science, **2**(1), pp. 59-68.

[17] Hedges, K. R. and Hill, P. G., 1974, “Compressible Flow Ejectors Part I — Development of a Finite-Difference Flow Model,” Journal of Fluids Engineering, Trans ASME, **96**, pp. 272-281.

[18] Gilbert, G. B. and Hill, P. G., 1973, “Analysis and Testing of Two-Dimensional Slot

Nozzle Ejectors with Variable Area Mixing Sections," NASA Contractor Report CR-2251.

[19] Neve, R. S., 1993, "Computational Fluid Dynamics Analysis of Diffuser Performance in Gas-Powered Jet Pumps," International Journal of Heat and Fluid Flow, **14**(4), pp. 401-407.

[20] Riffat, S. B., Gan, G. and Smith, S., 1996, "Computational Fluid Dynamics Applied to Ejector Heat Pumps," Applied Thermal Engineering, **16**(4), pp. 291-297.

[21] Bartosiewicz, Y., Aidoun, Z., Desevaux, P. and Mercadier, Y., 2005, "Numerical and Experimental Investigations on Supersonic Ejectors," International Journal of Heat and Fluid Flow, **26**, pp. 56-70.

[22] Bartosiewicz, Y., Aidoun, Z. and Mercadier, Y., 2006, "Numerical Assessment of Ejector Operation for Refrigeration Applications Based on CFD," Applied Thermal Engineering, **26**, pp. 604-612.

[23] Fox, R. W., McDonald, A. T. and Pritchard, P. J., 2003, *Introduction to Fluid Mechanics*, 6th Edition, John Wiley & Sons, Inc., Hoboken, NJ.

[24] Yapici, R. and Ersoy, H. K., 2005, "Performance Characteristics of the Ejector Refrigeration System Based on the Constant Area Ejector Flow Model," Energy Conversion and Management, **46**, pp. 3117-3135.

[25] Fluent Inc., 2006, *FLUENT 6.3 User's Guide*, Fluent Inc., Lebanon, NH.

[26] Snyder, L. E., 2004, "A Feasibility Study of Internal Evaporative Cooling for Proton Exchange Membrane Fuel Cells," Texas A&M University Thesis.

[27] Caimi, R. E. and Thaxton, E. A., 1993, "Supersonic Gas-Liquid Cleaning System,"

NASA conference publication: The Fourth National Technology Transfer Conference and Exposition, Volume 1 pp. 232-240.

APPENDIX A

MATLAB PROGRAM DEVELOPED FOR PARAMETRIC STUDIES

ON CONSTANT-PRESSURE EJECTOR MODEL

Main Programs

1) ER-AR_P1.m

```
% Main Program for constant-pressure gas ejector AR-ER plots
% It is an 1-D analytical model for constant-pressure gas ejector calculations
% There is a separate parameter input file
%
clear all;                              % clear previous variables, clear the figures

load parameters;                        % load the input data
P_S0=para{8};

PR=[1.0,0.98,0.95,0.90,0.80,0.70];      % vector of P1/P_s0


for L=1:6
   P1(L)=P_S0*PR(L);                    % vector of P1
end

N=30;
ER=zeros(N,1);                          % initialize the ER vector
AR=zeros(N,6);                          % initialized the AR vector

for I=1:10
   ER(I)=I*0.1;                         % give arbitrary value to ER
end

for I=11:19
   ER(I)=ER(10)+(I-10)*1;
end

for I=20:28
   ER(I)=ER(19)+(I-19)*10;
end

for I=29:N
   ER(I)=ER(28)+(I-28)*50;
end
```

```
for K=1:6
   P1_TMP=P1(K);
   for J=1:N
      ER_TMP=ER(J);
      [AR_M2T,AR_M2P1,AR_P1T]=ARM2T(P1_TMP,ER_TMP);      % call function ARM2T
      AR(J,K)=AR_M2T;                                    % AR
   end
end

% Plot the AR vs.ER
figure(1);
plot(AR(1:N,1),ER(1:N),'-',AR(1:N,2),ER(1:N),'--',AR(1:N,3),ER(1:N),'-',AR(1:N,4),ER(1:N),'--
',AR(1:N,5),ER(1:N),'-',AR(1:N,6),ER(1:N),'--')
title(sprintf('Entrainment Ratio vs.Area Ratio'))
xlabel('AR')
ylabel('ER')
legend('P1/P_S0=1.0','P1/P_S0=0.98','P1/P_S0=0.95','P1/P_S0=0.90','P1/P_S0=0.80','P1/P_S0=0.70')
```

2) ER-CR-AR.m

```
% Main Program for constant-pressure ejector for the relationship of ER, AR and CR
%
clear all;                    % clear previous variables, clear the figures

load parameters;              % load input data
P_S0=para{8};

PR=0.95;                      % P1/P_s0=0.95
P1=P_S0*PR;                   % P1

N=30;
ER=zeros(N,1);                % initialize the ER vector
AR=zeros(N,1);                % initialize the AR vector
CR=zeros(N,1);                % initialize the CR vector

% Give arbitrary values to ER
for I=1:10
   ER(I)=I*0.1;
end

for I=11:19
   ER(I)=ER(10)+(I-10)*1;
end

for I=20:28
   ER(I)=ER(19)+(I-19)*10;
end

for I=29:N
```

```
   ER(I)=ER(28)+(I-28)*50;
end

% calculate CR and AR
for J=1:N
   ER_TMP=ER(J);
   [AR_M2T,AR_M2P1,AR_P1T]=ARM2T(P1,ER_TMP);
   [CR_TP]=PRCR(P1,ER_TMP);
   CR(J)=CR_TP;
   AR(J)=AR_M2T;
end

% Plot the ER vs.AR
figure(1);
plot(AR,ER,'-')
title(sprintf('Entrainment Ratio vs.Area Ratio'))
xlabel('AR')
ylabel('ER')

% Plot the CR vs.AR
figure(2);
plot(AR,CR,'-')
title(sprintf('Compression Ratio vs.Area Ratio'))
xlabel('AR')
ylabel('CR')

% Plot the CR vs.ER
figure(3);
plot(ER,CR,'-')
title(sprintf('Compression Ratio vs.Entrainment Ratio'))
xlabel('ER')
ylabel('CR')
```

3) AR-Mm2-CR.m

```
% Main Program developed to investigate the relationships of AR, M_m2 and CR
%
clear all;                    % clear previous variables, clear the figures

load parameters;              % load input data
P_S0=para{8};

PR=0.95;                      % give arbitrary value, P1/P_S0=0.95
P1=P_S0*PR;

N=30;
ER=zeros(N,1);                % initialize the ER vector
AR=zeros(N,1);                % initialize the AR vector
CR=zeros(N,1);                % initialize the CR vector
M_M2=zeros(N,1);              % initialize the M_m2 vector
```

```
% give arbitrary value to ER

for I=1:10
   ER(I)=I*0.1;
end

for I=11:19
   ER(I)=ER(10)+(I-10)*1;
end

for I=20:28
   ER(I)=ER(19)+(I-19)*10;
end

for I=29:N
   ER(I)=ER(28)+(I-28)*50;
end

% calculate M_M2, CR, AR

for J=1:N
   ER_TMP=ER(J);
   [AR_M2T,AR_M2P1,AR_P1T]=ARM2T(P1,ER_TMP);
   [CR_TP]=PRCR(P1,ER_TMP);
   [MM2_TMP]=MM2(P1,ER_TMP);
   M_M2(J)=MM2_TMP;
   CR(J)=CR_TP;
   AR(J)=AR_M2T;
end

% Plot the M_m2 vs.AR
figure(1);
plot(AR,M_M2,'-')
title(sprintf('M_M2 vs.Area Ratio'))
xlabel('AR')
ylabel('M_M2')

% Plot the M_m2 vs.CR
figure(2);
plot(M_M2,CR,'-')
title(sprintf('Compression Ratio vs.M_M2'))
xlabel('M_M2')
ylabel('CR')
```

Subroutines

4) ParametersInput.m

```
clear all; clf;          % clear previous variables, clear the figures

% input the boundary conditions
GAMMA_P=1.4;          % Primary stream gas specific heat ratio, Cp/Cv
GAMMA_S=1.66;         % Secondary stream gas specific heat ratio, Cp/Cv
MW_P=28.97;           % Primary stream gas molecular weight, kg/kg-mol
MW_S=4;               % Secondary stream gas molecular weight, kg/kg-mol
P0_P=264.7            % Primary stream stagnation pressure, psia
P0_S=34.7             % Secodnary stream stagnation pressure, psia
T0_P=300;             % Primary stream gas stagnation temperature, K
T0_S=300;             % Secodnary stream gas stagnation temperature, K
DT=0.0145;            % Nozzle throat diameter, inch
D1=0.02;              % Nozzle exit diameter, inch
D2=0.17;              % Mixing chamber diameter, inch
D3=0.20;              % Diffuser exit diameter, inch
ETA_N=0.95;           % Nozzle isentropic efficiency coefficient
ETA_D=0.96;           % Diffuser isentropic efficiency coefficient

% Gas constant
R_BAR=8312;           % Universal gas constant, J/(kg-mol.K)
R_P=R_BAR/MW_P;       % Primary stream gas constant, J/(kg.K)
R_S=R_BAR/MW_S;       % Secondary stream gas constant, J/(kg.K)

% Units conversion
P0_P=P0_P*6894.76;    % Primary stream stagnation pressure, Pa
P0_S=P0_S*6894.76;    % Secodnary stream stagnation pressure, Pa
DT=DT*2.54/100;       % Nozzle throat diameter, m
D1=D1*2.54/100;       % Nozzle exit diameter, m
D2=D2*2.54/100;       % Mixing chamber diameter,m
D3=D3*2.54/100;       % Diffuser exit diameter, m

% Area calculations
AT=pi*DT*DT/4;        % Nozzle throat area, m2
A1=pi*D1*D1/4;        % Nozzle exit area, m2
A2=pi*D2*D2/4;        % Mixing chamber area, m2
A3=pi*D3*D3/4;        % Diffuser exit area, m

%*****************************
para{1}=GAMMA_P;
para{2}=GAMMA_S;
para{3}=R_P;
para{4}=R_S;
para{5}=T0_P;
para{6}=T0_S;
para{7}=P0_P;
para{8}=P0_S;
para{9}=AT;
para{10}=A1;
para{11}=A2;
para{12}=A3;
para{13}=ETA_N;
para{14}=ETA_D;
```

```
%*****************************
save parameters para
```

5) NOZZLE.m

```
function [M_P,P_P1,AR_P1T,P_PT,T_PT,C_PT]=NOZZLE(M_P1);

load parameters;

GAMMA_P=para{1};
R_P=para{3};
T_P0=para{5};
P_P0=para{7};
AT=para{10};
ETA_N=para{13};

TMP1=2/(GAMMA_P+1);
TMP2=GAMMA_P/(GAMMA_P-1);

P_PT=P_P0*(TMP1^TMP2);
T_PT=T_P0*TMP1;
C_PT=sqrt(R_P*T_P0*TMP1*GAMMA_P);
V_PT=C_PT;

TMP3=(GAMMA_P+1)/(GAMMA_P-1);
TMP4=sqrt((GAMMA_P/R_P)*(TMP1^TMP3));
TMP5=sqrt(T_P0);
TMP6=AT*P_P0;

M_P=(TMP6/TMP5)*TMP4;

TMP7=ETA_N*(1+(GAMMA_P-1)*M_P1*M_P1/2);
TMP8=1-1/ETA_N+1/TMP7;
P_P1=P_P0*(TMP8^TMP2);
AR_P1T=(1/M_P1)*(TMP1^(TMP3/2))/(TMP8^(TMP3/2));
% end of function
```

6) ARM2T.m

```
function [AR_M2T,AR_M2P1,AR_P1T]=ARM2T(P1,ER);

M_P1=MP1(P1);

[AR_M2P1]=ARM2P1(P1,ER);
[M_P,P_P1,AR_P1T,P_PT,T_PT,C_PT]=NOZZLE(M_P1);
AR_M2T=AR_M2P1*AR_P1T;

% end of function
```

7) FUN2.m

```
function [F2]=FUN2(GAMMA,M);

F2TM1=1+(GAMMA-1)*M*M/2;
F2TM2=sqrt(GAMMA*F2TM1);

F2=M*F2TM2;
% end of function
```

8) MP1.m

```
function [M_P1]=MP1(P1);

load parameters;
GAMMA_P=para{1};
P_P0=para{7};
ETA_N=para{13};

PR=P1/P_P0;
MP1T1=GAMMA_P-1;
MP1T2=2/MP1T1;
MP1T3=MP1T1/GAMMA_P;

TM1=ETA_N*(1-PR^MP1T3);
TM2=TM1/(1-TM1);

M_P1=sqrt(MP1T2*TM2);
% end of function
```

9) MS1.m

```
function [M_S1]=MS1(P1);

load parameters;
GAMMA_S=para{2};
P_S0=para{8};

PR_S=P1/P_S0;
MS1T1=GAMMA_S-1;
MS1T2=2/MS1T1;
MS1T3=-MS1T1/GAMMA_S;

TM1_S=PR_S^MS1T3-1;
```

```
M_S1=sqrt(MS1T2*TM1_S);
% end of function
```

10) MIX.m

```
function [GAMMA_M,R_M,T_M0,TR_M0P0]=MIX(ER);

load parameters;
GAMMA_P=para{1};
GAMMA_S=para{2};
R_P=para{3};
R_S=para{4};
T_P0=para{5};
T_S0=para{6};

GMTM1=1/(GAMMA_P-1);
GMTM2=GAMMA_P/(GAMMA_P-1);
GMTM3=1/(GAMMA_S-1);
GMTM4=GAMMA_S/(GAMMA_S-1);
GMTM5=R_S/R_P;

GAMMA_M=(GMTM2+GMTM4*GMTM5*ER)/(GMTM1+GMTM3*GMTM5*ER);
R_M=(R_P+ER*R_S)/(1+ER);

TR=T_S0/T_P0;
TR_M0P0=(GMTM2+GMTM4*GMTM5*TR*ER)/(GMTM2+GMTM4*GMTM5*ER);
T_M0=T_P0*TR_M0P0;
% end of function
```

11) MM2.m

```
function [M_M2]=MM2(P1,ER);

load parameters;
GAMMA_P=para{1};
GAMMA_S=para{2};
R_P=para{3};
R_S=para{4};
P_P0=para{7};

RR_SP=R_S/R_P;
GMR_SP=GAMMA_S/GAMMA_P;
TR_S1P1=TRS1P1(P1);
M_P1=MP1(P1);
M_S1=MS1(P1);
ZETA=M_P1+ER*M_S1*sqrt(GMR_SP*RR_SP*TR_S1P1);

[GAMMA_M,R_M,T_M0,TR_M0P0]=MIX(ER);
```

```
GMR_MP=GAMMA_M/GAMMA_P;
RR_MP=R_M/R_P;
PR_POP1=P_P0/P1;
SAI=(1+ER)*sqrt(GMR_MP*RR_MP*TR_M0P0)*(PR_POP1^((GAMMA_P-1)/(2*GAMMA_P)));

CR=ZETA/SAI;
M_M2=CR*sqrt(1-CR*CR*(GAMMA_M-1)/2);
% end of function
```

12) ARM2P1.m

```
function [AR_M2P1]=ARM2P1(P1,ER);

load parameters;
GAMMA_P=para{1};
R_P=para{3};
T_P0=para{5};

M_P1=MP1(P1);
F2_P=FUN2(GAMMA_P,M_P1);

[GAMMA_M,R_M,T_M0,TR_M0P0]=MIX(ER);
M_M2=MM2(P1,ER);
F2_M=FUN2(GAMMA_M,M_M2);
RR_MP=R_M/R_P;

AR_M2P1=sqrt(TR_M0P0*RR_MP)*(F2_P/F2_M)*(1+ER);
% end of function
```

13) TRS1P1.m

```
function [TR_S1P1]=TRS1P1(P1);

load parameters;
GAMMA_P=para{1};
GAMMA_S=para{2};
T_P0=para{5};
T_S0=para{6};
P_P0=para{7};
P_S0=para{8};

TRTM1=(GAMMA_P-1)/GAMMA_P;
TRTM2=-(GAMMA_S-1)/GAMMA_S;
TRTM3=T_S0/T_P0;
TRTM4=P_P0/P1;
TRTM5=P_S0/P1;

TR_S1P1=TRTM3*(TRTM4^TRTM1)*(TRTM5^TRTM2);
```

```
% end of function
```

14) PRCR.m

```
function [CR]=PRCR(P1,ER);

load parameters;
P_S0=para{8};
ETA_D=para{14};

[GAMMA_M,R_M,T_M0,TR_M0P0]=MIX(ER);
M_M2=MM2(P1,ER);
M_M3=M_M2;

TP1=ETA_D*M_M3*M_M3*(GAMMA_M-1)/2;
TP2=GAMMA_M/(GAMMA_M-1);

PR_40M3=(1+TP1)^TP2;
PR_M3P1=1;
PR_P1S0=P1/P_S0;

CR=PR_40M3*PR_M3P1*PR_P1S0;
% end of function
```

APPENDIX B

MATLAB PROGRAM DEVELOPED FOR PARAMETRIC STUDIES

ON CONSTANT-AREA EJECTOR MODEL

Main Programs

1) ER-AR-variousP1.m

```
% Main Program for the relationship of ER-AR
% The pressure ratio P1/P_S0 are 0.95, 0.90, 0.80, 0.70, 0.60, 0.50.
% P_S0 is fixed so that P1 is various according to the pressure ratio of P1/P_s0.
% It is an 1-D analytical model for constant-pressure gas ejector calculations
% There is a separate parameter input file
clear all;                                  % clear previous variables, clear the figures

load parameters;                            % load input data
P_S0=para{8};

PR=[0.95,0.90,0.80,0.70,0.60,0.50];         % P1/P_S0 vector

for L=1:6
   P1(L)=P_S0*PR(L);                        % P1
end

N=41;
AR=zeros(N,1);                              % initialize AR vector
DR=zeros(N,1);                              % initialize DR vector
ER=zeros(N,6);                              % initialize ER vector

% give arbitrary values to AR
for I=1:10
   AR(I)=I*1.0;
end

for I=11:28
   AR(I)=AR(10)+(I-10)*5.0;
end

for I=29:36
   AR(I)=AR(28)+(I-28)*50.0;
end

for I=37:N
```

```
   AR(I)=AR(36)+(I-36)*100.0;
end

% calcualte ER
for K=1:6
   P1_TMP=P1(K);
   M_P1=MP1(P1_TMP);
   M_S1=MS1(P1_TMP);
   for J=1:N
      AR_TMP=AR(J);
      [ER_TP]=OMEGA(M_P1,M_S1,AR_TMP);
      ER(J,K)=ER_TP;
   end
end

% convert ER to DR
for I=1:N
   DR(I)=sqrt(AR(I));
end

% write AR and ER to EXCEL files
wk1write('CAAR.xls',AR);
wk1write('CAER.xls',ER);

% Plot the ER vs.AR
figure(1);
plot(AR(1:N),ER(1:N,1),'-',AR(1:N),ER(1:N,2),'--',AR(1:N),ER(1:N,3),'-',AR(1:N),ER(1:N,4),'--
',AR(1:N),ER(1:N,5),'-',AR(1:N),ER(1:N,6),'--')
title(sprintf('Entrainment Ratio vs.Area Ratio'))
xlabel('Area Ratio of Mixing Chamber to Nozzle Throat')
ylabel('Entrainment Ratio')
legend('P1/P_S0=0.95','P1/P_S0=0.90','P1/P_S0=0.80','P1/P_S0=0.70','P1/P_S0=0.60','P1/P_S0=0.50')

% Plot the ER vs.DR
figure(2);
plot(DR(1:N),ER(1:N,1),'-',DR(1:N),ER(1:N,2),'--',DR(1:N),ER(1:N,3),'-',DR(1:N),ER(1:N,4),'--
',DR(1:N),ER(1:N,5),'-',DR(1:N),ER(1:N,6),'--')
title(sprintf('Entrainment Ratio vs.Area Ratio'))
xlabel('Diameter Ratio of Mixing Chamber to Nozzle Throat')
ylabel('Entrainment Ratio')
legend('P1/P_S0=0.95','P1/P_S0=0.90','P1/P_S0=0.80','P1/P_S0=0.70','P1/P_S0=0.60','P1/P_S0=0.50')
```

2) ER-AR-variousT0.m

```
% Main Program for plots of ER-AR,for various temperature ratio of T_S0/T_P0
% T_P0 is fixed at 300K, T_S0 is various according to the value of T_S0/T_P0
% P1 is a fixed value, P1=0.90*P_S0
% It is an 1-D analytical model for constant-area gas ejector calculations
% There is a separate parameter input file
%
```

```
clear all;                                  % clear previous variables and figures

load parameters;                            % load input data
P_S0=para{8};
T_P0=para{5};

TR=[0.90,0.95,1.0,1.05,1.10,1.20,1.30];     % Temperature ratio of T_S0/T_P0 vector
PR=0.90;                                    % Pressure ratio P1/P_S0 is given as 0.90
P1=P_S0*PR;                                 % Calculate P1

N=41;
AR=zeros(N,1);                              % Initialize AR vector
DR=zeros(N,1);                              % Initialize DR vector
ER=zeros(N,7);                              % Initialize ER vector
TS0=zeros(7,1);                             % Initialize T_S0 vector

for L=1:7
   TS0(L)=T_P0*TR(L);                       % Calculate T_S0
end

% Give arbitrary values to AR
for I=1:10
   AR(I)=I*1.0;
end

for I=11:28
   AR(I)=AR(10)+(I-10)*5.0;
end

for I=29:36
   AR(I)=AR(28)+(I-28)*50.0;
end

for I=37:N
   AR(I)=AR(36)+(I-36)*100.0;
end

M_P1=MP1(P1);                               % Calculate M_P1
M_S1=MS1(P1);                               % Calculate M_S1

for K=1:7
   TS0_TMP=TS0(K);
   for J=1:N
      AR_TMP=AR(J);
      [ER_TP]=OMEGA(M_P1,M_S1,AR_TMP,TS0_TMP);    % Calculate ER, call function OMEGA
      ER(J,K)=ER_TP;
   end
end

for I=1:N
   DR(I)=sqrt(AR(I));                                % Convert AR to DR
end
```

```
% Plot the ER vs.AR
figure(1);
plot(AR(1:N),ER(1:N,1),'-',AR(1:N),ER(1:N,2),'--',AR(1:N),ER(1:N,3),'-',AR(1:N),ER(1:N,4),'--
',AR(1:N),ER(1:N,5),'-',AR(1:N),ER(1:N,6),'--',AR(1:N),ER(1:N,7),'-')
title(sprintf('Entrainment Ratio vs.Area Ratio'))
xlabel('Area Ratio of Mixing Chamber to Nozzle Throat')
ylabel('Entrainment Ratio')
legend('T_S0/T_P0=0.90','T_S0/T_P0=0.95','T_S0/T_P0=1.0','T_S0/T_P0=1.05','T_S0/T_P0=1.10','T_S0/
T_P0=1.20','T_S0/T_P0=1.30')

% Plot the ER vs.AR
figure(2);
plot(DR(1:N),ER(1:N,1),'-',DR(1:N),ER(1:N,2),'--',DR(1:N),ER(1:N,3),'-',DR(1:N),ER(1:N,4),'--
',DR(1:N),ER(1:N,5),'-',DR(1:N),ER(1:N,6),'--',DR(1:N),ER(1:N,7),'-')
title(sprintf('Entrainment Ratio vs.Area Ratio'))
xlabel('Diameter Ratio of Mixing Chamber to Nozzle Throat')
ylabel('Entrainment Ratio')
legend('T_S0/T_P0=0.90','T_S0/T_P0=0.95','T_S0/T_P0=1.0','T_S0/T_P0=1.05','T_S0/T_P0=1.10','T_S0/
T_P0=1.20','T_S0/T_P0=1.30')
```

3) CR-ER.m

```
% Main Program for plots of ER-CR, ER-M_M3
% ER and M_M3 are clacualted by using arbitrary AR values
% P1 is a fixed value, P1=0.90*P_S0
% It is an 1-D analytical model for constant-area gas ejector calculations
% There is a separate parameter input file
%
clear all;                    % clear previous variables, clear the figures

load parameters;              % load input data
P_S0=para{8};

PR=0.90;                      % P1/P_S0=0.90
P1=P_S0*PR;                   % calcualte P1

N=41;
AR=zeros(N,1);                % initialize AR vector
ER=zeros(N,1);                % initialize ER vector
MM3A=zeros(N,1);              % initialize M_M3A vector, there are two solutions for each AR
MM3B=zeros(N,1);              % initialize M_M3B vector, there are two solutions for each AR
CR=zeros(N,1);                % initialize CR vector

for I=1:10
   AR(I)=I*1.0;               % give arbitrary values to AR
end

for I=11:28
   AR(I)=AR(10)+(I-10)*5.0;   % give arbitrary values to AR
```

```
end

for I=29:36
   AR(I)=AR(28)+(I-28)*50.0;       % give arbitrary values to AR
end

for I=37:N
   AR(I)=AR(36)+(I-36)*100.0;      % give arbitrary values to AR
end

M_P1=MP1(P1);                  % calucalte M_P1
M_S1=MS1(P1);                  % calucalte M_S1
for J=1:N
   AR_TMP=AR(J);
   [ER_TP]=OMEGA(M_P1,M_S1,AR_TMP);            % calucalte ER
   [MM3_1,MM3_2]=MM3(M_P1,M_S1,ER_TP);         % calucalte M_M3
   [CR_TP]=PREJ(AR_TMP,ER_TP,M_P1,MM3_1,P1);   % calucalte CR

   ER(J)=ER_TP;
   MM3A(J)=MM3_1;
   MM3B(J)=MM3_2;
   CR(J)=CR_TP;
end

% Plot the AR_S1P1 vs.ER
figure(1);
plot(ER,MM3A,'-',ER,MM3B,'--')
title(sprintf('MM3 vs.ER'))
xlabel('Entrainment Ratio')
ylabel('MM3')

% Plot the AR_S1P1 vs.ER
figure(2);
plot(ER,MM3A,'-')
title(sprintf('MM3 vs.ER'))
xlabel('Entrainment Ratio')
ylabel('MM3')

% Plot the AR_S1P1 vs.ER
figure(3);
plot(ER,CR,'-')
title(sprintf('CR vs.ER'))
xlabel('Entrainment Ratio')
ylabel('Compression Ratio')
```

4) AR-AR-variousGAMMA.m

```
% This a program developed to investigate the impact of specific heat ratio on the ejector performance
% ER is plotted against AR for various gamma_s/gamma_p, with gamma_p fixed
% P1 is a fixed value, P1=0.90*P_S0
```

```
% It is an 1-D analytical model for constant-area gas ejector calculations
% There is a separate parameter input file
%
clear all;                                          % clear previous variables, clear the figures

load parameters;                                    % load input data
GAMMA_P=para{1};
P_S0=para{8};

GR=[0.80,0.90,1.0,1.20,1.40,1.60,1.80];             % gamma_s/gamma_p ratio vector
PR=0.90;                                            % P1/P_S0 =0.90
P1=P_S0*PR;                                         % calculate P1

N=41;
AR=zeros(N,1);                                      % initialize the AR vector
DR=zeros(N,1);                                      % initialize the DR vector
ER=zeros(N,7);                                      % initialize the ER vector
GAMMA_S=zeros(7,1);                                 % initialize the GAMMA_S vector

for L=1:7
   GAMMA_S(L)=GAMMA_P*GR(L);                        % calcualte GAMMA_S
end

% give arbitrary values to AR
for I=1:10
   AR(I)=I*1.0;
end

for I=11:28
   AR(I)=AR(10)+(I-10)*5.0;
end

for I=29:36
   AR(I)=AR(28)+(I-28)*50.0;
end

for I=37:N
   AR(I)=AR(36)+(I-36)*100.0;
end

M_P1=MP1(P1);                                       % calculate M_P1
for K=1:7
   GAMMAS=GAMMA_S(K)
   M_S1=MS1(P1,GAMMAS)                              % calculate M_S1
   for J=1:N
      AR_TMP=AR(J);
      [ER_TP]=OMEGA(M_P1,M_S1,AR_TMP,GAMMAS);    % calcualte ER
      ER(J,K)=ER_TP;
   end
end

for I=1:N
   DR(I)=sqrt(AR(I));                                    % convert AR to DR
```

```
end

% Plot the ER vs.AR
figure(1);
plot(AR(1:N),ER(1:N,1),'-',AR(1:N),ER(1:N,2),'--',AR(1:N),ER(1:N,3),'-',AR(1:N),ER(1:N,4),'--
',AR(1:N),ER(1:N,5),'-',AR(1:N),ER(1:N,6),'--',AR(1:N),ER(1:N,7))
title(sprintf('Entrainment Ratio vs.Area Ratio'))
xlabel('Area Ratio of Mixing Chamber to Nozzle Throat')
ylabel('Entrainment Ratio')
legend('gamma_s/gamma_p=0.8','gamma_s/gamma_p=0.9','gamma_s/gamma_p=1.0','gamma_s/gamma_p
=1.2','gamma_s/gamma_p=1.4','gamma_s/gamma_p=1.6','gamma_s/gamma_p=1.8')

% Plot the ER vs.AR
figure(2);
plot(DR(1:N),ER(1:N,1),'-',DR(1:N),ER(1:N,2),'--',DR(1:N),ER(1:N,3),'-',DR(1:N),ER(1:N,4),'--
',DR(1:N),ER(1:N,5),'-',DR(1:N),ER(1:N,6),'--',DR(1:N),ER(1:N,7),'-')
title(sprintf('Entrainment Ratio vs.Area Ratio'))
xlabel('Diameter Ratio of Mixing Chamber to Nozzle Throat')
ylabel('Entrainment Ratio')
legend('gamma_s/gamma_p=0.8','gamma_s/gamma_p=0.9','gamma_s/gamma_p=1.0','gamma_s/gamma_p
=1.2','gamma_s/gamma_p=1.4','gamma_s/gamma_p=1.6','gamma_s/gamma_p=1.8')
```

5) ER-AR-variousETAN.m

```
% This a program developed to investigate the impact of primary nozzle efficiency coefficient
% ETA_N on the ejector performance curve ER
% ER is plotted against AR for various ETA_N
% P1 is calcualted according to the primary nozzle geometry and ETA_N values

clear all;                          % clear previous variables, clear the figures

load parameters;                    % load input data
P_P0=para{7};
P_S0=para{8};

ETA_N=[0.98,0.95,0.90,0.85,0.8,0.7,0.60];     % define ETA_N vector

N=41;
AR=zeros(N,1);                      % initialize AR vector
DR=zeros(N,1);                      % initialize DR vector
ER=zeros(N,7);                      % initialize ER vector

% give arbitrary values to AR
for I=1:10
   AR(I)=I*1.0;
end

for I=11:28
   AR(I)=AR(10)+(I-10)*5.0;
end
```

```
for I=29:36
   AR(I)=AR(28)+(I-28)*50.0;
end

for I=37:N
   AR(I)=AR(36)+(I-36)*100.0;
end

% Calcualte P1, ER
for K=1:7

   ETA_TMP=ETA_N(K)
   [M_P1,PR_P1P0]=CFMP1(ETA_TMP);          % calcualte P1 according to nozzle geometry, by
                                              least square data fit skill
   P1=P_P0*PR_P1P0
   PR_P1S0=P1/P_S0

   M_S1=MS1(P1);                           % calcualte M_S1
  for J=1:N
     AR_TMP=AR(J);
     [ER_TP]=OMEGA(M_P1,M_S1,AR_TMP,ETA_TMP); % calculate ER
     ER(J,K)=ER_TP;
  end
end

for I=1:N
   DR(I)=sqrt(AR(I));              % convert AR to DR
end

% Plot the ER vs.AR
figure(1);
plot(AR(1:N),ER(1:N,1),'-',AR(1:N),ER(1:N,2),'--',AR(1:N),ER(1:N,3),'-',AR(1:N),ER(1:N,4),'--
',AR(1:N),ER(1:N,5),'-',AR(1:N),ER(1:N,6),'--',AR(1:N),ER(1:N,7),'-')
title(sprintf('Entrainment Ratio vs.Area Ratio'))
xlabel('Area Ratio of Mixing Chamber to Nozzle Throat')
ylabel('Entrainment Ratio')
legend('eta_n=0.98','eta_n=0.95','eta_n=0.90','eta_n=0.85','eta_n=0.80','eta_n=0.70','eta_n=0.60')

% Plot the ER vs.DR
figure(2);
plot(DR(1:N),ER(1:N,1),'-',DR(1:N),ER(1:N,2),'--',DR(1:N),ER(1:N,3),'-',DR(1:N),ER(1:N,4),'--
',DR(1:N),ER(1:N,5),'-',DR(1:N),ER(1:N,6),'--',DR(1:N),ER(1:N,7),'-')
title(sprintf('Entrainment Ratio vs.Diameter Ratio'))
xlabel('Diameter Ratio of Mixing Chamber to Nozzle Throat')
ylabel('Entrainment Ratio')
legend('eta_n=0.98','eta_n=0.95','eta_n=0.90','eta_n=0.85','eta_n=0.80','eta_n=0.70','eta_n=0.60')
```

Subroutines

6) ParametersInput.m

```
clear all; clf;          % clear previous variables, clear the figures

% input the boundary conditions
GAMMA_P=1.4;          % Primary stream gas specific heat ratio, Cp/Cv
GAMMA_S=1.66;         % Secondary stream gas specific heat ratio, Cp/Cv
MW_P=28.97;           % Primary stream gas molecular weight, kg/kg-mol
MW_S=4;               % Secondary stream gas molecular weight, kg/kg-mol
P0_P=264.7;           % Primary stream stagnation pressure, psia
P0_S=34.7;            % Secodnary stream stagnation pressure, psia
T0_P=300;             % Primary stream gas stagnation temperature, K
T0_S=300;             % Secodnary stream gas stagnation temperature, K
DT=0.0145;            % Nozzle throat diameter, inch
D1=0.0195;            % Nozzle exit diameter, inch
D2=0.17;              % Mixing chamber diameter, inch
D3=0.20;              % Diffuser exit diameter, inch
ETA_N=0.95;           % Nozzle isentropic efficiency coefficient
ETA_D=0.96;           % Diffuser isentropic efficiency coefficient

% Gas constant
R_BAR=8312;           % Universal gas constant, J/(kg-mol.K)
R_P=R_BAR/MW_P;       % Primary stream gas constant, J/(kg.K)
R_S=R_BAR/MW_S;       % Secondary stream gas constant, J/(kg.K)

% Units conversion
P0_P=P0_P*6894.76;    % Primary stream stagnation pressure, Pa
P0_S=P0_S*6894.76;    % Secodnary stream stagnation pressure, Pa
DT=DT*2.54/100;       % Nozzle throat diameter, m
D1=D1*2.54/100;       % Nozzle exit diameter, m
D2=D2*2.54/100;       % Mixing chamber diameter,m
D3=D3*2.54/100;       % Diffuser exit diameter, m

% Area calculations
AT=pi*DT*DT/4;        % Nozzle throat area, m2
A1=pi*D1*D1/4;        % Nozzle exit area, m2
A2=pi*D2*D2/4;        % Mixing chamber area, m2
A3=pi*D3*D3/4;        % Diffuser exit area, m2

AR_P1T=(D1/DT)*(D1/DT);

%*****************************
para{1}=GAMMA_P;
para{2}=GAMMA_S;
para{3}=R_P;
para{4}=R_S;
para{5}=T0_P;
para{6}=T0_S;
para{7}=P0_P;
para{8}=P0_S;
para{9}=AT;
```

```
para{10}=A1;
para{11}=A2;
para{12}=A3;
para{13}=ETA_N;
para{14}=ETA_D;
para{15}=AR_P1T;
%*****************************
save parameters para
```

7) CFMP1.m

```
function [MP1_N,PR_N]=CFMP1(ETA);

load parameters;
AR_NOZZLE=para{15};

N=40;
MP1_CF=zeros(N,1);
AR_CF=zeros(N,1);
PR_CF=zeros(N,1);

A=1.0;
B=2.6;
DM=(B-A)/N;

for I=1:N
   MP1_CF(I)=1.0+I*DM;
end

for J=1:N
      MP1_TMP=MP1_CF(J);
      [PR1,AR1]=NOZLCF(MP1_TMP,ETA);
      PR_CF(J)=PR1;
      AR_CF(J)=AR1;
end


X=AR_CF;
Y=MP1_CF;
P=polyfit(X,Y,6);

MP1_N=polyval(P,AR_NOZZLE);
[PRTMP,ARTMP]=NOZLCF(MP1_N,ETA);
PR_N=PRTMP;
% end of function
```

8) NOZLCF.m

```
function [PR_P1P0,AR_P1T]=NOZZLE(MP1,ETA_TMP);
```

```
load parameters;
GAMMA_P=para{1};

TMP1=(GAMMA_P+1);
TMP2=(GAMMA_P-1);
TMP3=GAMMA_P/(GAMMA_P-1);
TMP4=(GAMMA_P+1)/(2*(GAMMA_P-1));
TMP5=ETA_TMP*(1+TMP2*MP1*MP1/2);
TMP6=1-1/ETA_TMP;

PR_P1P0=(TMP6+1/TMP5)^TMP3;
AR_P1T=(1/MP1)*((2/TMP1)^TMP4)/((TMP6+1/TMP5)^TMP4);
% end of function
```

9) FUN5.m

```
function [F5]=FUN5(M,ETA_N);

load parameters;
GAMMA_P=para{1};
%ETA_N=para{13};

TM1=2/(GAMMA_P+1);
TM2=(GAMMA_P+1)/(2*(GAMMA_P-1));
TM3=(GAMMA_P-1)/2;
TM4=ETA_N*(1+TM3*M*M);
TM5=1-1/ETA_N+1/TM4;

F5=(1/M)*(TM1^TM2)/(TM5^TM2);
% end of function
```

10) FUNP.m

```
function [FP]=FUNP(ETA,GAMMA,M);

FP_TM1=(ETA-1)/ETA;
FP_TM2=(GAMMA-1)*M*M/2;
FP_TM3=GAMMA/(GAMMA-1);

FP=(FP_TM1*FP_TM2+1)^FP_TM3;
% end of function
```

11) FUNT.m

```
function [FT]=FUNT(GAMMA,M);
```

```
FT_TM1=(GAMMA+1)/(2*(GAMMA-1));
FT_TM2=1+(GAMMA-1)*M*M/2;

FT=FT_TM2^FT_TM1;
% end of function
```

12) MS1.m

```
function [M_S1]=MS1(P1);

load parameters;

GAMMA_S=para{2};
P_S0=para{8};

PR_S=P1/P_S0;
MS1T1=GAMMA_S-1;
MS1T2=2/MS1T1;
MS1T3=-MS1T1/GAMMA_S;

TM1_S=PR_S^MS1T3-1;

M_S1=sqrt(MS1T2*TM1_S);
% end of function
```

13) OMEGA.m

```
function [ER_TMP]=OMEGA(MP1,MS1,AR,ETA_N);

load parameters;
GAMMA_P=para{1};
GAMMA_S=para{2};
R_P=para{3};
R_S=para{4};
T_P0=para{5};
T_S0=para{6};
P_P0=para{7};
P_S0=para{8};
%ETA_N=para{13};

T1=P_S0/P_P0;
T2=T_P0/T_S0;
T3=R_P/R_S;
T4=GAMMA_S/GAMMA_P;
T5=MS1/MP1;

F5=FUN5(MP1,ETA_N);
FT_S=FUNT(GAMMA_S,MS1);
```

```
FT_P=FUNT(GAMMA_P,MP1);
FP=FUNP(ETA_N,GAMMA_P,MP1);

ERTM1=T1*T5;
ERTM2=sqrt(T2*T3*T4);
ERTM3=AR/F5-1;
ERTM4=FT_P/(FT_S*FP);

ER_TMP=ERTM1*ERTM2*ERTM3*ERTM4;
% end of function
```

14) MP1.m

```
function [M_P1]=MP1(P1);

load parameters;
GAMMA_P=para{1};
P_P0=para{7};
ETA_N=para{13};

PR=P1/P_P0;
MP1T1=GAMMA_P-1;
MP1T2=2/MP1T1;
MP1T3=MP1T1/GAMMA_P;

TM1=ETA_N*(1-PR^MP1T3);
TM2=TM1/(1-TM1);

M_P1=sqrt(MP1T2*TM2);
% end of function
```

15) FUN2.m

```
function [F2]=FUN2(GAMMA,M);

F2TM1=1+(GAMMA-1)*M*M/2;
F2TM2=sqrt(GAMMA*F2TM1);

F2=M*F2TM2;
% end of function
```

16) FUN4.m

```
function [F4]=FUN4(GAMMA,M);

F4TM1=(1+GAMMA*M*M)/M;
```

```
F4TM2=(GAMMA-1)/2;
F4TM3=1+F4TM2*M*M;
F4TM4=1/sqrt(GAMMA*F4TM3);

F4=F4TM1*F4TM4;
% end of function
```

17) ALPHA.m

```
function [ALFA]=ALPHA(MP1,MS1,ER);

load parameters;

GAMMA_P=para{1};
GAMMA_S=para{2};
R_P=para{3};
R_S=para{4};
T_P0=para{5};
T_S0=para{6};

[GAMMA_M,R_M,T_M0,TR_M0P0]=MIX(ER);

F4_S=FUN4(GAMMA_S,MS1);
F4_P=FUN4(GAMMA_P,MP1);

TR=T_S0/T_P0;
RR=R_S/R_P;

TRM=T_M0/T_P0;
RRM=R_M/R_P;

TMP1=sqrt(TR*RR);
TMP2=sqrt(TRM*RRM);

ALFA=(TMP1*F4_S*ER+F4_P)/(TMP2*(1+ER));
% end of function
```

18) MIX.m

```
function [GAMMA_M,R_M,T_M0,TR_M0P0]=MIX(ER);

load parameters;

GAMMA_P=para{1};
GAMMA_S=para{2};
R_P=para{3};
R_S=para{4};
T_P0=para{5};
T_S0=para{6};
```

```
GMTM1=1/(GAMMA_P-1);
GMTM2=GAMMA_P/(GAMMA_P-1);
GMTM3=1/(GAMMA_S-1);
GMTM4=GAMMA_S/(GAMMA_S-1);
GMTM5=R_S/R_P;

GAMMA_M=(GMTM2+GMTM4*GMTM5*ER)/(GMTM1+GMTM3*GMTM5*ER);
R_M=(R_P+ER*R_S)/(1+ER);

TR=T_S0/T_P0;
TR_M0P0=(GMTM2+GMTM4*GMTM5*TR*ER)/(GMTM2+GMTM4*GMTM5*ER);
T_M0=T_P0*TR_M0P0;
% end of function
```

19) MM3.m

```
function [MM3_1,MM3_2]=MM3(MP1,MS1,ER);

[GAMMA_M,R_M,T_M0,TR_M0P0]=MIX(ER);
[ALFA]=ALPHA(MP1,MS1,ER);

C1=ALFA*ALFA-2;
C2=2*GAMMA_M/(GAMMA_M-1);
C3=(GAMMA_M-1)/GAMMA_M;
C4=GAMMA_M-1;
C5=ALFA*ALFA-C2;

TERM1=sqrt(C1*C1+2*C3*C5);
TERM2=C4*C5
TERM3=-C1+TERM1
TERM4=-C1-TERM1

MM3_1=sqrt(TERM3/TERM2);
MM3_2=sqrt(TERM4/TERM2);
% end of function
```

20) PREJ.m

```
function [CR]=PREJ(AR,ER,MP1,MM3,P1);

load parameters;

P_S0=para{8};
ETA_D=para{14};

[GAMMA_M,R_M,T_M0,TR_M0P0]=MIX(ER);

TP1=ETA_D*MM3*MM3*(GAMMA_M-1)/2;
```

```
TP2=GAMMA_M/(GAMMA_M-1);

PR_40M3=(1+TP1)^TP2;
[PR_M3P1]=PRM3P1(AR,ER,MP1,MM3);
PR_P1S0=P1/P_S0;

CR=PR_40M3*PR_M3P1*PR_P1S0;
% end of function
```

21) PRM3P1.m

```
function [PR_M3P1]=PRM3P1(AR,ER,MP1,MM3);

load parameters;

GAMMA_P=para{1};
R_P=para{3};
T_P0=para{5};

[AR_M3P1]=ARM3P1(AR,MP1);
AR_P1M3=1/AR_M3P1;
[GAMMA_M,R_M,T_M0,TR_M0P0]=MIX(ER);

T1=T_M0/T_P0;
T2=R_M/R_P;
T3=sqrt(T1*T2);

F2P=FUN2(GAMMA_P,MP1);
F2M=FUN2(GAMMA_M,MM3);

PR_M3P1=T3*AR_P1M3*F2P*(1+ER)/F2M;
% end of function
```

22) ARM3P1.m

```
function [AR_M3P1]=ARM3P1(AR,MP1);

[M_P,P_P1,AR_P1T,P_PT,T_PT,C_PT]=NOZZLE(MP1);

AR_M3P1=AR/AR_P1T;
% end of function
```

23) NOZZLE.m

```
function [M_P,P_P1,AR_P1T,P_PT,T_PT,C_PT]=NOZZLE(M_P1);
```

```
load parameters;

GAMMA_P=para{1};
R_P=para{3};
T_P0=para{5};
P_P0=para{7};
AT=para{10};
ETA_N=para{13};

TMP1=2/(GAMMA_P+1);
TMP2=GAMMA_P/(GAMMA_P-1);

P_PT=P_P0*(TMP1^TMP2);
T_PT=T_P0*TMP1;
C_PT=sqrt(R_P*T_P0*TMP1*GAMMA_P);
V_PT=C_PT;

TMP3=(GAMMA_P+1)/(GAMMA_P-1);
TMP4=sqrt((GAMMA_P/R_P)*(TMP1^TMP3));
TMP5=sqrt(T_P0);
TMP6=AT*P_P0;

M_P=(TMP6/TMP5)*TMP4;

TMP7=ETA_N*(1+(GAMMA_P-1)*M_P1*M_P1/2);
TMP8=1-1/ETA_N+1/TMP7;
P_P1=P_P0*(TMP8^TMP2);
AR_P1T=(1/M_P1)*(TMP1^(TMP3/2))/(TMP8^(TMP3/2));
% end of function
```

APPENDIX C

MATLAB PROGRAM DEVELOPED FOR PARAMETRIC STUDIES

ON GENERALIZED EJECTOR MODEL

Main Programs

1) General-Features.m

```
% This is a program developed to investigate the general features of generalized ejector model
% Relationships of MU, TAO, ER, ENTROPY,M_P1, M_S1, M_M3, etc. will be plotted as figures
% Values of MU are given arbitrary
% It is an 1-D analytical model for generalized ejector model
% There is a separate parameter input file
%
clear all;                          % clear previous variables, clear the figures

THETA=1.2;                          %  theta=1.2, arbitrary given
AR_M2T=80;                          %  KAPPA=80, arbitrary given

N=500;
TESTMU=zeros(N-1,1);                %  initialize MU vector
ENTROPY=zeros(N-1,1);               %  initialize total entropy,i.e.,delta_S_total, vector
ENTROMIX=zeros(N-1,1);              %  initialize entropy component, delta_s_mix, vector
ENTROPX=zeros(N-1,1);               %  initialize entropy component, delta_s_x, vector
ERR=zeros(N-1,1);                   %  initialize ER vector
MMIX=zeros(N-1,1);                  %  initialize M_MIX vector
TM2=zeros(N-1,1);                   %  initialize T_M2 vector
PRS0M=zeros(N-1,1);                 %  initialize TAO vector
MUTAO=zeros(N-1,1);                 %  initialize MU*TAO vector
MS1S=zeros(N-1,1);                  %  initialize M_S1 vector
MP1S=zeros(N-1,1);                  %  initialize M_P1 vector

DETAMU=1.0/N;

for K=1:N-1
   TESTMU(K)=K*DETAMU;              % give arbitrary values to MU
end

for J=1:N-1

   MU=TESTMU(J);
   [M_S1]=MS1(MU);                                  % calcualte M_S1
```

```
   [ARS1P1,ARS1M2,ARP1M2]=ARS(THETA,AR_M2T);     % calculate area ratios
   [M_P1,MP1SQ]=MP1(MU);                          % calculate M_P1
   [S_PX,PR_0I0X]=SPX(MU,M_P1);                   % calculate entropy change
                                                  % component delta_S_shock

   [ER]=OMEGA(M_P1,M_S1,THETA,AR_M2T);            % calcualte ER
   [GAMMA_M,R_M,T_M0,TR_M0P0]=MIX(ER);            % calcualte properties of mixed flow
   [TR_P1S1]=TRP1S1(M_P1,M_S1);                   % calcualte temperature ratio of T_P1/T_S1
   [D]=TMD(M_P1,M_S1,ARS1M2,ARP1M2);              % calcualte temporary parameter D
   [E]=TME(ER,M_S1,ARS1M2);                       % calcualte temporary parameter E
   [TAO1,TAO2]=TAO(ER,MU,D,E,GAMMA_M);            % calcualte TAO, there are two solutions

   PR_S0M2=TAO2;                                  % the supersonic TAO is discarded,and subsonic is kept

   [M_M2,MM2SQ]=MM2(GAMMA_M,MU,D,PR_S0M2);        % calculate M_M2

   [TR_M2P1]=TRM2P1(M_M2,ER,M_P1);                % calculate the temperature ratio of T_M2/T_P1
   [PR_1M2]=PR1M2(MU,PR_S0M2);                    % calculate the pressure ratio of P1/P_M2
   [S_MIX]=SMIX(M_M2,M_P1,M_S1,ER,MU,PR_S0M2);    % calculate the entropy change
                                                  % component of delta_s_mix
   [S_TOT]=STOT(M_M2,M_P1,M_S1,ER,MU,PR_S0M2);    % calculate the total entropy change
                                                  % delta_S

   PRS0M(J)=PR_S0M2;
   TM2(J)=T_M0/TFUN(GAMMA_M,M_M2);
   ENTROPX(J)=S_PX/(1+ER);
   ENTROMIX(J)=S_MIX;
   ENTROPY(J)=S_TOT;

   MUTAO(J)=TESTMU(J)*PRS0M(J);

   ERR(J)=ER;
   MMIX(J)=M_M2;

   MS1S(J)=M_S1;
   MP1S(J)=M_P1;
end

ER_MAX=max(ERR);                                  % find the maximum ER value

% Plot total entropy change and its two components against MU
figure(1);
plot(TESTMU,ENTROPY,'-',TESTMU,ENTROPX,'-.',TESTMU,ENTROMIX,'--')
title(sprintf('Entropy Change vs.MU'))
xlabel('MU')
ylabel('delta_S')
legend('s_total','s_shock,','s_mixing')

% Plot ER against MU
figure(2);
plot(TESTMU,ERR,'-')
title(sprintf('ER vs.MU'))
xlabel('MU')
```

```
ylabel('ER')

% Plot M_MIX against MU
figure(3);
plot(TESTMU,MMIX,'-')
title(sprintf('Mach Number of Mixed Flow vs.MU'))
xlabel('MU')
ylabel('M_MIX')

% Plot total entropy change against MU
figure(4);
plot(TESTMU,ENTROPY,'-')
title(sprintf('Total Entropy Change vs.MU'))
xlabel('MU')
ylabel('delta_S')

% Plot T_M2 against MU
figure(5);
plot(TESTMU,TM2,'-')
title(sprintf('Mixing Flow Temperature vs.MU'))
xlabel('MU')
ylabel('T_M2')

% Plot TAO against MU
figure(6);
plot(TESTMU,PRS0M,'-')
title(sprintf('TAO vs.MU'))
xlabel('MU')
ylabel('TAO')

% Plot M_P1, M_S1 and normalzied ER against MU
figure(10);
plot(TESTMU,ERR/ER_MAX,'-',TESTMU,MP1S,'--',TESTMU,MS1S,'-.')
title(sprintf('ER,M_P1 and M_S1vs.MU'))
xlabel('MU')
ylabel('ER and Mach Numbers')
legend('ER','M_P1','M_S1')
```

2) OPTIMAL_CURVES.m

```
% This is a program developed to plot the optimal ER as a function of AR for various theta
% Values of MU calcualted at M_S1=1, i.e. the secondary stream is choked at station 1.
% It is an 1-D analytical model for generalized ejector model
% There is a separate parameter input file
%
clear all;                                  % clear previous variables, clear the figures

load parameters;                            % load the input data
GAMMA_S=para{2};
```

```
N=100;
THE_TA=[1.0,1.2,1.4,1.6,1.8,2.0];          % the THETA vector, arbitrary given

AR_M2T=zeros(N,1);                         % initialize the AR (KAPPA) vector
ERR=zeros(N,6);                            % initialize the ER vector
ENTROPY=zeros(N,6);                        % initialize the total entropy change vector
MMIX=zeros(N,6);                           % initialize the M_MIX vector
PRS0M=zeros(N,6);                          % initialize TAO vector
PCR=zeros(N,6);                            % initialize the CR vector

for I=1:N
   AR_M2T(I)=10*I;                         % give arbitrary values to AR
end

MU=CHOKE(GAMMA_S);                         % calculate MU, which corresponds to the choked secondary
stream
[M_S1]=MS1(MU);                            % calculate M_S1, actually, M_S1=1
[M_P1,MP1SQ]=MP1(MU);                      % calculate M_P1
[S_PX,PR_0I0X]=SPX(MU,M_P1);               % calculate delta_S due to the primary stream shock
[TR_P1S1]=TRP1S1(M_P1,M_S1);               % calculate the temperature ratio of _P1/T_S1

for K=1:6
   THETA=THE_TA(K);

for J=1:N

   AR=AR_M2T(J)
   [ARS1P1,ARS1M2,ARP1M2]=ARS(THETA,AR);  % calculate area ratios
   [ER]=OMEGA(M_P1,M_S1,THETA,AR);         % calculate ER
   [GAMMA_M,R_M,T_M0,TR_M0P0]=MIX(ER);    % calcualte properties of MIXED flow

   [D]=TMD(M_P1,M_S1,ARS1M2,ARP1M2);       % calcualte the temporary parameter D
   [E]=TME(ER,M_S1,ARS1M2);                % calcualte the temporary parameter E
   [TAO1,TAO2]=TAO(ER,MU,D,E,GAMMA_M);    % calcualte TAO, there are two solutions for TAO

   PR_S0M2=TAO2;                           % supersonic solution of TAO is discarded

   [M_M2,MM2SQ]=MM2(GAMMA_M,MU,D,PR_S0M2);   % calculate M_M2
   [TR_M2P1]=TRM2P1(M_M2,ER,M_P1);         % calcualte the temperature ratio of T_M2/T_P1
   [PR_1M2]=PR1M2(MU,PR_S0M2);             % calcualte the pressure ratio of P1/P_M2
   [S_MIX]=SMIX(M_M2,M_P1,M_S1,ER,MU,PR_S0M2);  % calcualte the entropy change
                                                % due to the flow mixing
   [S_TOT]=STOT(M_M2,M_P1,M_S1,ER,MU,PR_S0M2); % calculate the total entropy change

   [CR]=PRCR(M_M2,GAMMA_M,PR_S0M2);           % calcualte CR

   ENTROPY(J,K)=S_TOT;
   ERR(J,K)=ER;
   MMIX(J,K)=M_M2;
   PRS0M(J,K)=PR_S0M2;
   PCR(J,K)=CR;
end
end
```

```
% Plot the ER vs.AR for various THETA
figure(1);
plot(AR_M2T,ERR(1:N,1),'-',AR_M2T,ERR(1:N,2),'-',AR_M2T,ERR(1:N,3),'-',AR_M2T,ERR(1:N,4),'-
',AR_M2T,ERR(1:N,5),'-',AR_M2T,ERR(1:N,6),'-')
title(sprintf('Optimal ER vs.AR'))
xlabel('AR')
ylabel('ER')
legend('theta=1.0','theta=1.2','theta=1.4','theta=1.6','theta=1.8','theta=2.0')

% Plot the CR vs.AR for various THETA
figure(2);
plot(AR_M2T,PCR(1:N,1),'-',AR_M2T,PCR(1:N,2),'-',AR_M2T,PCR(1:N,3),'-',AR_M2T,PCR(1:N,4),'-
',AR_M2T,PCR(1:N,5),'-',AR_M2T,PCR(1:N,6),'-')
title(sprintf('Optimal CR vs.AR'))
xlabel('AR')
ylabel('CR')
legend('theta=1.0','theta=1.2','theta=1.4','theta=1.6','theta=1.8','theta=2.0')
```

3) CONP_THETA.m

```
% This is a program developed to investigate the relationship between generalized ejector model
% and the constant-pressure mixing model. Should the assumption of constant-pressure mixing possible,
% there exist some values of MU so that the curve of TAO will intersect with the curve of 1/MU.
% The curves of TAO vs. MU are plotted together with 1/MU for various THETA
% AR (KAPPA) is set to be arbitrary value of 100.
% It is an 1-D analytical model for generalized ejector model
% There is a separate parameter input file
%
clear all;        % clear previous variables, clear the figures

THE_TA=[1.0,1.1,1.2,1.3,1.4,1.5];          % The vector of THETA
AR_M2T=100;                                % AR (KAPPA)=100

N=500;
TESTMU=zeros(N-1,1);                       % initialize the MU vector
ERR=zeros(N-1,6);                          % initialize the ER vector
PRS0M=zeros(N-1,6);                        % initialize the TAO vector
TAO_CP=zeros(N-1,1);                       % initialize the vector of 1/MU

DETAMU=1.0/N;

for K=1:N-1                                % calcualte 1/MU
   TESTMU(K)=K*DETAMU;
   TAO_CP(K)=1/TESTMU(K);
end

for J=1:N-1

   MU=TESTMU(J);
```

```
   [M_S1]=MS1(MU);                          % calcualte M_S1
   [M_P1,MP1SQ]=MP1(MU);                    % calcualte M_P1

   for I=1:6

      THETA=THE_TA(I);
      [ARS1P1,ARS1M2,ARP1M2]=ARS(THETA,AR_M2T);     % calculate area ratios
      [ER]=OMEGA(M_P1,M_S1,THETA,AR_M2T);           % calculate ER
      [GAMMA_M,R_M,T_M0,TR_M0P0]=MIX(ER);           % calculate properties of mixed flow
      [D]=TMD(M_P1,M_S1,ARS1M2,ARP1M2);             % calculate the temporary parameter of D
      [E]=TME(ER,M_S1,ARS1M2);                      % calculate the temporary parameter of E
      [TAO1,TAO2]=TAO(ER,MU,D,E,GAMMA_M);   % calculate TAO, there are two solutions of TAO

      PRS0M(J,I)=TAO2;                              % discarded supersonic solution of TAO
      ERR(J,I)=ER;
   end

end

% Plot TAO vs. MU, as well as 1/MU vs. Mu
figure(1);
plot(TESTMU,PRS0M(1:N-1,1),'-',TESTMU,PRS0M(1:N-1,2),'-',TESTMU,PRS0M(1:N-1,3),'-
',TESTMU,PRS0M(1:N-1,4),'-',TESTMU,PRS0M(1:N-1,5),'-',TESTMU,PRS0M(1:N-1,6),'-
',TESTMU,TAO_CP,'--')
title(sprintf('MU and TAO'))
xlabel('MU')
ylabel('TAO')
legend('theta=1.0','theta=1.1','theta=1.2','theta=1.3','theta=1.4','theta=1.5','TAO_CP')

% Plot ER vs. MU
figure(2);
plot(TESTMU,ERR(1:N-1,1),'-',TESTMU,ERR(1:N-1,2),'-',TESTMU,ERR(1:N-1,3),'-
',TESTMU,ERR(1:N-1,4),'-',TESTMU,ERR(1:N-1,5),'-',TESTMU,ERR(1:N-1,6),'-')
title(sprintf('ER vs. MU'))
xlabel('MU')
ylabel('ER')
legend('theta=1.0','theta=1.1','theta=1.2','theta=1.3','theta=1.4','theta=1.5')
```

4) CONP_AR.m

```
% This is a program developed to investigate the relationship between generalized ejector model
% and the constant-pressure mixing model. Should the assumption of constant-pressure mixing possible,
% there exist some values of MU so that the curve of TAO will intersect with the curve of 1/MU.
% The curves of TAO vs. MU are plotted together with 1/MU for various KAPPA (AR)
% THETA is set to be arbitrary value of 1.0, or set to be constant-area ejector
%
clear all;                          % clear previous variables, clear the figures

THETA=1.0;                          % THETA set to be 1.0, i.e., constant-area ejector
KAPPA=[20,60,100,140,400,600];              % KAPPA (AR) vector
```

```
N=500;
TESTMU=zeros(N-1,1);                    % initialize the MU vector
ERR=zeros(N-1,6);                       % initialize the ER vector
PRS0M=zeros(N-1,6);                     % initialize the TAO vector
TAO_CP=zeros(N-1,1);                    % initialize the 1/MU vector

DETAMU=1.0/N;

for K=1:N-1
   TESTMU(K)=K*DETAMU;                  % calculate the 1/MU value
   TAO_CP(K)=1/TESTMU(K);
end

for J=1:N-1

   MU=TESTMU(J);
   [M_S1]=MS1(MU);                      % calculate M_S1
   [M_P1,MP1SQ]=MP1(MU);                % calcualte M_P1

   for I=1:6

      AR_M2T=KAPPA(I);
      [ARS1P1,ARS1M2,ARP1M2]=ARS(THETA,AR_M2T); % calculate area ratios
      [ER]=OMEGA(M_P1,M_S1,THETA,AR_M2T);       % calculate ER
      [GAMMA_M,R_M,T_M0,TR_M0P0]=MIX(ER);       % calculate properties of mixed flow
      [D]=TMD(M_P1,M_S1,ARS1M2,ARP1M2);         % calculate the temporary parameter of D
      [E]=TME(ER,M_S1,ARS1M2);                  % calculate the temporary parameter of E
      [TAO1,TAO2]=TAO(ER,MU,D,E,GAMMA_M);       % calculate TAO

      PRS0M(J,I)=TAO2;
      ERR(J,I)=ER;
   end

end

% Plot TAO vs. MU,as well as 1/MU for various AR
figure(1);
plot(TESTMU,PRS0M(1:N-1,1),'-',TESTMU,PRS0M(1:N-1,2),'-',TESTMU,PRS0M(1:N-1,3),'-
',TESTMU,PRS0M(1:N-1,4),'-',TESTMU,PRS0M(1:N-1,5),'-',TESTMU,PRS0M(1:N-1,6),'-
',TESTMU,TAO_CP,'--')
title(sprintf('MU and TAO'))
xlabel('MU')
ylabel('TAO')
legend('kappa=20','kappa=60','kappa=100','kappa=140','kappa=400','kappa=600','TAO_CP')
```

5) SolutionSURFACE.m

```
% This is a program developed to generate the surface plot of ER against P_P0/P_S0 and P_b/P_S0
% It is an 1-D analytical model for generalized ejector model
```

```
% There is a separate parameter input file
%
clear all;                          % clear previous variables, clear the figures

load parameters;                    % load input data
GAMMA_S=para{2};
P_S0=para{8};

PR0=2;
PRBS0=0.05;

N=15;
M=30;
THETA=1.0;
AR=100;

PR_P0S0=zeros(N,1);
PP0=zeros(N,1);
TAOMAXS=zeros(N,1);
TAOMINS=zeros(N,1);
PRBS0_MIN=zeros(N,1);
PRBS0_MAX=zeros(N,1);
MU_CF=zeros(M,N);
PRBS=zeros(M,1);
PRSOB=zeros(M,1);
ERR=zeros(M,N);

for P=1:N
   PR_P0S0(P)=P*PR0;
   PP0(P)=PR_P0S0(P)*P_S0;
end

for Q=1:M
   PRBS(Q)=0.50+PRBS0*Q;
   PRSOB(Q)=1/PRBS(Q);
end

for I=1:N

   P_P0=PP0(I);
   [TAOMAX,TAOMIN]=TAOLM(THETA,AR,P_P0);
   TAOMAXS(I)=TAOMAX;
   TAOMINS(I)=TAOMIN;

   for J=1:M
      TAO_CF=PRSOB(J);
      if ( TAO_CF<TAOMIN | TAO_CF>TAOMAX)
        ER=0;
      else
        MU_CF(I,J)=CFMU(THETA,AR,TAO_CF,P_P0);
        MU=MU_CF(I,J);

       [M_S1]=MS1(MU);
```

```
        [M_P1,MP1SQ]=MP1(MU,P_P0);

        [ARS1P1,ARS1M2,ARP1M2]=ARS(THETA,AR);
        [ER]=OMEGA(M_P1,M_S1,THETA,AR);
      end

     ERR(J,I)=ER;
  end
end

for R=1:N
   for S=1:M
      A=imag(ERR(S,R));
      B=abs(A);
      if ( B > 0 )
         ERR(S,R)=0;
      end
   end
end

for K=1:N
   PRBS0_MIN(K)=1/TAOMAXS(K);
   PRBS0_MAX(K)=1/TAOMINS(K);
end

% Plot the ER surface
figure(1);
surf(PR_P0S0,PRBS,ERR)
title(sprintf('ER Surface'))
xlabel('P_P0/P_S0')
ylabel('P_b/P_SO')
zlabel('ER')
```

6) Limitations_opt.m

```
% This is a program developed to generate the surface plot of optimal ER
% Relationship between optimal ER and the parameters of AR, THETA, CR are investigated and plotted
% The total entropy change is plotted to investigate the feasibility of ejector design
%

clear all;        % clear previous variables, clear the figures

load parameters;
GAMMA_S=para{2};

N=100;
THE_TA=[1.0,1.2,1.4,1.6,1.8,2.0];

AR_M2T=zeros(N,1);
ERR=zeros(N,6);
```

```
ENTROPY=zeros(N,6);
MMIX=zeros(N,6);
PRS0M=zeros(N,6);
PCR=zeros(N,6);

for I=1:N
   AR_M2T(I)=10*I;
end

MU=CHOKE(GAMMA_S);
[M_S1]=MS1(MU);
[M_P1,MP1SQ]=MP1(MU);
[S_PX,PR_0I0X]=SPX(MU,M_P1);
[TR_P1S1]=TRP1S1(M_P1,M_S1);

for K=1:6
   THETA=THE_TA(K);

for J=1:N

   AR=AR_M2T(J);
   [ARS1P1,ARS1M2,ARP1M2]=ARS(THETA,AR);
   [ER]=OMEGA(M_P1,M_S1,THETA,AR);
   [GAMMA_M,R_M,T_M0,TR_M0P0]=MIX(ER);

   [D]=TMD(M_P1,M_S1,ARS1M2,ARP1M2);
   [E]=TME(ER,M_S1,ARS1M2);
   [TAO1,TAO2]=TAO(ER,MU,D,E,GAMMA_M);

   PR_S0M2=TAO2;

   [M_M2,MM2SQ]=MM2(GAMMA_M,MU,D,PR_S0M2);
   [TR_M2P1]=TRM2P1(M_M2,ER,M_P1);
   [PR_1M2]=PR1M2(MU,PR_S0M2);
   [S_MIX]=SMIX(M_M2,M_P1,M_S1,ER,MU,PR_S0M2);
   [S_TOT]=STOT(M_M2,M_P1,M_S1,ER,MU,PR_S0M2);

   [CR]=PRCR(M_M2,GAMMA_M,PR_S0M2);

   ENTROPY(J,K)=S_TOT;
   ERR(J,K)=ER;
   MMIX(J,K)=M_M2;
   PRS0M(J,K)=PR_S0M2;
   PCR(J,K)=CR;
end
end

% Plot the ER vs.AR
figure(1);
plot(AR_M2T,ERR(1:N,1),'-',AR_M2T,ERR(1:N,2),'-',AR_M2T,ERR(1:N,3),'-',AR_M2T,ERR(1:N,4),'-
',AR_M2T,ERR(1:N,5),'-',AR_M2T,ERR(1:N,6),'-')
title(sprintf('Optimal ER vs.AR'))
xlabel('AR')
```

```
ylabel('ER')
legend('theta=1.0','theta=1.2','theta=1.4','theta=1.6','theta=1.8','theta=2.0')

figure(2);
plot(AR_M2T,PCR(1:N,1),'-',AR_M2T,PCR(1:N,2),'-',AR_M2T,PCR(1:N,3),'-',AR_M2T,PCR(1:N,4),'-
',AR_M2T,PCR(1:N,5),'-',AR_M2T,PCR(1:N,6),'-')
title(sprintf('Optimal CR vs.AR'))
xlabel('AR')
ylabel('CR')
legend('theta=1.0','theta=1.2','theta=1.4','theta=1.6','theta=1.8','theta=2.0')

figure(3);
surf(THE_TA,AR_M2T,ERR)
title(sprintf('ER vs. AR and theta'))
xlabel('AR')
ylabel('theta')
legend('ER')

figure(4);
surf(THE_TA,AR_M2T,PCR)
title(sprintf('CR vs. AR and theta'))
xlabel('AR')
ylabel('theta')
legend('CR')

figure(5);
surf(THE_TA,AR_M2T,ENTROPY)
title(sprintf('ENTROPY vs. AR and theta'))
xlabel('AR')
ylabel('theta')
legend('ENTROPY')
```

7) Limitations_S-MU-AR.m

```
% This is a program developed to generate the surface plot total entropy change
% against the parameters of AR and MU
% The ENTROPY surface give the ejector design limitations
%
clear all;        % clear previous variables, clear the figures

load parameters;
GAMMA_S=para{2};

THETA=1.0;

N=100;
M=100;

AR_M2T=zeros(N,1);
ERR=zeros(N,M);
```

```
ENTROPY=zeros(N,M);
MMIX=zeros(N,M);
PRS0M=zeros(N,M);
PCR=zeros(N,M);

for I=1:N
   AR_M2T(I)=10*I;
end

DETAMU=0.50/M;

for K=1:M
   TESTMU(K)=0.50+(K-1)*DETAMU;
end

for I=1:M
   MU=TESTMU(I);
   [M_S1]=MS1(MU);
   [M_P1,MP1SQ]=MP1(MU);
   [S_PX,PR_0I0X]=SPX(MU,M_P1);
   [TR_P1S1]=TRP1S1(M_P1,M_S1);

   for J=1:N

      AR=AR_M2T(J);
      [ARS1P1,ARS1M2,ARP1M2]=ARS(THETA,AR);
      [ER]=OMEGA(M_P1,M_S1,THETA,AR);
      [GAMMA_M,R_M,T_M0,TR_M0P0]=MIX(ER);

      [D]=TMD(M_P1,M_S1,ARS1M2,ARP1M2);
      [E]=TME(ER,M_S1,ARS1M2);
      [TAO1,TAO2]=TAO(ER,MU,D,E,GAMMA_M);

      PR_S0M2=TAO2;

      [M_M2,MM2SQ]=MM2(GAMMA_M,MU,D,PR_S0M2);
      [TR_M2P1]=TRM2P1(M_M2,ER,M_P1);
      [PR_1M2]=PR1M2(MU,PR_S0M2);
      [S_MIX]=SMIX(M_M2,M_P1,M_S1,ER,MU,PR_S0M2);
      [S_TOT]=STOT(M_M2,M_P1,M_S1,ER,MU,PR_S0M2);

      [CR]=PRCR(M_M2,GAMMA_M,PR_S0M2);

      ENTROPY(J,I)=S_TOT;
      ERR(J,I)=ER;
      MMIX(J,I)=M_M2;
      PRS0M(J,I)=PR_S0M2;
      PCR(J,I)=CR;
   end
end

% Surface plot of DELTA_S_TOT vs. AR and MU
figure(1);
```

```
surf(TESTMU,AR_M2T,ENTROPY)
title(sprintf('Total Entropy Change'))
xlabel('MU')
ylabel('AR')
legend('Delta_S')
```

8) Limitations_S-MU-theta.m

```
% This is a program developed to generate the surface plot total entropy change
% against the parameters of THETA and MU
% The ENTROPY surface give the ejector design limitations
%
clear all;          % clear previous variables, clear the figures

load parameters;
GAMMA_S=para{2};

AR=100;
N=20;
M=100;

THE_TA=zeros(N,1);
ERR=zeros(N,M);
ENTROPY=zeros(N,M);
MMIX=zeros(N,M);
PRS0M=zeros(N,M);
PCR=zeros(N,M);

for I=1:N
   THE_TA(I)=1.0+(I-1)*(1.0/N);
end

DETAMU=0.50/M;

for K=1:M
   TESTMU(K)=0.50+(K-1)*DETAMU;
end

for I=1:M
   MU=TESTMU(I);
   [M_S1]=MS1(MU);
   [M_P1,MP1SQ]=MP1(MU);
   [S_PX,PR_0I0X]=SPX(MU,M_P1);
   [TR_P1S1]=TRP1S1(M_P1,M_S1);

   for J=1:N

      THETA=THE_TA(J);
      [ARS1P1,ARS1M2,ARP1M2]=ARS(THETA,AR);
      [ER]=OMEGA(M_P1,M_S1,THETA,AR);
```

```
      [GAMMA_M,R_M,T_M0,TR_M0P0]=MIX(ER);

      [D]=TMD(M_P1,M_S1,ARS1M2,ARP1M2);
      [E]=TME(ER,M_S1,ARS1M2);
      [TAO1,TAO2]=TAO(ER,MU,D,E,GAMMA_M);

      PR_S0M2=TAO2;

      [M_M2,MM2SQ]=MM2(GAMMA_M,MU,D,PR_S0M2);
      [TR_M2P1]=TRM2P1(M_M2,ER,M_P1);
      [PR_1M2]=PR1M2(MU,PR_S0M2);
      [S_MIX]=SMIX(M_M2,M_P1,M_S1,ER,MU,PR_S0M2);
      [S_TOT]=STOT(M_M2,M_P1,M_S1,ER,MU,PR_S0M2);

      [CR]=PRCR(M_M2,GAMMA_M,PR_S0M2);

      ENTROPY(J,I)=S_TOT;
      ERR(J,I)=ER;
      MMIX(J,I)=M_M2;
      PRS0M(J,I)=PR_S0M2;
      PCR(J,I)=CR;
   end
end

% Surface plot DELTA_S_TOT vs. MU and THETA
figure(1);
surf(TESTMU,THE_TA,ENTROPY)
title(sprintf('Total Entropy Change'))
xlabel('MU')
ylabel('theta')
legend('Delta_S')
```

Subroutines

9) ParametersInput.m

```
clear all; clf;                 % clear previous variables, clear the figures
% input the boundary conditions
GAMMA_P=1.4;            % Primary stream gas specific heat ratio, Cp/Cv
GAMMA_S=1.4;            % Secondary stream gas specific heat ratio, Cp/Cv
MW_P=28.97;             % Primary stream gas molecular weight, kg/kg-mol
MW_S=28.97;             % Secondary stream gas molecular weight, kg/kg-mol
P0_P=364.7;             % Primary stream stagnation pressure, psia
P0_S=34.7;              % Secodnary stream stagnation pressure, psia
T0_P=300;               % Primary stream gas stagnation temperature, K
T0_S=300;               % Secodnary stream gas stagnation temperature, K
DT=0.0145;              % Nozzle throat diameter, inch
```

```
D1=0.04;                    % Nozzle exit diameter, inch
D2=0.17;                    % Mixing chamber diameter, inch
D3=0.20;                    % Diffuser exit diameter, inch
ETA_N=0.95;                  % Nozzle isentropic efficiency coefficient
ETA_D=0.96;                 % Diffuser isentropic efficiency coefficient

% Gas constant
R_BAR=8312;                 % Universal gas constant, J/(kg-mol.K)
R_P=R_BAR/MW_P;             % Primary stream gas constant, J/(kg.K)
R_S=R_BAR/MW_S;              % Secondary stream gas constant, J/(kg.K)

% Area ratio of A_P1 to A_t
ARP1T=(D1/DT)*(D1/DT);

% Units conversion
P0_P=P0_P*6894.76;          % Primary stream stagnation pressure, Pa
P0_S=P0_S*6894.76;          % Secodnary stream stagnation pressure, Pa
DT=DT*2.54/100;             % Nozzle throat diameter, m
D1=D1*2.54/100;             % Nozzle exit diameter, m
D2=D2*2.54/100;             % Mixing chamber diameter,m
D3=D3*2.54/100;             % Diffuser exit diameter, m

% Area calculations
AT=pi*DT*DT/4;       % Nozzle throat area, m2
A1=pi*D1*D1/4;       % Nozzle exit area, m2
A2=pi*D2*D2/4;       % Mixing chamber area, m2
A3=pi*D3*D3/4;       % Diffuser exit area, m2

%*****************************
para{1}=GAMMA_P;
para{2}=GAMMA_S;
para{3}=R_P;
para{4}=R_S;
para{5}=T0_P;
para{6}=T0_S;
para{7}=P0_P;
para{8}=P0_S;
para{9}=AT;
para{10}=A1;
para{11}=A2;
para{12}=A3;
para{13}=ETA_N;
para{14}=ETA_D;
para{15}=ARP1T;

%*****************************
save parameters para
```

10) ARS.m

```
function [ARS1P1,ARS1M2,ARP1M2]=ARS(THETA,AR_M2T);

load parameters;

AR_P1T=para{15};

ARP1M2=AR_P1T/AR_M2T;
ARS1P1=(AR_M2T*THETA/AR_P1T)-1;
ARS1M2=ARP1M2*ARS1P1;
% end of function
```

11) CFMP1.m

```
function [MP1_N,PR_N]=CFMP1(AR_NOZZLE);

N=40;
MP1_CF=zeros(N,1);
AR_CF=zeros(N,1);
PR_CF=zeros(N,1);

A=1.0;
B=2.6;
DM=(B-A)/N;

for I=1:N
   MP1_CF(I)=1.0+I*DM;
end

for J=1:N
      MP1_TMP=MP1_CF(J);
      [PR1,AR1]=NOZLCF(MP1_TMP);
      PR_CF(J)=PR1;
      AR_CF(J)=AR1;
end

X=AR_CF;
Y=MP1_CF;
P=polyfit(X,Y,8);

MP1_N=polyval(P,AR_NOZZLE);
[PRTMP,ARTMP]=NOZLCF(MP1_N);
PR_N=PRTMP;
% end of function
```

12) FUN2.m

```
function [F2]=FUN2(GAMMA,M);
```

```
F2TM1=1+(GAMMA-1)*M*M/2;
F2TM2=sqrt(GAMMA*F2TM1);

F2=M*F2TM2;
% end of function
```

13) GTS.m

```
function [G1,G2,G3,G4,G5,G6]=GTS(GAMMA);

G1=GAMMA/(GAMMA+1);
G2=(GAMMA-1)/(GAMMA+1);
G3=GAMMA/(GAMMA-1);
G4=(GAMMA+1)/(GAMMA-1);
G5=(GAMMA-1)/GAMMA;
G6=(GAMMA+1)/GAMMA;
% end of function
```

14) MIX.m

```
function [GAMMA_M,R_M,T_M0,TR_M0P0]=MIX(ER);

load parameters;

GAMMA_P=para{1};
GAMMA_S=para{2};
R_P=para{3};
R_S=para{4};
T_P0=para{5};
T_S0=para{6};

GMTM1=1/(GAMMA_P-1);
GMTM2=GAMMA_P/(GAMMA_P-1);
GMTM3=1/(GAMMA_S-1);
GMTM4=GAMMA_S/(GAMMA_S-1);
GMTM5=R_S/R_P;

GAMMA_M=(GMTM2+GMTM4*GMTM5*ER)/(GMTM1+GMTM3*GMTM5*ER);
R_M=(R_P+ER*R_S)/(1+ER);

TR=T_S0/T_P0;
TR_M0P0=(GMTM2+GMTM4*GMTM5*TR*ER)/(GMTM2+GMTM4*GMTM5*ER);
T_M0=T_P0*TR_M0P0;
% end of function
```

15) MM2.m

```
function [M_M2,MM2SQ]=MM2(GAMMA_M,MU,D,TAO);

MM2SQ=(D*MU*TAO-1)/GAMMA_M;
M_M2=sqrt(MM2SQ);
% end of function
```

16) MP1.m

```
function [M_P1,MP1SQ]=MP1(MU);

load parameters;

GAMMA_P=para{1};
P_P0=para{7};
P_S0=para{8};
ARP1T=para{15};

[GM1,GM2,GM3,GM4,GM5,GM6]=GTS(GAMMA_P);

GTT1=GAMMA_P-1;
GTT2=2/(GAMMA_P+1);
GTT3=GM4;

TT1=((P_P0/P_S0)/ARP1T)^2;
TT2=2*GTT1*(GTT2^GTT3);
TT3=MU*MU+TT1*TT2;

MP1SQ=(-MU+sqrt(TT3))/(GTT1*MU);
M_P1=sqrt(MP1SQ);
% end of function
```

17) MS1.m

```
function [M_S1]=MS1(MU);

load parameters;

GAMMA_S=para{2};

MS1T1=GAMMA_S-1;
MS1T2=2/MS1T1;
MS1T3=-MS1T1/GAMMA_S;

TM1_S=MU^MS1T3-1;

M_S1=sqrt(MS1T2*TM1_S);
% end of function
```

18) NOZLCF.m

```
function [PR_P1P0,AR_P1T]=NOZLCF(MP1);

load parameters;
GAMMA_P=para{1};

TMP1=(GAMMA_P+1);
TMP2=(GAMMA_P-1);
TMP3=1+TMP2*MP1*MP1/2;
TMP4=TMP1/2;
TMP5=TMP1/TMP2;

AR_P1T=(1/MP1)*sqrt((TMP3/TMP4)^TMP5);
PR_P1P0=(TMP3)^(-GAMMA_P/TMP2);
% end of function
```

19) OMEGA.m

```
function [ER]=OMEGA(M_P1,M_S1,THETA,AR_M2T);

load parameters;
GAMMA_P=para{1};
GAMMA_S=para{2};
R_P=para{3};
R_S=para{4};
T_P0=para{5};
T_S0=para{6};

F2_S1=FUN2(GAMMA_S,M_S1);
F2_P1=FUN2(GAMMA_P,M_P1);
[ARS1P1,ARS1M2,ARP1M2]=ARS(THETA,AR_M2T);

TM1=ARS1P1;
TM2=sqrt((R_P*T_P0)/(R_S*T_S0));
TM3=F2_S1/F2_P1;

ER=TM1*TM2*TM3;
% end of function
```

20) PR1M2.m

```
function [PR_1M2]=PR1M2(MU,PR_S0M2);

PR_1M2=MU*PR_S0M2;
% end of function
```

21) SMIX.m

```
function [S_MIX]=SMIX(M_M2,M_P1,M_S1,ER,MU,PR_S0M2);

load parameters;
GAMMA_P=para{1};
GAMMA_S=para{2};
R_P=para{3};
R_S=para{4};

[GAMMA_M,R_M,T_M0,TR_M0P0]=MIX(ER);

TGM1=GAMMA_P/(GAMMA_P-1);
TGM2=GAMMA_S/(GAMMA_S-1);

[TR_M2P1]=TRM2P1(M_M2,ER,M_P1);
[TR_P1S1]=TRP1S1(M_P1,M_S1);
[PR_1M2]=PR1M2(MU,PR_S0M2);

PT1=1/(ER+1);
PT2=(R_P+ER*R_S)*log(PR_1M2);
PT3=ER*R_S*TGM2*log(TR_P1S1);
PT4=(R_P*TGM1+ER*R_S*TGM2)*log(TR_M2P1);

S_MIX=PT1*(PT2+PT3+PT4);
% end of function
```

22) SPX.m

```
function [S_PX,PR_0I0X]=SPX(MU,M_P1);

load parameters;
GAMMA_P=para{1};
R_P=para{3};
P_P0=para{7};
P_S0=para{8};

[GM1,GM2,GM3,GM4,GM5,GM6]=GTS(GAMMA_P);

[TFPX]=TFUN(GAMMA_P,M_P1);

PR_0I0X=((P_P0/P_S0)/MU)*(TFPX^(-GM3));

S_PX=R_P*log(PR_0I0X);
% end of function
```

23) STOT.m

```
function [S_TOT]=STOT(M_M2,M_P1,M_S1,ER,MU,PR_S0M2);

[S_PX,PR_0I0X]=SPX(MU,M_P1);
[S_MIX]=SMIX(M_M2,M_P1,M_S1,ER,MU,PR_S0M2);

WT=1/(1+ER);
S_TOT=WT*S_PX+S_MIX;
% end of function
```

24) TAO.m

```
function [TAO1,TAO2]=TAO(ER,MU,D,E,GAMMA_M);

GT1=GAMMA_M+1;
GT2=GAMMA_M-1;
GT3=2*GAMMA_M;
ET=(ER+1)/ER;
TMP=GT3*(ET/E)*(ET/E)-GT2*D*D;

NUM1=D+sqrt(D*D-TMP*GT1);
NUM2=D-sqrt(D*D-TMP*GT1);
DEN=TMP*MU;

TAO1=NUM1/DEN;
TAO2=NUM2/DEN;
% end of function
```

25) TFUN.m

```
function [TRS]=TFUN(GAMMA,M);

TRS=1+(GAMMA-1)*M*M/2;
% end of function
```

26) TMD.m

```
function [D]=TMD(M_P1,M_S1,ARS1M2,ARP1M2);

load parameters;
GAMMA_P=para{1};
GAMMA_S=para{2};

TERM1=ARP1M2*(1+GAMMA_P*M_P1*M_P1);
TERM2=ARS1M2*(1+GAMMA_S*M_S1*M_S1);

D=TERM1+TERM2;
```

```
% end of function
```

27) TME.m

```
function [E]=TME(ER,M_S1,ARS1M2);

load parameters;
GAMMA_S=para{2};
R_S=para{4};
T_S0=para{6};

[GAMMA_M,R_M,T_M0,TR_M0P0]=MIX(ER);
F2S1=FUN2(GAMMA_S,M_S1);

TM1=1/ARS1M2;
TM2=sqrt((R_S*T_S0)/(R_M*T_M0));
TM3=1/F2S1;

E=TM1*TM2*TM3;
% end of function
```

28) TRM2P1.m

```
function [TR_M2P1]=TRM2P1(M_M2,ER,M_P1);

load parameters;
GAMMA_P=para{1};

[GAMMA_M,R_M,T_M0,TR_M0P0]=MIX(ER);

TR_P0P1=TFUN(GAMMA_P,M_P1);
DEN=TFUN(GAMMA_M,M_M2);

TR_M2P1=TR_M0P0*TR_P0P1/DEN;
% end of function
```

29) TRP1S1.m

```
function [TR_P1S1]=TRP1S1(M_P1,M_S1);

load parameters;
GAMMA_P=para{1};
GAMMA_S=para{2};
T_P0=para{5};
T_S0=para{6};
```

```
TR_S=TFUN(GAMMA_S,M_S1);
TR_P=TFUN(GAMMA_P,M_P1);

TR_P1S1=(T_P0/T_S0)*(TR_S/TR_P);
% end of function
```

30) CHOKE.m

```
function [MU_STAR]=CHOKE(GAMMA);

TGM=-GAMMA/(GAMMA-1);
MU_STAR=(1+(GAMMA-1)/2)^TGM;
% end of function
```

31) PRCR.m

```
function [CR]=PRCR(M_M2,GAMMA_M,PS0M2);

load parameters;
ETA_D=para{14};

TP1=ETA_D*M_M2*M_M2*(GAMMA_M-1)/2;
TP2=GAMMA_M/(GAMMA_M-1);

PR_40M2=(1+TP1)^TP2;
CR=PR_40M2/PS0M2;
% end of function
```

32) CFMU.m

```
function [MU_CF]=CFMU(THETA,AR,TAO_CF,P_P0);

load parameters;
GAMMA_S=para{2};

M=60;
TESTMU=zeros(M,1);
PRS0M=zeros(M,1);

MU_OPT=CHOKE(GAMMA_S);
DETAMU=(1.0-MU_OPT)/M;

for K=1:M
   TESTMU(K)=MU_OPT+(K-1)*DETAMU;
end
```

```
for I=1:M
   MU=TESTMU(I);
   [M_S1]=MS1(MU);
   [M_P1,MP1SQ]=MP1(MU,P_P0);

      [ARS1P1,ARS1M2,ARP1M2]=ARS(THETA,AR);
      [ER]=OMEGA(M_P1,M_S1,THETA,AR);
      [GAMMA_M,R_M,T_M0,TR_M0P0]=MIX(ER);

      [D]=TMD(M_P1,M_S1,ARS1M2,ARP1M2);
      [E]=TME(ER,M_S1,ARS1M2);
      [TAO1,TAO2]=TAO(ER,MU,D,E,GAMMA_M);

      PRS0M(I)=TAO2;
end

X=TESTMU;
Y=PRS0M;
P=polyfit(Y,X,6);
MU_CF=polyval(P,TAO_CF);
% end of function
```

33) TAOLM.m

```
function [TAOMAX,TAOMIN]=TAOLM(THETA,AR,P_P0);

load parameters;
GAMMA_S=para{2};

MU_OPT=CHOKE(GAMMA_S);
MU_UP=0.995;
MUS=[MU_OPT,MU_UP];
TAOM=zeros(2,1);

for I=1:2
   MU=MUS(I);
   [M_S1]=MS1(MU);
   [M_P1,MP1SQ]=MP1(MU,P_P0);
   [ARS1P1,ARS1M2,ARP1M2]=ARS(THETA,AR);
   [ER]=OMEGA(M_P1,M_S1,THETA,AR);
   [GAMMA_M,R_M,T_M0,TR_M0P0]=MIX(ER);
   [D]=TMD(M_P1,M_S1,ARS1M2,ARP1M2);
   [E]=TME(ER,M_S1,ARS1M2);
   [TAO1,TAO2]=TAO(ER,MU,D,E,GAMMA_M);
   TAOM(I)=TAO2;
end

TAOMAX=TAOM(1);
TAOMIN=TAOM(2);
% end of function
```

APPENDIX D

MATLAB PROGRAM DEVELOPED FOR PARAMETRIC STUDIES

ON EJECTOR WORKING WITH TWO-PHASE FLOW

Main Programs

1) PRIMARYmixture.m

```
% Main Program for investigations of performance and limitations of ejector
%  working with gas-liquid two-phase mixture. The two-phase mixture is supplied
%  as the primary flow, and the single-component gas is supplied as the secondary flow.
% Ejector performance ER as well as its limitation based on the total entropy change are
%  investigated and plotted as surface figures against various parameters.
% The generalized ejector model is utilized for this study
% % There is a separate parameter input file
%

clear all;                    % clear previous variables, clear the figures

load parameters;              % load input data
GAMMA_S=para{2};
P_S0=para{8};
R_G=para{4};
CP_G=para{16};
CV_G=para{17};
CP_L=para{18};

PR0=2;
PRBS0=0.05;                   % P_b/P_S0=0.05
THETA=1.0;                    % THETA=1.0, i.e., constant-area gas ejector
AR=100;                       % AR(KAPPA)=100

N=15;
M=100;
NAR=50;
NTH=20;

DX=0.01;
RTP=zeros(M+1,1);             % initialize the vector of two-phase mixture gas constant, R_TP
GAMMATP=zeros(M+1,1);         % initialize the vector of two-phase mixture specific heat ratio,
GAMMA_TP
RG=zeros(M+1,1);              % initialize the vector of single-component gas constant, R_G
```

```
GAMMA_G=zeros(M+1,1);          % initialize the vector of single-component gas specific heat ratio,
GAMMA_G

PR_P0S0=zeros(N,1);            % initialize the vector of pressure ratio P_P0/P_S0
PP0=zeros(N,1);                % initialize the vector of primary inlet pressure P_P0
TAOMAXS=zeros(N,M+1);          % initialize the matrix of upper limits of TAO
TAOMINS=zeros(N,M+1);          % initialize the matrix of lower limits of TAO
PRBS0_MIN=zeros(N,M+1);        % initialize the matrix of lower limits of P_B/P_S0
PRBS0_MAX=zeros(N,M+1);        % initialize the matrix of upper limits of P_B/P_S0

AR_M2T=zeros(NAR,1);           % initialize the vector of AR
ER_AR=zeros(NAR,M+1);          % initialize the matrix of ER for AR as the variable
SAR=zeros(NAR,M+1);            % initialize the matrix of DELTA_S_TOTAL for AR as the variable

THE_TA=zeros(NTH+1,1);         % initialize the vector of THETA
ER_TH=zeros(NTH+1,M+1);        % initialize the matrix of ER for THETA as the variable
STH=zeros(NTH+1,M+1);          % initialize the matrix of DELTA_S_TOTAL for THETA as the
variable

for I=1:NAR
   AR_M2T(I)=15*I;             % give values to AR
end

for I=1:NTH+1
   THE_TA(I)=1.0+0.05*(I-1);   % give values to THETA
end

for I=1:M+1
   X(I)=(I-1)*DX;              % give values to X, the liquid quality
end

% calculate the thermodynamic properties of gas-liquid two-phase mixture
for J=1:M+1
   LQ=X(J);
   [R_TP,GAMMA_TP]=TWOPHASE(LQ,R_G,CP_G,CV_G,CP_L);
   RTP(J)=R_TP;
   GAMMATP(J)=GAMMA_TP;
   RG(J)=R_G;
   GAMMA_G(J)=CP_G/CV_G;
end

% Define boundary conditions
for P=1:N
   PR_P0S0(P)=P*PR0;
   PP0(P)=PR_P0S0(P)*P_S0;
end

% calculate the upper and lower limits of TAO
% calcualte the upper and lower limits of P_b/P_S0
for L=1:M+1
   RP=RTP(L);
   GP=GAMMATP(L);
```

```
   for K=1:N
      P_P0=PP0(K);
      [TAOMAX,TAOMIN]=TAOLM(THETA,AR,P_P0,RP,GP);
      TAOMAXS(K,L)=TAOMAX;
      TAOMINS(K,L)=TAOMIN;
      PRBS0_MIN(K,L)=1/TAOMAX;
      PRBS0_MAX(K,L)=1/TAOMIN;
   end
end

% should the P_b/P_S0 be a complex number, set it to be zero
for R=1:N
   for S=1:M+1
      A=imag(PRBS0_MIN(R,S));
      B=abs(A);
      if ( B > 0 )
         PRBS0_MIN(R,S)=0;
      end
   end
end

for U=1:M+1
   for V=1:N
      if ( PRBS0_MIN(V,U) == 0 )
         PRBS0_MIN(V,U)=PRBS0_MIN(V-1,U);
      end
   end
end

% calculate ER, DELTA_S_TOT for AR as the variable
P_P0=para{7};
MU=CHOKE(GAMMA_S);
[M_S1]=MS1(MU);
for L=1:M+1
   RP=RTP(L);
   GP=GAMMATP(L);
   [M_P1,MP1SQ]=MP1(MU,P_P0,GP);
   [S_PX,PR_0I0X]=SPX(MU,M_P1,P_P0,GP,RP);
   [TR_P1S1]=TRP1S1(M_P1,M_S1,GP);

   for J=1:NAR
      AR=AR_M2T(J);
      [ARS1P1,ARS1M2,ARP1M2]=ARS(THETA,AR);
      [ER]=OMEGA(M_P1,M_S1,THETA,AR,GP,RP);

      [GAMMA_M,R_M,T_M0,TR_M0P0]=MIX(ER,GP,RP);
      [D]=TMD(M_P1,M_S1,ARS1M2,ARP1M2,GP);
      [E]=TME(ER,M_S1,ARS1M2,GP,RP);
      [TAO1,TAO2]=TAO(ER,MU,D,E,GAMMA_M);

      PR_S0M2=TAO2;

      [M_M2,MM2SQ]=MM2(GAMMA_M,MU,D,PR_S0M2);
```

```
      [TR_M2P1]=TRM2P1(M_M2,ER,M_P1,GP,RP);
      [PR_1M2]=PR1M2(MU,PR_S0M2);
      [S_MIX]=SMIX(M_M2,M_P1,M_S1,ER,MU,PR_S0M2,GP,RP);
      [S_TOT]=STOT(M_M2,M_P1,M_S1,ER,MU,PR_S0M2,P_P0,GP,RP);

      A=real(S_TOT);
      B=abs(imag(S_TOT));
      if ( B > 0 )
         if ( A > 0 )
            SAR(J,L)=-A;
         else
            SAR(J,L)=A;
         end
      else
         SAR(J,L)=S_TOT;
      end

      ER_AR(J,L)=ER;
   end
end

% calculate ER, DELTA_S_TOT for THETA as the variable
AR=100;
for L=1:M+1
   RP=RTP(L);
   GP=GAMMATP(L);
   [M_P1,MP1SQ]=MP1(MU,P_P0,GP);
   [S_PX,PR_0I0X]=SPX(MU,M_P1,P_P0,GP,RP);
   [TR_P1S1]=TRP1S1(M_P1,M_S1,GP);

   for J=1:NTH+1
      THETA=THE_TA(J);
      [ARS1P1,ARS1M2,ARP1M2]=ARS(THETA,AR);
      [ER]=OMEGA(M_P1,M_S1,THETA,AR,GP,RP);

      [GAMMA_M,R_M,T_M0,TR_M0P0]=MIX(ER,GP,RP);
      [D]=TMD(M_P1,M_S1,ARS1M2,ARP1M2,GP);
      [E]=TME(ER,M_S1,ARS1M2,GP,RP);
      [TAO1,TAO2]=TAO(ER,MU,D,E,GAMMA_M);

      PR_S0M2=TAO2;

      [M_M2,MM2SQ]=MM2(GAMMA_M,MU,D,PR_S0M2);
      [TR_M2P1]=TRM2P1(M_M2,ER,M_P1,GP,RP);
      [PR_1M2]=PR1M2(MU,PR_S0M2);
      [S_MIX]=SMIX(M_M2,M_P1,M_S1,ER,MU,PR_S0M2,GP,RP);
      [S_TOT]=STOT(M_M2,M_P1,M_S1,ER,MU,PR_S0M2,P_P0,GP,RP);

      A=real(S_TOT);
      B=abs(imag(S_TOT));
      if ( B > 0 )
         if ( A > 0 )
            STH(J,L)=-A;
```

```
        else
           STH(J,L)=A;
        end
     else
        STH(J,L)=S_TOT;
     end

     ER_TH(J,L)=ER;

  end
end

% Surface plots of the parameters, ER, DETA-S, TAO_MAX, TAO_MIN, etc.
figure(1);
surf(X,PR_P0S0,PRBS0_MIN)
hold on
surf(X,PR_P0S0,PRBS0_MAX)
hold off
title(sprintf('P_b/P_S0 Surface'))
xlabel('X')
ylabel('P_P0/P_S0')
zlabel('P_b/P_S0')

figure(2);
plot(PR_P0S0,PRBS0_MIN(1:N,1),'-',PR_P0S0,PRBS0_MIN(1:N,26),'-
.',PR_P0S0,PRBS0_MIN(1:N,51),'--',PR_P0S0,PRBS0_MIN(1:N,76),'-
',PR_P0S0,PRBS0_MIN(1:N,M+1),'-.')
legend('x=0,P_b/P_S0 min','x=0.25,P_b/P_S0 min','x=0.50,P_b/P_S0 min','x=0.75,P_b/P_S0
min','x=1.0,P_b/P_S0 min')
hold on
plot(PR_P0S0,PRBS0_MAX(1:N,1),'-',PR_P0S0,PRBS0_MAX(1:N,26),'-
.',PR_P0S0,PRBS0_MAX(1:N,51),'--',PR_P0S0,PRBS0_MAX(1:N,76),'-
',PR_P0S0,PRBS0_MAX(1:N,M+1),'-.')
legend('x=0,P_b/P_S0 max','x=0.25,P_b/P_S0 max','x=0.50,P_b/P_S0 max','x=0.75,P_b/P_S0
max','x=1.0,P_b/P_S0 max')
hold off
title(sprintf('P_b/P_S0 Surface'))
xlabel('P_P0/P_S0')
ylabel('P_b/P_S0')

figure(3);
surf(X,AR_M2T,ER_AR)
title(sprintf('ER Surface'))
xlabel('X')
ylabel('AR')
zlabel('ER')

figure(4);
surf(X,THE_TA,ER_TH)
title(sprintf('ER Surface'))
xlabel('X')
ylabel('THETA')
zlabel('ER')
```

```
figure(5);
surf(X,AR_M2T,SAR)
title(sprintf('Entropy Surface'))
xlabel('X')
ylabel('AR')
zlabel('Delta_S')

figure(6);
surf(X,THE_TA,STH)
title(sprintf('Entropy Surface'))
xlabel('X')
ylabel('THETA')
zlabel('Delta_S')
```

Subroutines

2) ParametersInput.m

```
clear all; clf;          % clear previous variables, clear the figures

% input the boundary conditions
GAMMA_P=1.4;          % Primary stream gas specific heat ratio, Cp/Cv
GAMMA_S=1.4;          % Secondary stream gas specific heat ratio, Cp/Cv
MW_P=28.97;           % Primary stream gas molecular weight, kg/kg-mol
MW_S=28.97;           % Secondary stream gas molecular weight, kg/kg-mol
P0_P=364.7;           % Primary stream stagnation pressure, psia
P0_S=34.7;            % Secodnary stream stagnation pressure, psia
T0_P=300;             % Primary stream gas stagnation temperature, K
T0_S=300;             % Secodnary stream gas stagnation temperature, K
DT=0.0145;            % Nozzle throat diameter, inch
D1=0.04;              % Nozzle exit diameter, inch
D2=0.17;              % Mixing chamber diameter, inch
D3=0.20;              % Diffuser exit diameter, inch
ETA_N=0.95;           % Nozzle isentropic efficiency coefficient
ETA_D=0.96;           % Diffuser isentropic efficiency coefficient

CP_S=1.01*1000;       % Secondary stream specific heat Cps, J/(kg.K)
CV_S=0.72*1000;       % Secondary stream specific heat Cvs, J/(kg.K)
CP_L=4.186*1000;      % Liquid water specific heat at 25 degree,J/(kg.K)

% Gas constant
R_BAR=8312;           % Universal gas constant, J/(kg-mol.K)
R_P=R_BAR/MW_P;       % Primary stream gas constant, J/(kg.K)
R_S=R_BAR/MW_S;       % Secondary stream gas constant, J/(kg.K)

% Area ratio of A_P1 to A_t
ARP1T=(D1/DT)*(D1/DT);
```

```
% Units conversion
P0_P=P0_P*6894.76;     % Primary stream stagnation pressure, Pa
P0_S=P0_S*6894.76;     % Secodnary stream stagnation pressure, Pa
DT=DT*2.54/100;        % Nozzle throat diameter, m
D1=D1*2.54/100;        % Nozzle exit diameter, m
D2=D2*2.54/100;        % Mixing chamber diameter,m
D3=D3*2.54/100;        % Diffuser exit diameter, m

% Area calculations
AT=pi*DT*DT/4;         % Nozzle throat area, m2
A1=pi*D1*D1/4;         % Nozzle exit area, m2
A2=pi*D2*D2/4;         % Mixing chamber area, m2
A3=pi*D3*D3/4;         % Diffuser exit area, m2

%*****************************
para{1}=GAMMA_P;
para{2}=GAMMA_S;
para{3}=R_P;
para{4}=R_S;
para{5}=T0_P;
para{6}=T0_S;
para{7}=P0_P;
para{8}=P0_S;
para{9}=AT;
para{10}=A1;
para{11}=A2;
para{12}=A3;
para{13}=ETA_N;
para{14}=ETA_D;
para{15}=ARP1T;
para{16}=CP_S;
para{17}=CV_S;
para{18}=CP_L;

%*****************************
save parameters para
```

3) ARS.m

```
function [ARS1P1,ARS1M2,ARP1M2]=ARS(THETA,AR_M2T);

load parameters;
AR_P1T=para{15};

ARP1M2=AR_P1T/AR_M2T;
ARS1P1=(AR_M2T*THETA/AR_P1T)-1;
ARS1M2=ARP1M2*ARS1P1;
% end of function
```

4) CHOKE.m

```
function [MU_STAR]=CHOKE(GAMMA);

TGM=-GAMMA/(GAMMA-1);
MU_STAR=(1+(GAMMA-1)/2)^TGM;
% end of function
```

5) FUN2.m

```
function [F2]=FUN2(GAMMA,M);

F2TM1=1+(GAMMA-1)*M*M/2;
F2TM2=sqrt(GAMMA*F2TM1);

F2=M*F2TM2;
% end of function
```

6) GTS.m

```
function [G1,G2,G3,G4,G5,G6]=GTS(GAMMA);

G1=GAMMA/(GAMMA+1);
G2=(GAMMA-1)/(GAMMA+1);
G3=GAMMA/(GAMMA-1);
G4=(GAMMA+1)/(GAMMA-1);
G5=(GAMMA-1)/GAMMA;
G6=(GAMMA+1)/GAMMA;
% end of function
```

7) MIX.m

```
function [GAMMA_M,R_M,T_M0,TR_M0P0]=MIX(ER,GAMMA_P,R_P);

load parameters;
%GAMMA_P=para{1};
GAMMA_S=para{2};
%R_P=para{3};
R_S=para{4};
T_P0=para{5};
T_S0=para{6};

GMTM1=1/(GAMMA_P-1);
GMTM2=GAMMA_P/(GAMMA_P-1);
```

```
GMTM3=1/(GAMMA_S-1);
GMTM4=GAMMA_S/(GAMMA_S-1);
GMTM5=R_S/R_P;

GAMMA_M=(GMTM2+GMTM4*GMTM5*ER)/(GMTM1+GMTM3*GMTM5*ER);
R_M=(R_P+ER*R_S)/(1+ER);

TR=T_S0/T_P0;
TR_M0P0=(GMTM2+GMTM4*GMTM5*TR*ER)/(GMTM2+GMTM4*GMTM5*ER);
T_M0=T_P0*TR_M0P0;
% end of function
```

8) MM2.m

```
function [M_M2,MM2SQ]=MM2(GAMMA_M,MU,D,TAO);

MM2SQ=(D*MU*TAO-1)/GAMMA_M;
M_M2=sqrt(MM2SQ);
% end of function
```

9) MP1.m

```
function [M_P1,MP1SQ]=MP1(MU,P_P0,GAMMA_P);

load parameters;
%GAMMA_P=para{1};
%P_P0=para{7};
P_S0=para{8};
ARP1T=para{15};

[GM1,GM2,GM3,GM4,GM5,GM6]=GTS(GAMMA_P);
GTT1=GAMMA_P-1;
GTT2=2/(GAMMA_P+1);
GTT3=GM4;
TT1=((P_P0/P_S0)/ARP1T)^2;
TT2=2*GTT1*(GTT2^GTT3);
TT3=MU*MU+TT1*TT2;

MP1SQ=(-MU+sqrt(TT3))/(GTT1*MU);
M_P1=sqrt(MP1SQ);
% end of function
```

10) MS1.m

```
function [M_S1]=MS1(MU);
```

```
load parameters;
GAMMA_S=para{2};

MS1T1=GAMMA_S-1;
MS1T2=2/MS1T1;
MS1T3=-MS1T1/GAMMA_S;

TM1_S=MU^MS1T3-1;

M_S1=sqrt(MS1T2*TM1_S);
% end of function
```

11) OMEGA.m

```
function [ER]=OMEGA(M_P1,M_S1,THETA,AR_M2T,GAMMA_P,R_P);

load parameters;
%GAMMA_P=para{1};
GAMMA_S=para{2};
%R_P=para{3};
R_S=para{4};
T_P0=para{5};
T_S0=para{6};

F2_S1=FUN2(GAMMA_S,M_S1);
F2_P1=FUN2(GAMMA_P,M_P1);
[ARS1P1,ARS1M2,ARP1M2]=ARS(THETA,AR_M2T);

TM1=ARS1P1;
TM2=sqrt((R_P*T_P0)/(R_S*T_S0));
TM3=F2_S1/F2_P1;

ER=TM1*TM2*TM3;
% end of function
```

12) PR1M2.m

```
function [PR_1M2]=PR1M2(MU,PR_S0M2);

PR_1M2=MU*PR_S0M2;
% end of function
```

13) SMIX.m

```
function [S_MIX]=SMIX(M_M2,M_P1,M_S1,ER,MU,PR_S0M2,GAMMA_P,R_P);
```

```
load parameters;
%GAMMA_P=para{1};
GAMMA_S=para{2};
%R_P=para{3};
R_S=para{4};

[GAMMA_M,R_M,T_M0,TR_M0P0]=MIX(ER,GAMMA_P,R_P);

TGM1=GAMMA_P/(GAMMA_P-1);
TGM2=GAMMA_S/(GAMMA_S-1);

[TR_M2P1]=TRM2P1(M_M2,ER,M_P1,GAMMA_P,R_P);
[TR_P1S1]=TRP1S1(M_P1,M_S1,GAMMA_P);
[PR_1M2]=PR1M2(MU,PR_S0M2);

PT1=1/(ER+1);
PT2=(R_P+ER*R_S)*log(PR_1M2);
PT3=ER*R_S*TGM2*log(TR_P1S1);
PT4=(R_P*TGM1+ER*R_S*TGM2)*log(TR_M2P1);

S_MIX=PT1*(PT2+PT3+PT4);
% end of function
```

14) SPX.m

```
function [S_PX,PR_0I0X]=SPX(MU,M_P1,P_P0,GAMMA_P,R_P);

load parameters;

%GAMMA_P=para{1};
%R_P=para{3};
%P_P0=para{7};
P_S0=para{8};

[GM1,GM2,GM3,GM4,GM5,GM6]=GTS(GAMMA_P);
[TFPX]=TFUN(GAMMA_P,M_P1);

PR_0I0X=((P_P0/P_S0)/MU)*(TFPX^(-GM3));

S_PX=R_P*log(PR_0I0X);
% end of function
```

15) STOT.m

```
function [S_TOT]=STOT(M_M2,M_P1,M_S1,ER,MU,PR_S0M2,P_P0,GAMMA_P,R_P);

[S_PX,PR_0I0X]=SPX(MU,M_P1,P_P0,GAMMA_P,R_P);
[S_MIX]=SMIX(M_M2,M_P1,M_S1,ER,MU,PR_S0M2,GAMMA_P,R_P);
```

```
WT=1/(1+ER);
S_TOT=WT*S_PX+S_MIX;
% end of function
```

16) TAO.m

```
function [TAO1,TAO2]=TAO(ER,MU,D,E,GAMMA_M);

GT1=GAMMA_M+1;
GT2=GAMMA_M-1;
GT3=2*GAMMA_M;
ET=(ER+1)/ER;
TMP=GT3*(ET/E)*(ET/E)-GT2*D*D;

NUM1=D+sqrt(D*D-TMP*GT1);
NUM2=D-sqrt(D*D-TMP*GT1);
DEN=TMP*MU;

TAO1=NUM1/DEN;
TAO2=NUM2/DEN;
% end of function
```

17) TAOLM.m

```
function [TAOMAX,TAOMIN]=TAOLM(THETA,AR,P_P0,RP,GP);

load parameters;
GAMMA_S=para{2};

MU_OPT=CHOKE(GAMMA_S);
MU_UP=0.995;
MUS=[MU_OPT,MU_UP];
TAOM=zeros(2,1);

for I=1:2

   MU=MUS(I);
   [M_S1]=MS1(MU);
   [M_P1,MP1SQ]=MP1(MU,P_P0,GP);

   [ARS1P1,ARS1M2,ARP1M2]=ARS(THETA,AR);
   [ER]=OMEGA(M_P1,M_S1,THETA,AR,GP,RP);
   [GAMMA_M,R_M,T_M0,TR_M0P0]=MIX(ER,GP,RP);

   [D]=TMD(M_P1,M_S1,ARS1M2,ARP1M2,GP);
   [E]=TME(ER,M_S1,ARS1M2,GP,RP);
   [TAO1,TAO2]=TAO(ER,MU,D,E,GAMMA_M);
```

```
   TAOM(I)=TAO2;
end

TAOMAX=TAOM(1);
TAOMIN=TAOM(2);
% end of function
```

18) TFUN.m

```
function [TRS]=TFUN(GAMMA,M);

TRS=1+(GAMMA-1)*M*M/2;
% end of function
```

19) TMD.m

```
function [D]=TMD(M_P1,M_S1,ARS1M2,ARP1M2,GAMMA_P);

load parameters;
%GAMMA_P=para{1};
GAMMA_S=para{2};

TERM1=ARP1M2*(1+GAMMA_P*M_P1*M_P1);
TERM2=ARS1M2*(1+GAMMA_S*M_S1*M_S1);

D=TERM1+TERM2;
% end of function
```

20) TME.m

```
function [E]=TME(ER,M_S1,ARS1M2,GAMMA_P,R_P);

load parameters;
GAMMA_S=para{2};
R_S=para{4};
T_S0=para{6};

[GAMMA_M,R_M,T_M0,TR_M0P0]=MIX(ER,GAMMA_P,R_P);
F2S1=FUN2(GAMMA_S,M_S1);

TM1=1/ARS1M2;
TM2=sqrt((R_S*T_S0)/(R_M*T_M0));
TM3=1/F2S1;

E=TM1*TM2*TM3;
% end of function
```

21) TRM2P1.m

```
function [TR_M2P1]=TRM2P1(M_M2,ER,M_P1,GAMMA_P,R_P);

load parameters;
%GAMMA_P=para{1};

[GAMMA_M,R_M,T_M0,TR_M0P0]=MIX(ER,GAMMA_P,R_P);

TR_P0P1=TFUN(GAMMA_P,M_P1);
DEN=TFUN(GAMMA_M,M_M2);

TR_M2P1=TR_M0P0*TR_P0P1/DEN;
% end of function
```

22) TRP1S1.m

```
function [TR_P1S1]=TRP1S1(M_P1,M_S1,GAMMA_P);

load parameters;
%GAMMA_P=para{1};
GAMMA_S=para{2};
T_P0=para{5};
T_S0=para{6};

TR_S=TFUN(GAMMA_S,M_S1);
TR_P=TFUN(GAMMA_P,M_P1);

TR_P1S1=(T_P0/T_S0)*(TR_S/TR_P);
% end of function
```

23) TWOPHASE.m

```
function [R_TP,GAMMA_TP]=TWOPHASE(X,R_G,CP_G,CV_G,CP_L);

R_TP=R_G/(1+X);

GN=CP_G+X*CP_L;
GD=CV_G+X*CP_L;
GAMMA_TP=GN/GD;

% end of function
```

VITA

Name:	Chaqing Liao
Address:	Department of Nuclear Engineering, Texas A&M University, 3133 TAMU, College Station, TX 77843-3133
Email Address:	lchaqing@gmail.com
Education:	B.S., Electrical Engineering, Zhejiang University, 1996 M.E., Nuclear Engineering, Texas A&M University, 2004 Ph.D., Nuclear Engineering, Texas A&M University, 2008